

THE UNIVERSITY
of EDINBURGH

Contribution of the centriolar protein Trichoplein to endothelial cell function in brain vasculature

Eleonora Mameli

Doctor of Philosophy (PhD)

The University of Edinburgh

2023

Author's declaration

I declare that this PhD thesis has been entirely written by me as a result of the work I have performed during my PhD, under the supervision of Dr Andrea Caporali and Professor Giles Hardingham. This research was conducted at the Queen Margaret Research Institute, Centre for Cardiovascular Science, in Edinburgh. The high-content drug screening was performed by the Edinburgh Phenotypic Assay Centre with the professional help of Dr Andrea Martello. The mass spectrometry analysis was performed by the Mass Spectrometry Facility Core of the University of Edinburgh. The RNA sequencing was performed by Beijing Genomics Institute (BGI, Beijing, China). The imaging of the multiplex immunohistochemistry on the brain sections from $Tchp^{EC}$ mice was performed at CNR Institute of Molecular Genetics "Luigi Luca Cavalli-Sforza", Unit of Bologna at IRCCS Istituto Ortopedico Rizzoli with the professional help of Dr Spartaco Santi. This PhD thesis has not previously been submitted for a higher degree.

Eleonora Mameli
10th May 2023

Acknowledgements

Here I am at the end of this journey and I would like to thank some people who had a fundamental role in it.

A big thank you to my supervisor Andrea Caporali, for the support during these years and for always being available and happy to help. His encouragement and valuable feedback helped me progress towards the end of this journey.

I want to thank my co-supervisor Giles Hardingham for the advice he has provided during these years of PhD studies. A big thank you also to the other members of the thesis committee, Megan Holmes and Barry McColl, who helped with precious feedback and support during the PhD.

I would like to acknowledge the collaborators who helped my work take shape. Thank you to Spartaco Santi, Stefan Szymkowiak and Eva Jover Garcia for their guidance and help.

I would also like to thank Diana for sharing with me the joys and sorrows of PhD life.

I am extremely grateful to my family for all the support and encouragement over these years. My parents Rita and Salvatore, who taught me the importance of hard work and determination, and my brother Daniele, for being a loyal confidant and a friend.

Many thanks to my friends Antonella, Francesca, Themis and Chris for making me feel at home abroad and for the many awesome moments, that made such a difference during the pandemic years.

Finally, a special thanks to Steven, who brings light-heartedness into my life every day.

List of publications and achievements

Publications

Mameli, E., Martello, A. & Caporali, A. (2022) Autophagy at the interface of endothelial cell homeostasis and vascular disease, *Febs j.* **289**, 2976-2991.

Starikova, E., Mammedova, J., Ozhiganova, A., Lebedeva, A., Malashicheva, A., Semenova, D., Khokhlova, E., Mameli, E., Caporali, A., Wills, J. & Sokolov, A. (2021) Protective Role of Mytilus edulis Hydrolysate in Lipopolysaccharide-Galactosamine Acute Liver Injury, Frontiers in Pharmacology. 12, 1018.

Achievements and presentations

"Defective autophagy impairs endothelial cell function and barrier integrity." Poster presentation at International Vascular Biology Meeting, San Francisco Bay, 2022 – awarded the Moor Instrument Travel Award by British Microcirculation and Vascular Biology Society and the ASIP 2022 Trainee Scholar Award by the American Society for Investigative Pathology.

"Defective autophagy and proteotoxicity impair endothelial cell function." Oral presentation at the 3-minute thesis competition at the Centre for Cardiovascular Science Symposium 2021 – awarded the first prize.

Competition in the anti-ageing team in Merck Innovation Cup 2022, Merck headquarters, Darmstadt, Germany

"Defective autophagy impairs endothelial cell function and blood-brain barrier integrity." Oral presentation at the Joint Meeting between the German Society for Microcirculation and Vascular Biology and the British Microcirculation and Vascular Biology Society, Berlin, 2022. Awarded the Trainee Scholar Award by British Microcirculation and Vascular Biology Society.

"Defective autophagy impairs endothelial cell function and blood-brain barrier integrity". Oral Presentation at the Blood-Brain Barrier ECR's Symposium, 2021, University of Nottingham

"Defective autophagy and proteotoxicity impair endothelial cell function". Poster presentation at the EVBO Vascular Biology Summer School, 2021

"Trichoplein regulated Endothelial Cell function through the control of Autophagy". Poster presentation at the Scottish Cardiovascular Forum, 2020, University of Strathclyde, Glasgow

Abstract

Age-related cerebrovascular dysfunction plays a critical role in the pathogenesis of the cerebrovascular disease, vascular dementia and Alzheimer's disease, but therapeutic development has been largely unsuccessful until now. Endothelial cells (ECs) are a fundamental component of the neurovascular unit. Their dysfunction has been established as an early event in the pathogenesis of cerebrovascular disease and vascular dementia, leading to dysregulation of cerebral blood flow and blood-brain barrier damage. In this context, identifying novel genes associated with endothelial dysfunction will help understand the role of ECs in blood-brain barrier integrity and address new therapeutic targets.

Trichoplein (TCHP) was initially characterised as a ubiquitously expressed keratin filament-binding protein associated with cell division and cilia formation. Moreover, TCHP has been reported to regulate ER-mitochondria tethering and promote mitophagy, a specialised form of autophagy necessary for the turnover/remodelling of mitochondria. In the lab, we previously demonstrated a pivotal role for the centriolar protein TCHP in linking endothelial cell function with the control of autophagy, showing that the depletion of TCHP in ECs impairs migration and sprouting and triggers cellular inflammation. In line with this, the endothelial-specific deletion of Tchp ($Tchp^{EC}$) in mice decreased the blood flow recovery and vascularisation following hind-limb ischaemia. Protein aggregates were detected in ECs from $Tchp^{EC}$ mice and ECs from patients with coronary artery disease. However, the presented preliminary data regarding the role of TCHP in brain vasculature has not been explored yet.

My PhD project aims to characterise the role of TCHP in brain microvascular ECs *in vitro* and *in vivo* and to reveal its role in blood-brain barrier integrity.

For this study, I generated mice with endothelial selective Tchp knock-out ($Tchp^{EC}$) by breeding the conditional knock-out mice with mice carrying Cre recombinase under the VE-cadherin promoter. RNA sequencing demonstrated the up-regulation of matrix-metalloproteinases and chemokine signalling pathways in the brain ECs isolated from $Tchp^{EC}$ mice. The analysis of the *in vitro* permeability by Electric Cell-substrate Impedance Sensing (ECIS®) revealed an impaired barrier function in ECs

lacking TCHP. Furthermore, $Tchp^{EC}$ mice administered with the fluorescently labelled tracer dextran presented a higher tracer accumulation in the brain than WT mice, showing a loss of blood-brain barrier integrity. In addition, the presence of protein aggregates was confirmed in the cytoplasm of brain microvascular ECs lacking TCHP. The proteomic characterisation of the insoluble-protein fraction revealed RNA-binding and proteasome-associated proteins, suggesting the toxicity of these aggregates for the cells. Finally, a pharmacological screening identified an FDA-approved compound activating autophagy and, thus, restoring EC function and reducing expression of inflammatory genes in EC lacking TCHP.

Collectively, this study presents the novel role played by TCHP in the cerebrovascular endothelium and identifies a new mechanism by which the silencing of TCHP could link endothelial dysfunction to impaired blood-brain barrier integrity.

Lay summary

Age-related vessel dysfunction is an important step during the development of cerebrovascular diseases, such as vascular dementia. Endothelial cells are a thin layer that lines the blood vessels and are fundamental for keeping the integrity of the blood-brain barrier, maintaining the homeostasis of the brain and avoiding the entrance of external substances. A malfunction of endothelial cells leads to cerebrovascular dysfunction, causing the deregulation of cerebral blood flow and damage to blood-brain barrier integrity. Identifying new genes involved in endothelial cell homeostasis in this context is essential to identify new therapies.

We previously discovered that Trichoplein (TCHP) is important for the correct function of endothelial cells through the regulation of autophagy, a process that cells use to keep their homeostasis or to survive in low-nutrient conditions. Moreover, we identified that TCHP is downregulated in endothelial cells of patients with diabetes and coronary artery disease.

Therefore, I investigated the role of TCHP in the endothelial cells of the blood-brain barrier to understand its role in the brain. To perform this study, I used a mouse model lacking TCHP only in endothelial cells ($Tchp^{EC}$).

I demonstrated that endothelial cells lacking TCHP are inflamed, similar to what happens during ageing. Furthermore, $Tchp^{EC}$ mice showed a reduced vessel density and leakage of the blood-brain barrier. Moreover, I confirmed the accumulation of protein aggregates in the brain's endothelial cells of $Tchp^{EC}$ mice as a sign of reduced autophagy. Finally, I identified an approved drug that can restore autophagy and reduce the accumulation of protein aggregates.

For the first time, I present here the role of TCHP in regulating endothelial cell function in the brain and its contribution to the blood-brain barrier integrity.

Table of contents

AUTHOR'S DECLARATION 1

ACKNOWLEDGEMENTS 2

LIST OF PUBLICATIONS AND ACHIEVEMENTS 3

ABSTRACT 4

LAY SUMMARY 6

TABLE OF CONTENTS 7

LIST OF FIGURES 11

LIST OF TABLES 12

LIST OF ABBREVIATIONS 13

1. CHAPTER 1 INTRODUCTION 18

THE ROLE OF ECS IN THE HOMEOSTASIS AND DISEASE OF BRAIN VASCULATURE 18
THE NEUROVASCULAR UNIT 18
THE BLOOD-BRAIN BARRIER IN PHYSIOLOGICAL CONDITIONS 19
ENDOTHELIAL CELLS 20
PERICYTES 24
ASTROCYTES 26
MICROGLIA 26
NEURONS 27
THE BBB IN CEREBROVASCULAR DISEASE 28
NEUROINFLAMMATION 29
AUTOPHAGY IN EC HOMEOSTASIS AND VASCULAR DISEASE 31
THE AUTOPHAGIC PROCESS 31
AUTOPHAGY IN EC HOMEOSTASIS 34
DYSREGULATION OF EC AUTOPHAGY IN VASCULAR DISEASE 35
TRICHOPLEIN 40
IDENTIFICATION AND FUNCTION 44
TCHP AND REGULATION OF MITOCHONDRIA 44
TCHP AND REGULATION OF CYTOSKELETON AND CILIUM 45
TCHP AND REGULATION OF AUTOPHAGY IN ECS 46
$TCHP^{EC}$ MOUSE MODEL 48
HYPOTHESIS AND AIMS 51

CHAPTER 2 MATERIALS AND METHODS 53

MOUSE MODEL 53

GENOTYPING **53**
CELL CULTURE METHODS AND REAGENTS **55**
TRANSFECTION OF HBMVECS AND HBEC-5I AND TRANSDUCTION OF HUVECS **55**
ISOLATION AND CULTURE OF BRAIN MICROVASCULAR ECS FROM ADULT MICE **56**
IMPEDANCE-BASED SCRATCH ASSAY AND BARRIER FUNCTION ASSAYS **56**
PROTEIN MASS SPECTROMETRY **57**
PHENOTYPIC SCREENING ASSAY **58**
IMAGE ACQUISITION 58
IMAGE ANALYSIS 58
DATA ANALYSIS 58
***IN VITRO* TREATMENT** **59**
RNA EXTRACTION AND QUANTITATIVE REAL-TIME ANALYSIS **59**
RNA-SEQUENCING ANALYSIS **60**
GELATINE ZYMOGRAPHY **61**
IMMUNOCYTOCHEMISTRY **61**
IMMUNOHISTOCHEMISTRY **62**
PROTEOSTAT® AGGRESOME **64**
IMAGE ANALYSIS **65**
PROTEIN AGGREGATES QUANTIFICATION 65
CELL PROFILER WORKFLOW FOR CO-LOCALIZATION 65
PCM1 DISTRIBUTION 66
P62 PUNCTA ANALYSIS 66
ANGIOTOOL ANALYSIS 67
ZO-1 ANALYSIS 67
BBB PERMEABILITY ASSAY **68**
FLOW CYTOMETRY **68**
TISSUE COLLECTION: BONE MARROW 68
TISSUE COLLECTION: BRAIN 69
FLOW CYTOMETRY ANALYSIS 69
STATISTICS **70**

CHAPTER 3 CONTRIBUTION OF TCHP KNOCK-OUT TO IMPAIRED HOMEOSTASIS OF BRAIN ECS **72**

INTRODUCTION **72**
HYPOTHESIS AND AIMS **74**
RESULTS **76**
ISOLATION OF ECS FROM THE BRAIN OF TCHP^{EC} MICE 76
BULK RNA-SEQ OF TCHP^{EC} AND WT MICE MICROVASCULAR ECS 79
BIOINFORMATIC AND NETWORK ANALYSIS OF UP-REGULATED DEGS 81
METALLOPROTEINASE ACTIVITY IN TCHP^{EC} AND WT MICE MICROVASCULAR ECS 86
VALIDATION OF DOWN-REGULATED GENES IN HUMAN BRAIN MICROVASCULAR ECS LACKING TCHP 89
ANALYSIS OF THE EFFECTS OF TCHP KNOCK-OUT ON THE FUNCTIONALITY OF MICROVASCULAR ECS 92
LOCALISATION OF TCHP IN MICROVASCULAR ECS 94
CHARACTERISATION OF THE EFFECTS OF TCHP KNOCK-OUT ON CELLULAR ORGANELLES 97
LACK OF TCHP AFFECTS CAV-1 LOCALISATION 99
DISCUSSION **101**
TCHP KNOCK-DOWN ELICITS INFLAMMATION AND IMPAIRS BARRIER FUNCTION 101
EFFECTS OF TCHP KNOCK-DOWN ON NO-SGC-CGMP PATHWAY 105
TCHP LOCALISES IN THE CENTRIOLAR SATELLITES AND AFFECTS TRANSCYTOSIS 106
CONCLUSIONS AND FUTURE DIRECTIONS 108

CHAPTER 4 PHENOTYPIC CHARACTERISATION OF BRAIN VASCULATURE OF ENDOTHELIAL-SPECIFIC TCHP KNOCK-OUT MICE 111

INTRODUCTION 111
HYPOTHESIS AND AIMS 113
RESULTS 115
***IN VIVO* ANALYSIS OF VESSELS PERMEABILITY IN WT AND TCHP^{EC} MICE 115**
IMMUNOHISTOCHEMICAL CHARACTERISATION OF NEUROVASCULAR UNIT 117
ANALYSIS OF VESSELS NETWORK IN TCHP^{EC} BRAIN 119
FLOW CYTOMETRY ANALYSIS OF IMMUNE CELLS IN THE BRAIN OF TCHP^{EC} AND WT MICE 121
OPTIMISATION OF THE GATING STRATEGIES ON BONE MARROW 121
ANALYSIS OF IMMUNE CELLS RECRUITMENT IN THE BRAIN OF WT AND TCHP^{EC} MICE 123
DISCUSSION 127
KNOCK-OUT OF TCHP IS ASSOCIATED WITH INCREASED BBB VASCULAR PERMEABILITY 127
CONTRIBUTION OF TCHP KNOCK-OUT TO ALTERED VASCULAR FUNCTION AND NEUROINFLAMMATION 129
CONCLUSIONS AND FUTURE DIRECTIONS 130

CHAPTER 5 CHARACTERISATION OF AUTOPHAGY IN ECS AND IN VITRO SCREENING TO IDENTIFY COMPOUNDS TO RESTORE AUTOPHAGIC FLUX 132

INTRODUCTION 132
HYPOTHESIS AND AIMS 134
RESULTS 135
LACK OF TCHP CAUSES IMPAIRMENT OF AUTOPHAGY IN BRAIN MICROVASCULAR ENDOTHELIAL CELLS 135
TCHP KNOCK-OUT CAUSES ACCUMULATION OF PROTEIN AGGREGATES IN BRAIN MICROVASCULAR ECS 137
EVALUATION OF PROTEIN AGGREGATES BY MASS SPECTROMETRY 139
..... 142
DRUG SCREENING TO IDENTIFY AUTOPHAGY ACTIVATOR COMPOUNDS 142
..... 145
VALIDATION OF DRUG SCREENING IN VITRO – GUANABENZ, MILRINONE, CALPAIN INHIBITOR II 145
GUANABENZ REDUCES P62 AND LC3-I PUNCTA ACCUMULATION AND INFLAMMATION 146
DISCUSSION 149
TCHP KNOCK-DOWN IMPAIRS AUTOPHAGY IN BRAIN MICROVASCULAR ECS 149
PROTEINS INVOLVED IN STRESS GRANULES IN TCHP KNOCK-DOWN ENDOTHELIAL CELLS 150
GUANABENZ RESTORES AUTOPHAGY AND REDUCES THE ACCUMULATION OF PROTEIN AGGREGATES 152
CONCLUSIONS AND FUTURE DIRECTIONS 155

CHAPTER 6 DISCUSSION 157

TCHP KNOCK-OUT IMPAIRS BRAIN MICROVASCULAR ECS HOMEOSTASIS 158
TCHP KNOCK-OUT AFFECTS VASCULAR PERMEABILITY *IN VIVO* 159
TCHP AND THE REGULATION OF AUTOPHAGY IN BRAIN ECS 160
SUMMARY OF KEY FINDINGS 161
LIMITATIONS OF THE STUDY 162
FUTURE PERSPECTIVES 163
CHARACTERISATION OF TCHP^{EC} MOUSE MODEL: ANALYSIS OF CEREBRAL BLOOD FLOW AND BEHAVIOURAL TESTS 163
ANALYSIS OF BBB IMPAIRMENT 166
***IN VITRO* AND *IN VIVO* TESTS OF GUANABENZ 167**
CONCLUSIVE REMARKS 168

REFERENCES 169

List of figures

Figure 1.1|The neurovascular unit. 19
Figure 1.2| ECs in the BBB. 23
Figure 1.3| Blood-brain barrier in health and disease. 31
Figure 1.4| Three types of autophagy. 33
Figure 1.5| The interplay of autophagy with homeostasis, inflammation and senescence in ECs. 35
Figure 1.6| Dysregulation of EC autophagy in vascular disease. 40
Figure 1.7| TCHP regulates EC homeostasis by stabilizing PCM1. 48
Figure 1.8| TCHP^{EC} mouse model. 50
Figure 2.1|Regions targeted by the primers listed above in Tchp^{EC} and WT mice. 54
Figure 3.1| Isolation of microvascular ECs from the brain of Tchp^{EC} and WT mice for transcriptomic analysis. 78
Figure 3.2| Transcriptomic analysis of microvascular ECs isolated from the brain of Tchp^{EC} and WT mice. 80
Figure 3.3| Parametric Gene Set Enrichment Analysis of ECs from Tchp^{EC} mice. 81
Figure 3.4| KEGG pathway analysis and Network analysis of upregulated genes in ECs from Tchp^{EC} mice. 83
Figure 3.5| TCHP knock-out affects brain microvascular endothelial cells transcriptome in Tchp^{EC} mice. 84
Figure 3.6| TCHP knock-out affects brain microvascular endothelial cell transcriptome in Tchp^{EC} mice sorted with MACS®. 85
Figure 3.7| TCHP knock-out affects HBMVECs transcriptome. 86
Figure 3.8| Gelatin zymography of MMP1, MMP2 and MMP9 activity in the brain of WT and Tchp^{EC} mice. 87
Figure 3.9| Gelatine zymography of MMP1, MMP2 and MMP9 activity in control and Tchp Knock-down HBMVECs. 88
Figure 3.10| Gene Ontology analysis and Network analysis of downregulated genes in ECs from Tchp^{EC} mice. 90
Figure 3.11| TCHP knock-out affects brain microvascular endothelial cell transcriptome in Tchp^{EC} mice. 91
Figure 3.12| TCHP knock-out affects HBMVECs transcriptome. 92
Figure 3.13| TCHP knock-out affects EC function. 93
Figure 3.14| Tchp knock-out impairs ZO-1. 94
Figure 3.15| Colocalization of TCHP-V5 and centriolar satellite proteins, mitochondria and endoplasmic reticulum in HBEC-5i. 96
Figure 3.16| Analysis of cellular organelles in HBMEC-5i. 98
Figure 3.17| Analysis of cellular organelles in HBMVECs. 99
Figure 3.18| Analysis of CAV-1 in HBMEC-5i. 100
Figure 4.1| Analysis in vivo of vessel permeability in WT and Tchp^{EC} mice. 116
Figure 4.2| Tchp knockout increases vascular permeability in the hearth of Tchp^{EC} mice. 117
Figure 4.3| Immunohistochemical characterization of the neurovascular unit of WT and Tchp^{EC} mice. 118
Figure 4.4| Analysis of vascular network in the brain of WT and Tchp^{EC} mice. 120
Figure 4.5| Optimization of the protocol for flow cytometry analysis of the immune cells of the bone marrow of WT and Tchp^{EC} mice. 121
Figure 4.6| Gating strategy for flow cytometry analysis of immune cells in bone marrow from WT and Tchp^{EC} mice. 122
Figure 4.7| Protocol for flow cytometry analysis of cells from the brain of WT and Tchp^{EC} mice. 123
Figure 4.8| Gating strategy for flow cytometry analysis of immune cells in the brain from WT and Tchp^{EC} mice. 124
Figure 4.9| Quantification of flow cytometry analysis of immune cells in brain from Tchp^{EC} and WT mice. 126
Figure 5.1|TCHP knock-down causes impairment of autophagy in HBMVECs. 136
Figure 5.2| TCHP knock-down causes accumulation of protein aggregates in brain microvascular ECs. 138

Figure 5.3| Analysis of aggregate composition by Mass Spectrometry. 140
Figure 5.4|Stress granules markers in TCHP knock-down ECs. 141
Figure 5.5| Principal component analysis of the screened compounds. 143
Figure 5.6| Test in vitro of small molecules and compounds to decrease protein aggregates accumulation. 146
Figure 5.7| Effect of Guanabenz on autophagy and on TCHP–regulated target genes. 147
Figure 5.8| Effect of Guanabenz on TCHP–regulated target genes. 148
Figure 6.1| Characterization of cerebral blood flow and BBB integrity in $Tchp^{EC}$ mouse. 166
Figure 6.2| TCHP knockdown affects MFSD2A expression. 167

List of tables

Table 2.1| List of primers used to genotype $Tchp^{EC}$ and WT mice. 54
Table 2.2| List of mouse and human Sybr green primers used to assess gene expression in ECs isolated from $Tchp^{EC}$ and WT mice and HBMVECs. 60
Table 2.3| List of primary antibodies used in the study. 64
Table 2.4| List of secondary antibodies used in the study. 64
Table 5.1| List of compounds reversing p62 accumulation in TCHP knock-down cells ranked as positivity score. 144
Table 5.2: Analysis of kinase inhibitors reversing P62 accumulation in TCHP knock-down cells ranked as positivity score. 145

List of abbreviations

4E-BP : eIF4E-binding protein

AMPK : AMP-activated protein kinase

ANG2 *:* Angiopoietin 2

ATG : autophagy-related genes

BBB : blood-brain barrier

BCRP : breast cancer resistance protein

BECN1 : Beclin1

CAD : coronary artery disease

cAMP : adenosine 3',5'-cyclic monophosphate

CAV : Caveolin

CCL5 : chemokine (C-C motif) ligand 5

CLDN-1 : Claudin-1

CLDN-11 : claudin-11

CLDN-5 : Claudin-5

CNS : central nervous system

DEGs : differentially expressed genes

DHA : docosahexaenoic acid

ECs : Endothelial cells

EGFR : Epidermal growth factor receptor

EGM : endothelial cell growth medium

eIF2 : eukaryotic initiation factor 2

eNOS : Endothelial NO synthase

ER : endoplasmic reticulum

ESAM : endothelial cell-specific adhesion molecules

FCS : foetal calf serum

Fgf2 : fibroblast growth factor 2

Fgfbp1 *:* fibroblast growth factor-binding protein-1

FOX1 : forkhead box factor 1

G3BP : Ras-GTPase-activating protein SH3 domain-binding protein 1

GABARAP : Gamma-aminobutyric acid receptor-associated protein

GADD34 : growth arrest and DNA damage-inducible transcript 34

Glut-1 : glucose transporter isoform 1

GO : gene ontology

HAECs : human aortic endothelial cells

HBMVECs : Human Brain Microvascular ECs

HBSS : Hank's balanced salt solution

HDAC : histone deacetylase

HMGB1 : high mobility group box-1

HUVECs : human umbilical vein endothelial cells

I/R : ischaemia/reperfusion

ICAM : intercellular adhesion molecule

IFN-γ : interferon

IL-1β : Interleukin 1β

IL-6 : interleukin-6

IMPC : mouse phenotyping consortium

JAM : junctional adhesion molecules

Keap1 : Kelch-like ECH-associated protein 1

Lama2 : laminin α2 chain

LC3 : Microtubule-associated protein light chain 3

LDL: low-density proteins

LIR : LC3-interacting region

LRP1 : lipoprotein receptor–related protein 1

LSR : lipolysis-stimulated lipoprotein receptor

MACS® : magnetic-activated cell sorting

Mad2 : mitotic arrest deficient 2

MAPK : mitogen-activated protein kinases

MCP-1 : monocyte chemoattractant protein-1

miR-503 : microRNA-503

MMP: metalloproteinase

mTORC1 : mammalian target of rapamycin complex 1

MW : molecular weight

NLRP1 : NOD-, LRR- and pyrin domain-containing protein 1

NLRP3 : NOD-, LRR- and pyrin domain-containing protein 3

NO : Nitric oxide

Nrf2 : nuclear factor erythroid 2–related factor 2

NVU : neurovascular unit

OATP : organic anion transporting polypeptide

oxLDL : oxidised low-density lipoprotein

P-gp : P-glycoprotein

P62 : SQSTM1/p62

PBS : phosphate buffer saline

PCA : principal component analysis

PCM1 : pericentriolar material 1

PCR : Polymerase Chain Reaction

Pdgfb : platelet-derived growth factor subunit B

PE : phosphatidylethanolamine

PERK : protein kinase RNA-like ER kinase

PGC-1α : peroxisome proliferator-activated receptor γ coactivator- 1α

PGSEA : parametric gene set analysis

PIP3P : phosphatidylinositol 3-phosphate

PKA : cAMP-dependent protein kinase A

RBPs : RNA-binding proteins

RFUs : Raw fluorescence unit

RNS : reactive nitrogen species

ROS : reactive oxygen species

RPE1 : retinal pigment epithelial-1

S1P : endothelial sphingosine-1-phosphate

S6K1 : p70 ribosomal S6 kinase 1

SASP : senescence-associated secretory phenotype

SDS : sodium dodecyl sulfate

Ser/Thr : serine/threonine

sGC : soluble guanylyl cyclase

Shh : Sonic hedgehog

SIRT1 : Sirtuin 1

TCHP : Trichoplein

$Tchp^{EC}$: Endothelial selective Tchp knock-out

TEER : transendothelial electrical resistance

TGFβ1: growth factor beta 1

TH : T-helper

TJ : tight junctions

TNF-α : tumour necrosis factor

Treg : T-regulatory

TRM : tetramethyl rhodamine

ULK1 : UNC51-like Ser/Thr kinase

UPR : unfolded protein response

VCAM : vascular cell adhesion molecule

VCP : valosin-containing protein

VEGF : vascular endothelial growth factor

VEGFR2 : vascular endothelial growth factor receptor 2

VPS : vacuolar protein sorting

VWF : Von Willebrand factor

WIPI : WD-repeat protein interacting with phosphoinositide

ZO - 1 : zonula occludens 1

Chapter 1

Introduction

1. Chapter 1 Introduction

The role of ECs in the homeostasis and disease of brain vasculature

The neurovascular unit

Brain vasculature includes 400 miles of the vascular network and the brain uses one-fifth of the cardiac output [4]. This is because homeostasis and correct brain functioning depend on an adequate blood supply, oxygen and nutrients like glucose, ATP, glycogen and phosphocreatine [5]. The tight relationship between the brain and vascular system is emphasised by the neurovascular unit (NVU) concept, first introduced in 2001 at the Stroke Progress Review Group meeting of the National Institute of Neurological Disorders and Stroke of the NIH [6]. The NVU is a highly organised multicellular system, including vascular cells (brain ECs, smooth muscle cells, pericytes), neurons and glial cells (astrocytes, microglia, oligodendrocytes) [7] (**Figure 1.1**).

The NVU regulates the neurovascular coupling, indicating the mechanism through which blood supply is matched to neuronal need by controlling vascular intraluminal diameter. Additionally, the crosstalk between the several cells of the NVU is fundamental for keeping the blood-brain barrier (BBB) integrity and for brain development [6, 8]. Alterations of the NVU precede and lead to the development of brain dysfunction. Changes in the cerebral blood flow cause hypoxia and BBB alterations cause impairment in the clearance of unwanted metabolites and delivery of nutrients. Finally, alterations in clearance pathways can cause the accumulation of proteins and proteinopathies [6]. The strict connection between the different types of cells in the NVU explains the link between cerebrovascular dysfunction and disease. As an example, a neurovascular dysfunction is an early event in the pathogenesis of Alzheimer's disease and it is increasingly recognised as a hallmark beside amyloid-β plaques and hyperphosphorylated tau neurofibrillary tangles [9]. NVU alterations are involved in the pathogenesis of vascular dementia, Alzheimer's disease, ischemic stroke, chronic inflammation, multiple sclerosis and brain tumour

[10, 11]. Therefore, understanding the mechanisms involved in the impairment of NVU is necessary to identify new treatments for cerebrovascular disease.

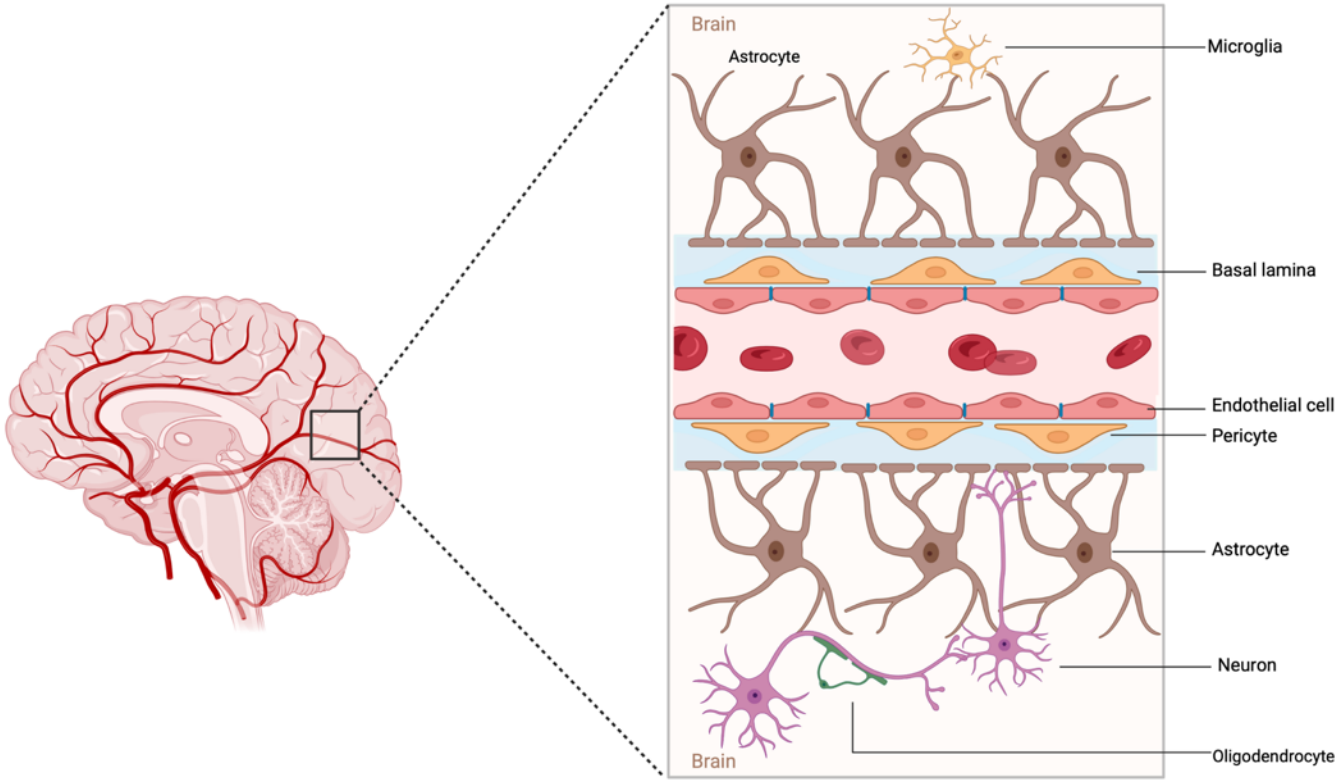


Figure 1.1|The neurovascular unit.

The NVU includes vascular cells (brain ECs, pericytes), neurons and glial cells (astrocytes, microglia, oligodendrocytes). Created with BioRender.com.

The blood-brain barrier in physiological conditions

The BBB is a multicellular system comprising ECs, pericytes and astrocytes, that takes part in the NVU with neurons, microglia and oligodendrocytes. The BBB is fundamental for keeping the central nervous system (CNS) microenvironment. Indeed, BBB regulates the transport of nutrients, such as glucose and amino acids, ions and O_2 inside the brain, using transport proteins. Furthermore, BBB protects the brain parenchyma from the entrance of exogenous compounds, pathogens, large hydrophilic molecules, plasma proteins and immune cells, protecting the brain from damage [10, 11]. Additionally, BBB separates central and peripheral neurotransmitters avoiding cross signalling [12]. BBB regulates paracellular and

transcellular transport through junctional complexes between ECs and the expression of specific receptors and pumps [13].

BBB was first discovered one century ago by Paul Elrich when he noted that a peripherally injected die did not stain the brain tissue [10]. The BBB is formed by microvascular ECs lining cerebral capillaries in the brain and spinal cord [14]. It is the most extensive blood-brain exchange interface, and the surface area in an adult arrives at 18 m^2 [10]. The main characteristics of the BBB are due to the specialised endothelium. Brain ECs are characterised by 1. lack of fenestrations; 2. the expression of tight junctions (TJ) that regulate the paracellular passage into the brain; 3. increased number of mitochondria; 4. lack of pinocytic activity and low rate of transcytosis to control the transcellular transport. The transport barrier includes efflux transporters such as P-glycoprotein (Pgp), breast cancer resistance protein (BCRP), and organic-transporting polypeptide (OATP) [10, 11]. Additionally, within ECs, drug-metabolizing enzymes, such as CYP 450, create a metabolic barrier [10]. Notably, this integrated barrier system protects the brain but also represents an obstacle to drug delivery into the CNS.

The following paragraphs will describe the several cellular species constituting the BBB (ECs, pericytes, astrocytes) and the NVU components neurons and microglia.

Endothelial cells

Brain ECs present different features compared to the peripheral system. They are characterised by a flattened appearance, expression of TJs, low caveolae transport and a high number of mitochondria, compared to ECs from other vascular beds. Genetic studies using global or condition transgenic mice reported Wnt7a/7b ligands and the Wnt/β-catenin pathway as the main drivers of angiogenesis and forming of the BBB [11]. Single-cell RNA sequencing revealed a different translatome associated with brain endothelial-specific transcription factors (Foxf2, Foxl2, Foxq1, Lef1, Ppard, Zfp551, and Zic3) that act downstream Wnt-β-catenin signalling during the embryogenesis of brain vasculature compared to other vascular districts. Interestingly, overexpression of Foxf2 and Zic3 in human umbilical vein endothelial cells (HUVECs) led to the production of BBB differentiation markers [15]. Notably,

there is a certain vascular heterogeneity in the BBB, and ECs morphology and molecular characteristics change depending on the area of the CNS [16, 17].

ECs form a sealed barrier via junctional complexes that block paracellular transport. TJs are intercellular junction complexes comprising integral membrane proteins such as occludin, claudins, junctional adhesion molecules (JAM), and endothelial cell-specific adhesion molecules (ESAM). The scaffolding proteins zonula occludens (ZO-1, ZO-2, ZO-3) allow them to link to the cytoplasm. Moreover, TJs mix with non-occludin adherens junctions (AJs), like the endothelial-specific VE-cadherin. Cadherin links to the actin cytoskeleton through catenins, forming contacts between cells. TJs and AJs interact particularly with ZO-1 and catenins, to influence TJs assembly [10, 18]. At the same time, signalling from TJs could regulate AJs expression. For example, VE-cadherin engagement through Akt activation and inhibition of β-catenin nuclear translocation promotes phosphorylation of the transcription factor forkhead box factor 1 (FOX1), thus inducing the transcription of TJ protein claudin-5 (CLDN-5) [19]. TJs prevent the lateral diffusion of bloodborne polar compounds and the diffusion of these molecules over the blood-brain barrier [20, 21]. CLDN-3, CLDN-5 and CLDN-12 are brain-specific and bind to claudins on adjacent cells, forming the TJ seal [22, 23]. CLDN-5 limits the movement of small molecules (<800 Da) across the BBB [13]. Additionally, CLDN-5 is necessary for TJ formation in BBB, since its embryonic ablation in mice causes postnatal brain oedema and death [24]. CLDN-1 is the second-highest expressed TJ. Loss of CLDN-1 happens in cancer, stroke and inflammation *in vitro* and *in vivo* [25-27]. Moreover, CLDN-11, a protein recently identified in brain ECs and capillaries, is essential for paracellular tightness via homophilic oligomerisation [28]. Its expression is significantly decreased in patients with multiple sclerosis and in a mouse model of experimental autoimmune encephalomyelitis (EAE) [29]. Occludin and claudins assemble into heteropolymers, allowing the diffusions of hydrophilic molecules and ions. Loss of 55 kDa occludin expression happens in brain tumours with concomitant BBB breakdown [10].

ESAM, JAM and nectins regulate TJ function and the transmigration of inflammatory cells across the BBB into the CNS [30]. Another class of TJ-associated proteins are the tricellular junctions, comprising tricellulin [31] and the lipolysis-stimulated lipoprotein receptor (LSR) [32]. They are localised where three cells connect. The role

of these tricellular junctions is not clear yet but genetic deletion of LSR results in the impairment of the barrier and leakiness to small molecules [33]. AJs are fundamental for the establishment of TJs [34]. VE-cadherin and N-cadherin represent the most expressed AJs in the ECs and they mediate the interaction between ECs and pericytes through peg and socket junctions. They also work as adhesion receptors through the proteins linked to their cytoplasmic tails [11].

The cytoskeleton provides inter-endothelial junctional integrity. It consists of actin microfilaments, intermediate filaments and microtubules. The actin cytoskeleton is essential in providing tension force to brain ECs that allows them to retain their shape, driven by the interaction of actin with myosin to form stress fibres. The polymerisation of actin fibres is essential for regular cellular physiological tasks such as cell cytokinesis or endo- and exocytosis [35]. Intermediate filaments are responsible for tensile strength; the major intermediate filament is vimentin which links to VE-cadherin [36]. Microtubules consist of α- & β- tubulin polymers involved in the rapid assembly of actin filaments and focal adhesions, cellular contraction and increased transendothelial migration [37].

ECs regulate the passage of molecules through the BBB into the CNS and from the CNS to the blood. Small lipophilic molecules, with a molecular weight (MW) < 400 Da can cross the BBB [38], while glucose and amino acids need carrier-mediated transporters. Larger molecules, such as insulin, iron transferrin and leptin, use receptor-mediated endocytosis [10, 39, 40]. Endothelial transporters play a crucial role in brain homeostasis. Active transport includes the glucose transporter isoform 1 (Glut-1), highly expressed during BBB formation and regulated by the Wnt/β-catenin pathway [24], amino acids transporters such as LAT1 and LAT2 [41] and ATP binding cassette family transporters, of which the most studied is Pgp, fundamental for brain homeostasis and involved in the pathogenesis of Alzheimer's disease [42] (**Figure 1.2**).

The third main feature that characterises brain ECs is the low rate of transcellular transport and reduced number of caveolae. Transcytosis can be clathrin-mediated, such as the transferrin receptor-mediated transport of iron [43], or non-clathrin mediated, including caveolae-mediated transcytosis [44]. Caveolae are 50-100 nm

membrane invaginations enriched in saturated phospholipids, sphingolipids, cholesterol and ethanolamine plasmalogens. Caveolae-mediated vesicle trafficking is strongly present in the ECs of peripheral tissues, such as the heart and lung, but much lower in the brain [45]. Andreone et al. described the regulation of caveolae-dependent transcytosis by the omega-3 fatty acid docosahexaenoic acid (DHA) transporter MFSD2A, which would control the luminal plasma membrane DHA lipid composition and consequently prevent caveolae transport, keeping the integrity of the blood-brain barrier [46]. The expression of MFSD2A increases in CNS during BBB formation and its ablation results in BBB leakiness because of the increase in vesicular traffic. Caveolin (CAV)-1 and CAV-2 are expressed in the ECs, but only CAV-1 is fundamental for caveolae formation [47].

Interestingly, CAV-1 interacts with β-catenin and weakens VE-cadherin-based AJs [48]. Studies in zebrafish demonstrated that transcytosis gradually stops with the establishment of the BBB function [49]. The same group reported that also in mice, the formation of the blood-retinal barrier is associated with a decrease in transcytosis [50].

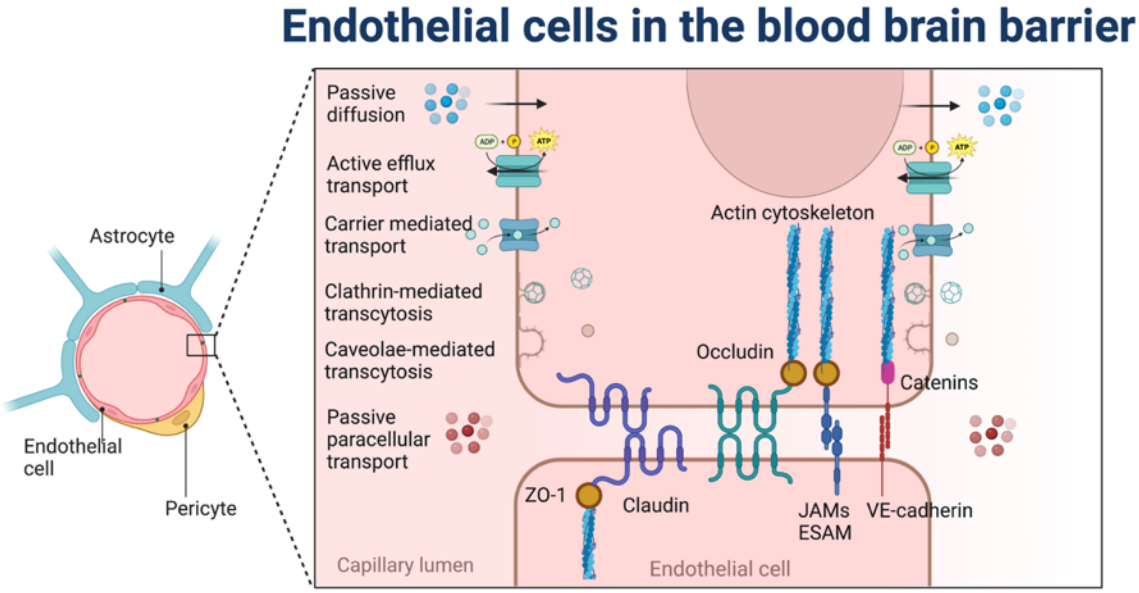


Figure 1.2| ECs in the BBB.

The ECs of the BBB constitute a tight barrier thanks to the presence of TJs (Claudin and occludin, JAMs, ESAM, linked to the actin cytoskeleton by ZO-1; and adherens junctions like VE-cadherin, linked to actin through catenins). Moreover, transport through the ECs is strictly regulated. Small molecules, with a MW< 400 Da can cross the BBB by passive diffusion and water-soluble agents can pass using passive paracellular transport. Active efflux transport includes ATP-binding cassette transporters such as Pgp and mostly eliminates substances from the brain. Carrier-mediated transport includes GLUT1 and LAT1 and LAT2. Finally, endocytosis, present at a lower level compared to other tissues, include clathrin-mediated and caveolae-mediated. Created with BioRender.com.

Pericytes

Pericytes have been considered support cells for many years. However, their involvement in neurovascular functioning has been clarified lately. Pericytes contact the underlying endothelium along the brain's microvasculature and are embedded within the basement membrane. Pericytes are involved in vascular development, cerebral blood flow regulation, keeping BBB integrity and, finally, neuroinflammation [51].

In the context of vascular development, the importance of pericytes is demonstrated by the fact that in pericyte-deficient mice, pericyte loss is associated with vascular dysfunction, reduced capillary perfusion and brain microcirculation and finally, BBB breakdown [52]. Pericytes play a role in angiogenesis and vascular stabilisation. Indeed, ECs secrete growth factors such as angiopoietin 1, transforming growth factor beta (TGF-β) and platelet-derived growth factor-BB (PDGF-BB), that make pericytes migrate to new vessels and stabilise vessel walls [53].

Regarding their involvement in keeping BBB stability, pericytes regulate the specific BBB endothelial gene expression in ECs and induce polarisation of the astrocytes' end feet around the blood vessel [54]. Armulik et al. showed that pericyte deficiency causes the passage of low-molecular-mass and high-molecular-mass tracers and increases endothelial transcytosis *in vivo*. Moreover, pericyte deficiency caused a decrease in the expression of polarised astrocyte end-foot AQP4, α-syntrophin and laminin α2 chain (Lama2) [54]. Pericyte also affected EC gene expression. The same group reported that the absence of pericytes causes the lack of the transporter MFSD2A. In contrast, regions of the capillary that kept contact with pericytes still presented the transporter, suggesting that pericytes control EC expression of MFSD2A directly through paracrine or juxtracrine signals. Furthermore, RNA-sequencing showed that the absence of pericytes causes loss of brain capillary transcriptome and gain of venous transcripts, and increased markers expressed normally only during development (fibroblast growth factor-binding protein-1 - Fgfbp1) and pathological angiogenesis (Angiopoietin 2 - Ang*2*) [55]. Transferrin receptor (CD71) expression was downregulated in ECs lacking pericytes coverage [54].

Pericytes morphology changes depending on their location. Grant et al. classified pericytes in adult mouse cortex as ensheathing pericytes characterised by shorter cell lengths and α-smooth muscle actin (α-SMA) in precapillary arterioles and mesh and thin-strand pericytes that present longer cell lengths and non-detectable α-SMA in capillaries [56]. Pericytes morphology plays a role in keeping BBB, as demonstrated by the irregular shape they present in the human median eminence, where leakage naturally happens, compared to the cortex [13, 57].

Pericytes interact with ECs through adhesion plaques and peg-and-socket junctions, formed by N-cadherin and connexin-43 hemichannels. Gap junctions allow the passage of ionic currents [11, 13]. Cell adhesion receptor CD146 regulate pericytes-EC interactions functioning as a co-receptor for PDGFRβ [58]. The loss of pericytes associated with ageing and disease could be due to the loss of the endothelial sphingosine-1-phosphate (S1P) receptor, which controls N-cadherin trafficking and, consequently, ECs-pericytes adhesion [59]. A reduction of S1P was observed in a mouse model of Alzheimer's disease and vascular dementia and is involved in neuroinflammation [13, 60].

Pericytes can relax or contract within the brain, regulating blood flow in response to neuronal activity. They indeed possess contractile proteins, such as α-SMA, myosin and tropomyosin. However, only the pericytes described above seem to be involved in regulating cerebral blood flow, but this is still unclear [61].

Even if neuroinflammation is principally due to microglia, astrocytes and infiltrating leucocytes, also pericytes are involved. Pericytes can release inflammatory molecules and metalloproteinase (MMP)9 when exposed to IL-1β or TNF-α, leading to BBB breakdown [62]. In addition, pericytes play a role in the recruitment of leukocytes inside the brain by opening intra-pericytes gaps. Indeed, pericyte-deficient mice presented reduced leukocyte trafficking [63, 64]. Finally, the reduction of pericyte coverage has been associated with Alzheimer's disease. Patients with Alzheimer's disease showed a 60% reduction in pericyte coverage [65]. Transgenic mice with pericyte deficiency presented an overexpression of Aβ precursor protein and reduced Aβ clearance low-density lipoprotein receptor–related protein 1 (LRP1) mediated, due to the lower number of pericytes [66].

Astrocytes

Astrocytes are the most present cell type in the CNS. They contact the outer basal membrane through the end feet, which produce the extracellular matrix proteins that constitute the basal membrane. Additionally, the end feet are characterised by the presence of water channel AQP4 and of the potassium channel Kir4.1, which regulate the water homeostasis in the NVU [24]. Astrocytes control perivascular fluid and solute movement via AQP4 channels and regulate the exchange between perivascular cerebrospinal fluid and interstitial fluid in CNS, regulating in this way also the clearance of toxins [67]. Astrocytes develop at late gestation stages (E17.5), so they are not involved in the development of the BBB, but only in its maintenance [11, 68]. In support of this, Sonic Hedgehog (Shh) stimulates the expression of the TJs CLDN-5 and occludin in ECs [69]. Chow & Gu demonstrated that in the retina, blood vessels develop a barrier postnatally when astrocytes are already present. At the same time, astrocytic signals alone are insufficient to induce a functional barrier since vessels present a leaky barrier phenotype [50]. Further proof of the role of astrocytes in the maintenance of the BBB is that deletion of astrocyte-derived laminin causes a decrease in AQP4 and reduced TJ proteins in ECs [70, 71].

Microglia

Microglia represent the brain's resident immune cell populations and the first line of defence in CNS. Microglia are involved in vascular growth during brain development, for example, through the secretion of Wnts [24]. Dudiki et al. reported that microglia regulate vascular architecture by a transforming growth factor beta 1 (TGFβ1)-dependent paracrine signalling [72]. Furthermore, Jobling et al. showed the presence of angiotensinogen in retinal microglia and the regulation of vessel diameter [73]. Microglia do not seem to have a role in barrier maintenance since their ablation does not increase BBB permeability [74].

In physiological conditions, microglia are in their homeostatic state, while in the presence of inflammatory stimuli, they undergo a rapid transformation into an active state. Activated microglia produces pro-inflammatory molecules, such as cytokine, chemokines and ROS, and can lead to neuroinflammation [75], by causing the disruption of BBB and neuronal damage [76]. Activation of microglia and disruption

of BBB is involved in cerebrovascular diseases, such as stroke [77] and Alzheimer's disease [78].

Haruwaka et al. showed that microglia initially have a protective effect on BBB, before phagocytosing BBB components, leading to leakage and neuroinflammation. Resident homeostatic microglia would migrate to the cerebral vessels in response to the endothelial release of chemokine (C-C motif) ligand 5 (CCL5), which would stimulate the secretion of microglial CLDN-5 to contact ECs and reinforce TJs. In late inflammation, microglia would be characterised by CD68-expressing phagocytic phenotype and phagocytise astrocytic end-feet negatively affecting BBB [79]. Reactive microglia downregulate CLDN-5, occludin, and ZO-1, causing BBB disruption [79]. Furthermore, reactive microglia can phagocyte ECs [80] and cortical synapses [81], affecting several components of the NVU.

Neurons

Neurons connect with astrocytic end feet in the proximity of BBB. They act like sensors in the CNS, communicating with astrocytes and leading to NVU regulation of cerebral blood flow. During vascular insult, they send signals that lead to the recruitment of microglia and the start of the inflammatory response [67]. During brain development, neural precursors and early neurons are the primary sources of Wnt7a and Wnt7b, promoting vascularisation [24]. Disturbed neural activity causes angiogenesis arrest in the associated brain area in the perinatal brain, highlighting the importance of neurons during brain development [82].

Neurons are involved in the regulation of BBB permeability. Increases in neural activity caused a change in BBB-related gene transcription in the vasculature of the visual cortex, with an increase in ANG2 [83], which can cause BBB disruption through antagonism of the ANG1-TIE2 pathway [84]. Neural stimulations using transcranial magnetic stimulation caused an increase in BBB permeability [85]. Furthermore, neural activity and the associated release of neurotransmitters act on cells of the NVU, affecting the BBB [86].

The BBB in cerebrovascular disease

The BBB is comprised of specialised ECs lining the brain's microcirculation. A tightly regulated BBB ensures limited permeability, aiding in preserving the homeostatic environment of the brain. As already reviewed, this is due to the contractile forces generated by the endothelial cytoskeleton and the adhesive forces of the TJ and AJ proteins, which are responsible for maintaining the integrity and restrictive nature of the BBB. Impairment of the blood-brain barrier and its increased permeability cause the entrance of plasma proteins and immune cells in the brain parenchyma, leading to neuroinflammation, involved in cerebrovascular and neurodegenerative disease [87].

A variety of different factors can disrupt the permeability of the BBB, including vasogenic agents such as histamine, vascular endothelial growth factor (VEGF), basic fibroblast growth factor and TGF-β, inflammatory mediators of cytokines (Interleukin 1β IL-1β, tumour necrosis factor TNF-α & interferon IFN-γ), chemokines (CCL2, CXCL8), matrix metalloproteinases (MMP2 & MMP9), free radicals (H2O2, OH- & NOO-) and prostaglandins (E2 & F2a) [88]. Increased paracellular permeability and low transendothelial electrical resistance (TEER) caused by these stimuli can be associated with alterations in the junctional complex, forming intercellular gaps and allowing large plasma proteins and inflammatory cells to break through.

Oxidative stress caused by increased production of reactive oxygen species (ROS) and reactive nitrogen species (RNS) causes endothelial dysfunction, impairment of TJs and activations of the MMPs [89]. Also, an increase in ROS species affects nitric oxide (NO) signalling and potassium channel function, leading to modification of cerebral blood flow. Decreased bioavailability of NO increases oxidative stress and endothelial dysfunction, leading to blood-brain barrier impairment [90].

Another factor involved in the disruption of the BBB is inflammation. Inflammation impairs BBB directly by affecting TJ assembly and Rho-kinase signalling involved in the internalisation of TJs [91], or indirectly by activating MMPs [92]. Pro-inflammatory cytokines activate apoptotic pathways and reduce TJs by upregulating the mitogen-activated protein kinases (MAPK) pathway [93]. Additionally, pro-

inflammatory cytokines cause increased expression of cell adhesion molecules that lead to leukocyte infiltration [89].

The variation in barrier dysfunction can range from mild transient TJ opening to complete perturbation and breakdown of the BBB. Specifically, the TJ and AJ proteins undergo phosphorylation and dephosphorylation by protein kinases and phosphatases at serine, threonine, or tyrosine residues affecting protein-protein interaction, protein localisation, distribution and degradation [94]. In addition, the actin cytoskeleton undergoes reorganisation whereby the actin filaments polymerise to form stress fibres. The association of actin with myosin results in the generation of contractile forces that disrupt the junctional complexes, forming small gaps in the barrier [95]. Downstream effects of changes in the TJs and AJs integrity include disruption of cell polarity, subsequently affecting the distribution and localisation of transporters and enzymes [96].

Neuroinflammation

BBB disruption and brain injury elicit neuroinflammation. First, inflammation leads to the activation of microglia, causing the release of pro-inflammatory mediators, such as cytokines, chemokines, ROS and interleukins (ILs), which increase the permeability of the BBB (**Figure 1.3**). This allows subsequent infiltration of peripheral leukocytes into the CNS, including T cells and monocytes [97]. Therefore, increased BBB permeability means that peripheral monocytes-derived macrophages can have a role in neuroinflammatory outcomes, leading to neuronal cell death and causing further microglial activation as a negative feedback loop. However, as reviewed above, activated microglia have been described as a double-edged sword, which can have both toxic and beneficial roles. Early migration of resident microglia to capillary walls in response to CCL5 release by brain ECs has been observed and results in TJ formation by microglia cells with ECs via expression of CLDN-5. Ablation of microglia or blockage of CCL5 signalling early on in inflammation increases BBB permeability [79]. Furthermore, at this stage, microglia release anti-inflammatory mediators such as interleukin-10 (IL-10), insulin-like growth factor 1 and neurotrophic factors to attempt to resolve the inflammation [98]. On the other hand, sustained inflammation causes microglia transformation to a phagocytic phenotype with the ability to release

pro-inflammatory mediators such as prostaglandins, TNF-α, interleukin-6 (IL-6), IL-1β, ROS and glutamate and thus contribute adversely to BBB damage [79].

The inflammation and the disruption of the BBB cause the infiltration of leukocytes into the brain, which are not present in physiological conditions. This is due to adhesion molecules such as intercellular adhesion molecule (ICAM) and vascular cell adhesion molecule (VCAM), selectins and leukocyte integrins on the surface of ECs, produced because of inflammation [99]. Among these leukocytes are the innate immune response molecules granulocytes (neutrophils, basophils, eosinophils), monocytes (macrophages and dendritic cells) and the adaptive immune system effectors, the lymphocytes ($CD4^+$ T-helper (TH) cells, $CD8^+$ cytotoxic T-cells and B cells) [100]. $CD4^+$ T-helper cells can be divided into different subsets; the pro-inflammatory TH1 and TH17 and the anti-inflammatory TH2 and T-regulatory (Treg). TH1 cells produce IFN-γ, TNF-α and IL-12 to trigger cell-mediated immunity and phagocytic-dependent inflammation and induce macrophage switching to a pro-inflammatory M1 phenotype. TH2 cells produce IL-4, IL-6, IL-10 and IL-13 to regulate antibody responses and TH17 cells predominately secrete IL-17 and IL-22. Treg cells secrete IL-10 and TGF-β to prevent excessive inflammatory responses, including autoimmunity, by regulating the other T-cell subsets and innate immune cells [101]. Infiltration of these immune cells affects vessel perfusion and leads to a consistent and chronic inflammation status. Furthermore, leukocytes produce ROS, causing activation of the NF-κB pathway and exacerbating inflammation [89].

Inflammation has been recognised as a key component of cerebrovascular and neurological diseases and in small vessel disease and vascular dementia, for example, there is always a combination of both acute and chronic inflammation [102]. Acute inflammation occurs with the stroke due to acute vessel blockage, leading to the activation of inflammation in response to hypoxia/ischaemia [103]. Chronic inflammation is thought to be related to the underlying hypoperfusion and BBB

changes and is likely more similar in pathophysiology to chronic neurodegenerative diseases such as Alzheimer's disease [104].

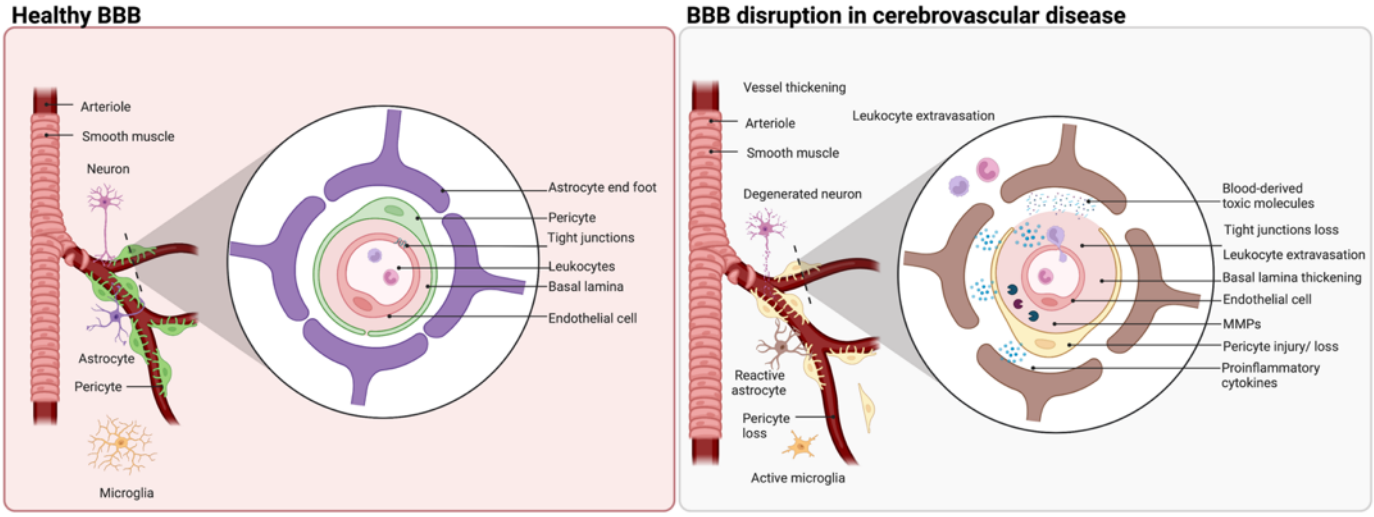


Figure 1.3| BBB in health and disease.

Components of the neurovascular unit in health and disease. In the pathogenesis of cerebrovascular disease, inflammation causes the loss of the tight barrier constituted by the ECs and pericytes coverage, causing the extravasation of immune cells and the entrance into the brain of blood-derived toxic molecules. This causes the activation of microglia and neurodegeneration. Created with BioRender.com

Autophagy in EC homeostasis and vascular disease

The autophagic process

Autophagy is an intracellular process that ensures cellular homeostasis and stress adaptation. Through autophagy, damaged organelles and harmful protein aggregates are degraded and their components are recycled to generate energy in adverse conditions. Three types of autophagy have been defined in literature: macroautophagy, microautophagy and chaperone-mediated autophagy (**Figure 1.4**). The macroautophagy process starts with the formation of the phagophore, a specialised membrane that engulfs the cytoplasmic material that must be eliminated, leading to the assembly of autophagosomes. Finally, the autophagosome mix with the lysosome to degrade its contents [105]. During microautophagy, lysosomes directly engulf the cytoplasmic material to eliminate. This second type of autophagy plays a role in maintaining organelles size, in cells survival during nitrogen starvation

and in maintaining membrane homeostasis [106]. Finally, chaperone-mediated autophagy is characterised by chaperone complexes and lysosome proteins that degrade proteins targeted by the specific motif [107] [3].

Macroautophagy, from now on just called autophagy, comprises initiation, elongation and maturation of autophagosomes. One of the main regulators is the multimeric protein mammalian target of rapamycin complex 1 (mTORC1), including serine/threonine (Ser/Thr) kinase mTOR, the regulatory protein RAPTOR, the assembly factor mLST8 and the two inhibitory subunits PRAS40 and DEPTOR. mTORC1 normally inhibits autophagy and promotes cell proliferation [108]. When the level of growth factors or aminoacids decreases under a certain threshold, mTORC1 inhibition of the complex formed by UNC51-like Ser/Thr kinase (ULK1), ATG13, FAK family kinase-interacting protein of 200 kDa and ATG101 stops and ULK1 autophosphorylates at Thr-180 [109]. This increases kinase activity, leading to the phosphorylation of RAPTOR and strengthening the inhibition of mTORC1. Additionally, activating AMP-activated protein kinase (AMPK) by metabolic demand during glucose or amino acid starvation leads to the inhibition of mTORC1 [110]. ULK1 activates the complex formed by phosphatidylinositol 3-kinase class III in complex with vacuolar protein sorting (VPS) 34, VPS15, Beclin1 (BECN1) and ATG14L, leading to the production of phosphatidylinositol 3-phosphate (PIP3P) [111]. Meanwhile, WD-repeat protein interacting with phosphoinositide (WIPI) binds PIP3P at the nascent autophagosome [3].

The following steps are controlled by autophagy-related genes (ATG). First, ATG12 binds to ATG5 and with ATG7 and ATG10, which act as E1 and E3-like enzymes, leading to the formation of the ATG12-ATG5-ATG16L1 complex. Then, ATG7 catalyses the conjugation of the ATG8 proteins to phosphatidylethanolamine (PE) on the phagophore membranes through the E2 enzyme ATG3 [112].

Mammals present several ATG8 orthologues: LC3A, LC3B, LC3C, GABARAP, GABARAPL1 and GABARAPL2 [112]. Microtubule-associated protein light chain 3 (LC3) and Gamma-aminobutyric acid receptor-associated protein (GABARAP) families have a non-redundant function during the autophagosome biogenesis, even if GABARAP seems to have a preponderant role since it binds essential ATG proteins over LC3 [113]. ATG8 proteins work as scaffold proteins during autophagosome

formation, binding protein subunits containing the sequence motif called LC3-interacting region (LIR) [114]. Simultaneously engaging with cargo and ATG8 family proteins on autophagosomes, the autophagy receptors containing LIR domain, such as SQSTM1/p62 (P62) and nuclear dot protein 52, physically link specified cellular material with the autophagy compartment [115].

Mature autophagosomes finally fuse with lysosomes, forming autolysosomes, and degrading the autophagosome's content.

It is not fully known how the translocation of ATG8 proteins to the phagophore happens. A pool of GABARAP is present in the centrosome and pericentrosomal region, regulating the development of autophagosomes during amino acid starvation. GABARAP binds pericentriolar material one (PCM1)[116], responsible for pericentrosomal localisation of centrosomal proteins and PCM1 controls the delivery of GABARAP to the autophagosome [3].

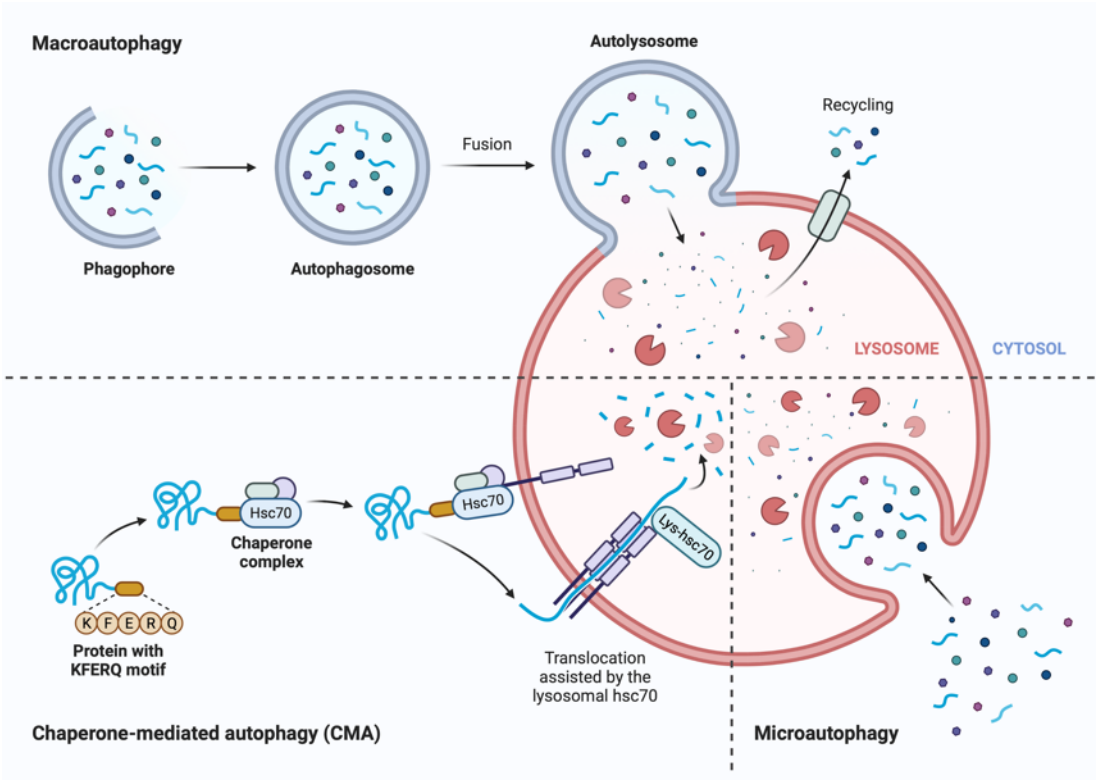


Figure 1.4| Three types of autophagy.

Macroautophagy process starts with the formation of the phagophore, a specialised membrane that engulfs the cytoplasmic material that must be eliminated, leading to the assembly of autophagosomes—finally, the autophagosome mix with the lysosome to degrade its contents. In chaperone-mediated autophagy, chaperone complexes and lysosome proteins degrade proteins targeted by the specific motif. In microautophagy, lysosomes directly engulf the cytoplasmic material to eliminate. Created with BioRender.com.

Autophagy in EC homeostasis

Autophagy regulates EC response to the surrounding environment and the angiogenic stimuli, which is important in regulating EC homeostasis.

Autophagy is involved in the proliferation and sprouting of ECs. Spengler et al. reported that VEGF transiently activates autophagic flux by an AMPK-dependent mechanism. This activation is regulated by the delayed activation of mTOR by VEGF [117]. Conversely, Domigan et al. showed that ablation of VEGF causes EC death via FOXO1-mediated fragmentation and increased autophagy [118]. Additionally, the cAMP-dependent protein kinase A (PKA) regulates vessel sprouting, determines endothelial quiescence through phosphorylation of ATG16L1 and reduces endothelial autophagy [119].

Shear stress induced by laminar flow promotes EC autophagy by activating Sirtuin 1 (SIRT1), an NAD^+-dependent histone deacetylase that directly deacetylates the promoters of numerous autophagy machinery components [120].

ECs require autophagic flux for the regulation of TJs and keeping barrier integrity. Decreased autophagy via siRNA silencing Atg5 caused an increased permeability ROS mediated. Moreover, autophagy is a defence mechanism against hypoxia, oxidised low-density lipoprotein (ox-LDL) and ROS. In line with this, whereas overexpressing ATG5 induces an increase in cell migration and angiogenic activities, inhibiting the autophagic process with 3-methiladenine or silencing of ATG5 causes a decrease in these two processes [121, 122].

In ECs, autophagy appears to have a role in controlling the secretion of Von Willebrand factor (VWF). The release of VWF from ECs is hampered by inhibiting the autophagic process, achieved by silencing ATG5 or ATG7 [124] or administering chloroquine [123], demonstrating that autophagy has anti-thrombotic properties. Endothelial NO synthase (eNOS) phosphorylation was disrupted and NO production decreased in response to laminar shear stress in ECs lacking ATG3 [124] or when bafilomycin was administered pharmaceutically [125]. In contrast, activation of autophagic flux under sustained laminar shear stress led to an increase in eNOS expression and an improvement in vascular tone in ECs. In addition, the NO

homologue endothelin 1, a marker of endothelial dysfunction, is inhibited by autophagy [124] (**Figure 1.5**).

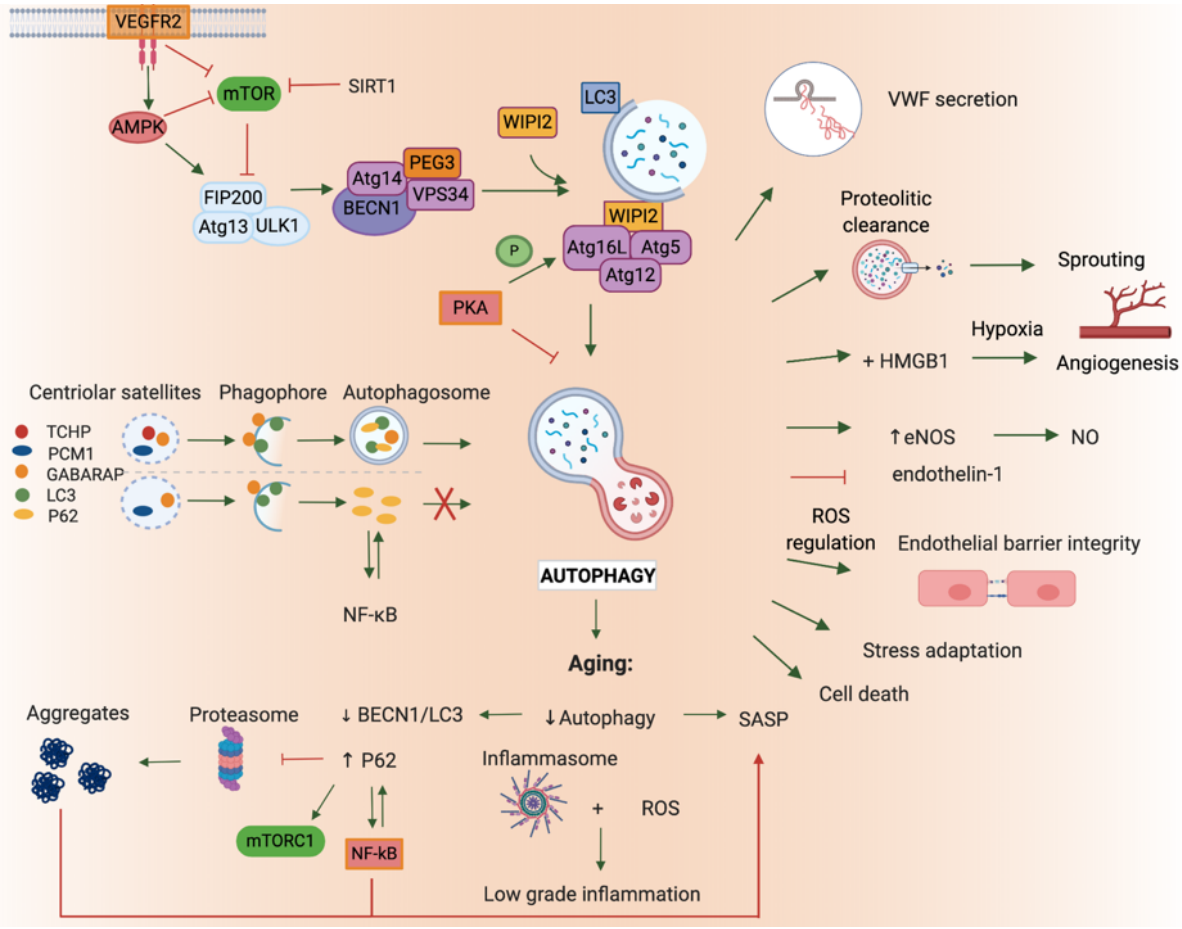


Figure 1.5| The interplay of autophagy with homeostasis, inflammation and senescence in ECs. From Mameli, E., Martello, A. & Caporali, A. (2022) Autophagy at the interface of endothelial cell homeostasis and vascular disease, *Febs j.* **289**, 2976-2991 [3].

Dysregulation of EC autophagy in vascular disease

Autophagic flux declines during ageing. The expression of autophagic markers is lower in ECs in aged mice compared to younger ones [126]. The decline of autophagy is associated with inflammation and endothelial senescence.

The decline of autophagic flux causes low-grade inflammation. Indeed, autophagy is important for the uptake of dysfunctional mitochondria that prevents excessive ROS production and the activation of inflammasomes. However, during ageing, the autophagic capacity declines and increased ROS production and aggregated proteins activate inflammasomes, leading to low-grade inflammation in several tissues. This

strengthens the inhibition of autophagy and accelerates the ageing process. Furthermore, the reduction in autophagy that occurs with ageing causes issues with cellular homeostasis function, activating nuclear factor (NF)-κB signalling and causing an age-related proinflammatory phenotype directly or through inflammasomes. Indeed, this mechanism could trigger the inflammatory danger sensor NLRP3 (NOD-, LRR- and pyrin domain-containing protein 3), and also NLRP1 in some tissues like the brain [127], and by this means stimulate inflammatory reactions in sensitive tissues [128]. Increased ROS interfere with NO functioning, affecting cerebral blood flow, platelet aggregation, endothelium apoptosis, preservation of endothelial progenitor cells, and anti-inflammatory properties.

Furthermore, peroxynitrite, the oxidative product of NO, causes severe cytotoxicity, leading to cellular death in cerebral vessels and other cell types, including neurons [129]. Mitochondrial-derived H_2O_2 activates NF-κB, leading to a pro-inflammatory shift in endothelial gene profiles [130]. In addition, oxidative stress damages the mitochondrial DNA [131]. An increase in pro-inflammatory cytokines such as IL-1β and IL-6 is associated with the senescence of endothelial cells.

Senescent EC accumulation may release senescence-associated secretory phenotype (SASP) inflammatory cytokines and impact nearby non-senescent cells, accelerating the onset and progression of vascular disease [3, 132].

The activation of NF-κB signalling is involved in inflammation and senescence. The interplay between P62, mTOR and NF-κB explains the connection between decreased autophagy and SASP transcription [133]. P62 activates NF-κB by inducing SASP synthesis through TRAF6 polyubiquitination [134]. Moreover, elevated P62 levels in autophagy-deficient cells prevent proteasomal degradation, resulting in the build-up of protein aggregates [3]. Finally, P62 can be a component of the mTORC1 complex and is required for mediating amino acid sensing to activate the mTOR pathway [135]. As a result, increased P62 expression may cause these pathways to become overactive and promote cellular senescence.

On the other hand, some studies demonstrated that senescence is not necessarily associated with an endothelial pro-inflammatory phenotype. Gamble et al. demonstrated the existence of a potentially anti-inflammatory senescent ECs population [136], induced by age-related stress [137] and by overexpression of the

vascular protective gene *ARHGAP18* [136]. According to the study, the anti-inflammatory senescent phenotype is mediated through caveolae and the consequent inhibition of NFκB pathway [137, 138]. It is important to consider the duality of senescence to both promote and limit inflammation.

Tissue remodelling factors like VEGF are released by some type of senescent ECs, for example in cancer, to drive tumorigenesis and tissue vascular remodelling effects [139]. Conversely, a recent study showed that counteracting the reduced VEGF signalling through a transgenic VEGF gain-of-function system or through adeno-associated virus (AAV)–assisted VEGF transduction provided protection from age-related capillary loss and increased healthy life span [140]. Depletion of senescence cells restores ageing-related changes but on the other hand is important to consider the role of senescence in the specific disease. Indeed, senescence can play a protective role, for example in tumour inhibition, tissue development and wound healing [138].

Inflammation components change with ageing. The age-related phenotype is associated with changes in blood-circulating molecules. A study by Yousef et al. demonstrated that factors in aged plasma caused the expression of VCAM-1 from EC in the brain, causing the tethering of leukocytes and inflammation [141]. The transfer of blood from young mice to old mice seemed to mitigate age-related phenotypes [142] [143]. Consequently, the change in ECs is due not only to cell-intrinsic properties but also to external factors.

The decline of autophagy leads to the accumulation of protein aggregates. In homeostatic conditions, insoluble aggregates tend to form aggresomes, that are transported via microtubules in the perinuclear region and here, the autophagic process clears them [144]. When the autophagy level is decreased, misfolded proteins accumulate in the cytoplasm, exacerbating cellular stress and inflammation [145]. In this context, the accumulation of the autophagic scaffold protein P62 due to the impairment of autophagy is associated with the inhibition of proteasome and protein translation. P62 activates eIF4E-binding protein (4E-BP) and p70 ribosomal S6 kinase 1 (S6K1), mTORC1 downstream effectors, that control protein translation [146]. Additionally, a shortage of nuclear factor erythroid 2–related factor 2 (Nrf2) and consequently increased Kelch-like ECH-associated protein 1 (Keap1) affected

P62, Atg12 and Atg7 levels in human ECs [147]. Consequently, the impairment of autophagic flux dysregulates protein translation and misfolded proteins clearance, in a loop that causes the accumulation of these aggregates. The link between protein aggregates and disease is well-established in neurological disorders. Still, recent literature demonstrates its role also in the pathogenesis of vascular diseases like atherosclerosis [148, 149] and diabetes [150, 151].

Impairment of autophagy is also associated with the formation of stress granules, biomolecular condensates constituted by translation factors, mRNAs, RNA-binding proteins (RBPs) and other proteins [152]. Stress granules assembling is elicited by cellular stress, which causes the phosphorylation of eIF2α, and reduces the availability of the eIF2α–GTP–tRNAiMet ternary complex that is required for translation initiation, thereby resulting in a blocked translation [153]. Circularised mRNA aggregates and binds RNA-binding proteins, such as TIA-1, TIAR, G3BP, CPEB1, and TTP, leading to the formation of stress granules [154]. Recent studies report that autophagy is involved in the clearance of stress granules and P bodies. Inhibiting autophagy through mutation or silencing Atg5 causes stress granule accumulation in baker's yeast. Buchan et al. defined this process targeting mRNP granules as granulophagy [155].

Furthermore, Seguin et al. demonstrated that inhibition of autophagy and the ubiquitin-selective chaperone valosin-containing protein (VCP) contributed to protein quality control, and impaired stress granules assembly and morphology [156]. Silva et al. reported that the mTOR-dependent inhibition of autophagy due to chronic stress was associated with the accumulation of RBPs, leading to the formation of stress granules and Tau aggregation in Tau transgenic mice. The same study also reported that the restoration of autophagy through mTOR pharmacological stimulation attenuated the accumulation of stress granules and Tau [157]. Collectively, autophagy contributes to the clearance of RBPs proteins involved in the formation of stress granules and stress granules themselves. The decline of autophagic flux due to disease or ageing leads to the accumulation of these aggregates, involved in cardiovascular [158] and neurodegenerative disease [159, 160] (**Figure 1.6**).

Dysfunctional autophagy affects vascular permeability and disrupts BBB. In ischaemia/reperfusion (I/R) injury, expression of histone deacetylase (HDAC) 9 increases, preventing autophagy, exacerbating inflammation and consequently affecting BBB integrity. Silencing of HDAC9 restored autophagy, leading to recovered expression of ZO-1, occludin and CLDN-5 [161]. Furthermore, autophagy restores decreased levels of ZO-1 and reduce ROS production and apoptosis in I/R injury [162]. Saha et al. showed that autophagy promotes a TJ barrier by increasing occludin through ERK 1/2 MAPK pathway [163]. Conversely, some studies reported a negative role for autophagy in ischaemia when autophagy would promote the degradation of CLDN-5 [164] and occludin in ECs formic BBB [165]. In this context, the silencing of Atg7 protects the brain against I/R injury during stroke and inhibition of autophagic flux in the diabetes mouse model would help recovery after brain ischaemia [3, 166]. Interestingly, studies *in vitro* and in zebrafish, reported that BBB disruption is associated with a redistribution of CLDN-5 in the cytosol through CAV-1. Therefore, autophagy has a protective action since it downregulated CAV-1 and cytoplasmic aggregated CLDN-5. Disruption of autophagic flux increases CLDN-5 aggregation and BBB impairment [167]. The exact mechanism through which autophagy regulates TJs and, consequently, BBB permeability is still not known. Still, several studies report autophagy inhibits CAV-1-mediated endocytosis and increases TJ expression in an ERK1/2 mitogen-activated protein kinase-dependent mechanism [168-170].

Finally, autophagy impairment is associated with increased inflammation and expression of MMP9. Knock-down of ATG5 increased the expression of MMP2 and MMP9 in endothelial progenitor cells, while treatment with autophagy activator rapamycin decreased the expression of MMP9. Furthermore, metformin treatment reduced MMP2 and MMP9 and increased autophagy via the AMPK/mTOR pathway [171]. Additionally, the activation of autophagy via high mobility group box-1 (HMGB1) and BECN1 by laminar shear stress inhibited inflammation in human aortic ECs (HAECs) [172].

Overall, modulation of autophagy represents a valuable target to reduce vascular and BBB impairment in cerebrovascular disease.

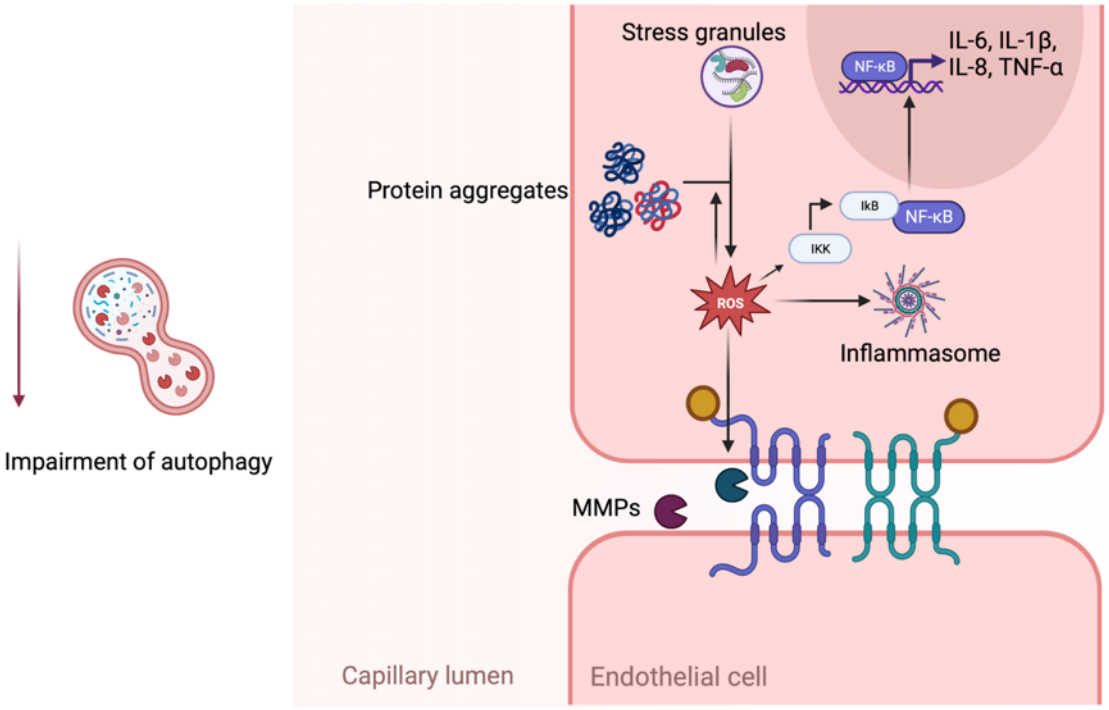


Figure 1.6| Dysregulation of EC autophagy in vascular disease.

Impairment of autophagy causes an accumulation of stress granules and protein aggregates, leading to ROS production and NF-kB and inflammasome activation. This causes a low-level inflammation and production of MMPs that damage endothelial junctions affecting the endothelial barrier. Created with BioRender.com.

Autophagy in cerebrovascular disease

Cerebrovascular disease

Cerebrovascular disease causes 15.4 thousand deaths per year in the UK, according to the last statistics data, and 160 thousand in the US, being the fifth cause of death worldwide [173]. These diseases include a range of conditions that affect blood flow in the brain, impairing the brain's function in a permanent or temporary way. Cerebrovascular disease includes conditions like stroke, transient ischaemic attack, aneurysm, vascular dementia, vascular malformations, and subarachnoid haemorrhage.

Among the cerebrovascular diseases, vascular dementia and ischemic stroke affect respectively 150,000 and 100,000 people per year in the UK [174]. Age-related cerebrovascular dysfunction plays a critical role in the pathogenesis of these diseases, but therapeutic development has been largely unsuccessful until now.

Vascular dementia

Vascular dementia represents the second most common type of dementia after Alzheimer's disease. Vascular dementia is caused by impairment in the blood supply to the brain and ischemic or haemorrhagic infarcts affecting multiple areas of the brain [175]. Symptoms include memory decline and neurological signs such as hemiparesis, bradykinesia, hyperreflexia, ataxia, verbal fluency and swallowing difficulties. In more affected patients dysarthria and aphasias may be present.

Three types of vascular dementia exist. Subcortical vascular dementia, multi-infarct dementia, and stroke-related dementia [176]. Subcortical vascular dementia is caused by small vessel disease. This condition affects arterioles, capillaries and small veins supplying the white matter and deep structures of the brain. The blood vessels change their morphology becoming stiff and twisted. The surrounding brain shows a lack of oxygen and nutrients. Multi-infarct dementia is caused by a series of mini-strokes and many regions are affected. The third type is stroke-related and it leads to the most serious damage. Risk factors for vascular dementia include age, hypertension, hypercholesterolemia, smoking, diabetes, cardiovascular and cerebrovascular disease.

Endothelial dysfunction has a pivotal role in small vessel disease and vascular dementia. This condition contributes to BBB damage, decrease in whole-brain or tissue-resting cerebral blood flow, loss of cerebral vasoreactivity, and increase in intracranial pulsatility [177]. The role of autophagy in vascular dementia is still unclear. Autophagy increased in several animal models of chronic cerebral hypoperfusion and in an oxygen-glucose deprivation model [178]. Another study demonstrated that chronic cerebral hypoperfusion upregulates autophagic flux through overexpression of beclin-1 and LC3-II/I and lysosomal dysfunction by decreasing the expression of LAMP1 [179]. Vascular dementia is also caused by

cerebral amyloid angiopathy, where the impaired autophagic process leads to amyloid plaque formation, impaired clearance of abnormal protein aggregates and collapse of blood vessels. A functioning autophagic flux prevents the deposition of abnormal proteins and clots, consequently keeping vascular homeostasis and preventing vascular dementia [180]. Chronic hypoperfusion leads to increased autophagy and loss of synaptic activity. Studies demonstrated that hypoperfusion is accompanied by increased hippocampal expression of the autophagic proteins LC3II/LC3I and that inhibition of autophagy by 3-Methiladenine restored synaptic remodelling and growth. On the contrary, rapamycin stimulation caused the loss in Synaptophysin and Postsynaptic density protein-95, two proteins that regulate synaptic functions, aggravating vascular dementia-induced changes in the synaptic and hippocampal plasticity [181, 182].

On the other hand, some studies present a protective role performed by autophagy in vascular dementia. Chronic cerebral hypoperfusion leads to mitochondrial loss and oxidative stress production, causing astrocyte and neuronal death. At the same time, reactive oxidative species inhibit mTOR and stimulate autophagy [183]. Autophagy plays a protective role in ischemic preconditioning. Overexpression of Heat shock protein B8 promoted autophagic flux and prevented the degradation of occluding and Cldn-5 in a rat middle cerebral artery occlusion/reperfusion model [184]. In the same way, 3-Methiladenine decreased the expression of LC3 and beclin-1 and increased the average value of brain oedema and BBB dysfunction and aggravated neurological deficits in a subarachnoid haemorrhage model of vascular dementia [185].

Autophagy can be considered a double-edged sword in the pathogenesis of vascular dementia. In the early stages of hypoperfusion, oxygen/glucose deficiency can trigger autophagy by activating AMPK and PI3K. At this stage, autophagy provides amino acids and energy. After a long period of ischemia, the ongoing activation of autophagy will cause apoptosis [178].

Cerebral ischemia and stroke

Cerebral ischemia is a mechanism of acute brain injury caused by impaired blood flow to the brain. If not treated it can cause cerebral infarctions or global hypoxic-ischemic encephalopathy. Cerebral ischaemia is also the leading cause of stroke (87% of all the strokes). Cerebral ischemia can be global or focal. Global is caused by systemic hypotension. It can be transient or prolonged, bringing in this last case to permanent neurological injury. Transient cerebral hypoperfusion can occur when autonomic and neurohormonal mechanisms that control blood pressure and heart rate are disrupted. Focal brain ischemia is caused by an obstruction of arterial blood flow to the brain, often as a result of thrombosis or embolism. If the ischemia persists long enough, irreversible neuronal loss occurs, resulting in an ischemic stroke [186].

Risk factors include heart conditions like atrial fibrillation, diabetes, obesity, hypertension, hyperlipidaemia and atherosclerosis, and sickle cell disease. Behavioural risk factors include smoking, excessive alcohol intake, and poor sleep.

The exact role of autophagy in ischemic stroke is not clear yet. On one hand, autophagy may contribute to endothelial damage and destruction of the BBB. Autophagy-lysosomal pathway activation following oxygen-glucose deprivation/reoxygenation promotes degradation of the TJs cldn-5 [187] and occludin [188]. On the other hand, during the reperfusion stage, upregulation of autophagy by microRNA-200c-3p has a protective action on ECs [189]. Conversely, the inhibition of autophagy protected brain ECs from oxygen-glucose deprivation/reoxygenation damage [190]. The activation of autophagy by Cav-1 leads to the degradation of ZO-1 in early reperfusion [191]. Li et al. found that EC autophagy has a beneficial effect on BBB integrity during I/R injury, showing that autophagy activation decreases ECs apoptosis, restores impaired levels of ZO-1 and ROS production induced by oxygen-glucose deprivation/reoxygenation [192]. Overall, autophagy represents an interesting target to regulate ischemic injury.

Trichoplein

Identification and function

TCHP, also called mitostatin, is a cytosolic 62 kDa protein. It was identified for the first time in 2005 as a keratin 8/18-binding protein in yeast [1]. The gene's open reading frame encodes for a 489 amino acids protein. The human TCHP presented a sequence similarity of 23% and 31% with human trichohyalin and mouse plectin, respectively (**Figure 1.8A**). Both these proteins were reported to link keratin intermediate filaments [193] and attach intermediate filaments to F-actin, in the case of plectin [194].

Vecchione et al. described TCHP as a tumour suppressor protein located on chromosome 12q24. Homozygous deletions and mutations of the TCHP gene were found in 5 to 11% of solid tumours, and its expression was found downregulated in bladder and breast tumours [195]. The same paper reported that the highest RNA expression was in the heart, skeletal muscle, kidney and liver. Moreover, a transcript of 5.5 kb was identified in the heart and skeletal muscle. Of note, mitostatin was localised in the mitochondria [195].

TCHP and regulation of mitochondria

Vecchione et al. localised TCHP on the outer membrane of mitochondria. Overexpression of TCHP was associated with changes in the mitochondrial network, fragmentation and perinuclear clustering [195]. In support of this, another study reported that TCHP localises at the interface between mitochondria and endoplasmic reticulum (ER) and controls the tethering between these two organelles in a mitofusin-2-dependent manner [196].

TCHP was associated with mitophagy in breast cancer, where decorin evoked TCHP would be stabilised by peroxisome proliferator-activated receptor γ coactivator- 1α (PGC-1α) and regulate mitophagy and angiostasis. The depletion of Tchp blocked mitophagy and increased VEGFA production [197]. In line with this, treating HUVECs and human aortic endothelial cells (HAECs) with the glycoprotein endorepellin evoked TCHP and Parkin induction downstream of vascular endothelial growth factor receptor 2 (VEGFR2), evoking pro-autophagic and mitophagy transcriptome [198].

Silvander et al. reported that keratins regulate cell mitochondria structure and function through mitofusin-2 and TCHP interactions in pancreatic cells. Losing keratin 8/18 would lead to irregular insulin vesicles and decreased insulin secretion. The decrease of keratins would be associated with mitochondria fragmentation and reduced cytochrome C, reduction of ATP and insulin, and decreased levels of mitofusin-2 and TCHP [199].

TCHP and regulation of cytoskeleton and cilium

TCHP was reported to have a role in correctly localising centrosomal proteins. Ibi et al. showed that TCHP localises in the subdistal zone of centrioles, where it binds the centrosomal proteins Odf2 and Ninein, controlling Ninein recruitment to the centrosome. Its deletion impaired microtubules anchoring at the centrosome in epithelial and non-epithelial cells [200]. Another study by Inagaki et al. confirmed the localisation of TCHP in centrioles in proliferating cells. TCHP binds the kinase Aurora A, regulating its activation, in centrioles in the G1 phase, suggesting it is required for G1 progression and suppressing primary cilia assembly. TCHP would indeed disappear in quiescent cells when primary cilia are present [201]. Additionally, the ubiquitin-proteasome machine would cause Aurora-A inactivation, removing trichoplein from mother centrioles and leading to axoneme extension in the ciliogenesis [202]. Epidermal growth factor receptor (EGFR) activated TCHP-Aurora A pathway via the deubiquitinase USP8 and suppressed ciliogenesis in retinal pigment epithelial-1 (RPE1) cells [203].

Previous studies in the lab confirmed the localisation of TCHP in the centriolar satellites of ECs, where it binds and stabilises PCM1 [2].

A recent study highlighted the importance of TCHP in promoting cell cycle progression in the G1/S phase by disassembling cilia. Deletion of TCHP causes entrance in the G0 phase, which could not be restored stopping the formation of the cilia [204]. In line with this, silencing of TCHP was linked with decreased levels of mitotic arrest deficient 2 (MAD2) and Cyclin B1, impairing mitotic progression and leading to DNA damage and chromosomal instability [205]. Additionally, the depletion of TCHP caused telomere dysfunction in HCT116 cells [206].

The role of TCHP in regulating ciliogenesis affects adipogenesis in mesenchymal progenitors and TCHP knock-out mouse model. Mesenchymal progenitors depleted of TCHP present long cilia and fail to differentiate in adipocytes. Furthermore, insulin-Akt signalling is inhibited because the elongated cilia prevent CAV-1 and GM3-positive lipid rafts from assembling at the cilium base where insulin receptors are located. This translates into body fat and smaller adipocytes in the Tchp knock-out mouse [207]. Finally, a recent study reported the involvement of TCHP in skeletal muscle regeneration. Downregulation of TCHP is involved in the elongation of primary cilia in fibro/adipogenic progenitors, promoting muscle regeneration and inhibiting adipogenesis via cilia-mediated insulin/Akt [208].

Overall, this evidence demonstrates the fundamental role of TCHP in the cytoskeleton as a regulator of centrosomal proteins and of the cilia, fundamental in keeping the morphology of the cells and also regulating the division and cell cycle progression.

TCHP and regulation of autophagy in ECs

Previously, in the lab, microRNA-503 (miR-503) was identified as a driver behind diabetes-induced impairment of the post-ischaemic reparative neovascularization [209, 210]. Following the identification of the miR-503 targets, TCHP was identified as a novel regulator of EC function.

My team has recently demonstrated that the depletion of TCHP in ECs impaired EC function by reducing autophagic flux, thus inducing premature cellular senescence [2]. Our data showed for the first time that TCHP is fundamental for autophagosome formation because it impacts the stability of PCM1 (centriolar satellite protein whose turnover is regulated by proteolytic degradation) and consequently of its binder GABARAP [211]. As previously reviewed, GABARAP is critical in the closure of the phagophore membrane and the fusion of autophagosomes with lysosomes. Therefore, TCHP downregulation impairs basal autophagy leading to the accumulation of unresolved autophagosomes, accumulation of P62 and unfolded protein aggregates (**Figure 1.7**). In addition, observed P62 accumulation in the cardiomyocytes and the vasculature of Tchp knock-out mice were described to impair autophagic flux.

Of note, TCHP knock-down was associated with activation of NF-κB signalling and treatment with the NF-κB inhibitor BAY11-7082 reduced P62 accumulation and mRNA levels of pro-inflammatory cytokines IL-8, IL-6 and IL-1B. Using ECs obtained from the vessel wall of patients with endothelial dysfunction and premature coronary artery disease (CAD), low levels of TCHP and high levels of P62 were detected and activation of the SASP gene signature. Treating ECs from patients with Torin-1 (mTOR inhibitor that restores autophagy) reduced the accumulation of P62 and aggregates [2].

Protein aggregates were also accumulated in the vessels and myocytes of limb muscles from Tchp knock-out mice (global knock-out). Furthermore, the team found that endothelial-specific disruption of Tchp gene expression in endothelial-specific Tchp knock-out mice *(*$Tchp^{EC}$) decreased blood flow recovery following hind-limb ischaemia.

Gene-level phenotypic associations studies associated TCHP with hypertension (p=5.21e-8), systolic and diastolic blood pressure (p=8.78e-13, p=3.84e-8), triglycerides (p=2.93e-6), cardiovascular disease (odds ratio=1.4623) [212]. Moreover, TCHP was inserted among potential effectors genes associated with stroke and stroke subtypes by a multi-ancestry genome-wide association study (GWAS) [213]. Additionally, phenome-wide association studies linked a missense mutation on TCHP (rs10774978) with vascular and heart problems (P= 6.24e-06) [214, 215] and CAD [216].

Therefore, because of TCHP's involvement in EC homeostasis, its role in autophagy regulation, and its association with hypertension and vascular and cerebrovascular disease, the goal of the following thesis is to investigate the role of TCHP in brain ECs.

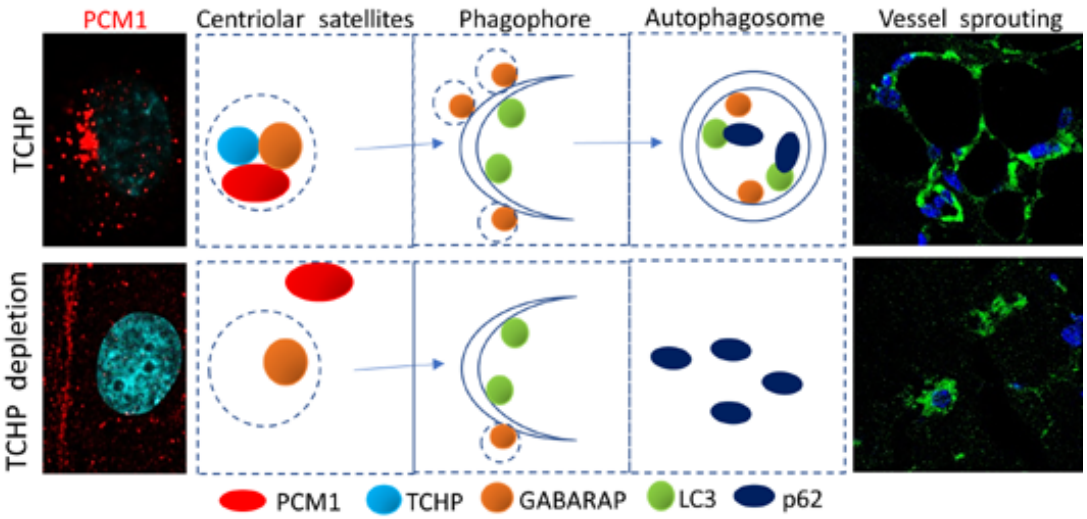


Figure 1.7| TCHP regulates EC homeostasis by stabilizing PCM1.

TCHP regulates the localisation of PCM1, stabilizing its link with the autophagic protein GABARAP and allowing autophagic flux in ECs. Depletion of TCHP affects vessel sprouting. From [2].

The endothelial-specific Tchp knock-out mice $Tchp^{EC}$ was generated by the Wellcome Trust Sanger Institute. $Tchp^{EC}$ mouse was created by breeding Tchp floxed mice with mice carrying the Cre recombinase under the VE-cadherin promoter (Cdh5-Cre). $Tchp^{tm1a(EUCOMM)Wtsi}$ endothelial-specific mouse originated from the original strain C57BL/6N-A^{tm1Brd} by inserting the L1L2_Bact_P cassette at position 114852212 of chromosome 5. The cassette comprises an FRT site, a lacZ sequence and a loxP site. The loxP site is followed by a neomycin resistance gene under the control of the human beta-actin promoter, SV40 polyA, another FRT site and a second loxP site [217]. Finally, a last loxP site is inserted downstream of the targeted exon. The critical exon is then cut by loxP sites [217]. A conditional ready allele is created by flp recombinase. Following cre expression generates $Tchp^{EC}$ mice (**Figure 1.8B**).

The international mouse phenotyping consortium (IMPC) characterised $Tchp^{tm1a(EUCOMM)Wtsi}$ mouse. The mouse presents increased circulating cholesterol

level (p=5.61x10e-15), increased circulating HDL and LDL cholesterol levels (2.16x10e-10; 7.35x10e-11) and abnormal incisor morphology (p=5.55x10e-5) [218] (**Figure 1.8C**).

Previous studies in the lab demonstrated reduced cardiac vascularisation and impairment of autophagic flux, highlighted by the accumulation of P62 in the cardiomyocytes and vessels of Tchp knock-out mice. Moreover, increased P62 was also observed in the liver and pancreas, suggesting autophagy impairment in other tissues [2]. Unpublished data in the lab showed that the $Tchp^{EC}$ mouse had decreased blood flow recovery following hind-limb ischaemia, confirming the endothelial dysfunction observed in the global knock-out mouse model (**Figure 1.8D**).

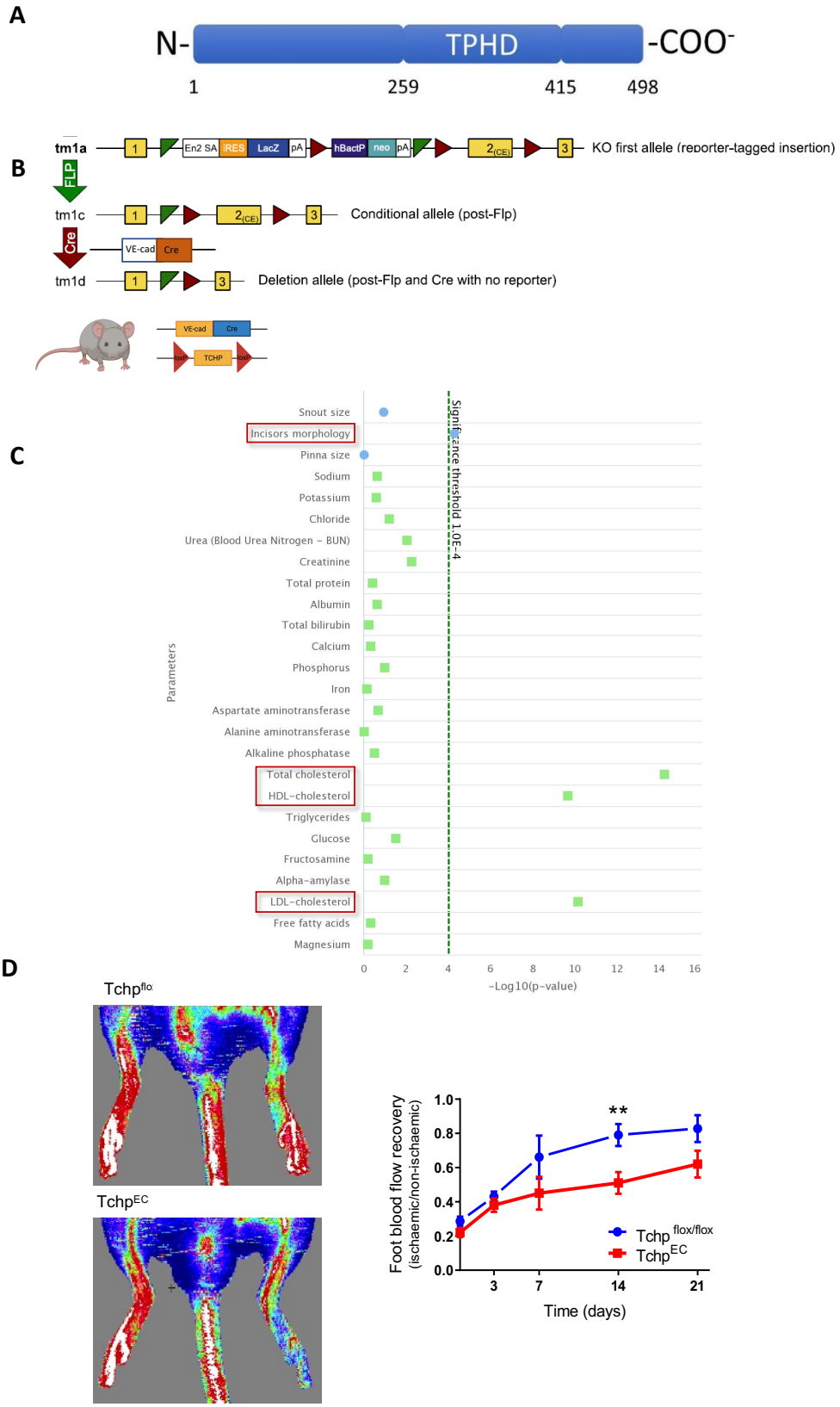


Figure 1.8| TCHP^{EC} mouse model.

A. TCHP was identified as a 498aminoacids keratin binding protein in epithelial cell. TPHD indicates the trichohyalin/plectin homology domain [1] **B.** Mutation details of Tchp^{EC} mouse. **C.** Phenotypic characterisation of Tchp^{EC} mouse by IMPC. The significant threshold is 1.0E-4. **D.** Foot blood flow recovery in Tchp$^{flox/flox}$ and Tchp^{EC} mice after hind-limb ischaemia. (n=5 per group; unpaired t test **p<0.01).

Hypothesis and aims

Age-related cerebrovascular dysfunction plays a critical role in the pathogenesis of cerebrovascular disease, but therapeutic development has been largely unsuccessful until now. ECs are an essential part of the NVU, and it has been demonstrated that their dysfunction occurs early in the pathophysiology of cerebrovascular disease. This dysfunction results in altered cerebral blood flow and disruption of the BBB. In this context, identifying novel genes associated with endothelial dysfunction will help understand the role of ECs in BBB integrity and address new therapeutic targets.

TCHP knock-down has been previously associated with endothelial dysfunction, senescence and altered blood flow in peripheral vascular beds. Additionally, TCHP has been demonstrated to stabilise autophagy in ECs, a process not yet clarified in the ECs of the BBB. However, its role in the microvascular brain ECs has not been studied yet.

Therefore, the hypothesis addressed in this PhD thesis is:

"*TCHP contributes to EC homeostasis in the brain vasculature. Therefore, its downregulation affects EC function and consequently BBB integrity*".

The aims of this project are:

- The characterisation of the role of TCHP *in vitro* in ECs isolated from $Tchp^{EC}$ mice and in human brain microvascular ECs.
- The characterisation of the role of TCHP *in vivo* in the endothelium of $Tchp^{EC}$ mice, focussing on vessel permeability, vessel network and neuroinflammation.
- To assess the role of TCHP in autophagy regulation in brain ECs from $Tchp^{EC}$ mice and human brain microvascular ECs and, finally, the screening of compounds that can restore impaired autophagic flux.

Chapter 2

Materials and Methods

Chapter 2 Materials and Methods

Mouse model

Animal experiments were performed following the Animals (Scientific Procedures) Act (UK) 1986 and under the auspices of the UK Home Office Project. $Tchp^{tm1a(EUCOMM)Wtsi}$ endothelial-specific mouse was generated by the Wellcome Trust Sanger Institute (Hinxton, United Kingdom).

$Tchp^{tm1a(EUCOMM)Wtsi}$ endothelial-specific mouse originated from the original strain C57BL/6N-A^{tm1Brd} by inserting the L1L2_Bact_P cassette at position 114852212 of chromosome 5. The cassette comprises an FRT site, a lacZ sequence and a loxP site. The loxP site is followed by a neomycin resistance gene under the control of the human beta-actin promoter, SV40 polyA, another FRT site and a second loxP site. Finally, a last loxP site is inserted downstream of the targeted exon at position 114855904. The critical exon is then cut by loxP sites. A conditional ready allele is created by flp recombinase. Following cre expression generates $Tchp^{EC}$ mice. $Tchp^{EC}$ mice are cre heterozygous.

Homozygous loxP , hemizygous Cre are crossed with homozygous loxP , noncarrier. The breeding generates experimental and control mice in a 1:1 ratio, following Mendelian inheritance. The male and female ratio is 1:1. Four breeding pairs of [Cdh5-cre x Tchp flox/flox = $Tchp^{EC}$] homozygous parents are required to generate a cohort of 14 homozygous mutant animals for the experiments. $Tchp^{EC}$ mice have an average litter size of 7, and 90% of mating is productive.

Male and female eight (young mice) to twenty-four (adult mice) weeks old were used for the study. Both genders were used as we did not detect differences in the phenotype.

Genotyping

Genomic DNA was isolated from the ears notch; tissue was treated with a first solution containing 25 mM NaOH, 0.2 mM EDTA, and dH_2O, digested for 45 minutes at 95°C and treated with 40 mM Tris and dH_2O. Next, DNA fragments were amplified

with Polymerase Chain Reaction (PCR) using GoTaq Hot Start Green Master mix (Promega corporation, Madison, USA).

Two PCRs were used for genotyping, one to detect VE-Cre and the second to detect Tchp floxed allele. For VE-Cre detection, after a primary denaturation at 94°C for 5 minutes, followed by 30 cycles (denaturation at 94° C for 15 seconds; annealing at 58° C for 15 seconds; elongation at 72°C for 5 seconds), the last step consisted in a final elongation at 72°C for 5 minutes. To detect Tchp floxed allele, after a primary denaturation at 94°C for 5 minutes, followed by 34 cycles (denaturation at 94° C for 30 seconds; annealing at 58° C for 30 seconds; elongation at 72°C for 45 seconds), last step consisted in a final elongation at 72°C for 5 minutes. Genotyping to confirm the expression of the transgene was performed using the following primers:

	PRIMER	SEQUENCE (5'>3')
TCHP	TCHP_111280_F	TAGGGACCCCCTCACTTTCC
	TCHP_111280_R	CCAATTCCTCCTCCAAGTGC
	CAS_R1_TERM	TCGTGGTATCGTTATGCGCC
VE-CRE	Cre-R107	GCCTGGCGATCCCTGAACATG
	VECP-F-219	CCCAGGCTGACCAAGCTGAG

Table 2.1| List of primers used to genotype Tchp^{EC} and WT mice.

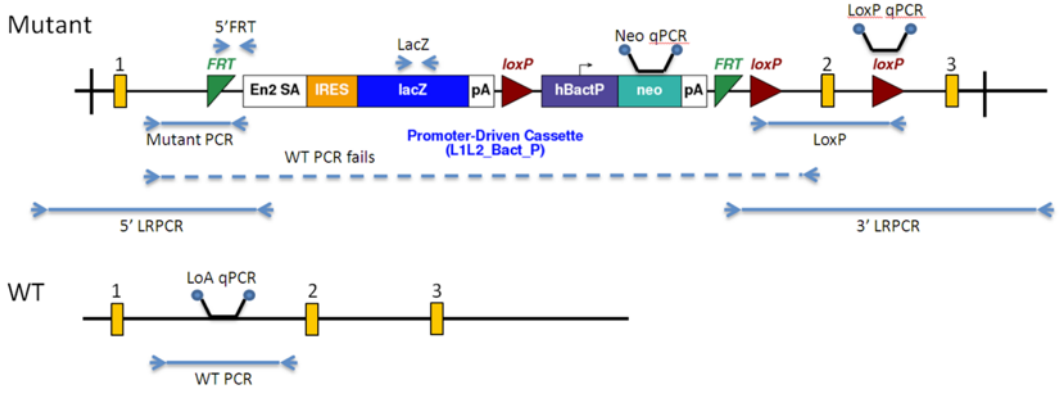


Figure 2.1|Regions targeted by the primers listed above in Tchp^{EC} and WT mice.

The resulting band sizes are 348 bp for Tchp^{EC} mice, 475 bp for wildtype (WT) mice, two bands of 348 bp and 475 bp for heterozygous mice. Mice that underwent the recombination with Cre presented a band at 350 bp.

Cell culture methods and reagents

Human Brain Microvascular ECs (HBMVECs) (ScienCell, Carlsbad, USA), HBEC-5i (ATCC-check, Manassas, USA) and ECs isolated from the brain of Tchp^{EC} and WT mice were grown in complete endothelial cell growth medium (EGM) MV2 (Promocell, Heidelberg, Germany), supplemented with 5% foetal calf serum (FCS). HUVECs (Lonza, Basel, Switzerland) were grown in complete endothelial basal medium 2 (Promocell, Heidelberg, Germany) and 2% FCS. Cells were kept in an incubator at 37°C and 5% CO2. HBMVECs, HBEC-5i and HUVECs were used between P2 and P6 passages.

Transfection of HBMVECs and HBEC-5i and transduction of HUVECs

HBMVECs and HBEC-5i were plated at a confluence of 30-50% in a 24-well plate or 6-well plate. Twenty-four hours later, they were transfected using lipofectamine RNAiMAX (Invitrogen, Waltham, USA) and Opti-MEM medium (Gibco, Waltham, USA) with siRNA targeting TCHP (SMARTpool: ON-TARGETplus TCHP siRNA - Dharmacon) or anti-miR negative control (Ambion, Waltham, USA) at a final concentration of 20nM, according to the manufacturer's instructions. 12 hours after the transfection, the medium was replaced with a fresh EGM-MV2 5% FCS medium.
Before transduction with lentivirus, HUVECs were plated at a confluence of 30-50% in a 6-well plate. They were then transduced at 20 MOI. Cells were incubated with the viral supernatant for 12 hours; then the medium was replaced with fresh 2% FCS medium. The pLKO DNA plasmid containing the shRNA sequence against human TCHP, was purchased from Sigma Aldrich (Mission®RNAi TRCN0000127662). The scrambled sequence shRNA plasmid was purchased from Addgene (plasmid #1864). Lentiviral vectors were produced by the Biomolecular Core of the Shared University Research Facilities at Edinburgh University. The packing plasmids used were pCMV-dR8.2 dvpr, plasmid #8455 from Addgene, and pCMV-VSVG, plasmid #8454 from Addgene respectively. TCHP-V5 (HsCD00444989) and empty vector (pLX304) are

from DNASU plasmid collection, and pBABEpuro GFP-LC3 from Addgene (plasmid #22405). Transduction was performed by Dr Andrea Caporali (University of Edinburgh).

Isolation and culture of brain microvascular ECs from adult mice

ECs from Tchp^{EC} mice were isolated employing a modified version of a pre-existing protocol [219]. After collecting the cerebrum from the skull of eight/twelve weeks old mice, cerebellum, olfactory bulb and meninges were removed. The tissue was then digested with collagenase/dispase for 1 hour 15 minutes at 37 º C and homogenised using a tissue grinder. Next, the homogenate was centrifuged at 800 g at 4 º C for 5 minutes and the resulting pellet was suspended in 18% dextran solution. After density centrifugation, cells were resuspended in Hanks' Balanced Salt Solution (HBSS) 1x and centrifuged at 500 x g for 5 min before being cultivated in pre-coated wells (10 μg/ml fibronectin, 0.2% gelatine). Outgrowing ECs were then selected by puromycin (8 μg/ml) (Thermo Fisher, Waltham, USA) treatment for 48 hours and grown to confluence within one week.

When ECs were sorted with the MACS® separator (Miltenyi Biotec, Bergisch Gladbach, Germany), after myelin removal, pellet was resuspended in wash buffer (0.5% (w/v) BSA, 2 mM EDTA in PBS) and 10 μl of CD31 MicroBeads (Miltenyi Biotec, Bergisch Gladbach, Germany) were added to the suspension. After incubation for 20 min at 4°C, cells were washed by adding 3 mL of wash buffer and centrifuged at 300 g for 5 min at 4°C. Supernatant was removed and pellet resuspended in 0.5 mL of wash buffer. Cell suspension was applied into MS column (Miltenyi Biotec, Bergisch Gladbach, Germany) through a 40 μm cell strainer. MS columns were washed 3 times with 0.5 mL wash buffer and finally, the MS columns were placed into 15 mL falcons and the fraction containing the magnetically labelled cells (CD31 - positive fraction) was flushed out by firmly applying the plunger supplied with the column.

Impedance-based scratch assay and barrier function assays

Migration and endothelial barrier function were measured using ECIS® using 8W1E and 8W10E+ array (Applied BioPhysics, North Greenbush, USA), respectively. 60,000 cells were grown on the arrays on top of gold electrodes for 24 hours. In the case of

ECs isolated from Tchp^{EC} and WT brains, 150,000 cells were plated on the array, selected by puromycin as previously described and grown for 7/10 days. Then, a constant small alternating current was applied at the bottom of the array (I) and the potential across (V) the electrodes was measured. Impedance (Z) was calculated as Ohm's law Z=V/I. For the migration assay, a wound in the cellular monolayer was generated by applying a 3-mA voltage pulse for 20 seconds and recovery of the layer was monitored by measuring resistance at 4000 Hz. Speed was determined as the time the cells re-establish the monolayer. For measuring barrier function, the cell monolayer was stimulated with thrombin (1 U/ml) (Sigma Aldrich, St.Louis, USA) or lipopolysaccharide (LPS) (1 nM) (Sigma Aldrich, St.Louis, USA) and impedance was recorded for 24 hours.

Protein Mass Spectrometry

Confluent HUVECs grown in T75 were harvested using a sodium dodecyl sulfate (SDS) lysis buffer (4% SDS, 150 mM NaCl, 50 mM Tris pH 7.5). Samples were vortexed, homogenised with a 21G needle, boiled for 5 minutes, and spun in a microcentrifuge at 17,000 g for 15 min at room temperature. The supernatant was retained as the soluble fraction. The pellet was washed with another volume of lysis buffer and spun at 17,000 g for 10 min. The washed pellet was resuspended in a volume equivalent to the supernatant of urea buffer (8M Urea, 1% SDS, Tris-HCl pH 8.0, 10mM DTT) and boiled with occasional vortexing until the solution was wholly clarified in all samples. The samples were then subjected to label-free quantification mass spectrometry, performed by the Mass Spectrometry Facility Core facility of the University of Edinburgh. Insoluble samples were cleared of detergents, reduced, alkylated and digested as reported [220]. The resulting peptide samples were separated on a Nanoflow Ultimate 3000 LC (Thermo Fisher, Waltham, USA) coupled online to a Q-Exactive plus mass spectrometer (Thermo Fisher, Waltham, USA). The raw mass spectrometric data files from LC-MS/MS were analysed using MaxQuant (Version 1.5.7.4).

Phenotypic screening assay

Image acquisition

A wide-field Imagexpress Micro XL high-content microscope (Molecular Devices, San Jose, USA) was used to image the plates. DAPI and Cy3 filter sets were used to visualise nuclei from 4 campuses within the well containing up to 200 cells per field of view using a 20× S Plan Fluor objective. The screening was performed by Edinburgh Phenotypic Assay Centre [EPAC], in collaboration with Dr Andrea Martello (University College London).

Image analysis

Images were analysed using MetaXpress Custom Module Editor (Molecular Devices, San Jose, USA) as previously published [2]. Background from P62 images was removed using a top hat filter (size = 10 pixels, shape = circle). Nuclei were first identified in the DAPI image using a user-defined intensity above the local threshold method and maximum (30 µm) and minimum (10 µm) widths. P62 puncta were then detected by using a user-defined intensity above background and maximum (1 µm) and minimum (0.5 µm) widths. Finally, a pseudo-whole cell was created by growing the mask by 50 pixels. The nuclear region was then subtracted from the whole-cell mask and the number of P62 puncta in cytoplasmic and nuclear regions was counted per cell.

Data analysis

Analysis was performed using Spotfire High Content Analyser software (PerkinElmer, Waltham, USA). Whole well averages were normalised to the negative controls by dividing all values on the plate by the median value for the negative control. Values were ranked between 0 and infinity, considering 1 as the median of the negative controls on that plate. For hit identification, control cells (no shRNA) were used as positive controls. An ensemble-based tree classifier was used to identify hit compounds with a cross-validated fivefold CV misclassification error of 0.4%. The following features were used: Cell Count; Nuclear Granules Nuclear Count Sum; Cytoplasmic Granules Nuclear Count Sum.

In vitro treatment

Subconfluent HUVECs or HBMVECs were treated with Guanabenz acetate (5 μM), Milrinone (5 μM), Calpain Inhibitor II (APExBIO, Houston, USA) (5 μM), or BAY11-7082 (0.3 μM) for 24 hours and then fixed with 4% paraformaldehyde and the supernatant collected for following analyses.

RNA extraction and quantitative real-time analysis

Total RNA was extracted using Qiazol reagent and RNeasy Mini Kit (Qiagen, Hilden, Germany), following the manufacturer's protocol. RNA quantification and quality control were conducted using Nanodrop Spectrometer (Nano-Drop Technologies, Wilmington, DE). RNA samples were stored at -80°C.

For gene expression analysis, cDNA was produced from total RNA (100-200 ng per reaction) using the QuantiTect Reverse Transcription Kit (Qiagen, Hilden, Germany) according to the manufacturer's instructions. Reverse transcription was performed in thermal cycler with the following steps: 2 minutes at 42°C, 5 minutes at 4°C, 30 minutes at 42°C, and 3 minutes at 95°C.

Real-time quantitative polymerase chain reaction (qPCR) was performed using Power SYBR Green dye (Applied Biosystem, Waltham, USA) in QuantStudio-5 (Applied Biosystem, Waltham, USA), with the following cycles: 2 minutes at 50 °C, 10 minutes at 95°C, 40 cycles of denaturation for 15 sec at 95°C, 1 min at 60°C. Each reaction was performed in duplicate. Quantification was performed by the $2^{-\Delta\Delta Ct}$method [221] normalising the Ct of the gene of interest to the Ct of the relative housekeeping gene (18s). The statistical analysis was performed considering the $2^{-\Delta Ct}$ of each condition. Sybr Green primers are listed in Table 2.2.

Gene	Forward	Reverse
hTCHP	CAGCCGTTACTTCAGGATGTC	GCTGCTCCCGGATTCTTCTTT
mTCHP	TGCACGCCTACCATTGTGAG	GTCGTTCAGCAATCAGCTTCC
18S	CCGAGGGCCTATCATCAACC	CCCCAGTAAAGTGCGGGTCATAA

hCCL5	CTGCTTTGCCTACATTGCCC	TCGGGTGACAAAGACGACTG
mCCL5	GCTGCTTTGCCTACCTCTCC	TCGAGTGACAAACACGACTGC
hCCL3	AGTTCTCTGCATCACTTGCTG	CGGCTTCGCTTGGTTAGGAA
mCCL3	TTCTCTGTACCATGACACTCTGC	CGTGGAATCTTCCGGCTGTAG
hCD36	AAGCCAGGTATTGCAGTTCTTT	GCATTTGCTGATGTCTAGCACA
mCD36	ATGGGCTGTGATCGGAACTG	GTCTTCCCAATAAGCATGTCTCC
hS100A4	GATGAGCAACTTGGACAGCAA	CTGGGCTGCTTATCTGGGAAG
mS100A4	TCCACAAATACTCAGGCAAAGAG	GCAGCTCCCTGGTCAGTAG
hSPP1	CTCCATTGACTCGAACGACTC	CAGGTCTGCGAAACTTCTTAGAT
mSPP1	AGCAAGAAACTCTTCCAAGCAA	GTGAGATTCGTCAGATTCATCCG
mHMGB2	TCCTGGTAGGCCAACAGGCT	AGCTAATGTTGAGCTGCACTTG
MABCB1A	AGGACAAAAGAAGGAACTTG	GATAAGGAGAAAAGCTGCAC
hGUCY1A1	TCAGCCCTACTTGTTGTACTCC	CAGAATAGCGATGTGGGAATCAC
hFGF2	GGAGTGTGTGCTAACCGTTACCTG	CTGCCCAGGTCCTGTTTTGG
mGucy1a1	CCCCTGGTCAGGTTCCTAAG	GGAGACTCCCTTCTGCATTCT
mGucy1a2	CCTTGCCTCAGACGATACACA	GCAGTCCGAGTACATTAGCAGT
mGucy1b1	TGCTGGTGATCCGCAATTATG	GGTTGAGGACTTTGCTTGCAG
mFgf2	GCGACCCACACGTCAAACTA	TCCCTTGATAGACACAACTCCTC
mPdgfb	CATCCGCTCCTTTGATGATCTT	GCGCTCGGGTCATGTTCAAGT
hMFSD2A	ATAGCTCTACAGTAGCTTCAC	TAGATACAGACAATGACCCC

Table 2.2| List of mouse and human Sybr green primers used to assess gene expression in ECs isolated from Tchp^{EC} and WT mice and HBMVECs.

RNA-sequencing analysis

Bulk RNA sequencing (RNA-seq) was performed by Beijing Genomics Institute (BGI, Beijing, China) on RNA extracted from ECs isolated from WT and Tchp^{EC} mice (n=3). Total RNA was assessed for quantity (Invitrogen Qubit) before library preparation. PolyA-enriched strand-specific RNA libraries were prepared by Beijing Genomics Institute and libraries were sequenced with DNBSEQ™ Sequencing Technology at an average of 30 million reads per sample (paired-end 2 x 150bp). The differential

expression was assessed using DESeq2 by comparing Tchp^{EC} with WT cells, performed as described in [222]. Analysis was performed using Dr Tom (https://www.bgi.com/global/service/dr-tom). Parametric gene set analysis was performed using iDEP96 (http://ge-lab.org/idep/); network analysis using GeneMania (https://genemania.org).

Gelatine zymography

Polyacrylamide gel (1 mm thickness) was prepared as follows. The running gel was made by mixing 2.8mL 1.5M Tris buffer, pH 8.8, 2mL 6mg/mL gelatine aqueous solution, 3.75mL 30% Acrylamide 29:1, 110uL 10% SDS, 50uL APS, 15uL TEMED. For stacking gel 2.9 mL ddH_2O, 1.25 mL 0.5M Tris buffer, pH 6.8, 0.834 mL 30% Acrylamide 29:1, 50 uL 10% SDS, 25 uL APS, 10 uL TEMED were added. 25 µl of samples (20 µl of cell supernatant and 5 µl of 5X loading dye) were charged into the gel and electrophoresis ran at 90 A for 1 hour and 45 minutes. After three washes with 2.5% TritonX100 to remove SDS residuals, the gel was placed into incubation buffer (1M TRIS pH 7.5, 10 mM CaCl2 ·2H_2O, 5 mM NaCl, 0.05 % Tween, ddH_2

O) overnight at 37 º C with gentle shaking. The following day, the gel was stained with Coomassie blue (Bio-Rad, Hercules, USA) for 60 minutes, washed with ddH_2O and de-stained with destaining solution (400 ml methanol, 100 ml acetic acid and 500 ml of ddH2O). Gel detection was performed with Odyssey CLx Imaging System - LICOR. Signals were quantified using Fiji-ImageJ and normalised on the number of cells counted at the moment of supernatant collection. Results have been plotted as fold-change with controls as reference group.

Immunocytochemistry

30,000 cells were plated on fibronectin-coated glass coverslips in 24-well tissue culture plates. Twenty-four hours later, the cells were rinsed with phosphate buffer saline (PBS) once and fixed for 15 min with 4% paraformaldehyde (PFA) in PBS at room temperature. Coverslips were rinsed twice with PBS. PFA was quenched with 20 mM Glycine in PBS for 30 min. After rinsing with PBS, cells were blocked for 1 hour in 2% BSA 0.1X Saponin in PBS. Slides were then incubated with the primary antibody

in 1% BSA 0.1X Saponin overnight at 4°C. Fixed cells were rinsed four times with 0.1X Saponin in PBS and incubated with secondary antibodies diluted 1:1000 in 1% BSA 0.1X Saponin for 1 hour protected from light at room temperature and washed four times with PBS. They were then stained with DAPI (Thermofisher, Waltham, USA) for 10 minutes protected from light and then washed with PBS. Coverslips were mounted on glass slides using Fluoromount-GR (SouthernBiotech, Birmingham, USA) and imaged on Zeiss LSM-780 confocal or Imager Z1 fluorescence microscope.

Immunohistochemistry

Hemi-brains from sixteen weeks old mice were dried for six hours in sucrose 15% and then overnight in sucrose 30% before being embedded in tissue-tek compound (OCT). 10-15 μm sections were cut on a cryostat set at -20 º C. Once sections were dried (30 minutes), slides were stored at -80 º C. On the day of the staining, slides were thawed at 37° C for 30 minutes and fixed with PFA 4% for 30 minutes. After a wash with 0.5% Triton in PBS for 30 minutes, they were blocked with 3% BSA in PBS for 1 hour. Finally, sections were stained with primary antibody in 3% BSA in PBS overnight at 4° C. The following day, they were washed 3 times (1 hour each) in 3% BSA in PBS with mild agitation and then stained with 2nd antibody in 3% BSA in PBS for 1 hour at room temperature. After 3 washes of 1 hour each with PBS, they were then incubated with DAPI (dilution 1:1000) (Thermofisher, Waltham, USA) for 10 minutes and washed again (30 minutes). Slides were mounted using Fluoromount-GR (SouthernBiotech, Birmingham, USA) and imaged on Zeiss LSM-780 confocal or Imager Z1 fluorescence microscope.

Primary antibody	**Manufacturer details**	**Dilution**
SQSTM1 rabbit polyclonal antibody	GeneTex, GTX100685-S	1:500
Tom20 mouse monoclonal antibody	Santa Cruz BiotechnologySC-17764	1:300
Tom20 rabbit polyclonal antibody	DO616	1:500

Caveolin-1 (D46G3) XP® Rabbit monoclonal antibody	Cell Signalling, 3267	1:400
Clathrin Heavy Chain (D3C6) XP® monoclonal antibody	Cell Signalling, 4796	1:50
PCM1 (G200) rabbit polyclonal antibody	Cell Signalling, 5213	1:500
α-Tubulin GT114 mouse monoclonal antibody	Abcam, ab184613	1:200
V5 Tag Monoclonal Antibody (TCM5) rabbit	Invitrogen, 14-6796-82	1:200
Vimentin mouse monoclonal antibody	Novus biologicals NBP1-92687	1:1000
Golgin-97 mouse monoclonal Antibody (CDF4)	Invitrogen, 14-9767-80	1:200
Calnexin rabbit polyclonal antibody	Abcam, ab22596	1:1000
Alexa Fluor™ 488 Phalloidin	Invitrogen A12379	1:400
Zonula occludens-1 polyclonal antibody	Invitrogen 40-2200	1:200
CD31 rabbit polyclonal antibody	Abcam ab28364	1:50
CD31/PECAM-1 rat monoclonal antibody (MEC13.3)	Novus Bioscience NB600-1475SS	1:100
GFAP rabbit polyclonal antibody	Sigma Aldrich G9269	1:400
AQP4 mouse monoclonal antibody	Elabscience E-AB-22025	1:100
PDGFRB goat polyclonal antibody	R&D AF1042-SP	1:50

Isolectin GS-IB_4 From *Griffonia simplicifolia*, biotin-XX Conjugate	Invitrogen I21414	1:100

Table 2.3| List of primary antibodies used in the study.

Secondary antibody	Manufacturer details	Dilution
Alexa fluor 647 Chicken anti-Rat IgG	Invitrogen A21472	1:100 (Immunohistochemistry)
Alexa Fluor 488 donkey anti-goat IgG (H+L)	Invitrogen A11055	1:100 (Immunohistochemistry) 1:1000 (Immunocytochemistry)
Alexa Fluor 405 Goat anti-Mouse IgG (H+L)	Invitrogen A31553	1:100 (Immunohistochemistry)
Alexa-Fluor 555 Goat anti-Rabbit IgG (H+L)	Invitrogen A21428	1:1000
Alexa Fluor 568 Goat anti-Rabbit IgG (H+L)	Invitrogen A-11011	1:1000
Alexa-Fluor 488\ Goat anti-Rabbit IgG (H+L)	Invitrogen A-11008	1:1000
Alexa-Fluor 488\ Goat anti-Mouse IgG (H+L)	Invitrogen Goat anti-Mouse IgG (H+L)	1:1000

Table 2.4| List of secondary antibodies used in the study.

PROTEOSTAT® Aggresome

Cells were grown directly on glass slides previously coated with 10µg/ml Fibronectin and 0.2% gelatin from porcine skin (Sigma, Burlington, USA). At the appropriate time cells were washed twice with 1X PBS and fixed with 4% formaldehyde (Alfa Aesar, Ward Hill, USA) for 30 minutes at room temperature. After being carefully washed 2 times with PBS, cells were permeabilised with permeabilising solution (0.5% Triton X-100, 3 mm EDTA, pH 8.0 in Assay Buffer 1x) on ice, and gently shaken for 30 minutes. Cells were then washed twice with 1X PBS and incubated with Dual Detection Reagent (1 µL of PROTEOSTAT® Aggresome Detection Reagent and 2 µL of

Hoechst 33342 Nuclear Stain in 2ml of 1x Assay Buffer) for 30 minutes at room temperature protected from light. Cells were then washed other 3-4 times with 1X PBS and the coverslips were mounted with 20 µl of Fluoromount-GR (SouthernBiotech, Birmingham, USA) on a microscope slide. Cells were analysed by Imager Z1 fluorescence microscope or Zeiss LSM-780 confocal using a standard rhodamine filter set for imaging the cell aggresome signal and a DAPI filter set for imaging the nuclear signal.

Image analysis

Protein aggregates quantification

Protein aggregates in HUVECs were quantified using the ImageJ macro AggreCount [223]. Settings were defined by selecting channels for nuclei and aggregates and identifying the appropriate threshold to apply to images. Size cut-offs and distance limits to the perinuclear regions were determined. Finally, the level of strictness to identify cell ROIs was chosen between 2.5,5 and 7.5. Once settings were determined, nuclei were processed via fluorescent signal enhancement, converted to a binary image and ROIs defines. Aggregates were then processed according to inserted processing steps and then converted to a binary image for ROI identification. Cells were processed via enhancement of fluorescent signal, conversion to a binary image and capture of ROIs. Finally, cells were segmented to capture ROIs and the final merged image with nucleus, aggregate and cell body ROIs was obtained. The macro then calculated the distance between aggregates and nuclei and aggregates located within the cytosol, perinuclear zone or nucleus. The number of aggregates per cell, aggregate area per cell, and average aggregate size were then calculated. The analysis was performed in a blinded manner by attributing a random number to the samples and using the automated system described above for the quantification.

Cell profiler workflow for co-localization

The images were processed and subjected to a 20-module co-localization workflow as described in [2]. The images were divided into separate channels and underwent pixel-based correlation, where the pixel intensities were compared in each image and

any initial correlation determined. Images were then thresholded and segmented. During the final image analysis stage, the images were further enhanced, and the objects of interest were refined. The software then calculated the number of pixels within a specific object in each channel. The area occupied by co-localized regions was then divided by the area of co-localized objects of interest and a per-image pixel fraction determined from the total object pixels. This information was then converted into a percentage co-localization or Pearson correlation and the data exported. The analysis was performed in a blinded manner by attributing a random number to the samples and using the automated system described above for the quantification.

PCM1 distribution

The image analysis software Cell Profiler was used to quantify PCM1 distribution. A detailed description of each stage of the Cell Profiler workflow is located on their website (http://cellprofiler.org). Radial integrated fluorescence intensity was measured by using eight concentric circles centred on the nucleus area (each nucleus then acted as a seed for subsequent 2 µm rings to be drawn radiating from its periphery), thus covering 16 µm radial distribution of individual cells. The sum of fluorescence integrated intensity of the inner four circles was considered as perinuclear and the sum of the outer four circles as the cytoplasm. Finally, the percentage of perinuclear localisation was calculated by dividing the sum of perinuclear fluorescence by total fluorescence ([perinuclear/[perinuclear + cytoplasm]] × 100). The analysis was performed in a blinded manner by attributing a random number to the samples and using the automated system described above for the quantification. The analysis of PCM1 distribution in HUVECs was performed by Dr Andrea Martello and presented in [2].

P62 and LC3 puncta analysis

The image analysis software Cell Profiler was used to measure P62 and LC3 puncta in the cells. Z-stacks were acquired with the 63× objective, 2× zoom and 1-µm interval between slices, to cover the entire volume of the cell. Alexa Fluor 555 or Alexa Fluor

488 fluorescence and DAPI signals were used to delineate the cytoplasmic area, and the number of puncta was measured only in the cytoplasm. For each cell, the number of puncta from each slice was normalised against the surface area of the cytoplasm and then added together to obtain the total puncta/cell. The analysis was performed in a blinded manner by attributing a random number to the samples and using the automated system described above for the quantification.

Angiotool analysis

The vascular network in brain sections was analysed with Angiotool [224]. 16-bit greyscale images, 1.0-pixel aspect ratio, displaying labelled vasculature on a dark background were uploaded in the software. Segmentation of the vessel profiles was achieved using a fast multiscale Hessian-based enhancement filter [225, 226]. Images were first convolved with fast recursive Gaussian kernel and tube-like structures and then computed based on a combination of the eigenvalues of the 2D Hessian matrix. After segmentation, vessels were skeletonised according to [227] and analysed. Morphometric parameters (vessel area, vessel length, number of junctions and lacunarity) were measured and exported. The analysis was performed in a blinded manner by attributing a random number to the samples and using the automated system described above. for the quantification.

ZO-1 analysis

To analyse ZO-1 distribution in confluent ECs, Tif images taken with 20x objective were uploaded on Ilastik [228] and segmented into nuclei, ZO-1, cytoplasm and background. Automated analysis was performed on Fiji using a macro developed by Dr Matthieu Vermeren (Imaging facility - Institute of Regeneration and Repair). Ten different areas per condition were analysed. The area covered by ZO-1, the mean fluorescence intensity, minimum and maximum values and the perimeter of ZO-1 were measured and reported. The analysis was performed in a blinded manner by attributing a random number to the samples and using the automated system described above for the quantification.

BBB permeability assay

Dextran tetramethyl rhodamine (TRM) 3 kDa (Invitrogen, Waltham, USA) was injected intraperitoneally in sixteen weeks old mice. Mice were then anaesthetised using isoflurane 5%. After 10 minutes, mice were perfused with PBS and the brain, kidney and heart were collected. Hemi-brain and heart were harvested for following homogenisation and quantification of tracer fluorescence; the other hemi-brain was later embedded in OCT for further histological analysis. The hemibrain was then homogenised at 1000 rpm, centrifuged at 15,000 g, 20 minutes at 4 °C and the obtained supernatant was analysed by spectrofluorometer to investigate the fluorescence of the tracer extravasated in the tissue. 50 µL of tissue supernatants were pipetted into a 384-well black plate and read using excitation/emission (nm) values of 550/580. Tissue supernatant from one sham animal (injected with PBS) was included to ensure proper background subtraction. Raw fluorescence unit (RFUs) were used to calculate the permeability index (PI) after subtracting the corresponding sham values according to the formula: Permeability index = (Tissue RFUs/g tissue weight). To prevent bias, the analysis was performed in a blinded manner attributing to each mouse a random number in an excel sheet.

Flow Cytometry

Tissue collection: bone marrow

After euthanasia, sixteen weeks old mice were aseptically dissected. Femurs were cut at both ends and a 23-gauge needle and a 10 cc syringe were used to flush out the bone marrow with ice-cold Hank's balanced salt solution (HBSS). Bone marrow was then smashed through a 70 µm cells strainer using a 5 ml plunger. After centrifugation at 1500 rpm for 7 min at 4°C, the supernatant was discarded. The pellet was resuspended with red blood cells lysis buffer (0.16 M NH_4Cl, 10 mM $KHCO_3$, 0.13 mM EDTA dissolved in sterile H_2O) and incubate for 5 minutes at room temperature. Lysis buffer was neutralised by adding 5 ml FBS. Cells were centrifuged at 1500 rpm for 5 minutes at 4°C and resuspended in ice-cold FACS buffer (PBS + 0.1% BSA + 25 mM HEPES).

Tissue collection: brain

Sixteen weeks old mice were anaesthetised through intraperitoneal injection of sodium pentobarbital (45mg/kg) and perfused with HBSS through ventricle puncture to exclude red blood cells from the final preparation. Cerebrum was then collected from the skull of the mice, and the cerebellum, olfactory bulb and meninges were removed. The tissue was then digested with collagenase/dispase for 1 h 15 min at 37 º C and homogenised using a tissue grinder as described in paragraph 2.5. The homogenate was centrifuged at 800 g at 4 º C for 5 min, and the resulting pellet was suspended in 35% isotonic Percoll containing 25 mM HEPES solution. After centrifugation at 800g for 30 min at 4º C with no brake, cells were resuspended in FACS buffer (PBS + 0.1% BSA + 25 mM HEPES), filtered in 40 μm to remove cell clumps and large debris and counted using a haemocytometer for the following normalisation after flow cytometry analysis.

Flow cytometry analysis

After the count, low affinity Fc receptors were blocked by incubation of cells with anti-CD16/32 antibody for 30 minutes. Then, cells were incubated with the following fluorochrome-conjugated mouse monoclonal antibodies for 30 minutes: antibody anti-mouse/human CD11B (clone M1/70, 1 μg/ml, BioLegend), anti-mouse P2Y12 (clone S16007D, 1 μg/ml, BioLegend), anti-mouse LY6G (clone IA8, 1 μg/ml, BioLegend), anti-mouse CD3 (clone 17A2, 1 μg/ml, BioLegend), anti-mouse CD19 (clone 6D5, 1 μg/ml, BioLegend), anti-mouse LY6-C (clone HK1.4, 1 μg/ml, BioLegend) and anti-mouse CD45 (clone 30-F11, 1 μg/ml, BioLegend). Single stain controls were prepared adding one drop (10 μl) of compensation beads (BD Pharmingen, Franklin Lakes, USA) to each fluorophore-conjugated antibody and left in ice for 20 minutes with gentle rotation. Unstained control was prepared using non-stained cells. After centrifugation at 400 g for 5 minutes, the supernatant was replaced with 200 μl FACS buffer and samples were stored in ice. DAPI (1:1000) was added before reading at 6LSR Fortessa (BD Biosciences, Franklin Lakes, USA) and analysed using FlowJo software.

Compensation was performed using single-labelled samples as references and positive staining regions were defined based on unstained samples. Gating and criteria for identifying discrete cell subpopulations are described in Chapter 4. For brain samples, the absolute number of cells of a specific subset was determined from the number of cells in the population divided by total viable cells, multiplied by the total viable cell yield from the hemisphere (derived from cell density calculated by haemocytometer on the single cell suspension) as described in [229]. Mean fluorescent intensities (MFI) of selected cell populations were derived from the software.

Statistics

Analyses were performed using GraphPad Prism 9. Unpaired t-test was used for comparisons between two normally distributed datasets. Welch's correction was applied in *in vivo* studies according to [230]. One-way ANOVA with Bonferroni correction for multiple comparisons or two-way ANOVA with Tukey's post hoc test was applied in the case of more than two datasets. Data have been tested for outliers using GraphPad Prism 9 and samples have been excluded in the case positive for outlier test. Data are expressed as mean ± SEM of at least three independent experiments. P value <0.05 was considered statistically significant.

Chapter 3

Contribution of TCHP knock-out to impaired homeostasis of brain ECs

Chapter 3 Contribution of TCHP knock-out to impaired homeostasis of brain ECs

Introduction

An adequate blood supply and functional integrity of blood vessels are fundamental for normal brain functioning. The cerebrovascular endothelium is a specialised interface between vasculature and the brain that regulates brain physiology and plays a critical role in the pathogenesis of the cerebrovascular disease. The brain relies on the exchange with the circulation and blood flow perfusion to get oxygen and nutrients like glucose, ATP, glycogen and phosphocreatine [5]. Furthermore, neuronal activity is matched by changes in blood flow through the neurovascular coupling, which is finely regulated by the endothelium.

The interaction between endothelial and other brain cell types, including neurons and glia (astrocytes, microglia, oligodendrocytes), has been summarised by the concept of the NVU [6], which emphasises the importance of the endothelium in brain function. The crosstalk between the cells of the NVU is fundamental for regulating cerebral blood flow and the BBB permeability [9]. Intercellular communication is disrupted in disease conditions triggered by hypoxia, oxidative stress and inflammation. In this context, ECs regulate the haemostatic status of cerebral vessels with antithrombotic and fibrinolytic activities and play an anti-inflammatory role in controlling the adhesion of inflammatory cells, such as neutrophils, monocytes and macrophages [231].

ECs form the BBB, where they function as a sealed cellular layer, actively controlling the influx of molecules or cells and generally limiting influx processes under normal conditions, both in a trans-cellular and inter-cellular manner. BBB ECs present a unique phenotype, characterised by TJs and specific polarised transport systems. TJs are intercellular junctional complexes composed of integral membrane proteins, such as occludin, claudins, JAMs, and ESAMs. They connect to the cytoplasm through the scaffolding proteins zonula occludens (ZO-1, ZO-2, ZO-3). Moreover, non-occludin adherens junctions are mixed with TJs. Between these, the endothelial-specific VE-cadherins. In the context of the BBB, TJs stop the diffusion of blood-borne

polar substances [20], the lateral diffusion of integral membrane proteins and lipids and maintain cell polarisation [21]. Furthermore, they also act as an intracellular signalling platform [22].

An essential characteristic of the brain ECs is the low rate of vesicular transport – transcytosis. Transcytosis pathways are divided into clathrin-mediated and non-clathrin-mediated [44]. Examples of clathrin-mediated transcytosis are transferrin receptor-mediated transport of iron [43] and the uptake of low-density proteins (LDL). In the case of non-clathrin-mediated vesicle trafficking pathways, several cellular machineries can be involved, such as dynamin, small GTPases, RhoGAP proteins, and coat proteins [44]. Non-clathrin-mediated transcytosis consists of large micrometre-scale pathways such as micropinocytosis and phagocytosis involving actin fibres and smaller than 200 bm scale processes involving dynamin. Caveolae-mediated vesicle trafficking is strongly present in the ECs of peripheral tissues, such as the heart and lung, but not in the brain. Caveolae are 50-100 nm membrane invaginations enriched in saturated phospholipids, sphingolipids, cholesterol and ethanolamine plasmalogens [45]. Andreone et al. described the regulation of caveolae-dependent transcytosis by the omega-3 fatty acid DHA transporter Mfsd2a, which would control the luminal plasma membrane DHA lipid composition and consequently prevent caveolae transport, keeping the integrity of the BBB [46]. Furthermore, Knowland et al. explained that transcytosis and endocytosis are increased 6 hours after ischemic stroke, as demonstrated by an increased level of CAV-1. The paracellular endothelial barrier is affected only after 48 hours, as highlighted by TJs' disruption [232].

Another leading mechanism responsible for BBB disruption is the excessive production of MMPs due to chronic hypoxia or inflammation induced by age-related vascular changes. MMPs facilitate the degradation of TJ proteins and the basement membrane [233].

Cerebrovascular diseases are associated with high levels of pro-inflammatory factors, which contribute to a pro-inflammatory microenvironment, thus facilitating vascular dysfunction and promoting endothelial apoptosis, mainly by activating NF-κB [130, 234, 235]. Inflammatory factors associated with an increased risk of developing

vascular cognitive impairment and dementia include TNF-α, IL-6, and IL-1β [236] and chemokines such as CCL3 and CCL5 [237-239].

Several mechanisms can lead to chronic inflammation. One of them is oxidative stress. Indeed, an increase in ROS can disturb the functionality of NO, which is a critical vasodilation factor that contributes to cerebral blood flow regulation and confers vascular protective effects, including inhibition of platelet aggregation, inhibition of endothelial apoptosis, preservation of endothelial progenitor cells, and anti-inflammatory properties. Mitochondrial-derived H_2O_2 activates NF-κB, leading to a pro-inflammatory shift in endothelial gene profiles [130]. In addition, oxidative stress damages mitochondrial DNA, further contributing to the pathogenesis of dementia [131]. An increase in pro-inflammatory cytokines is associated with the SASP and the secretion of growth factors, ROS, MMPs and proteases that contribute to ageing and the development of ageing-related disease.

ECs play a pivotal role in keeping the BBB integrity. It is thus essential to consider the barrier function as a critical parameter to be assessed when investigating brain endothelial cell function in vitro.

In this chapter, I will present the protocol used to isolate the ECs from the brain of $Tchp^{EC}$ mice without affecting the phenotype or the morphology typical of the ECs. Then, I will analyse the results of the bulk RNA-seq performed on the ECs from the brains of $Tchp^{EC}$ and WT mice, which demonstrated the activation of inflammatory pathways and MMPs in the ECs lacking TCHP. Finally, I will investigate how the knock-down of TCHP affects the cellular organelles, focusing on caveolae-mediated trafficking.

Hypothesis and aims

Given the inflammatory transcriptome and the association of SASP with TCHP knock-down [2] previously identified in HUVECs, I hypothesised that the lack of TCHP could cause a chronic inflammation status and thus affect barrier function in brain microvascular ECs. I verified this hypothesis both in ECs isolated from the brain of $Tchp^{EC}$ mice and HBMVECs lacking TCHP. Therefore, the hypothesis presented in this chapter is as follows:

“TCHP knock-out impairs brain EC homeostasis, causing inflammation and affecting barrier function”.

Aims:

- To assess a new protocol to isolate and cultivate primary brain ECs from adult mice.
- Characterisation of ECs from the brain of endothelial-specific Tchp knock-out mice and human brain microvascular ECs lacking TCHP.
- Characterisation of TCHP role in cellular organelles and molecular pathways in TCHP knock-down human brain microvascular ECs.

Results

Isolation of ECs from the brain of Tchp^{EC} mice

Microvascular ECs were isolated from 2-4 months old WT and Tchp^{EC} mice following a modified version of a pre-existent protocol [219] as reported in Chapter 2. (**Figure 3.1A**).

After the selection, the flow cytometry analysis performed to investigate the purity of the sample confirmed the presence of PECAM1 positive (CD31+) (ECs marker) and CD45 negative (CD45-) (haematopoietic cells' marker) cells. Furthermore, the microvascular ECs reached confluence within 7/8 days and were available for RNA extraction, protein collection or fixed with PFA 4% for the following immunocytochemistry. (**Figure 3.1B**).

Gene expression of endothelial markers (Cd31, Tek, Cldn5, Cdh5, Abcb1) and non-endothelial markers (Pdgfrb, Rgs5 and Gfap) in the ECs isolated and selected using puromycin were analysed by qPCR and compared with ECs sorted using MACS® (CD31+/CD45-). Data suggests that puromycin selection does not affect endothelial transporters or other endothelial markers. Furthermore, the immunocytochemistry analysis demonstrated that the ECs express the endothelial marker CD31 and the TJ ZO-1, ensuring that the ECs maintained their key characteristics (**Figure 3.1C**).

Finally, we tested their function *in vitro* through cell-impedance-based assays focussed on migration and barrier function. ECs were plated on ECIS® arrays, where a small alternating current (I) was applied across at the bottom of the array. This created a potential V across the electrodes measured by the instrument. The impedance Z was determined by Ohm's law Z = V/I. Migration was investigated through wound healing assay. The current was boosted by a 1000-fold to a milliampere, causing electroporation and forming a 250 µm wound. Healthy neighbouring cells migrate inward to replace the affected cells, and the instrument measured the change in impedance. The ECs isolated and selected by puromycin did not show a difference in the resistance before and after the wound, demonstrating that the selection did not affect the migration of the cells. Puromycin, an antibiotic, allows the selection of the brain ECs that present the P-glycoprotein pump, which consents the efflux of the antibiotic outside the cells, while it is toxic for the other

cell types (pericytes, red blood cells, astrocytes, microglia, neurons). This method secures the purity of the culture.

Moreover, the barrier function of the ECs in culture was analysed by treating the cells with thrombin (1 U/ml) or LPS (1 nM). At low alternating current frequency, the membrane impedance is high, and most of the current flows under the cells and through the tight spaces between the cells. Cells were stimulated with thrombin or LPS to investigate changes in transcellular resistance. In both cases, the treatment caused a transient drop in transcellular resistance, with a significant reduction compared with unstimulated control cells (**Figure 3.1D**).

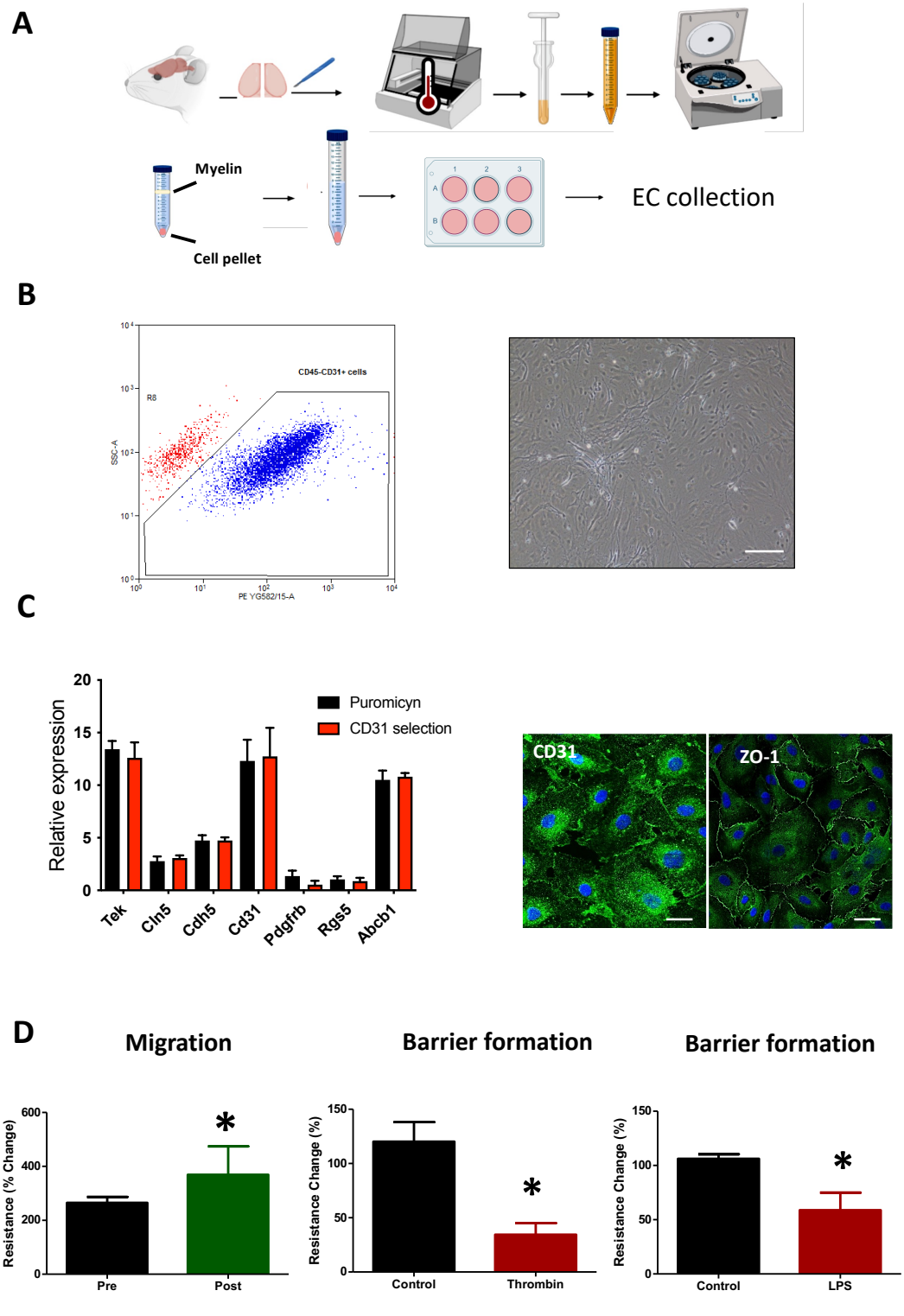


Figure 3.1| Isolation of microvascular ECs from the brain of Tchp^{EC} and WT mice for transcriptomic analysis.

A. Schematic representation from tissue acquisition to analysis. **B**. Left panel: flow cytometry characterization of mouse brain ECs after puromycin selection. Right panel: Representative image of mouse brain ECs after isolation and selection by puromycin treatment. Scale bar, 100µm. **C.** Left panel: Expression of endothelial and non-endothelial markers in mouse brain ECs after isolation and selection by puromycin and after CD31 selection using MACS® (CD31+/CD45-). Puromycin does not affect endothelial genes. Right panel: immunofluorescence staining of CD31 and ZO-1 fluorescent Intensity in mouse brain ECs after isolation.

D. On the left panel quantitative comparison of resistance changes (%) at 24h before and after wounding via electroporation in mice brain ECs after isolation and selection by puromycin. On the central panel, resistance change (ohms) with and without stimulation with thrombin (1 U/ml) over 24h. Thrombin stimulation caused a biphasic change in transcellular resistance, with a significant reduction compared with unstimulated control cells. On the right panel, quantification of resistance change (ohms) with and without stimulation with LPS (1 nM) over 24h. LPS stimulation caused a transient drop in transcellular resistance, with a significant reduction compared with unstimulated control cells. *P > 0.05, unpaired *t*-test (N=3 per group). Statistical analyses were performed on at least three independent experiments.

Bulk RNA-seq of Tchp^{EC} and WT mice microvascular ECs

To investigate the transcriptional changes caused by the knock-out of Tchp in the brain microvascular ECs, bulk RNA-seq (BGI genomics) was performed on ECs of WT and Tchp^{EC} mice collected after 7 days in culture (n=3). The RNA sequencing identified 807 differentially expressed genes (DEGs) in the samples of Tchp^{EC} mice compared to the control (**Figure 3.2A**), 602 upregulated and 205 downregulated, as highlighted by the Heatmap and the Volcano plot (**Figure 3.2B**).

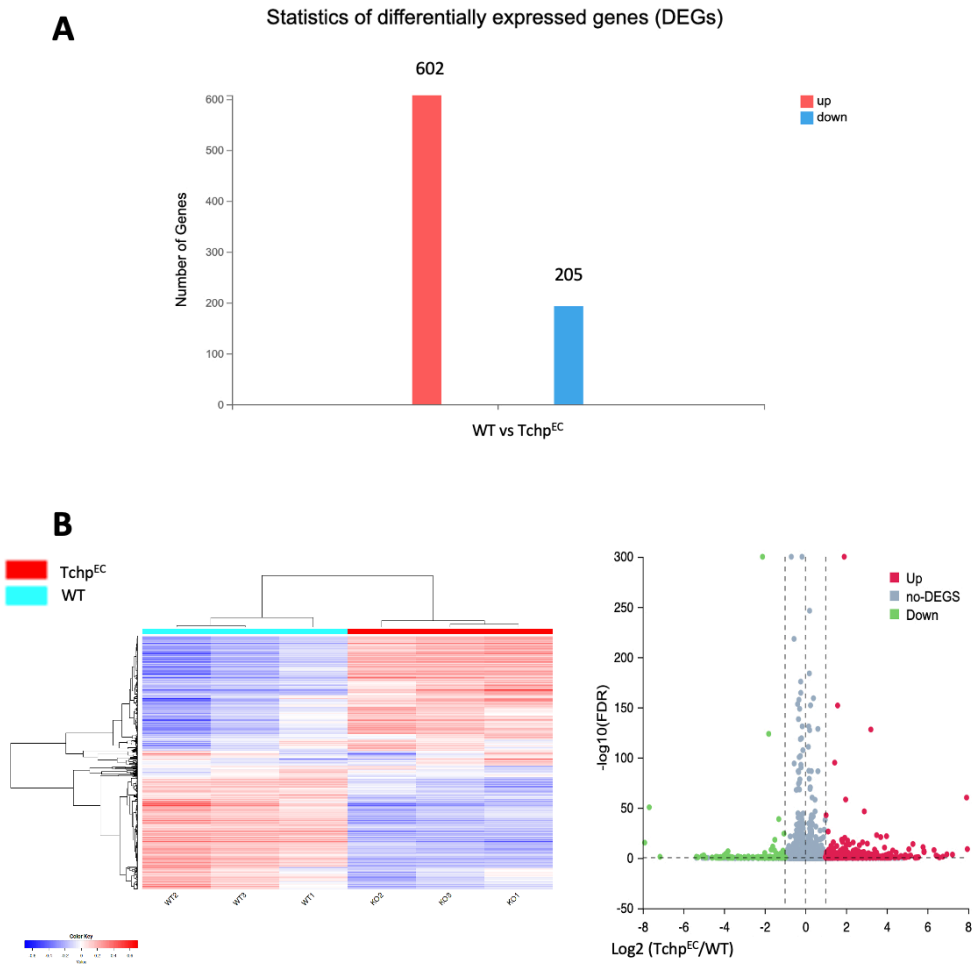


Figure 3.2| Transcriptomic analysis of ECs isolated from the brain of Tchp^{EC} and WT mice.

A. Statistics of DEGs in Tchp^{EC} ECs. DEG up-regulated 602 (in red). DEGs downregulated 205 (in blue). The analysis was performed using BGI Dr Tom. **B.** Left Panel: Heat map representation of differentially expressed genes identified by comparing Tchp^{EC} KO RNA-Seq samples to WT ECs. The horizontal axis is the log2 of sample (expression value +1), and the vertical axis is the gene.

The warmer the colour block is, the higher the expression level is, and the colder the colour block is, the lower the expression level is. The heat map was generated using iDEP96. Right Panel: Volcano plot depicting differentially expressed genes in WT and $Tchp^{EC}$ KO cells. The X-axis represents the fold change of the difference after conversion to log2, and the Y-axis represents the significance value after conversion to-log10. Red represents DEG up regulated, green represents DEG down regulated, and grey represents non-DEG. The Volcano plot was generated using BGI Dr. Tom.

The biological processes affected by the knock-out of Tchp in the brain were investigated using parametric gene set analysis (PGSEA). The analysis was conducted on the 807 DEGs. KEGG pathways analysis revealed the downregulation of ribosome and proteasome pathways ($p=4.36 \times 10^{-3}$). These data suggest that the downregulation of Tchp is linked with negative regulation of translation, in line with the phosphorylation of elf2α and the subsequent formation of stress granules and accumulation of protein aggregates, as will be further explained in chapter 5. Of note, autophagy of mitochondria appears between the suppressed pathway ($p=4.87 \times 10^{-3}$), in line with the previously published link between Tchp and autophagy in ECs [2] (**Figure 3.3A**).

The gene ontology (GO) analysis of cellular components annotations revealed enrichment of mitochondria and mitochondrial outer membrane ($p=4.52 \times 10^{-3}$) between the downregulated genes, in line with the role of Tchp in modulating mitochondria shape and juxtaposition with ER [196]. Stress fibres and contractile actin filament bundle ($p=6.11 \times 10^{-3}$) are between the activated pathways (**Figure 3.3B**), suggesting cytoskeleton modification associated with the knock-out of TCHP.

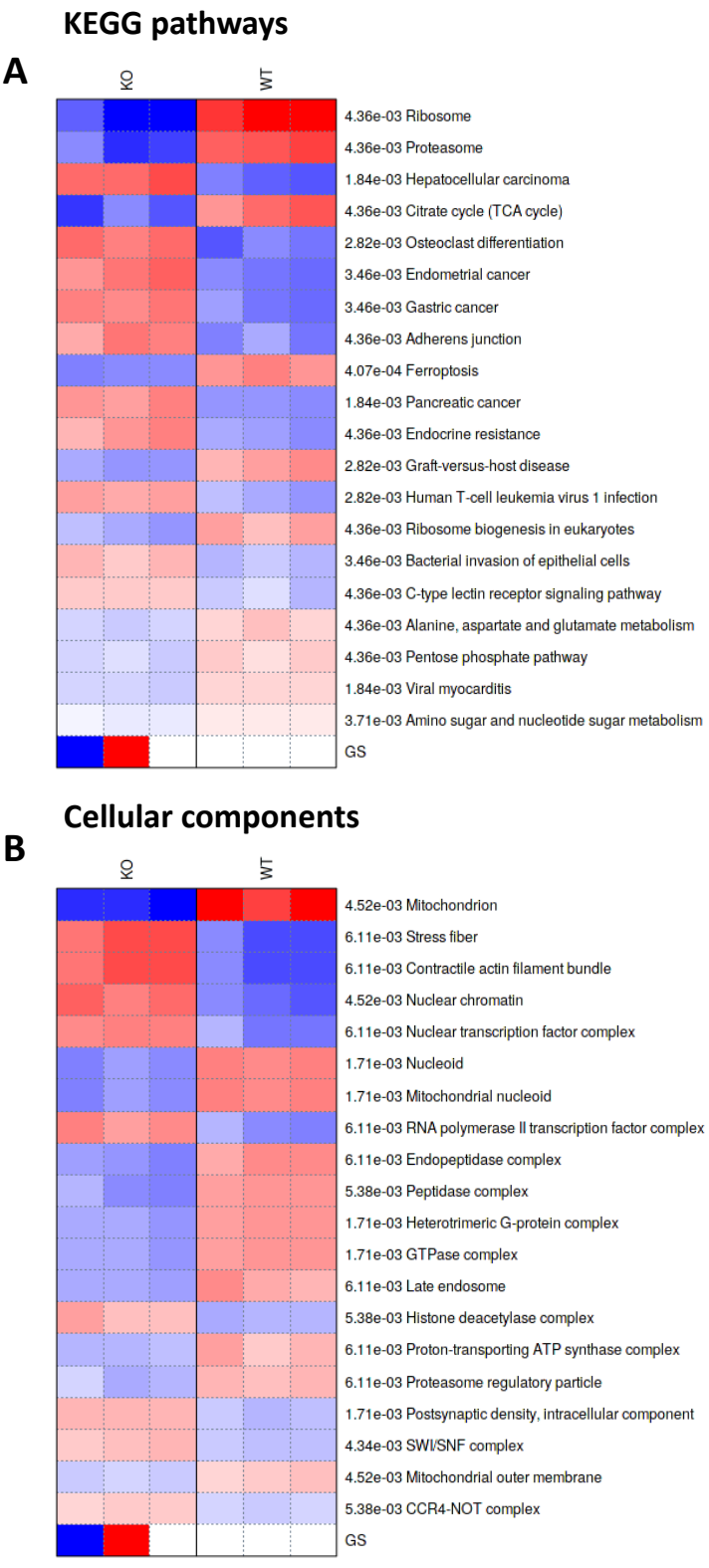


Figure 3.3| Parametric Gene Set Enrichment Analysis of ECs from Tchp^{EC} mice.

Heat-maps showing enriched pathways in ECs from WT and Tchp^{EC} mice using KEGG pathways (A) and Cellular components (B). Red and blue indicates activated and suppressed pathways. The tables were generated using iDEP96.

The 602 upregulated differentially expressed genes were further analysed using the BGI software Dr Tom. The upregulated DEGs were investigated using KEGG pathway enrichment analysis. The function of Qvalue <= 0.05 was regarded as a significant enrichment. “Cytokine-cytokine receptor interaction”, “ECM-receptor interaction”, “PPAR signalling”, “chemokine signalling”, “Cell adhesion molecule” and “Degradation of the extracellular matrix” were among the significantly enriched pathways `in $Tchp^{EC}$ mice (**Figure 3.4.A**). Among the genes upregulated are the chemokines Ccl5, Ccl7, Ccl11, the interleukin Il33, the receptor Cd36, Spp1 and Mmp9.

Since I was interested in the pro-inflammatory transcriptome in the ECs from $Tchp^{EC}$ mice, I further investigated interactions between the different DEGs involved in “cytokine-cytokine receptor interaction” and “ECM-receptor interaction” using GeneMania software [240]. Interactions (in red), co-expression (in purple), shared protein domains (in green), predicted interactions (in yellow) and co-localization (in blue) were analysed (**Figure 3.4.B**). The analyses revealed DEGs involved in neurodegenerative and cerebrovascular disorders that I further validated using qPCR. Ccl3 and Ccl5 belong to CCL3/CCR5 and CCL5/CCR5 axes and have a fundamental role in brain inflammation, stroke and pathogenesis of neurodegenerative disease [237-239]. Cd36 has been linked with neurovascular dysfunction and inflammasome activation in Alzheimer's disease pathogenesis [241, 242]. HMGBs mediate inflammatory responses in cerebral ischaemia injury [243, 244]. S100A4, a marker of endothelial-mesenchymal transition, and Spp1, a fibroblast marker, are both involved in disrupting the BBB [245-247]. Mmp9, a metalloproteinase, is associated with neuroinflammation and degradation of the BBB in neurodegenerative disorders [248, 249].

Up-regulated genes

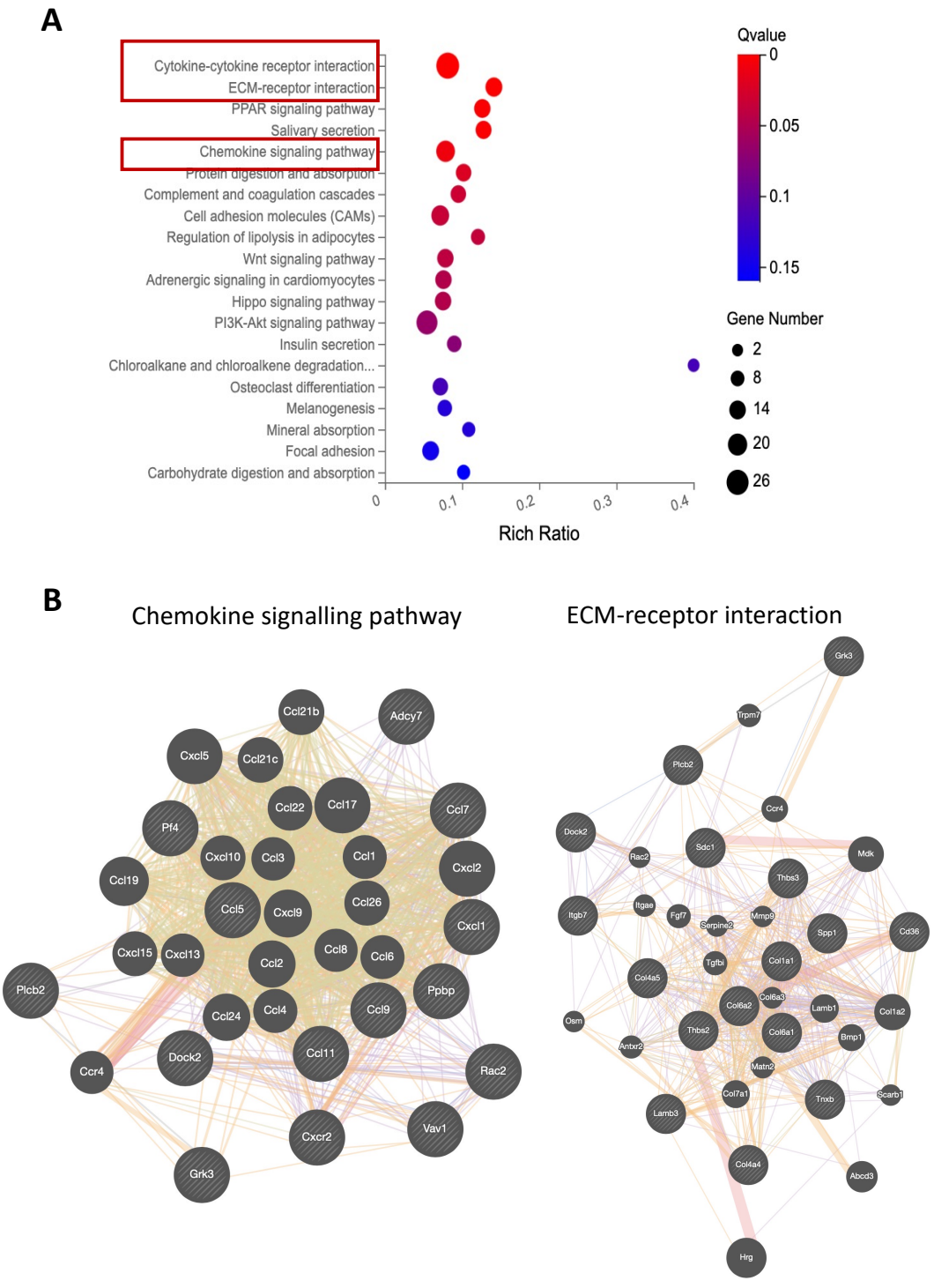


Figure 3.4| KEGG pathway analysis and Network analysis of upregulated genes in ECs from Tchp^{EC} mice.

A. Bubble chart showing enriched pathways in ECs from Tchp^{EC} mice using kegg_pathway annotation classification. The function of Qvalue <= 0.05 is regarded as a significant enrichment. The Bubble chart was generated using BGI Dr Tom. **B.** left Panel: Chemokine signalling network cluster with 17 genes. Red lines represent interactions, purple lines indicate co-expression, green lines indicate shared protein domains, yellow lines predicted interactions, blue lines indicate co-localization. Right Panel: ECM-receptor interaction network cluster with 17 genes. Red lines represent interactions, purple lines indicate co-expression, green lines indicate shared protein domains, yellow lines predict interactions, blue lines indicates co-localization. The network analysis was performed with GeneMania.

QPCR was performed to validate the expression of chemokine signalling pathways DEGs (Ccl3, Ccl5) and ECM receptor interaction genes (S100a4, Spp1, Cd36, Hmgb2, Mmp9). The validation was performed in RNA extracted from ECs of WT and Tchp^{EC} mice and from ECs sorted from WT and Tchp^{EC} mice using the magnetic-activated cell sorting (MACS®) from Miltenyi biotech. The qPCR and the following $2^{-\Delta\Delta Ct}$ analyses demonstrated a significant up-regulation of the chemokines Ccl3 (p=0.0259) and Ccl5 (p=0.0434), suggesting the presence of inflammation in the ECs of Tchp^{EC} mice. Also, the gene expression of the inflammatory receptor Cd36 was significantly upregulated in Tchp^{EC} compared to WT (p=0.0086), in support of the presence of an inflammatory transcriptome (**Figure 3.5**).

Cellular culture

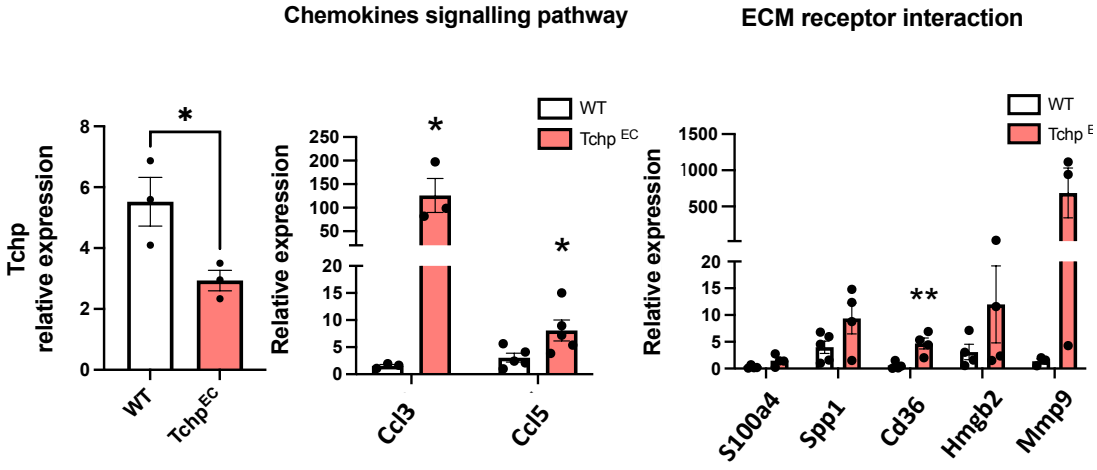


Figure 3.5| TCHP knock-out affects brain microvascular endothelial cells transcriptome in Tchp^{EC} mice.

A. Left panel: expression of Ccl3, Ccl5 in ECs from WT and TCHP^{EC} mice (unpaired *t*-test; Tchp= *P 0.0406, Ccl3 **P = 0.0259*; Ccl5 **P* = 0.0434). Right panel: expression of S100a4, Spp1, Cd36, Hmgb2, Mmmp9 in ECs from WT and TCHP^{EC} mice (unpaired *t*-test; Cd36 ***P* = 0.0086). Statistical analyses were performed on at least three independent experiments. Data are represented as mean ± standard error of the mean (SEM).

To exclude that the upregulation described above was due to the culture conditions, ECs from WT and Tchp^{EC} mice were sorted using MACS® system and magnetic beads conjugated antibodies (enrichment for CD31^{+}/CD45^{-}). The gene expression of Ccl3, Ccl5, S100a4, Spp1, Cd36, Hmgb2 and Mmp9 was investigated using qPCR. The upregulation of Ccl5 was confirmed in the ECs sorted from Tchp^{EC} mice (p= 0.0318) (Figure 3.6). Conversely, Cd36 upregulation was not observed, suggesting the previously shown upregulation was due to the culture conditions (**Figure 3.6**).

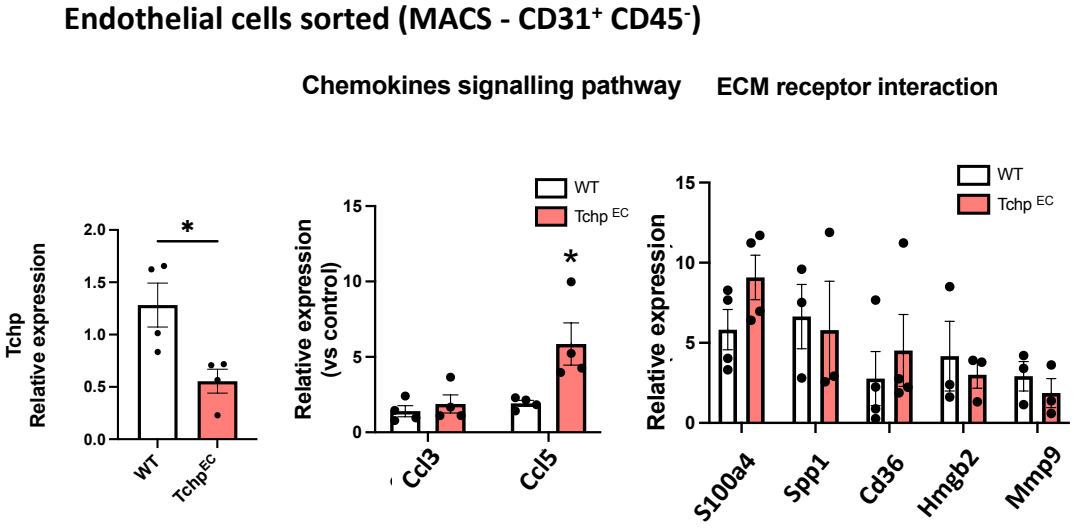


Figure 3.6| TCHP knock-out affects brain microvascular endothelial cell transcriptome in Tchp^{EC} mice sorted with MACS®.

Left panel: expression of Tchp, Ccl3, Ccl5 in ECs from WT and TCHP^{EC} mice sorted with MACS® (CD31+/CD45-) (unpaired *t*-test; Tchp= *P=0.0226, Ccl5 **P = 0.0318)* Right panel: expression of S100a4, Spp1, Cd36, Hmgb2, Mmp9 in ECs from WT and TCHP^{EC} mice sorted with MACS® (CD31+/CD45-) (unpaired *t*-test). Statistical analyses were performed on at least three independent experiments. Data are represented as mean ± SEM.

To confirm the inflammatory transcriptome identified in Tchp^{EC} mice in human cells, the gene expression of CCL5, S100A4, SPP1, CD36 and MMP9 was analysed in HBMVECs by qPCR. First, HBMVECs were transfected using siRNA oligonucleotides targeting TCHP or control anti-miR. Then, the expression levels were analysed. Finally, I analysed TCHP gene expression confirming the knock-down by transfection (p=0.0452). Interestingly, CCL5 upregulation was confirmed in HBMVECs (p=0.0348),

supporting the hypothesis that the inflammatory pathways are associated with the knock-down of TCHP (**Figure 3.7**).

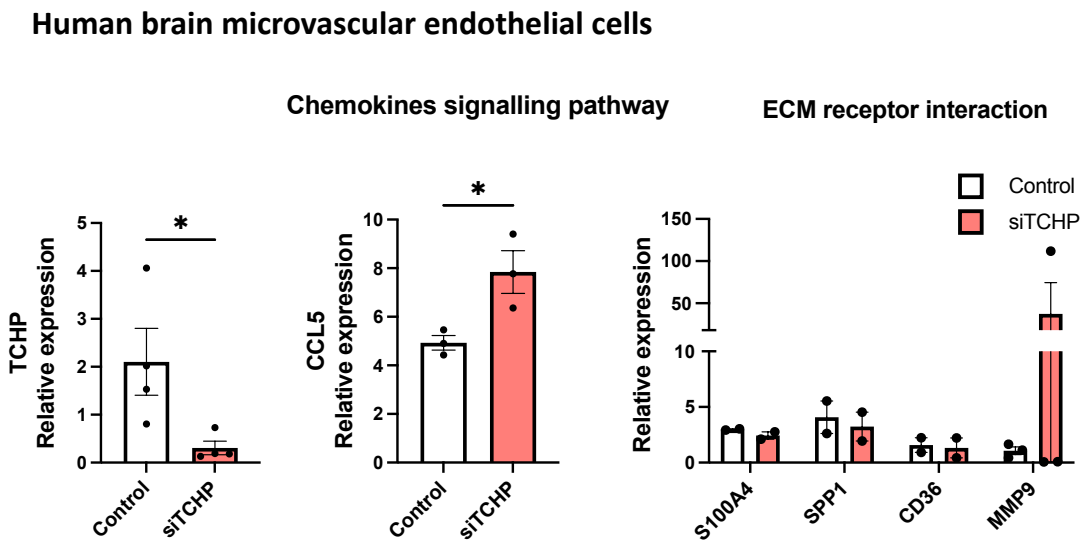


Figure 3.7| TCHP knock-down affects HBMVECs transcriptome.

A. Expression of TCHP, CCL5, S100A4, SPP1, CD36, MMP9 in control and TCHP Knock-down HBMVECs (unpaired *t*-test; TCHP **P = 0.0452*; CCL5 *P= 0.0348). Statistical analyses were performed on at least three independent experiments. Data are represented as mean ± SEM.

Metalloproteinase activity in Tchp^{EC} and WT mice microvascular ECs

The RNA sequencing analysis highlighted the activation of the "Degradation of the extracellular matrix" pathway in the ECs from the brain of Tchp^{EC} mice, notably of the matrix metalloproteinase Mmp9. The qPCR revealed a trend in the increased gene expression of Mmp9 in the ECs from Tchp^{EC} mice compared to the WT, though not statistically significant. To further investigate the upregulation of matrix metalloproteinases in Tchp^{EC} mice, protein levels of MMP9, MMP2 and MMP1 were analysed using gelatine zymography (**Figure 3.8A**). Metalloproteinase activity was normalised on the number of cells. The production of 97 kDa MMP9 increased in the ECs isolated from Tchp^{EC} brains, even if more replicates are necessary to confirm this statistically. On the other hand, 72 kDa MMP2/63 kDa MMP2 and 54 kDa MMP1 protein did not differ between WT and Tchp^{EC} ECs (**Figure 3.8B**).

To investigate if the inflammation associated with the knock-out of Tchp was due to the activation of the Nf-κB pathway as previously demonstrated in HUVECs lacking TCHP [2], ECs were treated with the Nf-κB inhibitor BAY11-7082 for 24 hours and the medium collected to be analysed by gelatine zymography. As a result, a reduction in MMP9 protein level was observed in Tchp^{EC} ECs, suggesting the involvement of Nf-κB, but more replicates are necessary to confirm this hypothesis (**Figure 3.8B**).

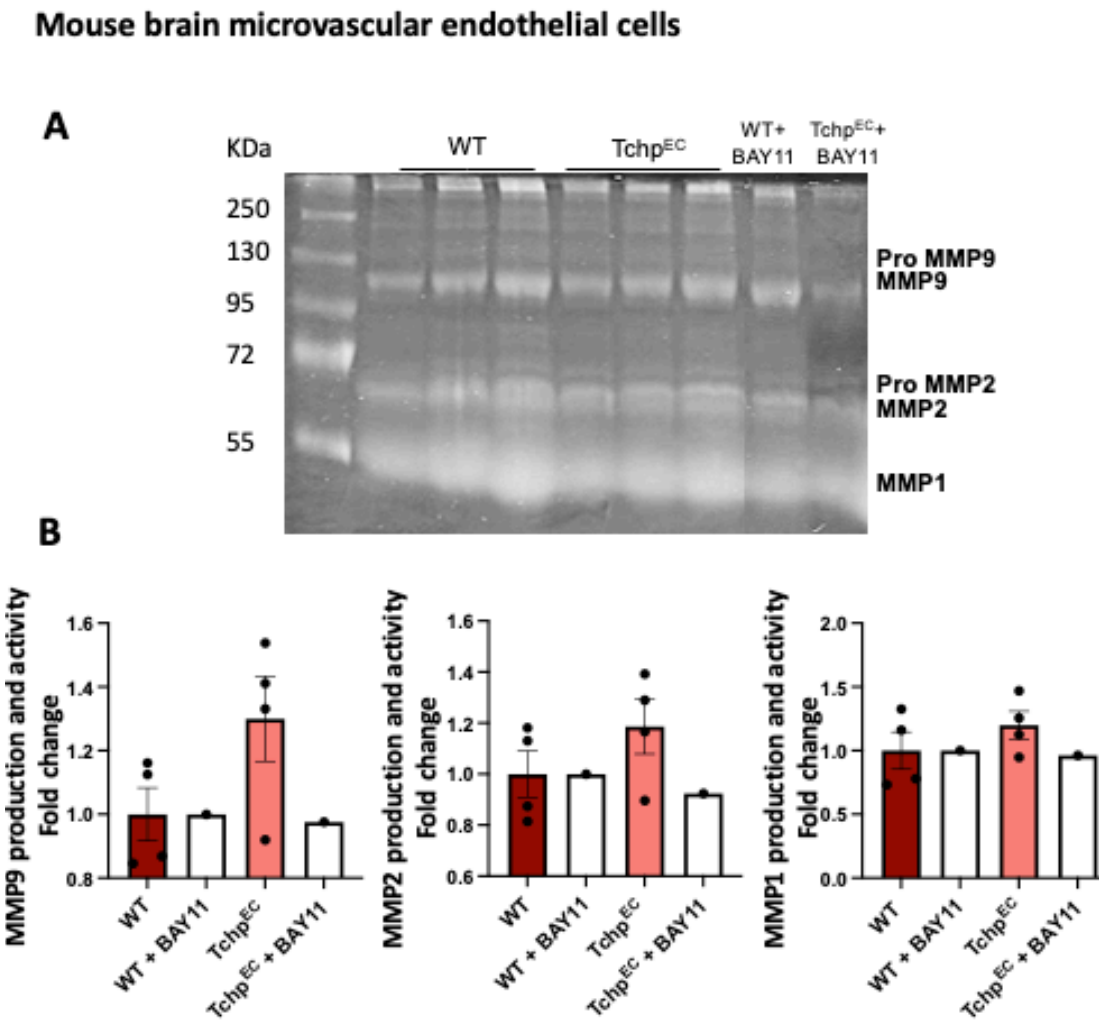


Figure 3.8| Gelatin zymography of MMP1, MMP2 and MMP9 activity in the brain of WT and Tchp^{EC} mice.

A. Representative image of gelatine zymography analysis of microvascular ECs of the brain of WT and Tchp^{EC} mice. **B**. Quantification of MMP1, MMP2 and MMP9 activities in ECs of Tchp^{EC} and WT mice and Tchp^{EC} and WT mice treated with BAY11-7082 300 nmol. Data are normalised on the number of cells. Statistical analyses were performed on at least three independent experiments except BAY11-7082 treatment. Data are represented as mean ± SEM.

The production of the MMPs was investigated in HBMVECs transfected with siRNA targeting TCHP and anti-miR as control using gelatine zymography (**Figure 3.9A**). Of note, 97 kDa MMP9 increased in the human ECs lacking TCHP (*P* = 0.0218), while 72 kDa MMP2/63 kDa MMP2 and 54 kDa MMP1 protein levels tend to be higher in TCHP knock-down ECs but without reaching a statistical significance (**Figure 3.9B**).

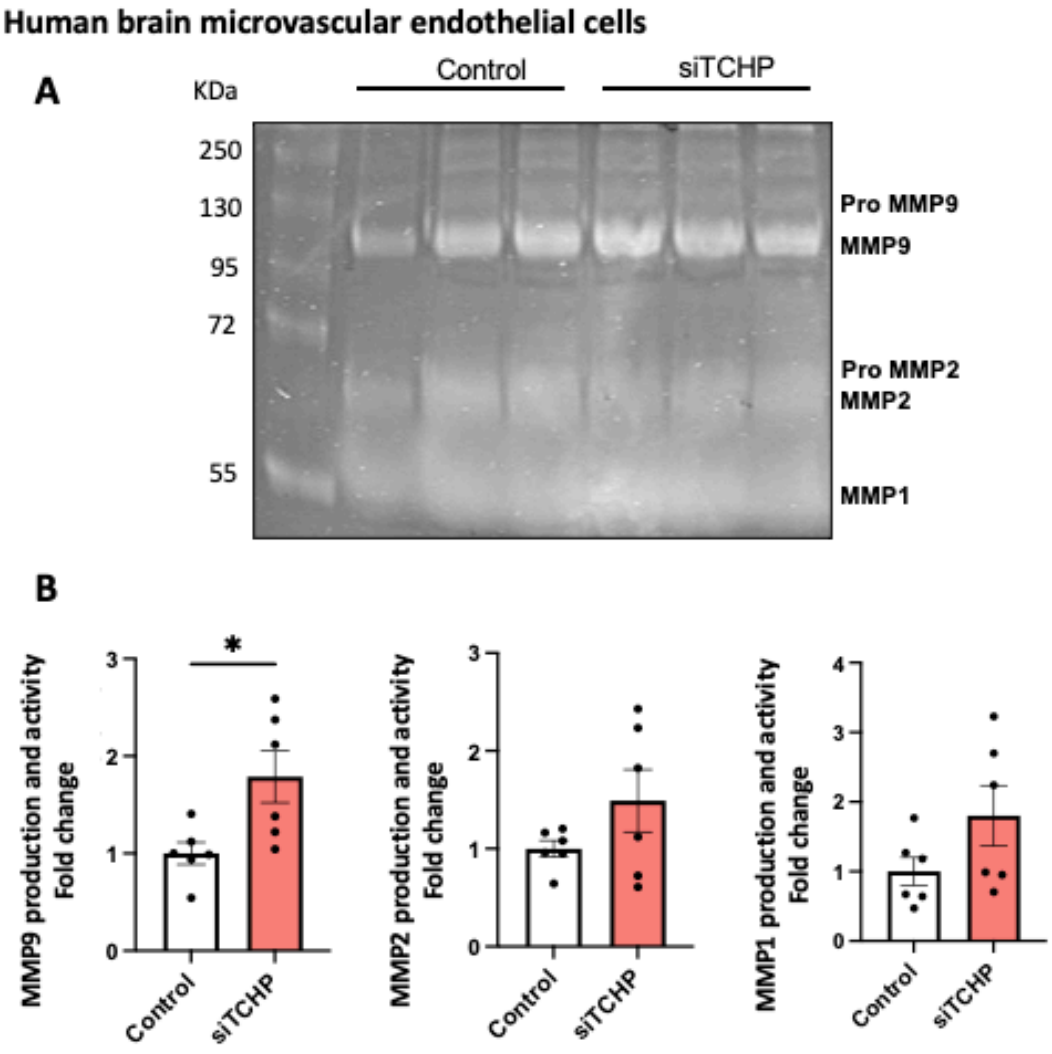


Figure 3.9 | Gelatine zymography of MMP1, MMP2 and MMP9 activity in control and Tchp Knock-down HBMVECs.

A. Representative image of gelatine zymography analysis of control and Tchp knock-down Human brain microvascular endothelial cells. **B.** Quantification of MMP1, MMP2 and MMP9 activities in control and Tchp knock-down human brain microvascular endothelial cells. (Unpaired *t*-test; MMP9 **P* = 0.0218). Data are normalised on the number of cells. Statistical analyses were performed on at least three independent experiments. Data are represented as mean ± SEM.

Validation of down-regulated genes in human brain microvascular ECs lacking TCHP

The 205 downregulated DEGs were further analysed using the BGI software Dr Tom. The downregulated DEGs were investigated using KEGG pathway enrichment analysis. The function of Qvalue <= 0.05 was regarded as a significant enrichment. “Gap junctions”, “cGMP-PKG signalling and pathway”, “Vascular Smooth muscle contraction” were among the significantly enriched pathways in the ECs from $Tchp^{EC}$ mice (**Figure 3.10A**). The following network analysis of the genes belonging to “Gap junctions” and “Vascular Smooth muscle contraction” showed that the guanylate cyclases Gucy1a1, Gucy1a2 and, Gucy1b1 are hub genes. Interestingly, Gucy1a1, Gucy1a2, and Gucy1b1 encode for soluble guanylyl cyclase (sGC) protein, and they are associated with hypertension, coronary artery disease and stroke [30, 31]. Furthermore, the impairment of the NO-sGC-cGMP signalling pathway has been observed in vascular dementia, Alzheimer's disease and general cognitive impairment (**Figure 3.10B**) [32, 33].

Down-regulated genes

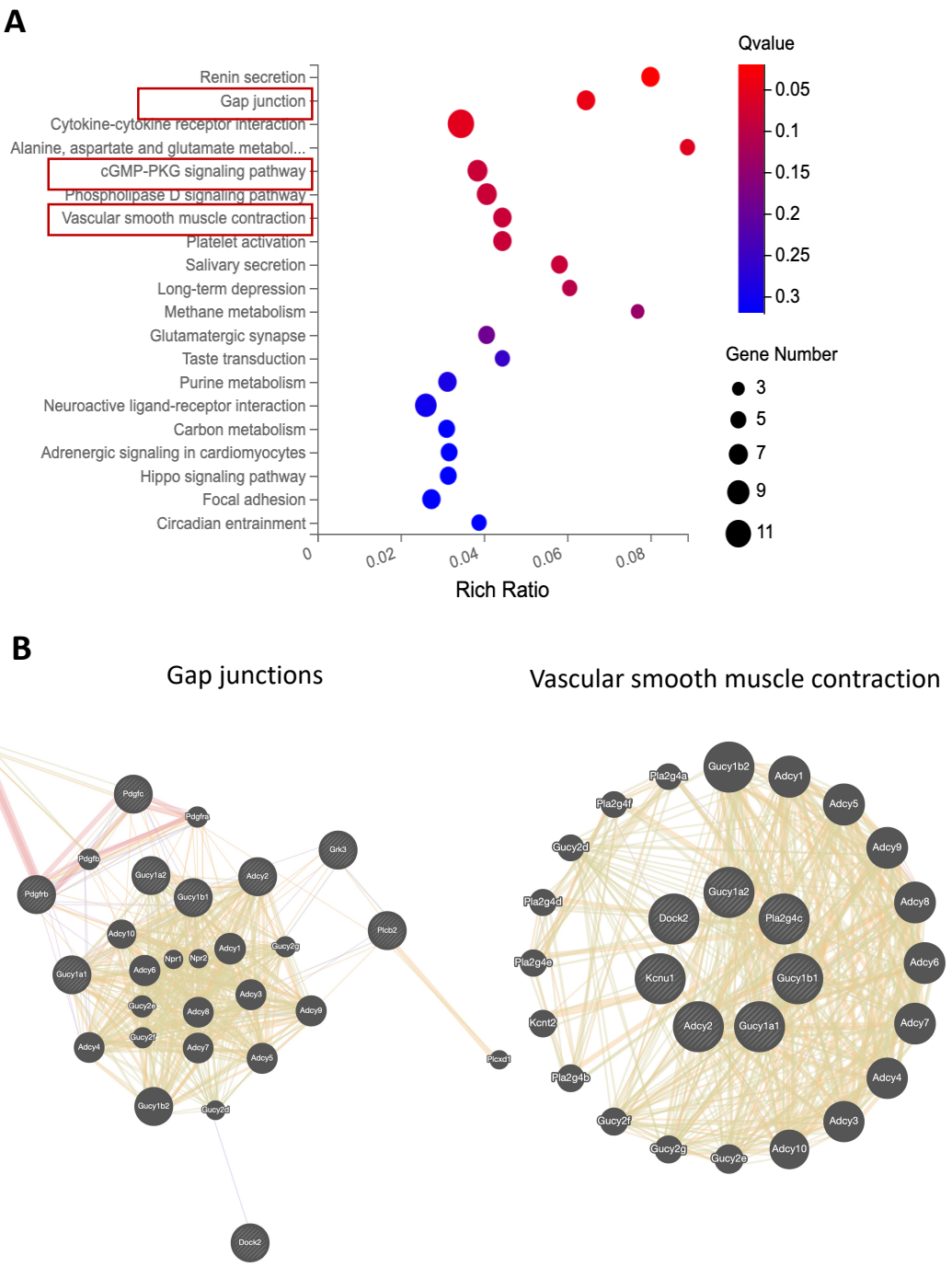


Figure 3.10| Gene Ontology analysis and Network analysis of downregulated genes in ECs from Tchp^{EC} mice.

A. Bubble chart showing enriched pathways in ECs from Tchp KO endothelial specific mice using kegg_pathway annotation classification. The function of Qvalue <= 0.05 is regarded as a significant enrichment. The Bubble chart was generated using BGI Dr.Tom. **B.** left Panel: Gap junctions network cluster with 6 genes. Red lines represent interactions, purple lines indicate co-expression, green lines indicate shared protein domains, yellow lines predicted interactions, blue lines indicates co-localization. Right Panel: Vascular Smooth Muscle Contraction with 6 genes. Red lines represent interactions, purple lines indicate co-expression, green lines indicate shared protein domains, yellow lines predicted interactions, blue lines indicates co-localization. The network analysis was performed with GeneMania.

QPCR was performed to validate the expression of the guanylate cyclases Gucy1a1, Gucy1a2, and Gucy1b1 on RNA extracted from confluent ECs isolated from the brain of WT and Tchp^{EC} mice. Furthermore, after further investigation of the core analysis, I decided to analyse the gene expression of fibroblast growth factor 2 (Fgf2) and platelet-derived growth factor subunit B (Pdgfb). Fgf2 induces angiogenesis through the activation of VEGF [250]. Pdgfb is secreted by ECs and stimulates proliferation, angiogenesis and cell survival by binding to Pdgrb. The qPCR and the following analysis demonstrated a significant down-regulation of Gucy1a1 (p= 0.047) and Fgf2 (p=0.0494) (**Figure 3.11A**).

Further validation was performed on RNA extracted from ECs sorted from WT and Tchp^{EC} mice using MACS® from Miltenyi biotech. Conversely to what was observed in the ECs isolated from WT and Tchp^{EC} mice, the gene expression levels of Gucy1a1 and Fgf2 did not decrease (**Figure 3.11B**).

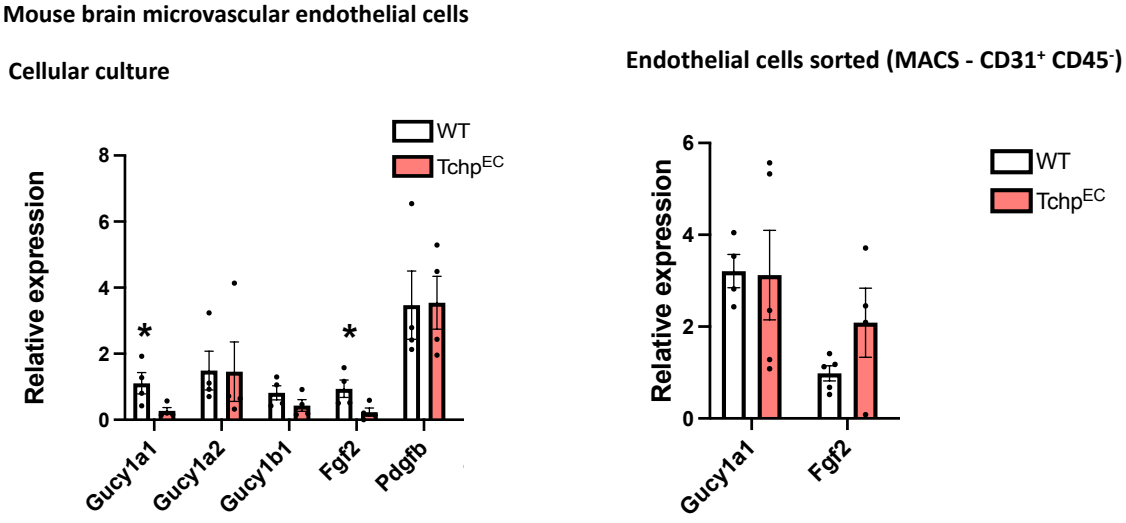


Figure 3.11| TCHP knock-out affects brain microvascular endothelial cell transcriptome in Tchp^{EC} mice.

On the left: expression of Gucy1a1, Gucy1a2, Gucy1b1, Fgf2, Pdgfb in ECs from WT and TCHP^{EC} mice (unpaired *t*-test; Gucy1a1 **P* = 0.047, Fgf2 *P=0.0494). On the right: expression of Gucy1a1, Gucy1a2, Gucy1b1, Fgf2, Pdgfb in ECs from WT and TCHP^{EC} mice sorted with MACS® (CD31+/CD45-). Statistical analyses were performed on at least three independent experiments. Data are represented as mean ± SEM.

To further investigate the downregulated DEGs identified in Tchp^{EC} mice in human cells, the gene expression of GUCY1A1 and FGF2 were analysed in HBMVECs by qPCR. First, HBMVECs were transfected using Tchp siRNA oligonucleotides or control siRNA. Then, gene expression levels were analysed using $2^{-\Delta\Delta Ct}$ quantification. A trend in the decrease of GUCY1A1 and FGF2 is present in TCHP knock-down HBMVECs and must be confirmed by increasing the statistical power (**Figure 3.12**).

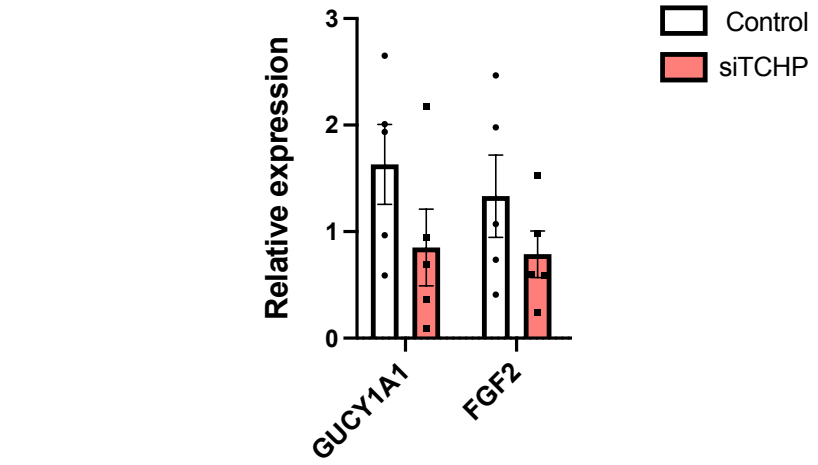


Figure 3.12| TCHP knock-out affects HBMVECs transcriptome.

Expression of GUCY1A1, FGF2 in control and TCHP knock-down HBMVECs. Statistical analyses (Mann Whitney) were performed on at least three independent experiments. Data are represented as mean ± SEM.

Analysis of the effects of TCHP knock-out on the functionality of microvascular ECs

The effects of the lack of Tchp on EC barrier function were investigated through permeability assay using the ECIS® instrument as described in the Material and Methods Chapter. ECs isolated from WT and Tchp^{EC} were grown in the ECIS® array for 7/10 days until confluence. The confluent monolayer of ECs was then kept in basal medium without growth factors for 4 hours and then resistance was recorded. The ECs from Tchp^{EC} brains showed lower resistance compared to the WT ECs. The analysis of the variance of the resistance peak showed a trend in decreasing in Tchp^{EC}

compared to the WT (**Figure 3.13A**). It is important to consider the difficulties in measuring the resistance opposed by the ECs from Tchp^{EC} brains because the cells do not easily form a confluent monolayer.

The permeability assay was then performed on HBMVECs using the ECIS® instrument to confirm the impairment of barrier function associated with the lack of TCHP. HBMVECs were transfected using TCHP siRNA oligonucleotides or control anti-miR and plated on the ECIS® array 2 days after the transfection. The resistance was measured after 3 days from the transfection. Of note, TCHP knock-down ECs presented a lower resistance compared to the control ($p<0.0001$), confirming the impairment of barrier function associated with TCHP knock-down (**Figure 3.13B**).

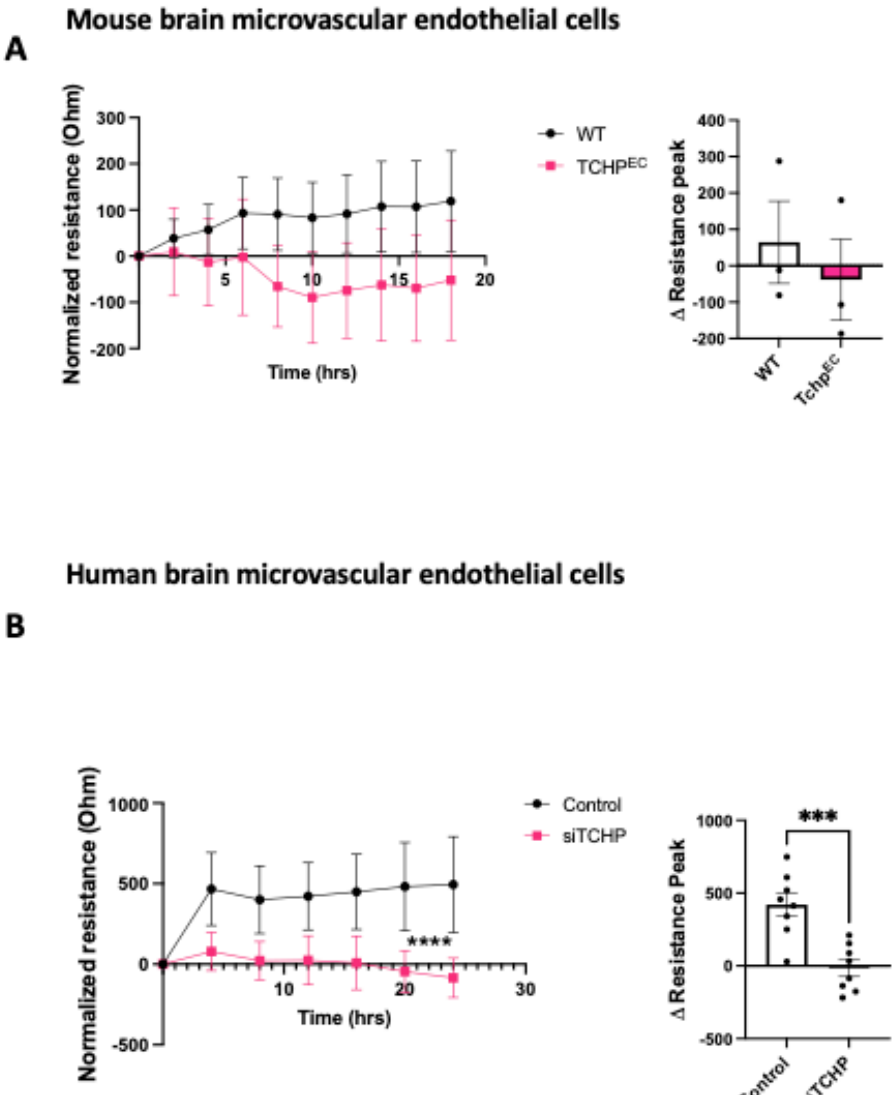


Figure 3.13| TCHP knock-out affects EC function.

A. Left panel: analysis of resistance changes on Tchp^{EC} and WT ECs. Right panel: quantification of resistance variation on Tchp^{EC} and WT ECs. **B.** Left panel: analysis of resistance changes in control and TCHP Knock-down Human Brain ECs (Area under the curve, unpaired t-test of the two AUCs **** $p<0.0001$). Right panel: quantification of resistance variation in TCHP knock-down human ECs and control (unpaired *t*-test *** p=<0.0005). Statistical analyses were performed on at least three independent experiments. Data are represented as mean ± SEM.

To understand the cause of the impaired barrier function associated with the lack of Tchp, I analysed the TJ protein ZO-1 by immunocytochemistry. The analysis of the mean intensity demonstrated significant impairment in ZO-1 in the ECs lacking TCHP ($p<0.0001$) compared to the control, supporting the impairment of barrier function observed using ECIS® (**Figure 3.14**).

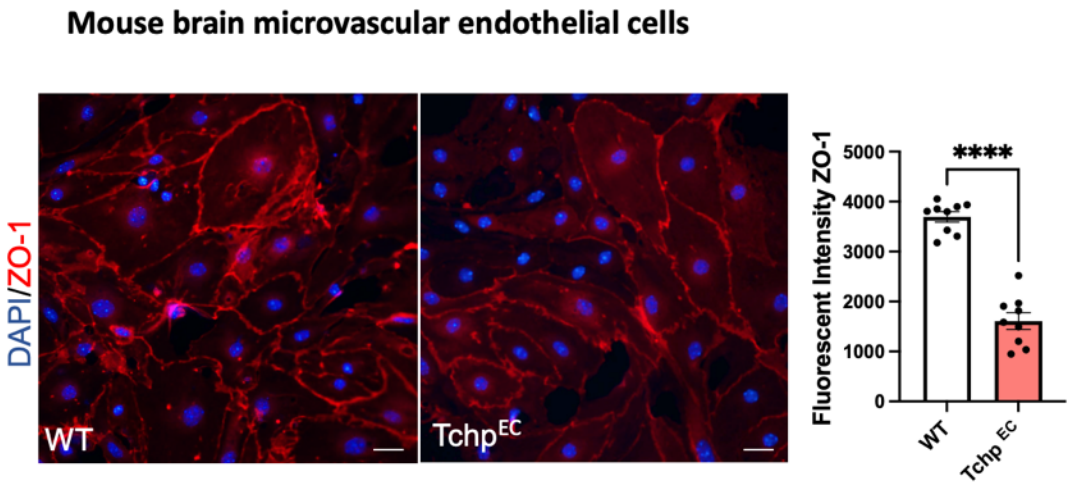


Figure 3.14| Tchp knock-out impairs ZO-1.

Immunocytochemistry and quantification of ZO-1 fluorescent intensity in ECs from WT and Tchp^{EC}. Scale bar=10 µm. (*N*. cells = 600, Unpaired t-test ****P<0.0001). Statistical analyses were performed on at least three independent experiments. Data are represented as mean ± SEM.

Localisation of TCHP in microvascular ECs

To confirm that also in HBMVECs TCHP localises in the centriolar satellites, as previously observed in HUVECs [2], I analysed the colocalisation of TCHP with PCM1, the mitochondrial import receptor subunit TOM20 and with the ER integral protein calnexin.

HBMEC-5i were transduced with TCHP-V5 lentivirus (20 MOI) and stained with antibodies anti-V5, anti-PCM1, anti-TOM20 and anti-Calnexin. Colocalisation was then analysed with Pearson correlation coefficient. The V5 epitope was chosen over commercially available antibodies for TCHP, which we found inaccurate and overstained cellular organelles not corresponding to TCHP. The study revealed that also in HBMVECs, TCHP colocalises with PCM1 in the pericentriolar matrix and

satellite region, in support of the binding of TCHP to PCM1 in these cells. Conversely, TCHP does not seem to localise in the mitochondria (anti-TOM20) or in the ER (anti-Calnexin).

The colocalisation of TCHP with PCM1 supports the hypothesis that also in HBMVECs, TCHP affects autophagy through the stabilisation of PCM1, fundamental for the formation of autophagosome through its binding to GABARAP (**Figure 3.15**).

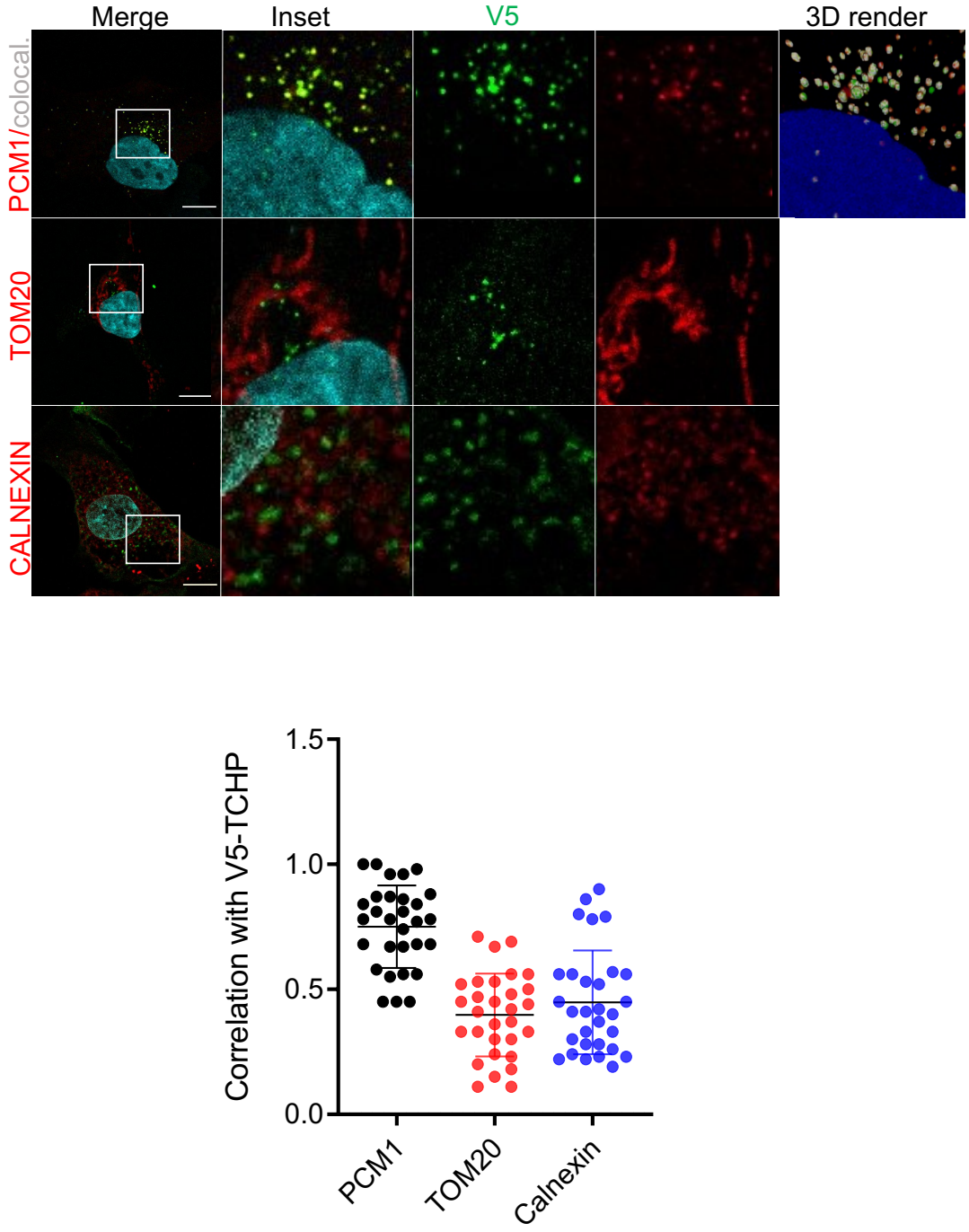


Figure 3.15| Colocalization of TCHP-V5 and centriolar satellite proteins, mitochondria and ER in HBEC-5i.

HBMEC-5i were transduced with TCHP-V5 lentivirus and stained for anti-PCM1 (in red), anti-TOM20 (in red), anti-Calnexin (in red) and anti-V5 (in green) antibodies. The co-localization of TCHP-V5 and PCM1 is white in the 3D rendering. Scale bars 10 µm. **B.** Analysis of co-localization of TCHP-V5 with mitochondria and ER: the two-channel intensity correlation of pixels corresponding to regions identified with TCHP-V5 and organelles (n=30 cells per replicate; Pearson co-localisation coefficient). Statistical analyses were performed on at least three independent experiments.

Characterisation of the effects of TCHP knock-out on cellular organelles

The knock-down of TCHP was previously associated with a change of localisation and intensity of the components of the endo-lysosomal pathway. Furthermore, TCHP knock-down caused modifications of the cytoskeleton [2]. For this reason, I decided to investigate how the knock-down affects several cellular organelles, focusing on transcytosis vesicles, intermediate filaments, endo-lysosomal pathway and cytoskeleton. Immunocytochemistry was performed to analyse CAV-1, vimentin, calnexin and clathrin, α-Tubulin and phalloidin.

CAV-1 is a scaffold protein of caveolae on the plasma membrane, which has an important role in endocytosis and in EC polarisation and migration [251]. α-Tubulin is a component of microtubules of the cytoskeleton that plays a fundamental role in the regulation of cell shape, migration and cell division. Clathrin is a scaffold protein fundamental for endocytosis. Calnexin is a chaperone protein belonging to ER essential for protein folding. Phalloidin staining was used to investigate actin and stress fibers, as suggested by the bulk RNA-seq and PGSEA analysis that highlighted these two activated pathways. Vimentin is a major intermediate filament that maintains cellular integrity and provides resistance against stress [252]. I was interested in observing if there was any disruption in the fibre network of vimentin due to the formation of stress fibers and, consequently, an increase in BBB permeability.

Opposite to what we previously observed in HUVECs, the immunocytochemistry anti-α-Tubulin and the staining anti-phalloidin did not highlight any defect in the cytoskeleton or formation of stress fibers in TCHP knock-down HBMEC-5i (**Figure 3.16A, 3.16B**). Furthermore, the immunocytochemistry did not show any modification in vimentin integrity (**Figure 3.16C**). The knock-down of TCHP did not affect the vesicles clathrin and calnexin (**Figure 3.16D, 3.16E**).

Of note, CAV-1 localisation changed from the edge of the plasma membrane to the abluminal plasma membrane and surrounding vesicle structures in the cytoplasm, suggesting TCHP knock-down affects caveolae-mediated transcytosis (**Figure 3.16F**).

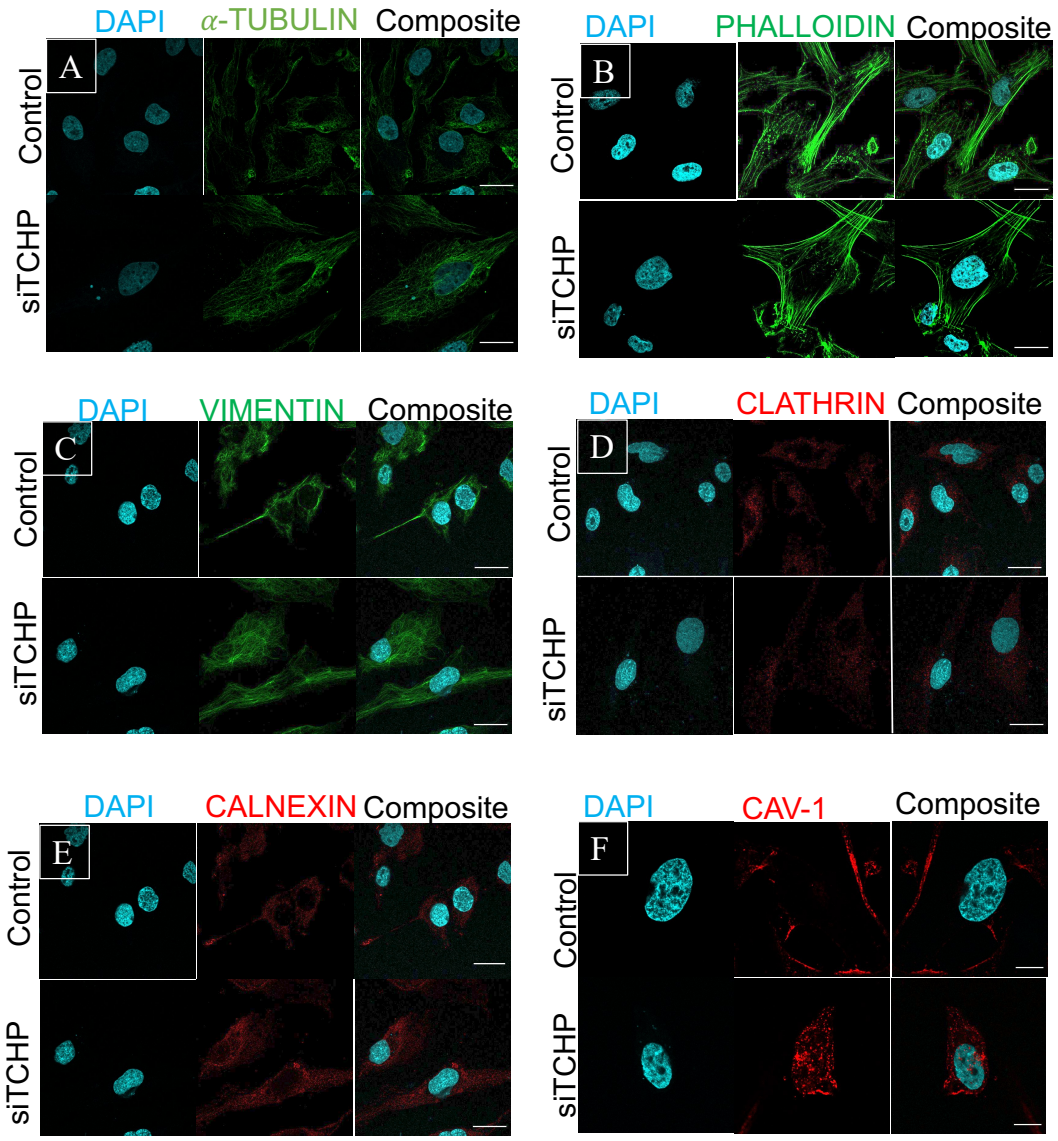


Figure 3.16| Analysis of cellular organelles in HBMEC-5i.

HBMEC-5i were transfected with TCHP siRNA or Anti-miR negative control and stained for **A.** anti-α-Tubulin . **B.** anti-phalloidin **C.** anti-vimentin **D.** anti-clathrin **E.** anti-calnexin **F**. anti-caveolin-1. Scale bars, 10 µm.

Lack of TCHP affects CAV-1 localisation

Since we observed the change in the localisation of CAV-1 in the HBMEC-5i, which were chosen for the first immunocytochemistry screening because easier to grow and handle for multiple experiments, I decided to analyse if the same phenotype occurs in non-immortalized HBMVECs.

The immunocytochemistry anti-CAV-1 confirmed that also in the primary cells, the knock-down of TCHP increases CAV-1 vesicles in the abluminal plasma membrane and in the cytoplasm (**Figure 3.17**).

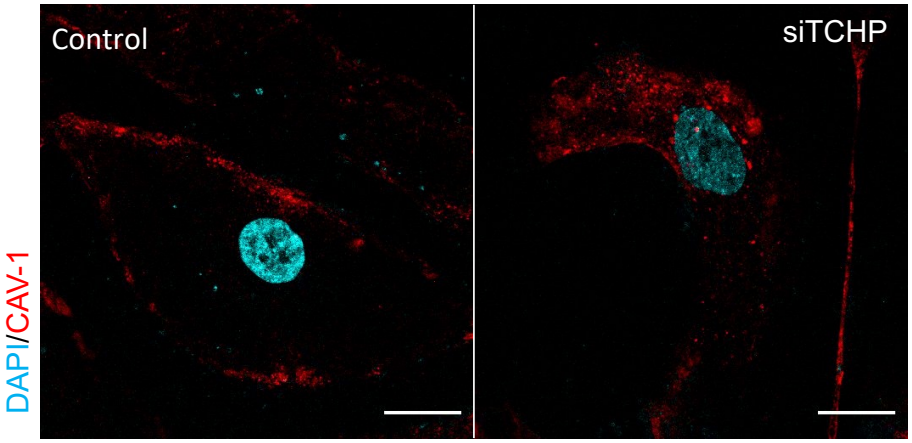


Figure 3.17| Analysis of cellular organelles in HBMVECs.

Immunocytochemistry analysis of anti-CAV-1 in HBMVECs. Scale bars, 10 µm.

The quantification of the mean intensity of CAV-1 in HBMEC-5i demonstrated the increased level of CAV-1 in the ECs lacking TCHP ($P<0.0001$), confirming TCHP mediated effect on caveolae-mediated transcytosis (**Figure 3.18**). It is well known that ECs from the central nervous system present a low level of transcytosis vesicles [46]; consequently, the increased levels of CAV-1 could affect the BBB integrity, in line with the impaired barrier function previously described *in vitro*.

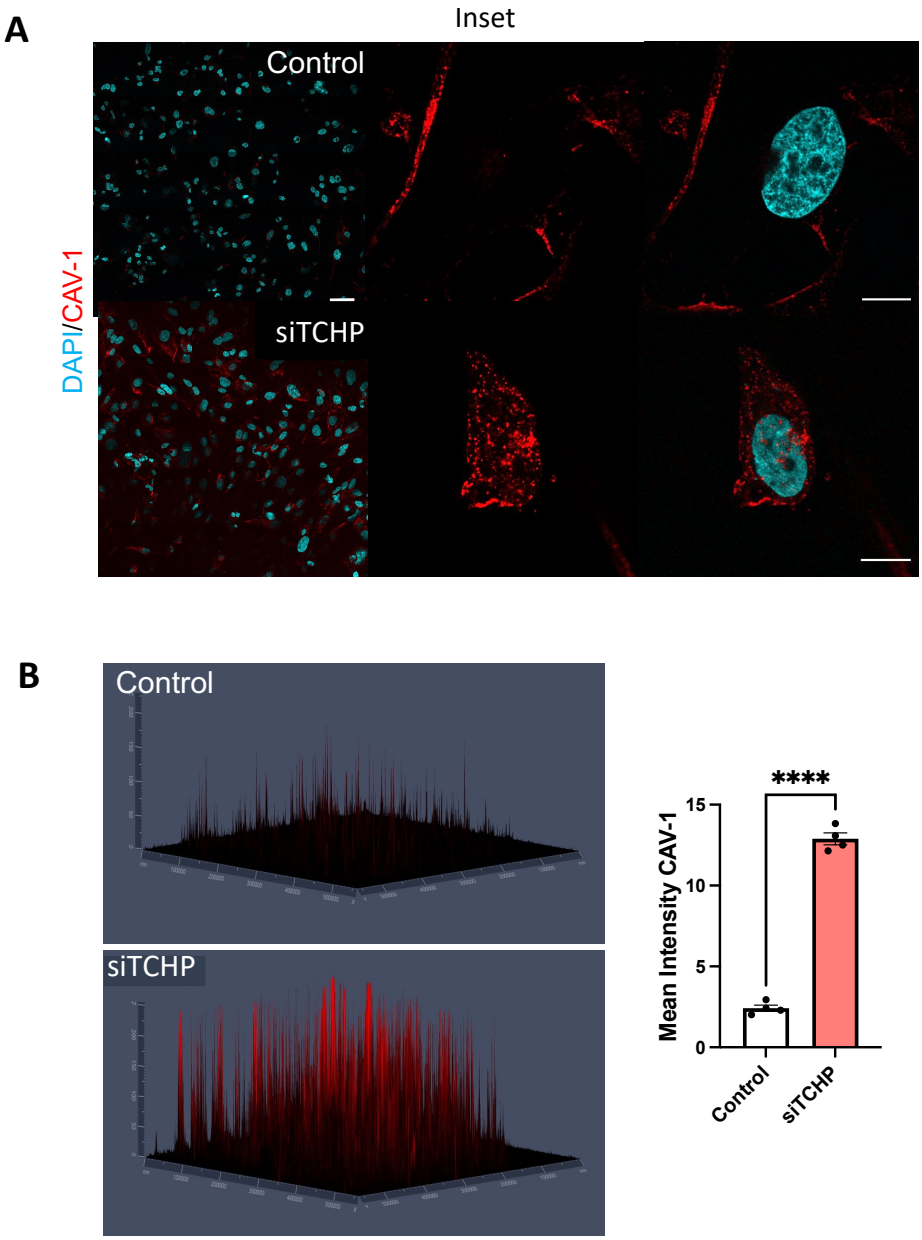


Figure 3.18| Analysis of CAV-1 in HBMEC-5i.

A. HBMEC-5i were transfected with TCHP siRNA or Anti-miR negative control and stained for anti-Caveolin-1. **B.** 2.5D profile showing the increased CAV-1 intensity in red in TCHP knock-down ECs and quantification (*N*. cells = 50, Unpaired t-test ****P<0.0001). Scale bars, 50 µm and 10 µm in the inset. Statistical analyses were performed on at least three independent experiments. Data are represented as mean ± SEM.

Discussion

This chapter aimed to characterise brain ECs lacking TCHP, either isolated from the brain of $Tchp^{EC}$ mice or human brain ECs transfected to get TCHP knock-down. The bulk RNA-seq and the following validation through qPCR demonstrated the activation of inflammatory pathways such as chemokine and cytokine signalling. Moreover, gelatine zymography confirmed the production of MMPs in HBMVECs as highlighted by the RNA-seq.

TCHP knock-down caused an impairment of barrier function both in ECs isolated from $Tchp^{EC}$ mice and HBMVECs, as demonstrated by the decrease of ZO-1 in ECs from $Tchp^{EC}$ mice brains and the increased production of MMP9.

Finally, the immunocytochemistry confirmed the colocalisation of TCHP with PCM1, as previously observed in HUVECs. Cytoskeleton proteins were not affected by the knock-down of TCHP, but an increased caveolae-mediated transport was observed in the TCHP knock-down HBMEC-5i and confirmed in HBMVECs.

Tchp knock-down elicits inflammation and impairs barrier function

TCHP knock-down was previously associated with an inflammatory transcriptome and SASP in HUVECs, demonstrated by an increased gene expression of the proinflammatory interleukins IL-6, IL-8, IL-1β and of the senescence marker p16 [2]. To investigate if the knock-out of Tchp was causing the same phenotype in the brain of $Tchp^{EC}$ mice, I performed bulk-RNA sequencing.

First, I isolated the ECs from the brain of WT and $Tchp^{EC}$ mice using a new protocol developed in collaboration with Dr Alessio Alfieri (University of Edinburgh). The protocol, presented in the "Materials and methods" chapter, allowed the isolation and culture of ECs that kept their morphology, such as the expression of TJ proteins, necessary to induce a high transendothelial resistance. This was demonstrated by the permeability assay performed using the ECIS® instrument when after treatment with LPS or thrombin, the resistance dropped, confirming the opening of the barrier between the ECs.

The bulk RNA-seq and the following PGSEA and KEGG pathway enrichment analysis highlighted the presence of stress fibers and contractile actin filament bundle, cytokine-cytokine receptor interaction, ECM-receptor interaction, PPAR signalling, chemokine signalling, cell adhesion molecules and degradation of the extracellular matrix among the activated pathways. The following immunocytochemistry analysis performed to investigate cytoskeleton modifications in TCHP knock-down ECs did not show any obvious difference in stress fibers and actin filaments compared to the control, opposite to what was previously observed in HUVECs [2].

The validation through qPCR on ECs from culture and sorted with MACS® from WT and $Tchp^{EC}$ brains demonstrated an increased gene expression of the chemokine Ccl5. This upregulation was also confirmed in TCHP knock-down HBMVECs. Ccl5, also known as RANTES (regulated upon activation, normal T cell expressed and secreted), belongs to CCL5/CCR5 axis and is associated with chronic inflammation in several diseases. It is involved in inflammation maintenance and attraction via haptotaxis of immune cells. Furthermore, it induces MMPs to stimulate the migration of cells into the site of inflammation [253]. CCL5 was found in the microcirculation of patients with Alzheimer's disease and its expression was upregulated by oxidative stress in brain ECs and associated with the recruitment of immune cells and increased neuronal death in a brain injury model [238, 254]. Consequently, its presence in the ECs of $TCHP^{EC}$ mice and TCHP knock-down HBMVECs suggest that the inflammatory transcriptome already observed in HUVECs is also present in the brain ECs lacking TCHP.

The pro-inflammatory transcriptome observed in ECs lacking TCHP could be due to the impairment of autophagy previously demonstrated in HUVECs, where TCHP acts as a regulator of autophagy through the stabilisation of the complex GABARAP-PCM1, fundamental for the formation of autophagosome [2]. Impaired autophagy within ECs has been recently linked with a pro-inflammatory phenotype [255]. EC autophagy normally declines with ageing, contributing to several vascular diseases. This was demonstrated by pharmacological interventions using spermidine [256], trehalose [126] and rapamycin [257], compounds that restored autophagy and reverted arterial ageing. Impairment of autophagy in vascular cells produces high levels of metabolic stress and compromises their functionality [258]. The decline of

autophagic capacity provokes low-grade inflammation. Indeed, autophagy is usually involved in clearing dysfunctional mitochondria, preventing excessive ROS production and activation of inflammasomes. During ageing, the decline of autophagy increases ROS production, and the uncleared aggregated proteins activate inflammasomes which provoke a low-grade inflammation. Furthermore, the impairment of autophagy causes an accumulation of P62, which leads to the activation of NF-κB via mTORC1 [135] or TRAF6 [134] polyubiquitination, leading to inflammation.

Previous studies carried out in the lab demonstrated that the downregulation of TCHP in HUVECs did not affect genes associated with angiogenesis like VEGFR1, PDGFB and PDGFA. The RNA-seq confirmed that these genes are not differently expressed in the knock-out ECs from the $Tchp^{EC}$ mouse compared to the control. Interestingly, Fgf2 is downregulated compared to the control, suggesting that angiogenesis could be affected by the knock-out in the brain ECs. Other genes of which we did not expect a difference in the knock-out are the ones associated with the Pgp pump, responsible for the exit of puromycin, because we already observed that puromycin was not affecting the expression of characteristic endothelial markers in vitro. This was confirmed by the RNA-seq.

The results of the RNA-seq and following mRNA validation must be confirmed at a protein level, by immunocytochemistry or immunohistochemistry and western blotting analyses.

The RNA sequencing analysis highlighted the activation of "Degradation of the extracellular matrix" pathway in the ECs from the brain of $Tchp^{EC}$ mice. The gelatine zymography analysis of the medium collected from the ECs from WT and $Tchp^{EC}$ mice revealed a trend of increased production of MMP9. In the HBMVECs, the knock-down of TCHP caused a statistically significant production of MMP9, supporting the data obtained from the KEGG pathway enrichment analysis. In line with this, the permeability assay performed using ECIS® demonstrated an impairment of barrier function in the TCHP knock-down HBMVECs and a trend in the ECs from the brain of $Tchp^{EC}$ mice. Furthermore, the immunocytochemistry analysis of ZO-1 confirmed impairment of the TJs in the ECs from the brain of $Tchp^{EC}$ mice, supporting the

decreased transendothelial and paracellular barrier resistance. In normal conditions, MMPs are involved in the remodelling of the extracellular matrix to support homeostatic processes, such as neurogenesis and angiogenesis [63]. In pathological conditions, though, MMPs are responsible for losing the BBB integrity by the digestion of TJ and basement membrane proteins. MMP9 is involved in the pathogenesis of multiple sclerosis, cerebral aneurysms, stroke, epilepsy, Alzheimer's disease, Parkinson's disease and brain cancer [248]. Elevated levels of MMP9 have been associated with white matter hyperintensities in non-stroke individuals [259]. Moreover, high levels of MMP9 have been found in Pdgfrb-null and Alzheimer's disease mouse models, associated with decreased collagen levels [260, 261].

In all these disorders, MMP9 is involved in neuroinflammation. The metalloproteinase can activate neuroinflammatory pathways indirectly or directly, indirectly through the interaction with cytokines, cell surface receptors, cell–cell adhesion molecules, or clotting factors [262, 263]. Directly activating neuroinflammatory pathways, such as TNF-α [264, 265]. It can also contribute to neuroinflammation-mediated neurotoxicity, affecting GABA and glycine level, modulating chloride channel activity, altering ECM-cell interaction, and starting the apoptotic pathway Fas/FasL [266, 267]. Overall, the activation of MMP9 could contribute to the inflammation present in the ECs of $Tchp^{EC}$ mice and cause the impairment of ZO-1 and barrier function. In the future, studies on CLDN-5 and occludin will be performed to understand if the knock-out of Tchp affects other TJ proteins and this will also be investigated in HBMVECs.

Interestingly, the treatment with the NF-κB inhibitor BAY11-7082 showed a reduction in the level of MMP9 in the ECs from $Tchp^{EC}$, suggesting that acting on NF-κB inflammatory pathway would also decrease MMP production.

To summarise, the knock-down of Tchp causes the activation of inflammatory pathways associated with increased production of MMP9 and impairment of barrier function. This inflammation could be due to an impairment of the autophagic process, as previously demonstrated in HUVECs , although the role of autophagy in maintaining brain EC homeostasis and BBB integrity is still unclear.

Effects of TCHP knock-down on NO-sGC-cGMP pathway

The bulk RNA-seq revealed the downregulation of genes associated with endothelial dysfunction in the ECs from Tchp^{EC} mice. Among these, Gucy1a1, Gucy1a2, Gucy1b1, genes that encode for sGC protein, consequently their modified transcriptomic could cause an impairment of NO-sGC-cGMP signalling pathway, fundamental for vasodilatation and platelet aggregation. Of particular interest, Gucy1a1 is associated with Moyamoya disease, a cerebrovascular disorder consisting of the progressive narrowing and blocking of the arteries of the basal ganglia.

The qPCR validation demonstrated a decrease in mRNA expression of Gucy1a1 and the angiogenesis regulator Fgf2 in the ECs from the brain of Tchp^{EC} mice. Conversely, the analysis of ECs sorted using MACS®, did not confirm the downregulation of these mRNAs. mRNAs expression was investigated both on sorted and culture cells because the literature demonstrates that culture induces changes in EC transcriptome. Several biological pathways are perturbed *in vitro*. King et al showed different canonical pathways significantly altered *in vitro* in primary hippocampal cell cultures compared to the hippocampal tissue [268]. Goldeman et al demonstrated that there are differences in mRNA expression in brain capillaries and brain endothelial *in vitro* cultures, such as efflux transporters, that can affect drug delivery studies [269]. ECs sorted are not affected by external factors such as the puromycin selection. Furthermore, differences in the metabolism and oxidative species have been demonstrated between culture and sorted cells [270].

The qPCR analysis showed a trend in the downregulation of GUCY1A1 and FGF2 mRNA expression in HBMVECs, but more replicates are necessary to confirm this. Differences between human and murine cultures are common. Indeed, even if humans and mice share 90% of the genes, species-specific differences between mouse ECs and human brain ECs must be considered. A benefit of human cell lines is that they are easier to culture compared to the primary cells isolated from mice. It is important to highlight that in this study only data coherent in both species are being considered for further investigations.

TCHP localises in the centriolar satellites and affects transcytosis

TCHP was previously localised in the pericentriolar matrix and satellite region in HUVECs, stabilising PCM1 and consequently the binding with the autophagic protein GABARAP [2]. To confirm the localisation of TCHP in brain ECs, I used HBEC-5i. I chose HBEC-5i over primary HBMVECs for the first screening because they can be grown in higher numbers for several immunocytochemistry analyses.

TCHP was previously associated with the tethering between ER and mitochondria. Vecchione et al. demonstrated that TCHP resides on the outer mitochondrial membrane, where it would interact with mitofusin 2 to promote a fission-like phenotype and the redistribution of mitochondria near nuclear membranes [195]. Cerqua et al. reported that TCHP regulates ER-mitochondria juxtaposition via mitofusin 2 and confers H_20_2-induced cell death resistance [196]. Furthermore, TCHP-enabled decorin evoked mitophagy in a breast cancer cell model [197]. Because of this strong association with ER and mitochondria, I investigated the colocalisation between TCHP, mitochondrial protein TOM20 and the ER protein calnexin.

The colocalisation analysis performed with Pearson analysis confirmed that TCHP colocalises with PCM1 also in HBMEC-5i, while the colocalisation coefficient was lower for ER (calnexin) and mitochondria (TOM20). This aligns with the hypothesis that TCHP knock-down impairs autophagy in brain ECs, causing inflammation and impairment of barrier function. The role of autophagy in the regulation of BBB integrity still needs to be clarified. Autophagy activation attenuates ECs apoptosis, reduces ROS production, and restores decreased levels of ZO-1, while autophagy impairment increases them [192]. Conversely, other studies identified a detrimental role for autophagy in ischemia. Inhibiting autophagy would improve recovery after brain ischaemia, and activation would promote the degradation of CLDN-5 [164] and occludin in brain ECs and capillaries [165]. Identifying the role of autophagy in brain ECs homeostasis is necessary to further understand its role in the pathogenesis of cerebrovascular diseases.

It was previously reported that TCHP interacts with the centrosomal proteins Odf2 and Ninein, localised in the mother centriole, regulating the anchoring of microtubules at the centrosome in proliferating cells [200]. Furthermore, it was

reported that TCHP knock-down causes modifications in the microtubule network, characterised by the absence of centrosome-anchored microtubule aster in HUVECs [2]. The examination of the cellular cytoskeleton showed no obvious change of actin filament or α-tubulin in HBMEC-5i. Furthermore, I did not observe any alterations in the stress fibres, conversely to what was highlighted by the PGSEA analysis of the bulk RNA-seq data. This could be due to the resistance of brain microvascular ECs to actin remodelling, as demonstrated by Reinitizet al., who reported that HBMECs resist cytoskeleton modification under shear stress [271].

Since TCHP was associated with regulating the tethering between ER and mitochondria [196], I investigated if the knock-down of TCHP affects ER. The immunocytochemistry analysis of calnexin, a chaperone protein belonging to ER, showed no modification caused by the TCHP knock-down.

Then, because of the emerging role of intermediate filaments in keeping the BBB integrity, I analysed vimentin. Vimentins bind focal adhesion, increasing resistance against shear stress by reinforcing the attachment of the cells to the matrix [272-274]. As said above, opposite to HUVECs, HBMECs resist actin modelling and elongation when exposed to shear stress; consequently, vimentin has a pivotal role in regulating cytoskeletal organisation [271]. Indeed, BBB permeability changes because of the formation of stress fibres and consequently actin reorganisation, which causes increasing tension in the cytoskeleton and cells are pulled away from each other because of contraction [252, 275]. Therefore, intermediate filaments are essential in keeping the BBB integrity. The immunocytochemistry analysis did not show modifications of vimentin, suggesting it is not affected by TCHP knock-down.

Finally, the lack of TCHP was reported to affect the endo-lysosomal pathway [2]. I analysed two main endocytosis processes in brain ECs: clathrin-dependent and caveolae-mediated endocytosis. The immunocytochemistry analysis of the scaffold protein clathrin showed no difference in TCHP knock-down compared to the control. Conversely, caveolin-1 mean fluorescent intensity was significantly higher in TCHP knock-down HBMEC-5i, and its localisation changed from the edge of the plasma membrane to the abluminal plasma membrane and surrounding vesicle structures in the cytoplasm. To confirm that the phenotype was not due to the use of immortalised cells, I established the change of CAV-1 intensity and localisation also in HBMVECs.

This suggests that TCHP knock-down affects caveolae-mediated endocytosis, while it does not affect clathrin-dependent endocytosis. An essential characteristic of the brain ECs is the low rate of vesicular transport. Indeed, caveolae-mediated vesicle trafficking is strongly present in the ECs of peripheral tissues, such as the heart and lung, but not in the brain. Emerging evidence demonstrates the importance of caveolae-mediated transcytosis in keeping the BBB functioning [50, 276]. Increased caveolae-mediated trafficking has been associated with increased brain permeability in the ischaemic stroke [232, 277]. It was reported that the transporter Mfsd2a prevents caveolae-mediated trafficking by regulating the lipid composition and, thus, holding BBB integrity [46]. Mfsd2a transporter has been associated with the formation of the BBB, and its genetic ablation results in disruption of the BBB from embryonic stages [276].

In the future, Mfsd2a expression will be investigated in ECs lacking TCHP to understand better the mechanism through which TCHP is involved in the increased caveolae transcytosis. Of note, TCHP has been associated with the regulation of adipogenesis. Yamakawa et al. reported that TCHP knock-out caused elongated cilia and consequently inhibited CAV-1, blocking lipid rafts from assembling around the ciliary base and affecting adipogenesis in a TCHP knock-down mouse model. Mesenchymal progenitors lacking TCHP fail to differentiate into adipocytes [207]. Further analysis is necessary to understand the exact mechanism through which TCHP affects transcytosis.

Conclusions and future directions

In this chapter, I characterised brain ECs lacking TCHP, either isolated from the brain of $Tchp^{EC}$ mice or human brain ECs transfected to get TCHP knock-down. To isolate the brain microvascular ECs, I have used a new protocol that allows the cultivation of the primary cells without losing their morphology**,** such as the expression of TJ proteins necessary to induce a high trans endothelial resistance.

The bulk RNA-seq and the following validation through qPCR demonstrated the activation of inflammatory pathways, such as chemokine and cytokine signalling, characterised by the upregulation of Ccl5. The knock-down of TCHP caused an

impairment of barrier function in both ECs isolated from $Tchp^{EC}$ mice and HBMVECs. In support of this hypothesis, ZO-1 was impaired in ECs from the $Tchp^{EC}$ brain, and MMP9 production increased in the ECs lacking TCHP. Finally, an increased caveolae-mediated transport was observed in the TCHP knock-down HBMEC-5i and confirmed in HBMVECs. The immunocytochemistry confirmed the colocalisation of TCHP with PCM1 as previously observed in HUVECs, suggesting the increase of inflammation and impairment of barrier function could be due to the impairment of autophagy previously observed in HUVECs.

Further investigations are necessary to clarify the connection between the increase of caveolae-mediated transcytosis and the downregulation of TCHP through the analysis of the transporter MFSD2A and lipidomic expression analysis of TCHP knock-down ECs.

Chapter 4

Phenotypic characterisation of brain vasculature of endothelial-specific Tchp knock-out mice

Chapter 4 Phenotypic characterisation of brain vasculature of endothelial-specific Tchp knock-out mice

Introduction

The BBB is comprised of specialised ECs lining the brain's microcirculation. These ECs are characterised by TJs, lack of fenestrations and specific transporters that protect the brain from toxic substances and harmful compounds and supply the brain with nutrients such as glucose, ATP, glycogen and phosphocreatine. Impairment of the BBB and its increased permeability cause the entrance of plasma proteins and immune cells in the brain parenchyma, leading to neuroinflammation, involved in cerebrovascular and neurodegenerative disease [87].

Endothelial dysfunction is involved in the opening of the BBB. Oxidative stress caused by increased production of ROS and RNS causes endothelial dysfunction, impairment of TJs and activations of MMPs [89]. Moreover, an increase in ROS affects NO signalling. In physiological conditions, NO controls cerebral blood flow through vessel dilatation and acts as a neurotransmitter to regulate vascular smooth muscle cells and Ca^{2+} levels, protecting neurons from excitotoxicity [278, 279]. Furthermore, decreased bioavailability of NO increases oxidative stress and endothelial dysfunction leading to BBB impairment [90]. ROS also impair potassium channel function, which is required for cerebrovascular dilatory responses [89].

Another factor that contributes to BBB impairment is inflammation. The pro-inflammatory cytokines and chemokines produced by several cells, including ECs, cause inflammation. Inflammation leads to the disruption of the BBB [87], directly through the impairment of TJ assembly and through the activation of Rho-kinase signalling involved in the internalisation of TJs [91], indirectly through the activation of MMPs [92]. Furthermore, pro-inflammatory cytokines can activate apoptotic pathways, upregulate the MAPK pathway and consequently reduce TJs and cause dysregulated transcytosis [93]. The pro-inflammatory cytokines also cause an increased expression of cell adhesion molecules which leads to leukocyte infiltration [89].

Microglia elicits neuroinflammation. Microglia represent the brain's resident immune cells and are activated by inflammatory stimuli [280]. Activated microglia

produces pro-inflammatory molecules, such as cytokine, chemokines and ROS [75], leading to neuroinflammation and BBB dysfunction [281]. Between the factors secreted by activated microglia are IL-1β, TNF, IL-6, and monocyte chemoattractant protein-1 (MCP-1) [282, 283]. These pro-inflammatory molecules cause necroptosis, leading to the death of ECs and consequently disrupting the BBB. In addition, excessive microglia activation affects the surrounding healthy neuronal tissue, which will secrete factors that stimulate inflammation and exacerbate neuroinflammation [76].

The inflammation and the disruption of the BBB cause the infiltration of leukocytes into the brain, which are not present in physiological conditions. This is due to adhesion molecules such as ICAM and VCAM, selectins and leukocyte integrins on the surface of ECs, produced because of inflammation [99]. Infiltration of these immune cells affects vessel perfusion and leads to a consistent and chronic inflammation status. Furthermore, leukocytes produce ROS, causing activation of the NF-κB pathway and exacerbating inflammation [89].

Pericytes play a role in the recruitment of leukocytes inside the brain by opening intra-pericytes gaps. These cells are also involved in neuroinflammation since they can release inflammatory molecules and MMP9 when exposed to IL-1β or TNF-α [284]. Furthermore, pericytes contribute to regulating cerebral blood flow, and pericyte death due to accumulation of Aβ has been demonstrated in Alzheimer's disease. Armulik et al. showed that pericytes are essential in keeping BBB integrity *in vivo.* Indeed, pericyte deficiency causes the passage of low-molecular-mass and high-molecular-mass tracers and increases endothelial transcytosis [54]. Furthermore, pericytes regulate the specific BBB ECs gene expression, impairing EC function when lost [54, 55].

Astrocytes are another important component for BBB integrity. Under pathological conditions, astrocytes activate and secrete inflammatory factors, such as VEGF-A and MMPs. Shan et al. described the secretion of VEGF-A and MMP9 in a mouse model of middle cerebral artery occlusion. The decrease of these two molecules improved BBB impairment [285]. Furthermore, astrocytes release IL-6, increase BBB permeability, and induce TJ reorganisation [286, 287].

Cerebrovascular alterations, including modified cerebral blood flow, structural alterations and reduced dilatory functions, have been reported in Alzheimer's disease, dementia, ageing and traumatic brain injury [288-290]. Patients with Alzheimer's disease present frequent deformations such as focal constrictions, twisting and looping [291-293]. Obenaus et al. reported that vascular network and complexity are reduced in a rat model of traumatic brain injury [290]. Furthermore, cerebral blood flow is usually reduced in vascular cognitive impairment, leading to neuronal death and white matter injury. Cerebrovascular alterations have been linked with ROS produced by NADPH oxidase [294, 295]. Indeed, ROS would sequester NO, stopping endothelial-mediated dilatation [296] and affecting potassium channel function [288, 297].

In this chapter, I will characterise the cerebral vasculature of Tchp^{EC} mice, focusing on BBB permeability and vascular network modifications. Furthermore, I will delve into the effects of Tchp knock-out on the permeability of the heart. Finally, I will investigate the recruitment of immune cells in the brain of Tchp^{EC} mice to understand if the knock-out of Tchp is associated with neuroinflammation.

Hypothesis and aims

Given the pro-inflammatory transcriptome observed in the ECs isolated from the brain of Tchp^{EC} mice and confirmed in HBMVECs, as well as the increased production of MMP9 and impairment in ZO-1, I decided to investigate the effects of the knock-out of Tchp on the BBB. Therefore, I have analysed vascular permeability, vascular network alterations and recruitment of immune cells in the brain of Tchp^{EC} mice.

The hypothesis presented in this chapter is: "Tchp knock-out affects cerebral vasculature, leading to increased permeability of the BBB and altering vascular network".

Aims:

- The characterisation *in vivo* of vessel permeability in the brain of WT and Tchp^{EC} mice.
- The characterisation of vessel network in the Tchp^{EC} brain.

- The analysis of immune cells in the brain of Tchp^{EC} and WT mice.

Results

In vivo analysis of vessels permeability in WT and Tchp^{EC} mice

Analysis of BBB permeability

In the previous chapter, I described the impairment of barrier function associated with Tchp knock-out in the ECs isolated from Tchp^{EC} mice and HBMVECs. To understand if this defect was also present *in vivo* and the effects at a BBB level, I treated 3 months old WT (males, n=3; females, n=3) and 3 months old Tchp^{EC} (males, n=6; female, n=2) mice with a low molecular weight fluorescent tracer, dextran (3 kDa). Permeability index calculations demonstrated that brains from Tchp^{EC} mice presented a higher permeability than the WT ones (P= 0.0352). The kidney was used as a control to check basal permeability in the other tissues. As expected, basal kidney permeability is greater than the brain since it presents a rich fenestrated endothelium (**Figure 4.1**).

Immunohistochemistry analysis was performed to confirm the extravasation of the fluorescent tracer from the vessels of Tchp^{EC} mice. Image processing and 3D reconstruction were conducted in collaboration with Dr Spartaco Santi (CNR Institute of Molecular Genetics "Luigi Luca Cavalli-Sforza", Unit of Bologna at IRCCS Istituto Ortopedico Rizzoli). The 3D reconstruction (**Figure 4.1C-A**) and the immunohistochemistry (**Figure 4.1C-B**) staining demonstrated the exit of the dextran outside the vessels (anti-CD31) in Tchp^{EC}. At the same time, in the WT mice, the tracer is restricted to the vasculature. This is in line with what the studies *in vitro* highlighted and suggests that the knock-out of Tchp is associated with increased permeability in the BBB.

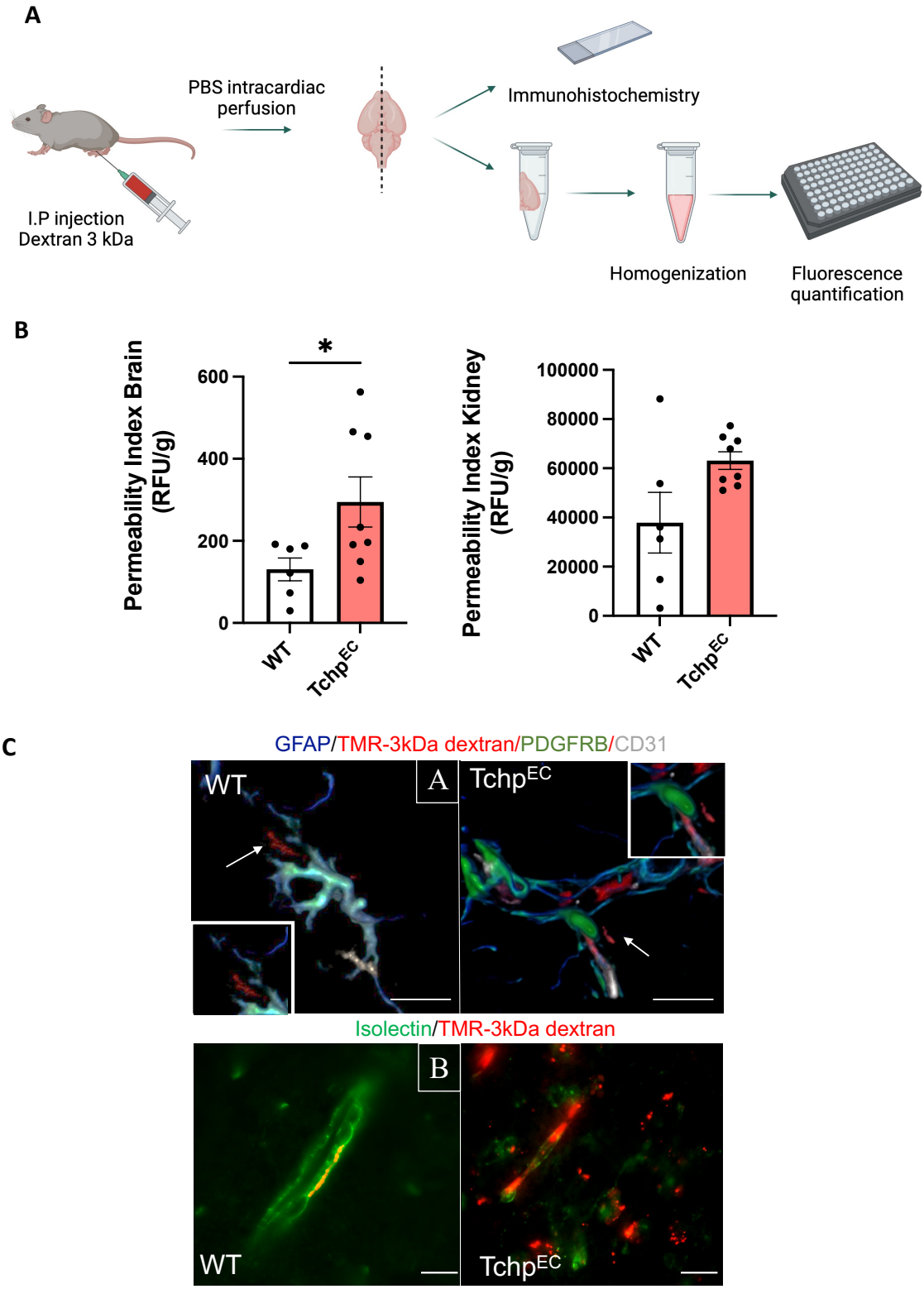


Figure 4.1| Analysis *in vivo* of vessel permeability in WT and Tchp^{EC} mice.

A. Protocol for the quantification of BBB permeability. **B.** Fluorescence quantification of brain permeability in WT (males, n=3; females n=3) and Tchp^{EC} (males, n=6; female, n=2) mice. Unpaired t-test, brain *P=0.0352. **C** Immunofluorescence staining for tracers to assess brain permeability changes in Tchp^{EC} mice. Increased permeability of 3 kDa TMR-dextran tracer (in red) can be visualized in Tchp^{EC} mice compared to WT. Staining for CD31 (A) and Isolectin in green (B) confirms the presence of vessels. Scale bar=10 µm.

Analysis of vessels permeability in heart and muscles of Tchp^{EC} mice

Tchp knock-out was previously associated with reduced cardiac vascularisation [2] and accumulation of p62 in Tchp knock-out mice. Furthermore, unpublished data from the lab demonstrated impaired EC function and re-vascularisation in adductor muscles from Tchp^{EC} mice after hind-limb ischemia. For this reason, I analysed vascular permeability in the heart (WT: males, n=3, females, n=3, Tchp^{EC}: males n=5, females n=2) and the adductor muscles (WT: n=3; Tchp^{EC} n=4) Tchp^{EC} and WT mice. The study showed an increased permeability in the heart of Tchp^{EC} mice (P= 0.0255), while no differences were observed in the adductor muscles. This suggests that the knock-out of Tchp affects brain ECs and ECs in other vascular beds, causing an increase in vascular permeability (**Figure 4.2**).

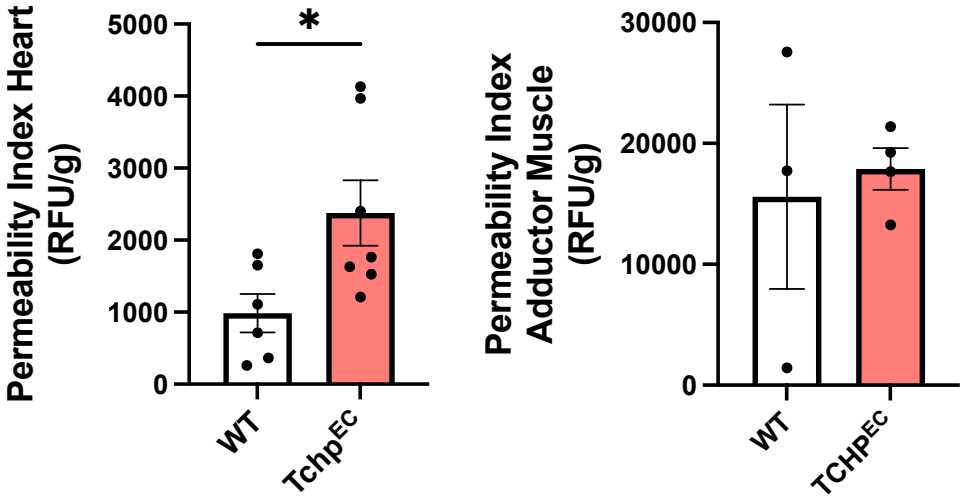


Figure 4.2| Tchp knockout increases vascular permeability in the hearth of Tchp^{EC} mice.

Analysis *in vivo* of heart and muscle permeability in WT and Tchp^{EC} mice. Unpaired t-test, heart *P=0.0255

Immunohistochemical characterisation of Neurovascular Unit

After fluorescence investigation through a spectrofluorometer, I performed immunohistochemistry to examine the distribution of the fluorescent tracer – dextran 3 kDa – in the brain of vessels of Tchp^{EC} mice. The hemibrain was embedded in an OCT, and slices of 20 μm were cut with a microtome-cryostat. The slices were

stained with anti-CD31 to highlight the ECs and DAPI. As shown in **Figure 4.3**, Tchp^{EC} brains showed enhanced tracer accumulation in the parenchyma compared to control mice, suggesting the presence of a leaky vasculature.

In addition to endothelial cells, pericytes and astrocytes were stained using antibodies anti-PDGFRB and anti-GFAP, as shown on the right panel of **Figure 4.3**. Multiplex immunohistochemistry was performed to analyse CD31, PDGFRB, GFAP, dextran and DAPI. Future studies will be involved in understanding the effects of Tchp knock-out in the other components of the NVU.

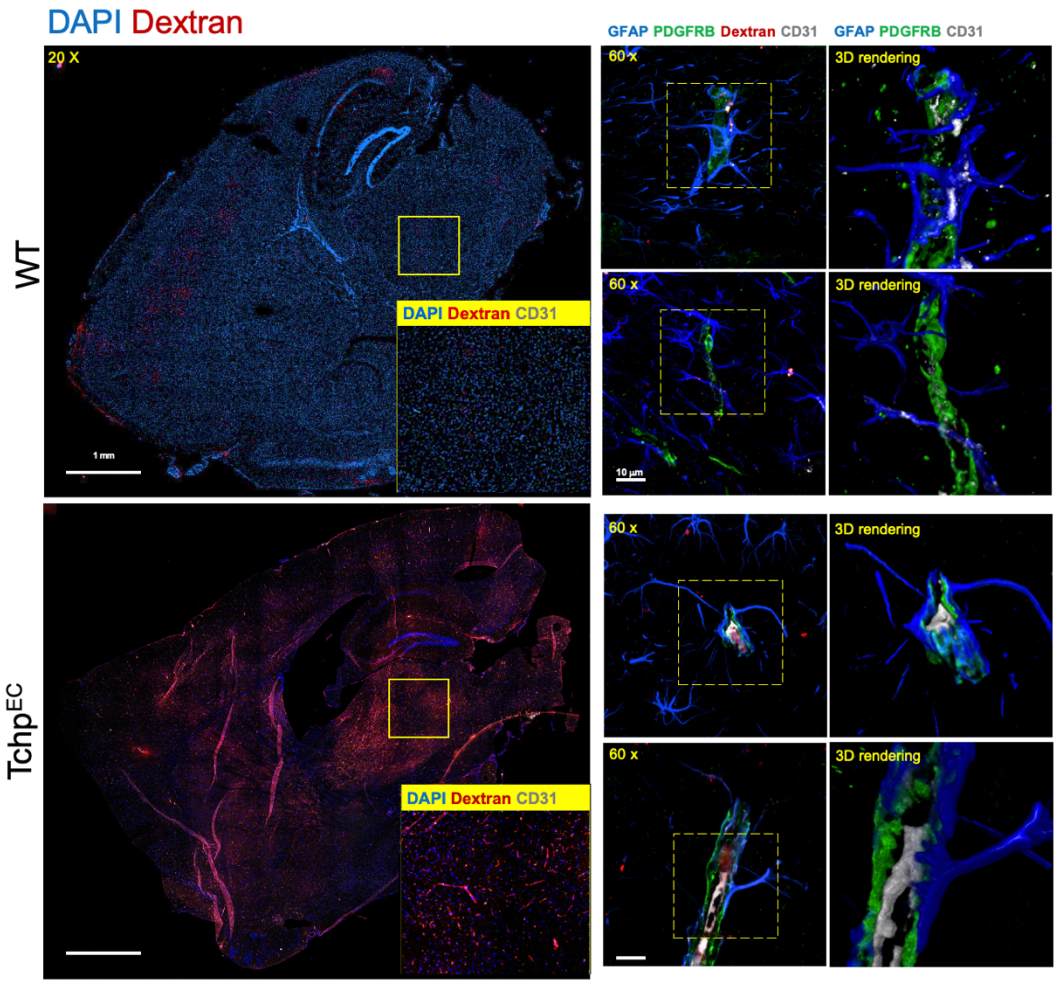


Figure 4.3| Immunohistochemical characterization of the neurovascular unit of WT and Tchp^{EC} mice.

On the left, TMR-Dextran tracer extravasation (red) into the brain is increased in Tchp^{EC} mice compared to control. On the right, characterization of the neurovascular unit of Tchp^{EC} and WT mice. The astrocytes are visible in blue (GFAP), pericytes in green (PDGFRB), endothelial cells in grey (CD31) and TRM-dextran in red. Scale bar 1 mm (left panel) and 10 µm (right panel).

Analysis of vessels network in Tchp^{EC} brain

Modifications of brain vasculature, including vascular network and blood flow, are features of cerebrovascular and neurodegenerative disease [290]. To assess the microvascular changes in the brain of Tchp^{EC} mice, a quantitative analysis of vessel parameters was performed using AngioTool on cerebral cortex sections of 2/3 months old WT and Tchp^{EC} mice (Cre transmitted by female parent). Vessel length, vessel area, lacunarity and the number of junctions were the parameters investigated on brain sections stained with isolectin B4 to stain endothelial cells.

The brain vasculature of Tchp^{EC} mice presented a reduced vessel area (P= 0.0328), decreased vessel length (P=0.0302) and decreased number of junctions (P=0.0099) compared to the control. Furthermore, the vessels from Tchp^{EC} brains showed an increased lacunarity (P=0.0424), indicating a reduction in structural homogeneity in Tchp^{EC} mice (**Figure 4.4**). Collectively, the data suggest that the downregulation of Tchp is associated with vascular alterations and modifications of vessel organisation.

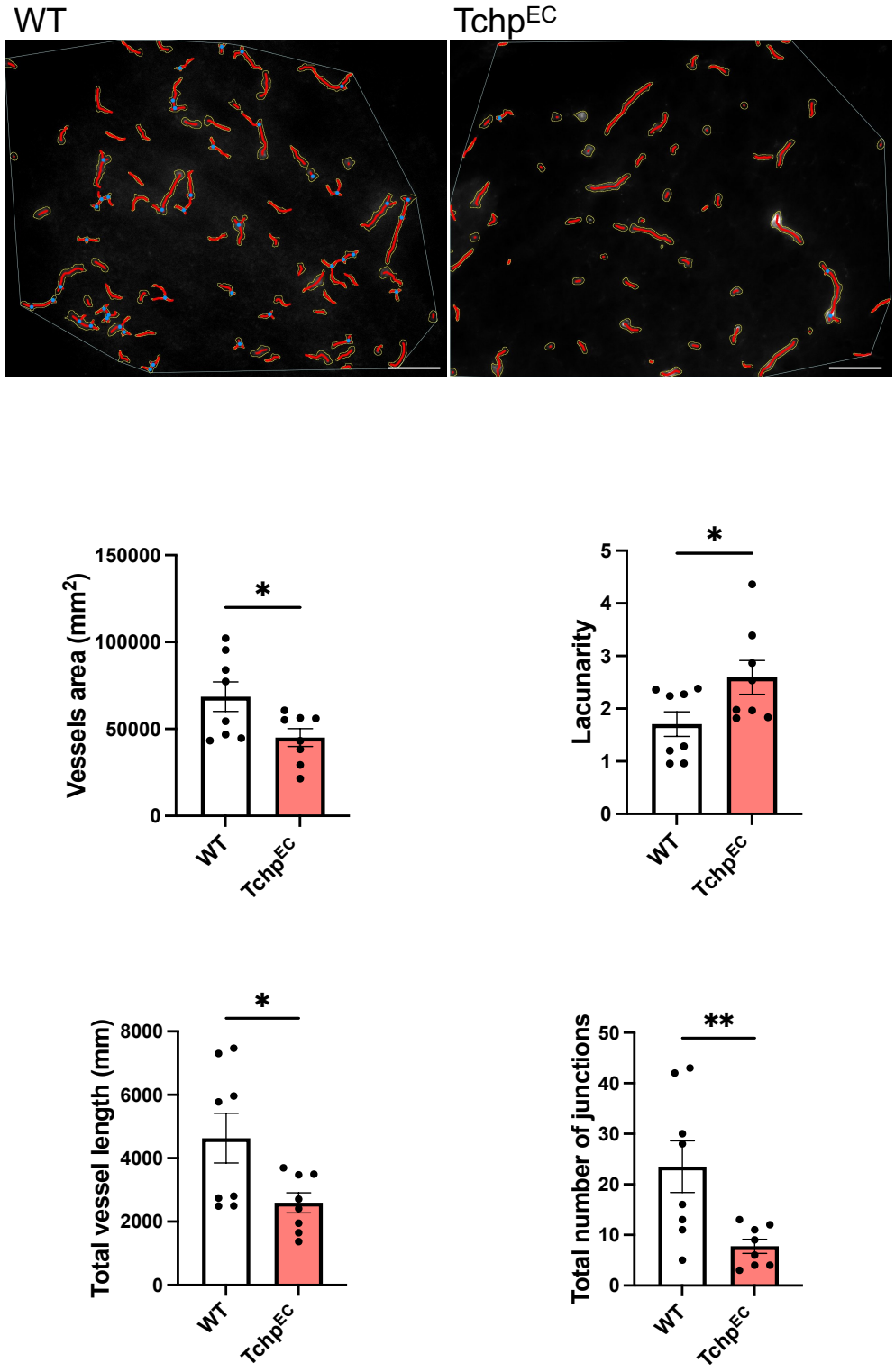


Figure 4.4| Analysis of vascular network in the brain of WT and Tchp^{EC} mice.

Immunohistochemistry and quantification of vessel area, lacunarity, vessel length, total number of junctions (n=3 unpaired t-test. Vessel area *P= 0.0328, lacunarity *P=0.0424, vessel length *P= 0.0302, total number of junctions **P=0.0099.) Scale bar 50 µm.

Flow Cytometry analysis of immune cells in the brain of Tchp^{EC} and WT mice

Optimisation of the gating strategies on bone marrow

Neuroinflammation is involved in the pathogenesis of several cerebrovascular and neurodegenerative diseases [298, 299]. Bulk RNA-seq analysis and gelatine zymography revealed a pro-inflammatory transcriptome and the increased production of MMP9 associated with Tchp knock-down (chapter 3); therefore, I decided to investigate the recruitment of immune cells in the brain of Tchp^{EC} mice.

To optimise the flow cytometry protocol, including the panel of antibodies and the gating strategy, I first analysed the bone marrow cells of WT mice. The gating strategy and the flow cytometry analysis were developed in collaboration with Dr Barry McColl's lab (Dementia Research Institute, University of Edinburgh) and the QMRI flow cytometry and cell sorting facility.

Bone marrow was collected from the femurs and after lysis of red blood cells, stained with anti-CD11B, anti-P2Y12, anti-LY6G, anti-CD3, anti-CD19, anti-LY6-C and anti-CD45 for detection of microglia, T-cells, B-cells, neutrophils, macrophages and monocytes. (**Figure 4.5**).

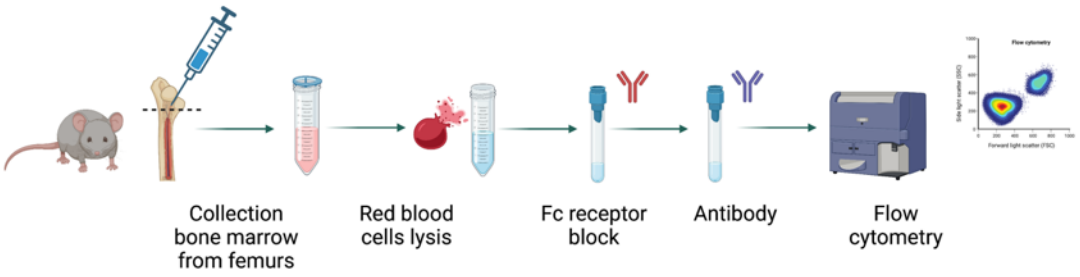


Figure 4.5| Optimization of the protocol for flow cytometry analysis of the immune cells of the bone marrow of WT and Tchp^{EC} mice.

Flow cytometry protocol, from the isolation of bone marrow to the reading with 6LSR Fortessa.

Fifty thousand live events were recorded for each specimen (WT n=3). After excluding the doublets and gating only the living cells, cells were divided into lymphoid cells ($CD11B^{-}CD45^{hi}$), monocyte-derived cells ($CD11B^{+}CD45^{hi}$) and microglia ($CD11B^{+}CD45^{mid/low}$). Lymphoid cells were then gated into B cells ($CD11B^{-}CD45^{hi}CD3^{-}CD19^{+}$) and T cells ($CD11B^{-}CD45^{hi}CD19^{-}CD3^{+}$), and monocyte-derived cells divided into neutrophils ($CD11B^{+}CD45^{hi}LY6G^{+}$) and macrophages ($CD11B^{+}CD45^{hi}LY6G^{-}LY6C^{-}$) and monocytes ($CD11B^{+}CD45^{hi}LY6G^{-}LY6C^{+}$). Finally, microglia was highlighted ($CD11B^{+}CD45^{low}LY6G^{-}LY6C^{-}$) (**Figure 4.6**).

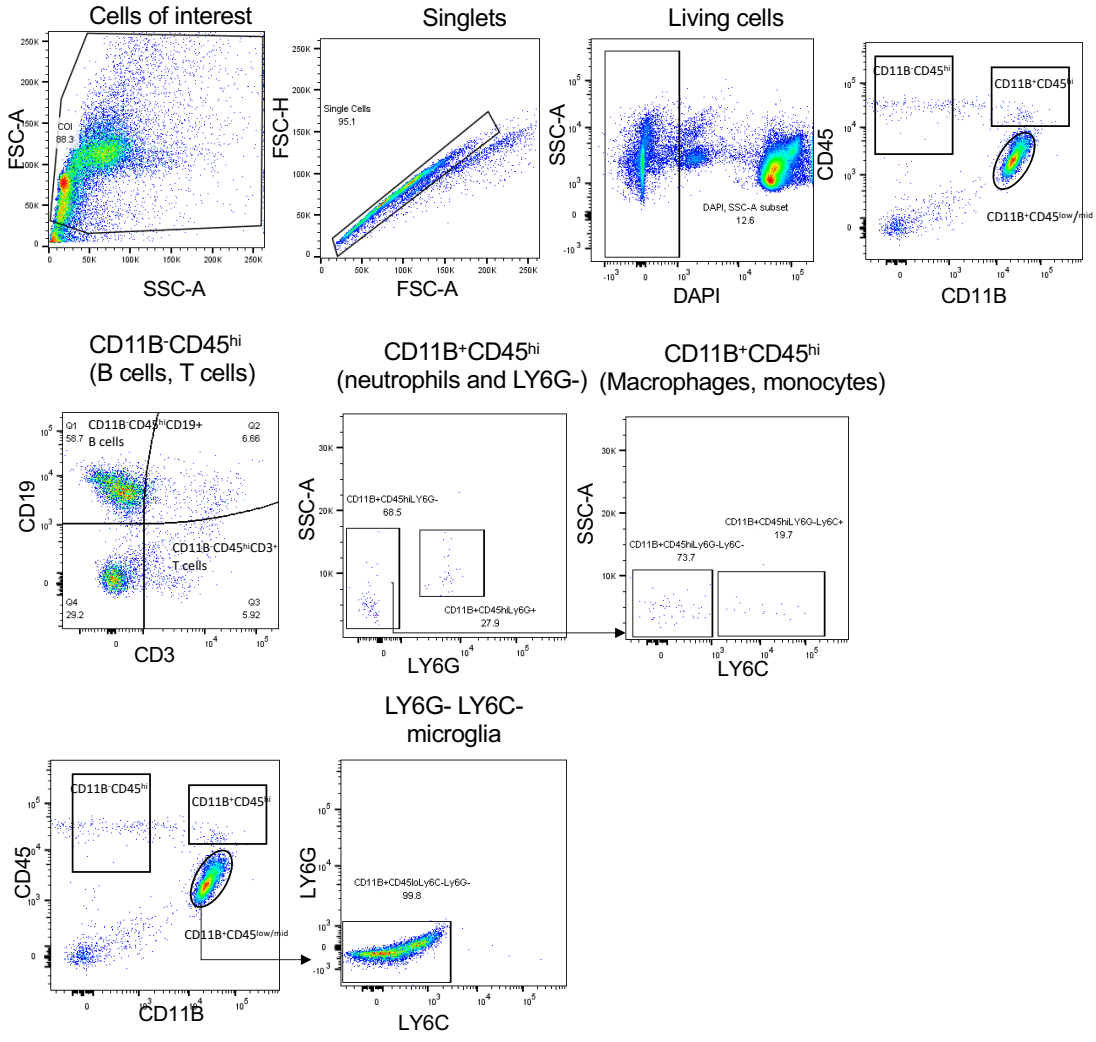


Figure 4.6| Gating strategy for flow cytometry analysis of immune cells in bone marrow

Femurs of WT mice (n=3) were flushed and processed to get bone marrow cells. Erythrocytes lysis was then performed. Antibody staining was performed for FACS analysis to detect T cells ($CD11B^{-}$ $CD45^{hi}$ $CD19^{-}$ $CD3^{+}$), B cells ($CD11B^{-}$ $CD45^{hi}$ $CD19^{+}$ $CD3^{-}$), Neutrophils ($CD11B^{+}$ $CD45^{hi}$ $LY6G^{+}$), Macrophages ($CD11B^{+}$ $CD45^{hi}$ $LY6G^{-}$ $LY6C^{+}$), Monocytes ($CD11B^{+}$ $CD45^{hi}$ $LY6G^{-}$ $LY6C^{-}$), Microglia ($CD11B^{+}$ $CD45^{lo}$ $LY6G^{-}$ $LY6C^{-}$). Data were acquired using FACSdiva software (BD bioscience) and analysed with FlowJo10.8.

Analysis of immune cells recruitment in the brain of WT and Tchp^{EC} mice

After optimising the flow cytometry analysis and gating strategy on bone marrow from WT mice, I finally performed the same analysis on the Tchp^{EC} brains (WT n=8, Tchp^{EC} n=8). Cells were analysed to determine the number of microglia, T-cells, B-cells, neutrophils, macrophages and monocytes (**Figure 4.7**).

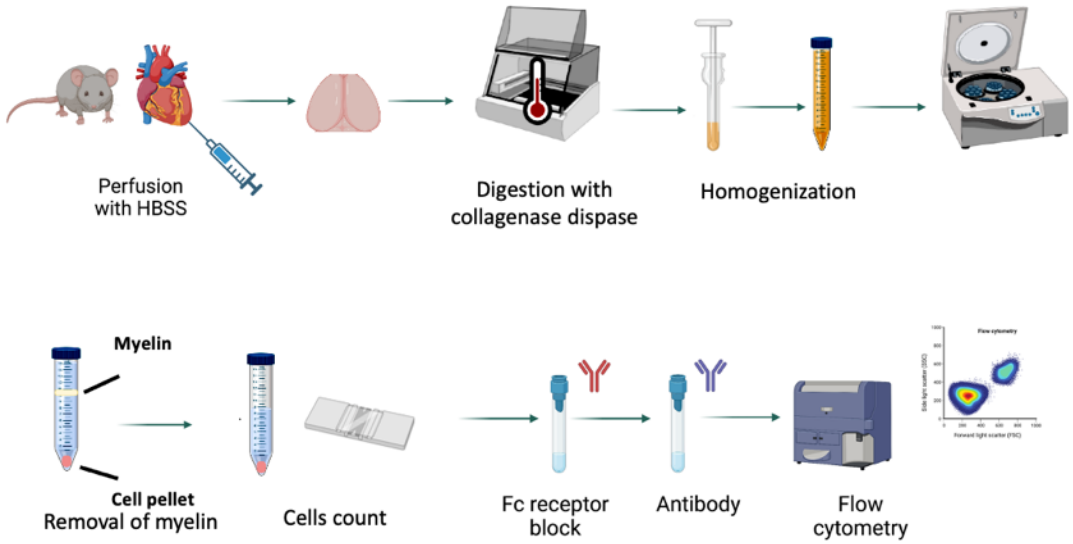


Figure 4.7| Protocol for flow cytometry analysis of cells from the brain of WT and Tchp^{EC} mice.

Flow cytometry protocol, from the tissue collection to the reading with 6LSR Fortessa.

Fifty thousand live events were recorded for each specimen, and the gating strategy was performed as described for the bone marrow (see paragraph "Optimisation of the gating strategies on bone marrow"). After acquisition using FACSdiva software (BD bioscience), data were analysed with FlowJo10.8 (**Figure 4.8**).

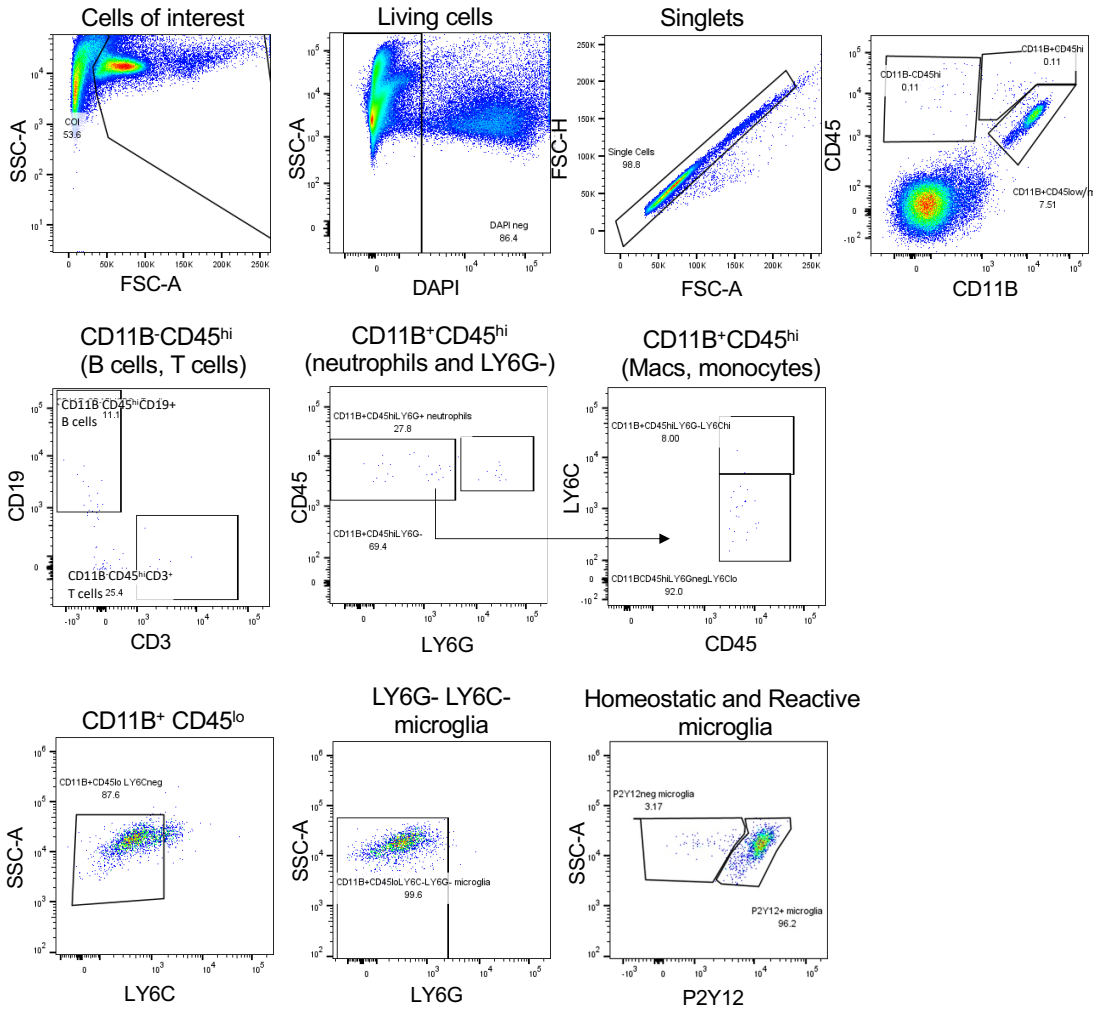


Figure 4.8| Gating strategy for flow cytometry analysis of immune cells in the brain from WT and Tchp^{EC} mice.

WT (n=8) and Tchp^{EC} (n=9) mice were perfused and brain digested using collagenase. Antibody staining was performed for FACS analysis to detect T cells (CD11B^{-} CD45^{hi} CD19^{-} CD3^{+}), B cells (CD11B^{-} CD45^{hi} CD19^{+} CD3^{-}), Neutrophils (CD11B^{+} CD45^{hi} LY6G^{+}), Macrophages (CD11B^{+} CD45^{hi} LY6G^{-} LY6C^{+}), Monocytes (CD11B^{+} CD45^{hi} LY6G^{-} LY6C^{-}), Microglia homeostatic (CD11B^{+} CD45^{lo} LY6G^{-} LY6C^{-} P2Y12^{+}), Microglia reactive (CD11B^{+} CD45$^{\uparrow}$ LY6G^{-} LY6C^{-} P2Y12$^{\downarrow}$). Data were acquired using FACSdiva software (BD bioscience) and analysed with FlowJo10.8.

Data were quantified using absolute number quantification normalising for the number of cells previously counted and mean fluorescent intensity. Recruitment of microglia, T cells, B cells, neutrophils, monocytes and macrophages were investigated. Data did not show differences in the number of lymphoid cells, macrophages, or monocytes.

I further investigated the mean fluorescent intensity of P2Y12 and CD45, interested in understanding if there was a microglia phenotype change towards reactive microglia. Indeed, whilst high expression of P2Y12 is a marker of resident quiescent microglia, decreased expression of P2Y12 is a feature of activated reactive microglia, reported in neuroinflammation and the pathogenesis of several cerebrovascular disease [300-304]. CD45 is upregulated in reactive microglia in Alzheimer's disease and multiple sclerosis [305]. The analysis did not reveal a difference in P2Y12 or CD45 in the brains of $Tchp^{EC}$ mice, suggesting the absence of reactive microglia (**Figure 4.9**).

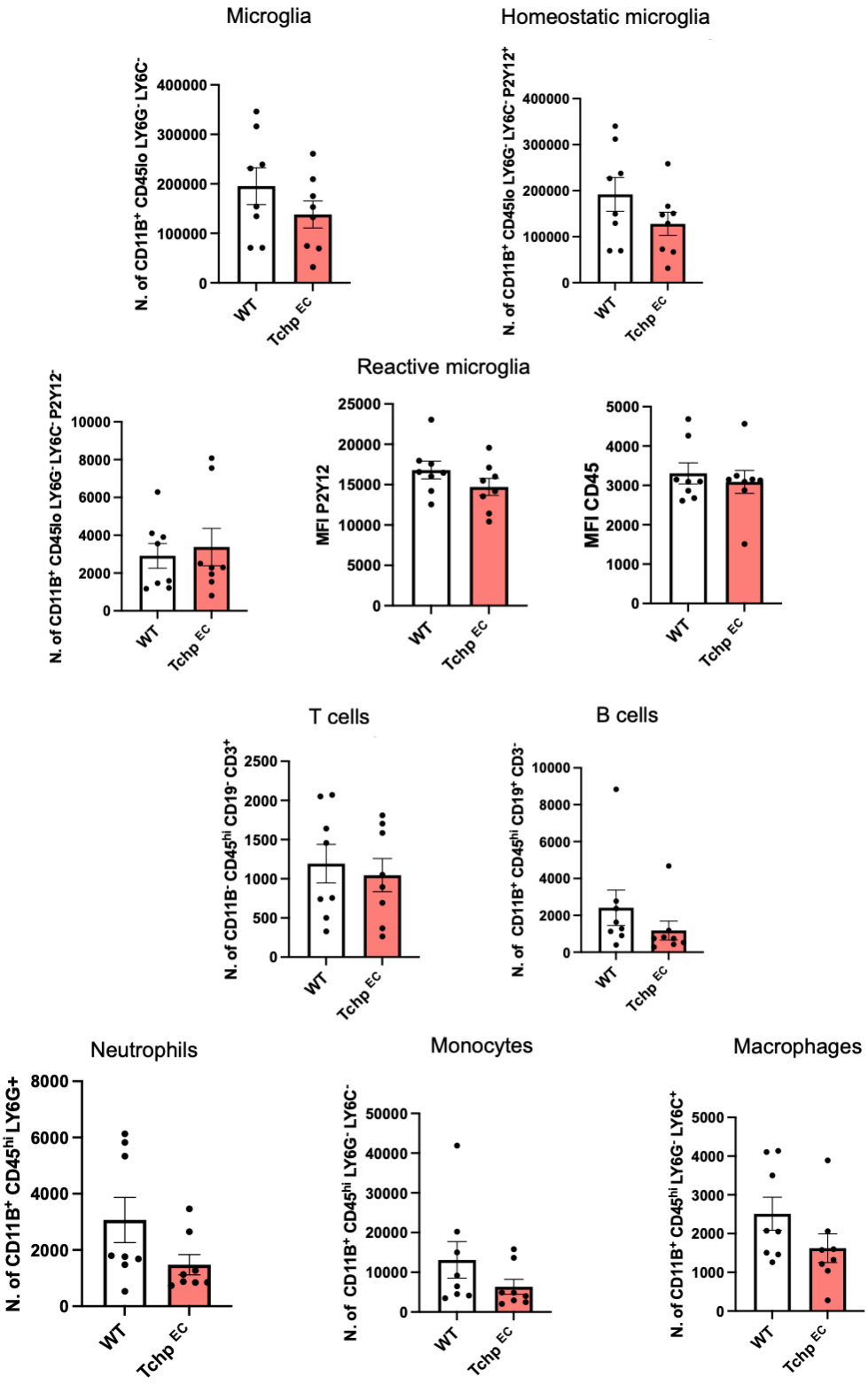


Figure 4.9| Quantification of flow cytometry analysis of immune cells in the brain from Tchp^{EC} and WT mice.

Quantification of flow cytometry analysis of immune cells in the brain of WT (n=8) and Tchp^{EC} (n=8) mice normalising for 50000 events. Statistical analyses were performed on at least three independent experiments. Data are represented as mean ± SEM.

Discussion

This chapter aimed to characterise the cerebral vasculature of Tchp^{EC} mice. The permeability assay performed by injecting dextran TRM 3 kDa revealed an increased accumulation of fluorescent tracer in the brain of Tchp^{EC} mice compared to the control, suggesting an impairment of the BBB. Furthermore, the assay demonstrated a higher permeability also in the hearts of Tchp^{EC} mice.

The analysis of the brain's vascular network of Tchp^{EC} mice using AngioTool showed significant alterations, decreased junctions, vessel length and reduced homogeneity of the vessels. Finally, flow cytometry analysis suggested that Tchp knock-out does not lead to the recruitment of inflammatory cells into the brain.

Knock-out of Tchp is associated with increased BBB vascular permeability

In the previous chapter, I described the impairment of barrier function associated with the knock-down of Tchp. ECs isolated from Tchp^{EC} brains and HBMVECs transfected with siRNA anti-TCHP demonstrated a decreased resistance when analysed using ECIS®, indicating impairment of barrier function in these cells. Furthermore, the impairment of ZO-1 and the increased production of MMP9 confirmed that the knock-down of Tchp affects the ECs barrier. Because of these results, I investigated the effects of Tchp knock-down on the BBB *in vivo*. The fluorescent tracer dextran TRM 3 kDa was administrated intraperitoneally in the mice, and after perfusion with PBS, the brain was collected for fluorescence quantification through spectrofluorimetric and immunohistochemistry. The following analysis demonstrated an increased vascular permeability in the BBB of Tchp^{EC} compared to the control, confirmed by the immunohistochemistry analysis, highlighting the exit of the fluorescent tracer dextran outside the vessels in Tchp^{EC} mice. This is in line with the previous results described *in vitro*. The increased production of MMP9 could explain the impairment observed in Tchp^{EC} mice. Elevation of MMP9 has been found in patients with small vessel disease [259], ischemic stroke [306, 307], and Alzheimer's disease [308]. In physiological conditions, MMP9 is required for the remodelling of the extracellular matrix necessary for processes like angiogenesis and neurogenesis [63], while in disease, MMP9's action

is exacerbated, causing a disruption of the BBB and leading to the access of inflammatory cells into the brain [309]. Not only does MMP9 act on the extracellular matrix, but also on TJs. Increased levels of MMP9 have been associated with a decrease of ZO-1, occludin and claudin-5 in a mouse model of Alzheimer's disease [261]

Furthermore, a reduction in ZO-1 was also associated with MMP2/MMP9 increase in ischaemic stroke [191]. This is in line with the data obtained from TCHP knock-down ECs. Future experiments will aim to characterise the nature of the leakage in the BBB by administering higher MW fluorescent tracers.

Of note, TCHP knock-down caused an increased permeability also in the heart of $Tchp^{EC}$ mice compared to the control. The heart of Tchp knock-out mice showed reduced cardiac vascularisation and impaired autophagy characterised by an accumulation of P62 [2]. This demonstrates that the effects of Tchp knock-out are extended to other vascular beds, not only the BBB. Also, the increased permeability in the heart of $Tchp^{EC}$ mice suggests that the increase in vascular permeability could be associated with the impairment of autophagy in $Tchp^{EC}$ mice.

The intraperitoneal injection (i.p) of the fluorescent dye was chosen over the intravenous (i.v) injection because easier to perform, but some limitations must be considered. It is more cost-intensive because a 2-fold higher amount of tracer is required compared to the i.v to obtain comparable serum fluorescence values [29]. The time of circulation for tracer adsorption into the bloodstream is higher compared to the one of the i.v (fifteen minutes vs the five minutes of the i.v). Also, an impaired vessel density could affect the amount of tracer that arrives at the brain. As presented in the discussion chapter, to confirm the results here described, MRI scan is being performed to demonstrate the increased vascular permeability compared to the WT, using the contrast reagent gadolinium.

The relationship between autophagy, TJs and EC integrity has been studied in the last few years. Shi et al. demonstrated that HDAC9 increases after I/R injury, suppressing autophagy, damaging the BBB's integrity and exacerbating inflammation. Gene silencing of HDAC9 recovered the decreased expression of ZO-1, Occludin and CLDN-5 by reactivating autophagy [161]. In support of this, Li et al. found that EC autophagy

restores decreased levels of ZO-1 and reduces ROS production and apoptosis in I/R injury [162]. Saha et al. showed that autophagy promotes a TJ barrier by increasing occludin through ERK 1/2 MAPK pathway [163]. Furthermore, the involvement of autophagy is also linked with the exacerbation of inflammation and the production of MMP9 [310].

In the future, investigations on astrocyte activation and coverage of pericytes are necessary to understand the effects of dysfunctional ECs on the NVU.

Contribution of Tchp knock-out to altered vascular function and neuroinflammation

Abnormal vascular function and morphology have been described in stroke, dementia, Alzheimer's disease and traumatic brain injury [288-290]. Furthermore, modifications of cerebral blood flow are a feature of the early stages of Alzheimer's disease and ageing-mild cognitive impairment [9]. To investigate how the knock-out of Tchp affected vascular function, I analysed the vascular morphology of sections of $Tchp^{EC}$ and WT brains using AngioTool [224]. The analysis demonstrated vascular network is significantly affected by EC Tchp knock-out, with a decrease in vessel area, total vascular length and junctions. Furthermore, the analysis showed inhomogeneity (increased lacunarity) of the vessels in the brain of $Tchp^{EC}$ mice compared to the WT. These results suggest a global reduction of vasculature compared to the control. This is in line with what is described in cerebrovascular disease. Alterations of vessel morphology have been described in patients with Alzheimer's disease [291] and traumatic brain injury [290]. The data confirm that the endothelial-specific knock-out of Tchp affects endothelial functionality leading to a global modification of the brain's vasculature.

Because we observed a pro-inflammatory phenotype in the ECs isolated from $Tchp^{EC}$ and impairment of ZO-1 compared to the control, I investigated the recruitment of immune cells in the brain of $Tchp^{EC}$. The flow cytometry analysis of the brain of $Tchp^{EC}$ mice did not show the recruitment of lymphoid cells (neutrophils, T cells, B cells) or macrophages and monocytes in the brain of $Tchp^{EC}$. We did not find evidences of

change of microglia in Tchp^{EC} compared to the controls, suggesting that Tchp knock-out does not cause microglia activation.

Conclusions and future directions

In this chapter, I characterised the brain vasculature of Tchp^{EC} mice. The permeability assay demonstrated impairment in the BBB of Tchp^{EC} mice compared to the WT, where dextran TRM 3 kDa exits from the vasculature in the surrounding tissue. Moreover, immunohistochemistry analysis demonstrated a reduction of vasculature and complexity in the brain of Tchp^{EC} mice. Finally, flow cytometry analysis showed no infiltration of immune cells or microglia activation in the brain of Tchp^{EC} mice.

The data highlights that endothelial-specific Tchp knock-out negatively affects the brain vasculature. This aligns with the inflammatory transcriptome and production of MMP9 described in the previous chapter. Future experiments will aim to investigate the other components of the NVU, focusing on the coverage of pericytes and activation of astrocytes, to understand better the role of Tchp in the ECs of the BBB.

Chapter 5

Characterisation of autophagy in ECs and *in vitro* screening to identify compounds to restore autophagic flux

Chapter 5 Characterisation of autophagy in ECs and *in vitro* screening to identify compounds to restore autophagic flux

Introduction

Autophagy is an intracellular process that ensures cellular homeostasis and stress adaptation. In addition, it allows the degradation of damaged organelles and harmful protein aggregates and, finally, the recycling of their components to generate energy in adverse conditions.

Three types of autophagy were described in the literature: microautophagy, macroautophagy and chaperone-mediated autophagy. Microautophagy consists of the engulfment of cytoplasmic material directly by the lysosomes [105]. Macroautophagy is characterised by the formation of double-membrane compartments called autophagosomes that carry the cytoplasmic material to degrade and finally fuse with lysosomes [311]. Finally, chaperone-mediated autophagy is characterised by chaperone complexes and lysosome proteins that degrade proteins targeted by specific motifs [107].

Autophagy regulates EC response to the surrounding environment and angiogenic stimuli in vascular disease. It also protects against ROS, hypoxia and ox-LDL. In line with this, inhibition of the autophagic process through 3-methiladenine or silencing of ATG5 causes a reduction of cell migration and angiogenic functions. In contrast, the overexpression of ATG5 causes an increase in these two processes [312]. Consequently, loss of autophagy could be involved in eliciting endothelial dysfunction in vascular disease. In support of this, inhibition of autophagy through bafilomycin [313] or silencing of ATG3 [125] decreases the level of eNOS and, consequently, the production of NO in response to shear stress. Furthermore, autophagy inhibits the marker of endothelial dysfunction endothelin-1, the counterpart of NO [124].

The role of autophagy in ECs also includes the regulation of VWF secretion. Indeed, inhibiting the autophagic process through the silencing of ATG5 or ATG7 [314] or treatment with chloroquine [123] impairs the secretion of VWF from ECs, indicating an anti-thrombotic role in autophagy.

Interestingly, the autophagic process in ECs contributes to regulating vascular permeability by maintaining barrier integrity by ROS regulation. The impairment of autophagy through small interfering RNA targeting ATG5 or pharmacological inhibition increases ROS production and EC permeability [315].

Autophagy is activated in pathological conditions to reinstate EC homeostasis and restore disease progression. In contrast, impaired autophagy under prolonged stress conditions, such as nutrient deprivation, hypoxia or oxidative stress, may be detrimental and lead to autophagic cell death.

Defective autophagy leads to the formation of protein aggregates of misfolded proteins, a hallmark of ageing and ageing-related disorders [144]. Insoluble aggregates are transported along the microtubules in the perinuclear region, where they are cleared through autophagy. When the autophagic process is impaired because of ageing or disease, the protein aggregates accumulate in the cytoplasm of the cell [145]. The accumulation of the autophagic protein P62 is associated with the inhibition of proteasome and protein translation. P62 is necessary to activate mTORC1 downstream effectors, eIF4E-binding protein and p70 ribosomal S6 kinase 1 (S6K1), which further control protein translation. Defective autophagy causing accumulation of P62 and dysregulation of protein translation leads to the accumulation of protein aggregates [146]. Protein aggregates have been associated with neurodegenerative [316] and cardiovascular diseases [148, 317].

Stress granules are another type of cytoplasmic aggregate composed of translation factors, mRNAs, RNA-binding proteins and other proteins [152]. Their assembling is triggered by stress, which causes the phosphorylation of eIF2α, and reduces the availability of the eIF2α–GTP–tRNAiMet ternary complex required for translation initiation, thereby resulting in a blocked translation [153]. The circularised mRNA, still attached to the preinitiation machinery, aggregate and binds RNA-binding proteins, causing the formation of stress granules. Between these RNA binding proteins, TIA-1, TIAR, G3BP, CPEB1, and TTP can initiate stress granules formation and overexpression of these proteins will promote their formation even under non-stressed conditions [154].

Recently, stress granules have been included in the category of biomolecular condensates, membrane-less organelles that can assemble through liquid–liquid

phase separation [318]. They are involved in physiological function but also diseases, such as neurodegeneration [319], cancer [320] and rare and viral infectious diseases [321]. Indeed, the changes in the formation, the dissolution or the properties of these condensates or stress granules due to ageing cause modifications in cellular senescence, gene expression, genomic instability, increased DNA damage, altered cell signalling, loss of protein quality control and stem cells exhaustion [322]. There is a strong interest in understanding condensates for treating protein aggregates disease.

In this chapter, I investigate the impairment of autophagic flux and the presence of stress granules and RNA-binding proteins in human microvascular ECs lacking TCHP. Finally, in collaboration with the drug screening facility, we performed a high-throughput screening to study compounds that could reduce the accumulation of protein aggregates by restoring autophagy and reducing inflammation.

Hypothesis and aims

Given the inflammatory phenotype associated with TCHP knock-out in the brain ECs and that a similar phenotype was previously observed in peripheral ECs lacking TCHP and linked with impairment of autophagic flux, we hypothesised the involvement of defective autophagy in the microvascular brain ECs lacking TCHP. Therefore, the hypothesis presented in this chapter is as follows:

"Lack of the centriolar protein TCHP causes an impaired autophagic process in brain microvascular ECs."

Aims:

- To assess the impairment of autophagy in the ECs of the brain of $Tchp^{EC}$ mice and TCHP knock-down human brain microvascular ECs.
- Characterisation of the protein aggregates due to the impairment of autophagic flux through mass spectrometry.
- *In vitro* screening of compounds that can restore autophagy and reduce inflammation in TCHP knock-down microvascular ECs.

Results

Lack of TCHP causes impairment of autophagy in brain microvascular endothelial cells

As presented in chapter 3, TCHP co-localises with PCM1 in the pericentriolar matrix and satellite region in human brain microvascular ECs, confirming what was previously observed in HUVECs. TCHP regulates the localisation of PCM1, and the knock-down of TCHP causes a delocalisation of the centriolar protein (**figure 5.1A**) [323]. The immunocytochemistry staining demonstrated that also, in HBMVECs, the depletion of TCHP caused a loss of PCM1 accumulation ($p = 0.003$) (**figure 5.1B**). PCM1 is a centriolar satellite protein which binds the autophagic protein GABARAP through a canonical LIR motif. Consequently, the destabilisation of PCM1 due to the loss of TCHP would affect autophagy [116]. In support of this, the knock-down of TCHP in human brain ECs causes an accumulation of the autophagic receptor P62 compared to the control ($p \leq 0.001$), indicating an impairment of the autophagic flux (**figure 5.1B**), as previously observed in HUVECs lacking TCHP.

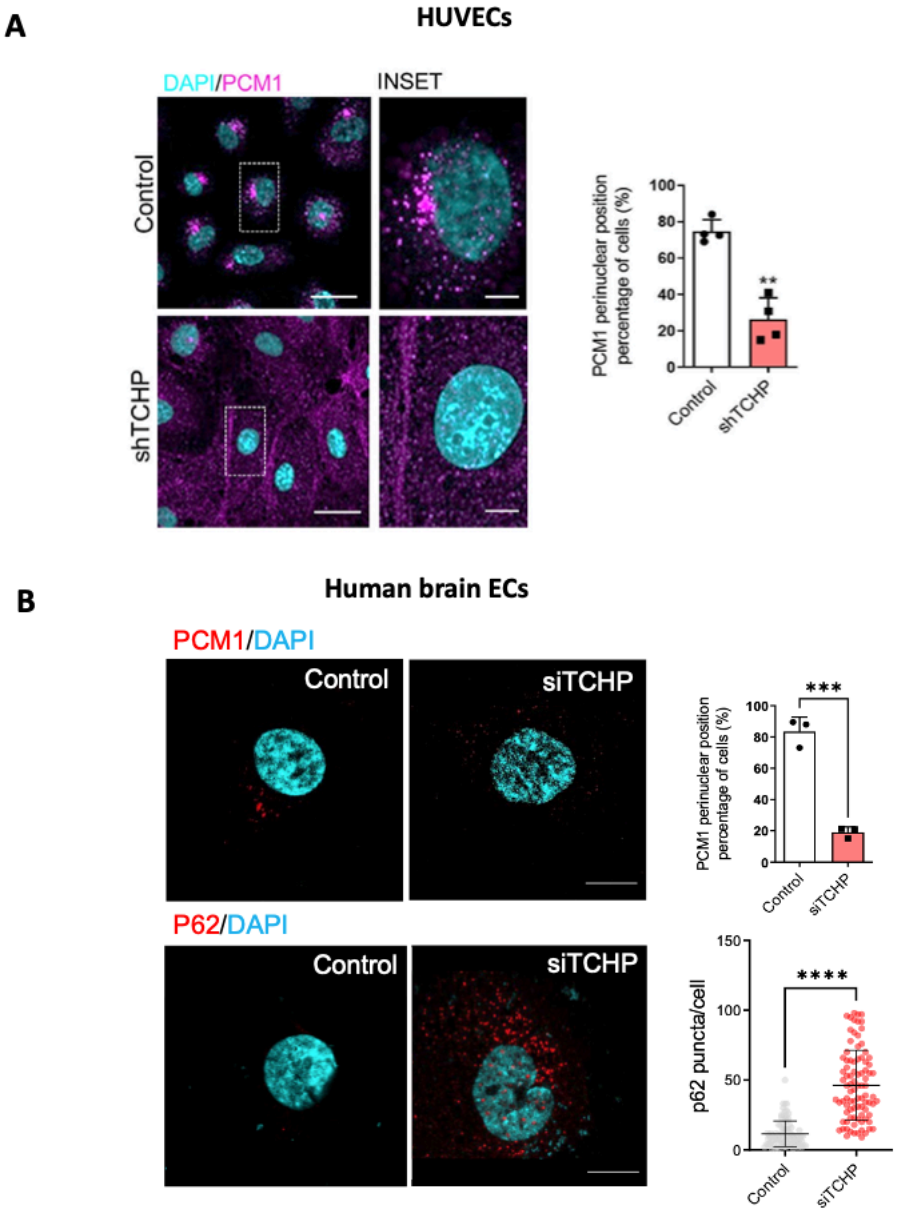


Figure 5.1|TCHP knock-down causes impairment of autophagy in HBMVECs.

A. TCHP knock-down or control HUVECs were stained for anti-PCM1 antibody. Taken from "Trichoplein binds PCM1 and controls endothelial cell function by regulating autophagy" by Martello A, et al.[2] **B.** Immunofluorescence staining anti-PCM1 (in red) and anti-P62 (in red) in control and TCHP knock-down human brain ECs. Nuclei are stained in Dapi (blue). Scale bars=A. 50 µm and 5 µm in the inset, B. 10 µm. Panel on the right: PCM1 quantification (n=3; unpaired t-test; ***p =0.003 vs control). P62 quantification (n=90 cells, unpaired t-test; ***p ≤ 0.001 vs control). Statistical analyses were performed on at least three independent experiments. Data are represented as mean ± SEM.

TCHP knock-out causes accumulation of protein aggregates in brain microvascular ECs

The impairment of protein degradation processes, such as autophagy or ubiquitin-proteasome system, causes the accumulation of protein aggregates. Insoluble aggregates tend to form aggresomes, that are transported via microtubules in the perinuclear region and here, the autophagic process clears them [144]. When the autophagy level is decreased, misfolded proteins accumulate in the cytoplasm, exacerbating cellular stress and inflammation [145].

PROTEOSTAT® dye is an analogue of Thioflavin T, which acts as a molecular rotor dye that fluorescence when it binds the cross-beta spine of quaternary protein structures found in misfolded and aggregated proteins (**figure 5.2A**). Using PROTEOSTAT® Aggresome Detection kit, we previously discovered the accumulation of protein aggregates in the cytoplasm of TCHP knock-down HUVECs compared to the controls in support of the hypothesis of the block of the autophagic process. Furthermore, the analysis of the HBMVECs confirmed the presence of aggresomes in the cytoplasm of TCHP knock-down ECs compared to the control (**figure 5.2B**). Moreover, the ECs from $Tchp^{EC}$ mice presented an increased presence of aggresomes, quantified using the Fiji macro Aggrecount. This suggests an impairment of autophagic flux also in ECs from the brain of $Tchp^{EC}$ mice (**figure 5.2C**).

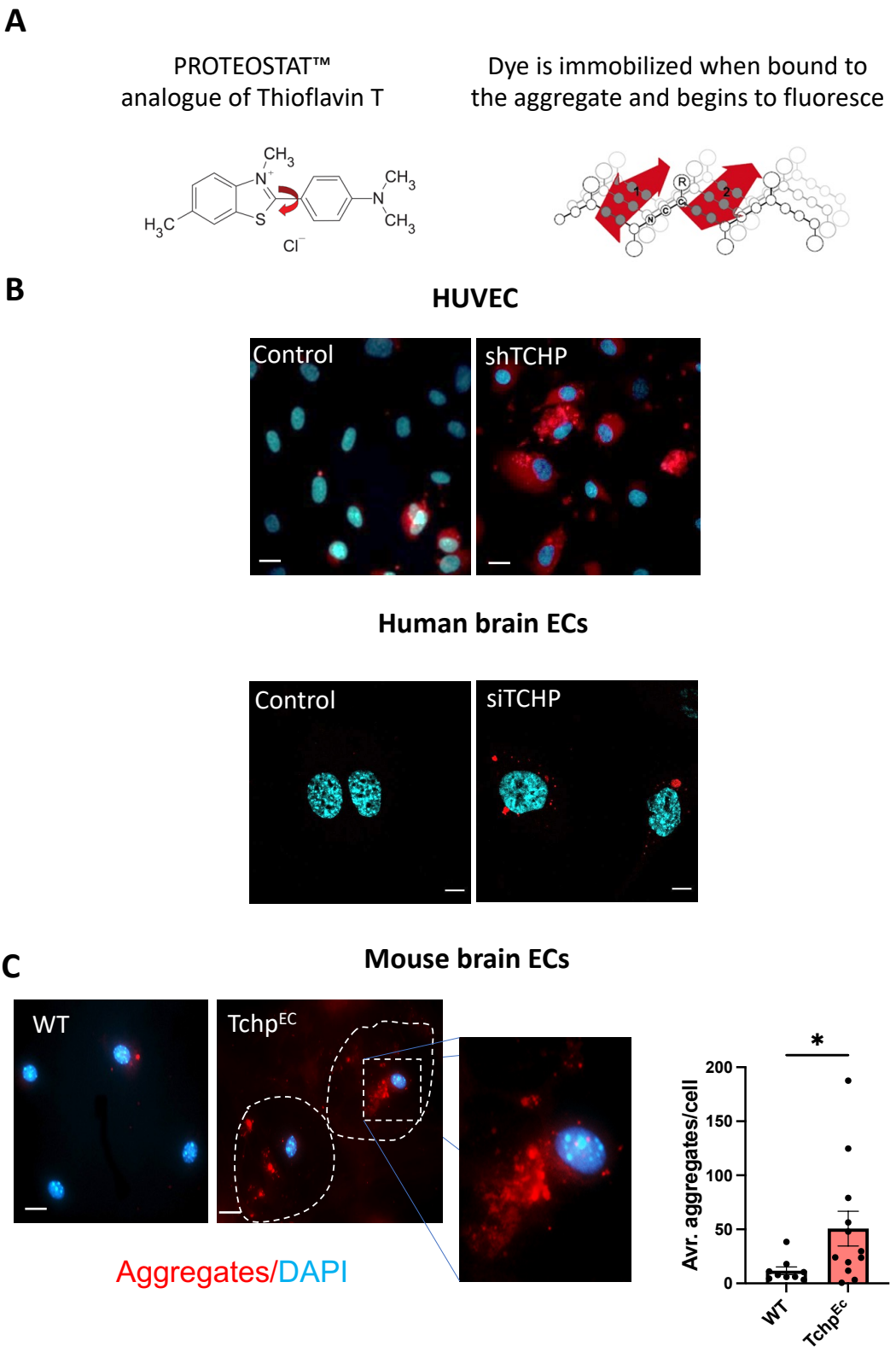


Figure 5.2| TCHP knock-down causes accumulation of protein aggregates in brain microvascular ECs.

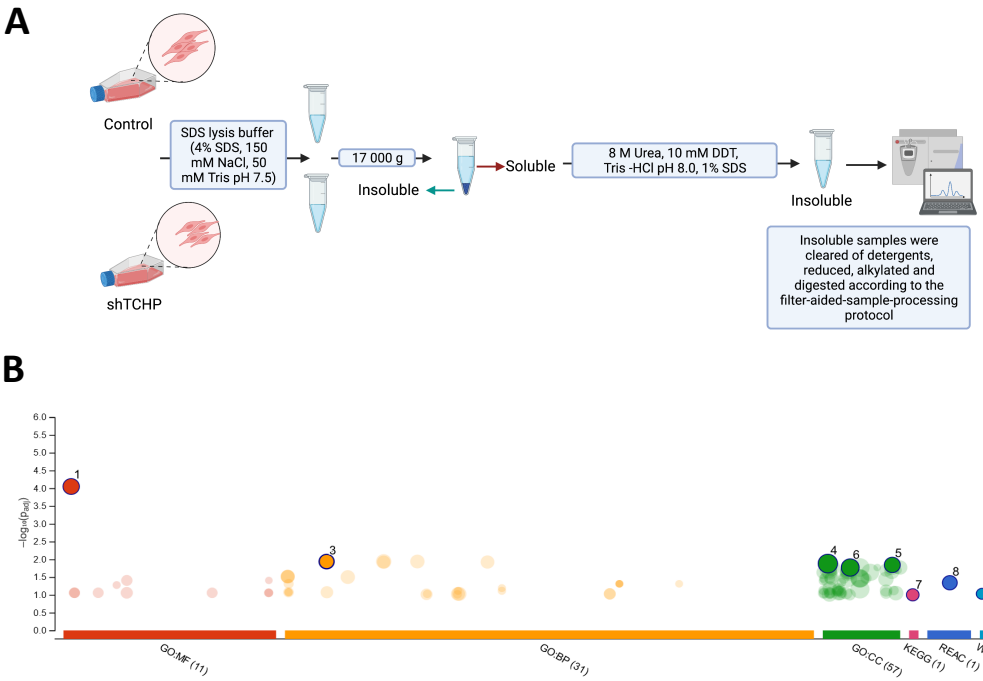
A. Schematic representation of PROTEOSTAT® assay. **B.** Staining of protein aggregates in control and TCHP knock-down HUVECs and human brain ECs. Aggregates are visible in red, and nuclei in blue (DAPI). **C.** Staining and quantification of protein aggregates in brain microvascular ECs of WT and TCHP knock-out mice using PROTEOSTAT® Aggresome Detection kit. Scale bars, 20 µm and 10 µm (Human brain ECs) ; (*n* = 245 cells; unpaired t-test; **P* = 0.0339). Statistical analyses were performed on at least three independent experiments. Data are represented as mean ± SEM.

Evaluation of protein aggregates by mass spectrometry

To evaluate the toxicity of the aggregates, their composition was analysed through mass spectrometry, in collaboration with the Mass Spectrometry Facility Core facility of the University of Edinburgh.

Since it is difficult to obtain the large number of brain microvascular ECs necessary to perform mass spectrometry, the analysis was performed on TCHP knock-down and control HUVECs. First, around 6 million cells were collected, and the insoluble fraction was separated from the soluble fraction in urea buffer. Cells were collected from two independent cultures. Then, label-free quantification liquid chromatography (LC)-MS/MS was performed to analyse the material enriched in the insoluble fraction (**Fig.5.3A**). A total of 2274 proteins were detected. 149 top-ranked proteins differing between controls and TCHP knock-down were identified using log2 fold change of 1 at the peptide and protein level. LFQ values were determined by the MaxQuant software suite. For data analysis, a cut-off of 3 peptides was used. Otherwise, that protein identification was removed from the dataset.

The gene ontology enrichment analysis of the highest-ranked proteins, performed using gProfiler software, revealed that RNA-binding, RNA processing, and miRNA processing-associated proteins are present in the aggregates (**Fig.5.3B**). Since RNA-binding proteins are associated with stress granules formation, hallmarks of neurodegenerative disorders, I further investigated these proteins by examining the RNA granules database (http://rnagranuledb.lunenfeld.ca) to identify the RNA-binding proteins associated with stress granules. Of note, between the RNA-binding proteins discovered by Mass Spectrometry MRPS9, MRPS14, MRPS24, SPATS2L, DDX10, GPATCH8, SMG8, LANCL1, TSR1, PLRG1, RSRC1, ATP8B1, UBAP2, PRRC2B, OAS2, NEXN, RIOK1, PTK6, ATP8B1 are RNA-binding proteins associated with stress granules (**Fig.5.4A**). Furthermore, MRPS9 and MRPS14 belong to the family of mitochondrial ribosomal proteins and are associated with neurodegenerative disease [324].



ID	Source	Term ID	Term Name	p_{adj} (query_1)
1	GO:MF	GO:0003723	RNA binding	8.948×10^{-5}
2	GO:BP	GO:0006396	RNA processing	1.153×10^{-2}
3	GO:BP	GO:0006397	mRNA processing	1.153×10^{-2}
4	GO:CC	GO:0005622	intracellular anatomical structure	1.316×10^{-2}
5	GO:CC	GO:1902494	catalytic complex	1.438×10^{-2}
6	GO:CC	GO:0032991	protein-containing complex	1.700×10^{-2}
7	KEGG	KEGG:03040	Spliceosome	9.981×10^{-2}
8	REAC	REAC:R-HSA-89...	Metabolism of RNA	4.561×10^{-2}
9	WP	WP:WP623	Oxidative phosphorylation	9.338×10^{-2}

Figure 5.3| Analysis of aggregate composition by Mass Spectrometry.

A. Schematic representation from protein acquisition to analysis. **B.** Enrichment analysis of Insoluble proteins collected from control and TCHP knock-down HUVECs. The plot was created using gProfiler software.

Stress granules are cytoplasmic RNA complexes that develop in the cells under stress conditions. Their formation depends on the phosphorylation of the α subunit of eukaryotic initiation factor 2 (eIF2), a component of the eIF2-GTP-tRNAiet ternary complex that stops translation through the block of polysome assembly [325]. The immunocytochemistry staining anti-phospho-elf2α revealed increased phosphorylation in the TCHP knock-down HUVECs compared to control, in support of the hypothesis of the accumulation of stress granules linked with TCHP knock-down (**Fig.5.4B**). Interestingly, immunofluorescence staining highlighted an increased expression of tristetraprolin (TTP) in the TCHP knock-down ECs. TTP is an

RNA-binding protein that induces stress granules assembly through the binding of untranslated mRNA [326]. Conversely, the immunocytochemistry of the deacetylase HDAC6, a component of stress granules that mediate their formation through the regulation of their components along microtubules [327], did not reveal a difference between control and TCHP knock-down ECs (**fig.5.4B**).

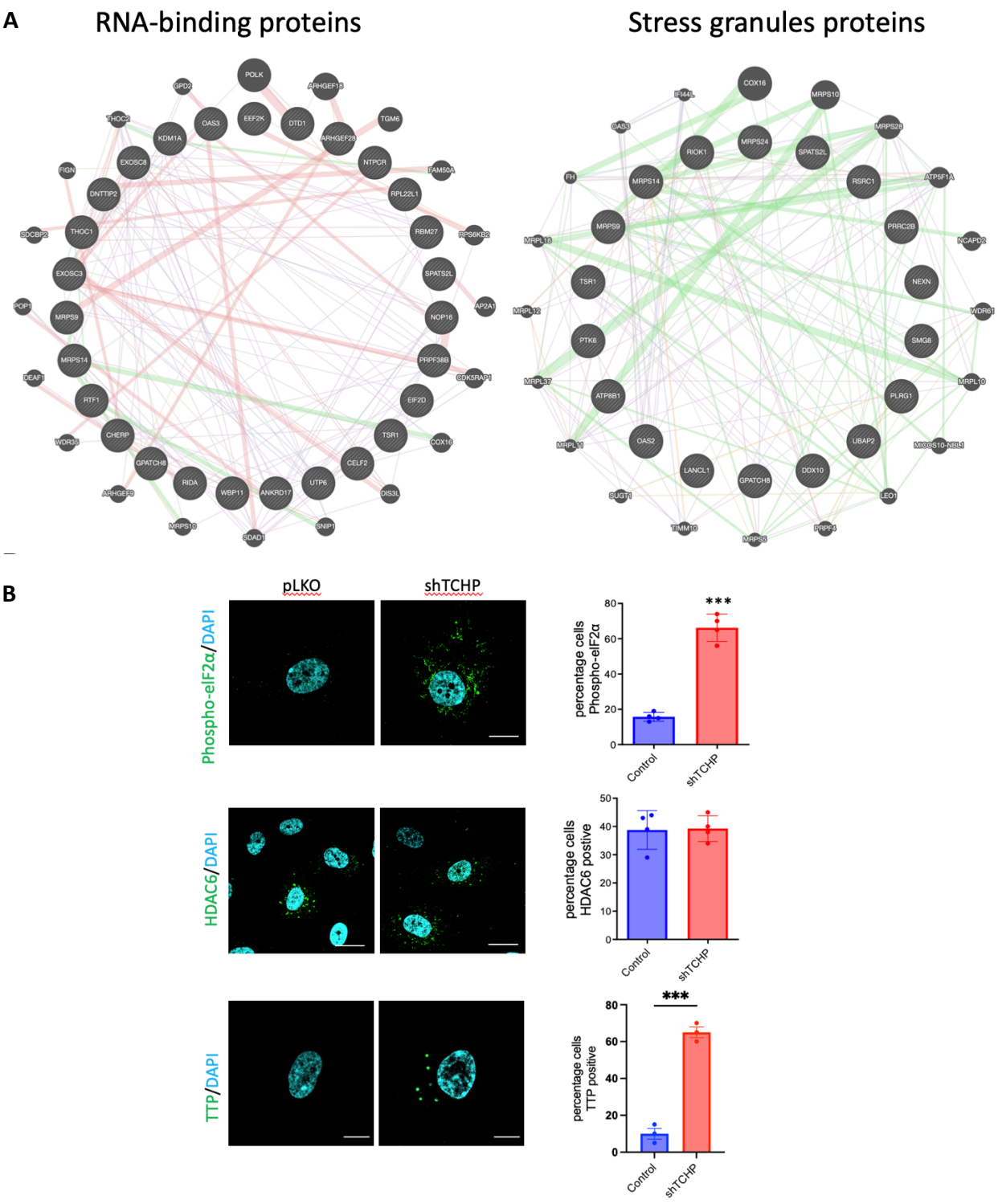


Figure 5.4|Stress granules markers in TCHP knock-down ECs.

A. Left panel: RNA binding proteins network cluster. Red lines represent interactions, purple lines indicate co-expression, green lines indicate shared protein domains, yellow lines predicted interactions and blue lines indicate co-localization.

Right Panel: Stress granules proteins network cluster. Red lines represent interactions, purple lines indicate co-expression, green lines indicate shared protein domains, yellow lines predicted interactions and blue lines indicate co-localization. **B.** Immunocytochemistry staining and quantification of phospho-elF2α, HDAC6, TTP in control and Tchp knock-down HUVECs (n. cells=90 from at least three different experiments, unpaired t-test, ***P <0.0001)

Drug screening to identify autophagy activator compounds

Detection of levels of P62 in the cells is a standard readout of autophagy. As a proof of concept, we have conducted a high-content phenotypic drug screen (in collaboration with Edinburgh Phenotypic Assay Centre; Prof Neil Carragher) to interrogate FDA-approved compounds (Prestwick FDA Approved Drug Library – 1280 compounds), which decrease the accumulation of P62 puncta in ECs lacking TCHP. Accordingly, candidate compounds that have reduced the accumulation of P62 in our cells were likely also to be regulators of autophagy. The analysis was performed considering the following features: cell number, the average nuclear intensity of P62 and whole-cell intensity of P62. Each compound was tested at a concentration of 0.33 μM, and 3.3 μM. HUVECs transfected with anti-miR negative control (20nM final concentration) were used as a positive control. HUVECs transfected with siRNA targeting TCHP (20nM final concentration) were treated with compounds 0.33 μM and 3.3 μM or with DMSO as a negative control. Finally, TCHP knock-down HUVECs not treated were used as an additional negative control.

Features were analysed using principal component analysis (PCA), and hits were identified using an Ensemble-based tree classification (**Fig.5.5**). The PCA analysis uses an orthogonal transformation to reduce the dimensionality of the dataset while preserving the most important patterns between the variables, which were cell number, the average nuclear intensity of P62 and whole-cell intensity of P62. The orthogonal axes, identified as principal components, capture the maximum variance in the data. The principal components are linear combinations of the original variables in the dataset and are ordered in decreasing order of importance. The first principal component (PC1) captures the most variation in the data and the second principal component (PC2) captures the maximum variance that is orthogonal to the first principal component. The red hits (siRNA + drug) highlighted in the **Fig. 5.5** indicate those compounds that are closer to the control media in blue. In green are represented the TCHP knock-out HUVECs treated with vehicle (siRNA DMSO) and in yellow are the TCHP knock-out HUVECs untreated (siRNA Media).

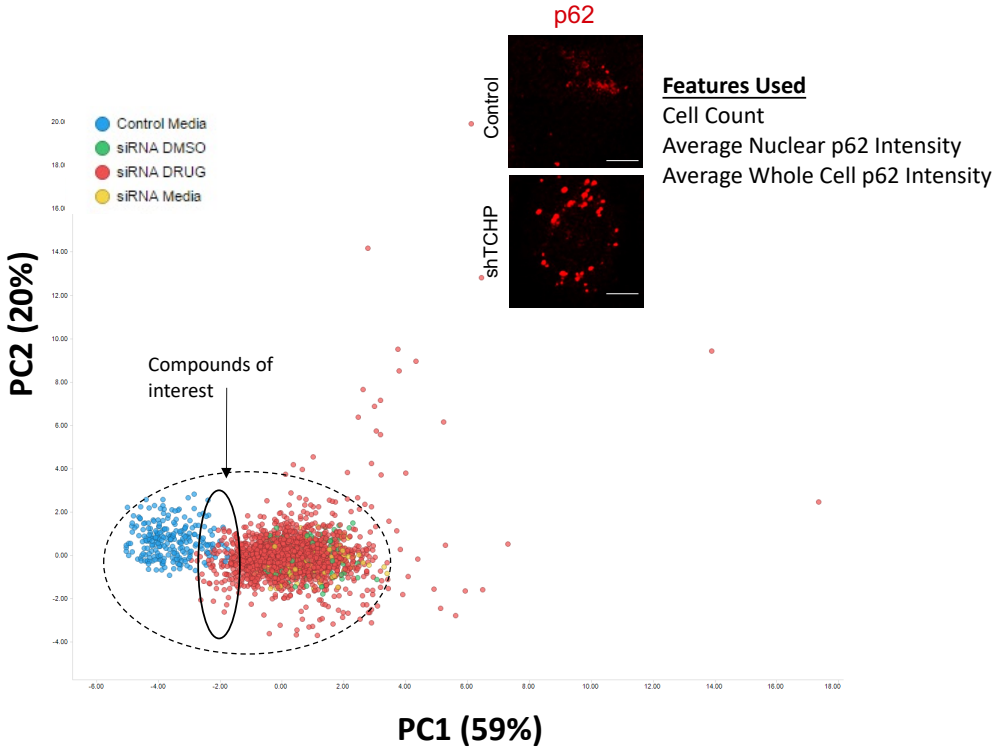


Figure 5.5| Principal component analysis of the screened compounds.

Principal components 1 and 2 are shown and their respective variance is indicated.

Compounds were ranked based on the positive score, from 1 in descending order, with compounds closer to 1 indicating the ones that shift towards the control media (**Table 5.1**). Two top compounds, Guanabenz and Milrinone, two FDA-approved compounds, were further tested *in vitro*. Guanabenz is an alpha2-selective adrenergic agonist used as anti-hypertensive agent, while Milrinone is a Phosphodiesterase 3A inhibitor that decreases inflammation in patients with heart failure [328].

Positivity score Control Media	Compounds
0.889501359	Guanabenz acetate
0.820095871	Dihydrostreptomycin sulfate
0.812883442	Milrinone
0.804299192	Canrenoic acid potassium salt
0.791489001	Bupropion hydrochloride
0.788091655	Ketoprofen
0.769178745	Sparfloxacin
0.759186341	Lidocaine hydrochloride
0.759019721	Glafenine hydrochloride
0.73735523	Urosiol
0.728166799	Meclofenamic acid sodium salt monohydrate
0.719715804	Diphenhydramine hydrochloride
0.719672213	Bumetanide
0.718243626	Nalmefene hydrochloride
0.695408307	Amitryptiline hydrochloride
0.69070317	Khellin
0.656091744	Chloropyramine hydrochloride
0.653425853	Acipimox
0.620913763	Benzbromarone
0.618527096	Primidone
0.606809239	Lodoxamide
0.598893691	Nitrofural
0.592990691	Cytarabine
0.59012072	R(-) Apomorphine hydrochloride hemihydrate
0.577642169	Proparacaine hydrochloride
0.548173872	Lincomycin hydrochloride
0.5427015	Chenodiol
0.524375105	Pancuronium bromide
0.493305059	Pinacidil
0.465435941	Thiethylperazine dimalate
0.405826488	Probenecid

Table 5.1| List of compounds reversing P62 accumulation in TCHP knock-down cells ranked as positivity score.

In red the compounds investigated *in vitro* using PROTEOSTAT® Aggresome Detection kit.

Moreover, a library of 176 compounds was screened, including protease and kinase inhibitors. The analysis generated a list of 25 hits. The top ones, apicidin and terreic acid, were excluded due to high toxicity, while splitomicin was eliminated for its negative effect on EC function (**Table 5.2**) [2]. Calpain inhibitor II, a kinase inhibitor previously known for restoring autophagy in diabetes and Huntington's disease [329, 330], was further investigated *in vitro*.

Kinase inhibitors

Chemical Name	Target	Positivity score control media
Splitomicin	SIRT-2 inhibitor	0.84
Apicidin	HDAC inhibitor	0.79
BAY 11-7082	IKK pathway	0.78
SB-202190	p38 MAPK	0.72
Terreic acid	BTK	0.70
TYRPHOSTIN AG 1288	Tyrosine kinases	0.69
Aminoresveratrol sulfate	SIRT1 activator	0.68
Daidzein	Negative control for Genistein	0.68
Epigallocatechin gallate	MMPs	0.66
N-Ethylmaleimide	Cysteine proteases	0.61
LY 294002	PI 3-K	0.57
E-64-C	Calpain; Cathepsins; Papain	0.57
Calpain Inhibitor II (ALLM)	Calpain; Cathepsins L, B	0.56
Tranylcypromine hemisulfate	Lysine demethylase inhibitor	0.53
Daidzein	Negative control for Genistein	0.53
GW 5074	cRAF	0.53
TYRPHOSTIN 46	EGFRK, PDGFRK	0.52
Lavendustin A	EGFRK	0.52
Nullscript	Scriptaid Neg control	0.50
Suramin·6Na	SIRT1 inhibitor	0.47
Roscovitine	CDK	0.46
Z-PLG-NHOH	MMPs	0.45
Piceatannol	Syk	0.44
ML-9Â·HCl	MLCK	0.43
SB-203580	p38 MAPK	0.42

Table 5.2: Analysis of kinase inhibitors reversing P62 accumulation in TCHP knock-down cells ranked as positivity score.

In red the small molecules investigated *in-vitro* using PROTEOSTAT® Aggresome Detection kit.

Validation of drug screening in vitro – Guanabenz, Milrinone, Calpain Inhibitor II

Sub-confluent cells were transduced with control and shRNA vectors targeting TCHP and treated with the selected compounds Guanabenz, Milrinone and Calpain Inhibitor II at the concentration of 5 μM or with DMSO for 24 hours. They were then fixed with 4% paraformaldehyde and stained using PROTEOSTAT® Aggresome Detection kit. The immunocytochemistry staining showed that Calpain inhibitor II and the phosphodiesterase 3A inhibitor Milrinone did not reduce the accumulation of aggregates in TCHP knock-down cells. Instead, the aggregates increased compared to the control. Conversely, the cells treated with the alpha-2 selective adrenergic agonist Guanabenz, show a significantly reduced presence of aggregates despite TCHP knock-down (**Figure 5.6**). Notably, Guanabenz can block eIF2α

dephosphorylation acting on protein phosphatase PP1C and consequently cause the block of the protein translation [331]. Moreover, recently Guanabenz acetate has been associated with the activation of autophagy through a similar mechanism [332].

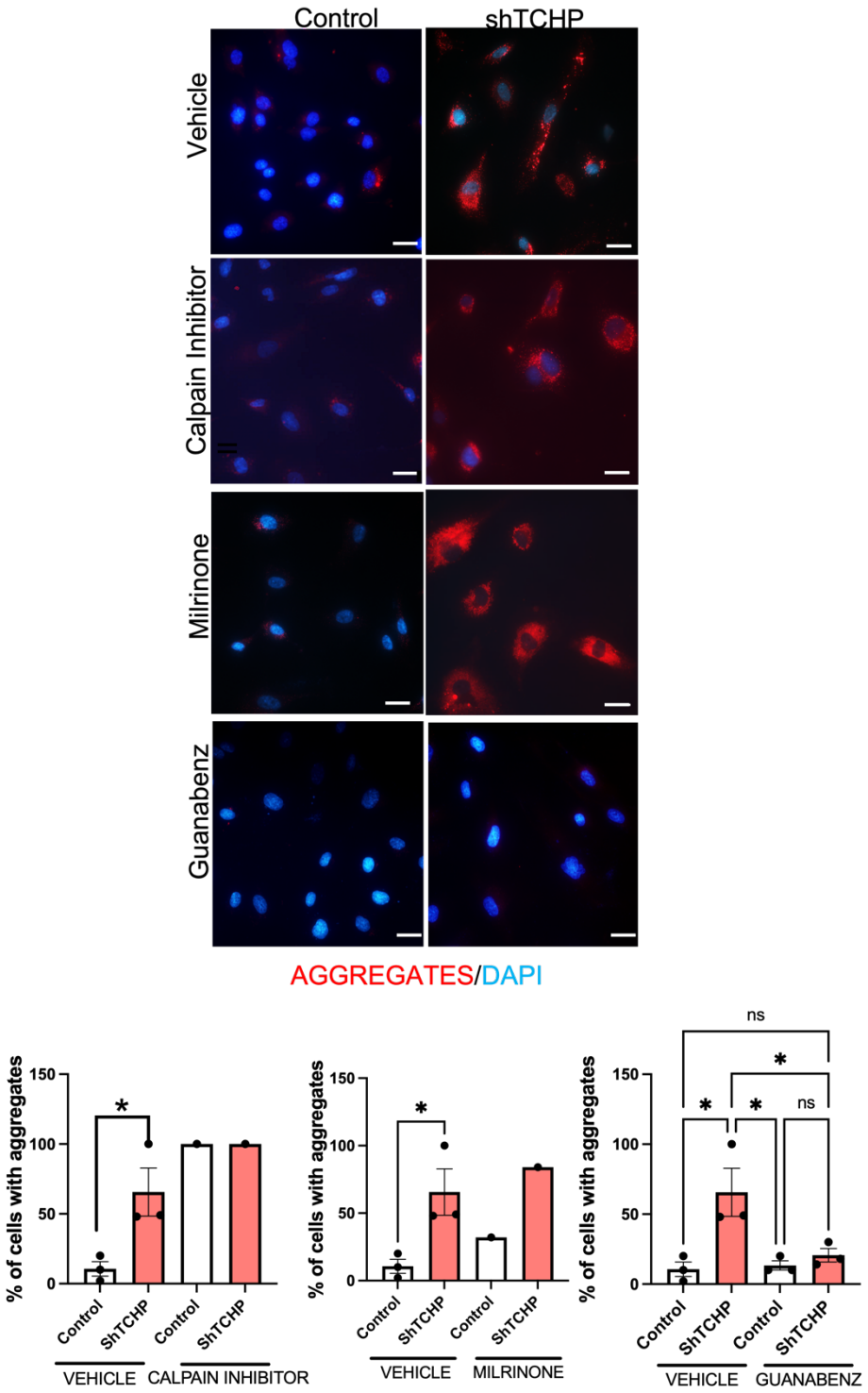


Figure 5.6| Test *in vitro* of small molecules and compounds to decrease protein aggregates accumulation.

Staining and quantification of protein aggregates in control and TCHP knock-down HUVECs either treated with vehicle (DMSO) or Guanabenz, Milrinone, Calpain Inhibitor II (5 µM). Scale bars, 20 µm; (*n* = 240 cells; Calpain Inhibitor : **P*= 0.0375 control vs shTCHP DMSO, *P=0.0133 control DMSO vs control Calpain Inhibitor II. Milrinone: *P= 0.0375 vs shTCHP. Guanabenz : two-way ANOVA Tukey post hoc test; **P* = 0.0184 control vs. shTCHP DMSO; $^{*}P$ = 0.0439 shTCHP DMSO vs. shTCHP Guanabenz, *P=0.0230 shTCHP vs control Guanabenz. F=8.359, DF=3). Statistical analyses were performed on at least three independent experiment. N experiment for calpain inhibitor and milrinone = 1. Data are represented as mean ± SEM.

Guanabenz reduces p62 and LC3-I puncta accumulation and inflammation

Since Guanabenz acetate decreased the accumulation of aggresomes in the cytoplasm of TCHP knock-down cells, I investigated if this action was linked with an activation of the autophagic flux. HUVECs were treated with Guanabenz (5 μM) or DMSO for 24 hours. The immunocytochemistry staining for P62 and the following quantification performed using CellProfiler, demonstrated a significant reduction of P62 puncta in the cytoplasm of TCHP knock-down cells treated with Guanabenz acetate compared to the controls treated with DMSO (**Fig.5.7A**). The decrease of P62 aligns with the hypothesis that Guanabenz can reduce the accumulation of aggregates reactivating autophagy. To confirm this, control and shRNA TCHP vectors were transduced with GFP-LCR lentiviral and treated with Guanabenz (5μM) for 24 hours. Interestingly, Guanabenz acetate could significantly reduce LC3-I puncta in TCHP knock-down cells ($p<0.0001$) compared to the control cells, indicating the reactivation of autophagy flux (**Fig.5.7B**).

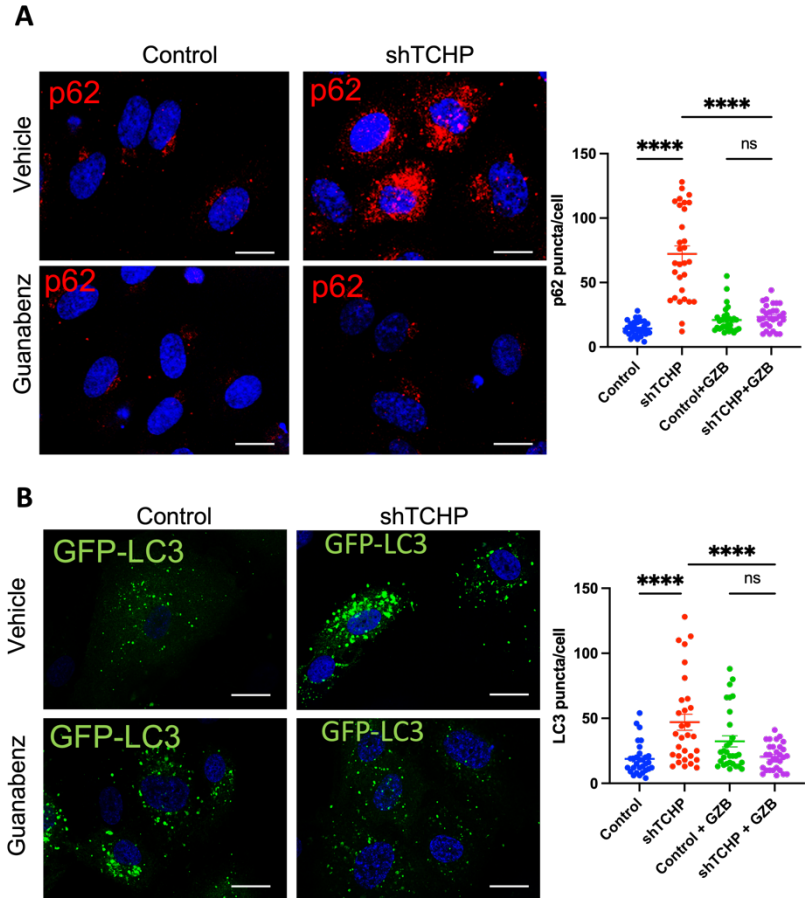


Figure 5.7| Effect of Guanabenz on autophagy and on TCHP–regulated target genes.

A. Immunocytochemistry and quantification of p62 in control and TCHP knock-down HUVECs either treated with vehicle (DMSO) or Guanabenz acetate (5 μM). **B.** Cells were transduced with control and shRNA TCHP vectors together with GFP-LCR lentiviral vector and treated with Guanabenz (5μM) for 24 hours. LC3 puncta per cell were analysed using CellProfiler software on n=60 cells/experimental conditions from three independent experiments . Scale bar 10 μm. Statistical analysis: Two-way ANOVA, Tukey post hoc test: ****$p<0.0001$, ns=not significant. For P62 puncta/cell: $F=58.85$; $DF=3$, for LC3 puncta/cell: $F=10.09$, $DF=3$.

Finally, I investigated if Guanabenz can decrease inflammation in the cells lacking TCHP. First, I addressed some target genes of TCHP, previously found upregulated in TCHP knock-down ECs [2]. The relative expression of the chemokine IL-8 ## increases significantly in TCHP knock-down ECs compared to the control (p=0.0124), while it decreases when cells are treated with Guanabenz (p=0.0007). Interestingly, the expression of the transcription factor FOXM1, a regulator of DNA damage, is upregulated in TCHP knock-down cells (p=0.0012), in support of the hypothesis of the genomic instability and the senescent phenotype. Notably, the Guanabenz treatment significantly reduced the increased expression of FOXM1 in the TCHP knock-down cells compared to the TCHP knock-down control (p= 0.0104) (**figure 5.8**).

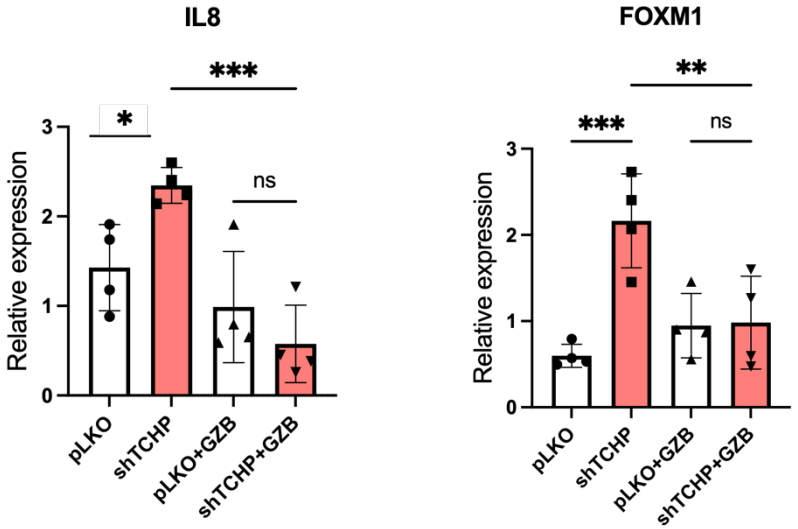


Figure 5.8| Effect of Guanabenz on TCHP–regulated target genes.

Cells were transduced with control and shRNA TCHP vectors and treated with Guanabenz (5µM) for 24 hours. Cells were transduced with control and shRNA TCHP vectors and treated with Guanabenz (5µM) for 24 hours. Expressions of IL8 and FOXM1 were determined by qPCR. Values are mean±SEM. Statistical analysis: Two-way ANOVA, Tukey post hoc test: **p<0.01; *p<0.05, ***p<0.001. Ns=statistically non-significant. IL8: F= 17.69, DF=3 FOXM1: F=20.29, DF=3.

Discussion

This chapter aimed to confirm the block of autophagic flux, previously linked with the knock-down of TCHP in HUVECs, in brain microvascular ECs and characterise the protein aggregates associated with this impairment. The analysis of the protein aggregates accumulated in the cytoplasm of TCHP knock-down ECs revealed the presence of RNA-binding proteins and other stress granules-related proteins, leading to the hypothesis of a biomolecular condensate nature of these aggregates. Aggregates and biomolecular condensates are a feature of ageing-associated disorders, and understanding the mechanisms that lead to their accumulation and toxicity is of interest to investigate new therapeutic targets and their involvement in the pathogenesis of these diseases.

Finally, the high-throughput screening revealed that an FDA-approved compound, Guanabenz, can reduce the accumulation of protein aggregates and decrease inflammation.

TCHP knock-down impairs autophagy in brain microvascular ECs

We previously discovered that TCHP is involved in the autophagy regulation in ECs through stabilising the centriolar protein PCM1. Consequently, impairment of TCHP causes the delocalisation of PCM1 and the degradation of its binding partner GABARAP, an autophagic protein necessary to form the autophagosome and accumulate the receptor protein P62. This has also been observed in patients with CAD [2].

I was interested in understanding if TCHP played the same role in the brain ECs. Immunocytochemistry demonstrated the delocalisation of PCM1 from centriolar satellites in TCHP knock-down human brain ECs and an accumulation of P62, confirming the hypothesis of the impairment of autophagic flux.

Of note, not only did we observe an accumulation of P62, but the brain ECs were also positive to the PROTEOSTAT®, a dye staining of protein aggregates. Furthermore, I confirmed their presence in the cytoplasm of both human microvascular ECs lacking TCHP and ECs isolated from the brain of $Tchp^{EC}$ mice. Protein aggregates are a hallmark of neurodegenerative disorders [333] and are involved in the pathogenesis

of the Lewy body [334], β-amyloid [335], huntingtin [336], and Tau [337]. In these pathologies, the aggregates are toxic and cause cell injury or death. Moreover, protein aggregates have been recently associated with ischaemic stroke when they aggravate cerebral ischaemic injury after cerebral ischaemia [317, 338]. The accumulation of these aggregates also demonstrates impairment of the protein clearance system, confirming the involvement of TCHP in the autophagic process in the brain ECs. The increased levels of P62 in the cytoplasm of the cells, caused by the impairment of the autophagic process, also inhibit the ubiquitin-proteasome system, enhancing the accumulation of the aggregates.

To conclude, these results confirm that TCHP localised in the centriolar satellites also in the brain microvascular ECs, stabilising PCM1 and affecting autophagosome formation.

Proteins involved in stress granules in TCHP knock-down endothelial cells

Stress granules are biomolecular condensates composed of translation factors, mRNAs, RNA-binding proteins and other proteins, whose assembling is triggered by cellular stress. Classically, the primary function of stress granules has been considered the translational arrest during a stress event. Their role has also been recognised in stress signalling, apoptosis induction, mRNA triage, expression regulation, biomolecular storage and inhibition of viral replication. They are involved not only in physiological function but in disease too. In support of the link between neurodegenerative disease and stress granules is the co-localisation between the stress granules and the pathological protein aggregates associated with these diseases [152]. Components of stress granules have been found in the aggregates of amyotrophic lateral sclerosis and Alzheimer's disease [339]. Therefore, I was interested in understanding if the protein aggregates observed in the cytoplasm of human TCHP knock-down ECs and from $Tchp^{EC}$ mice presented stress granules-related proteins. To evaluate that, I performed a mass spectrometry analysis of the insoluble fraction obtained from the control and HUVECs lacking TCHP. I chose to use HUVECs over the brain microvascular ECs because of the difficulties in obtaining many cells necessary to perform Mass spectrometry analysis.

The enrichment analysis demonstrated that RNA-binding, RNA processing, and mRNA processing-associated proteins are present in the aggregates. More specifically, RNA-binding proteins associated with stress granules were identified through enrichment analysis, supporting the hypothesis that the aggregates could be stress granules. Indeed, this category of proteins represents one of the main components of the stress granules, with TTP, TIA-1 and G3BP. In addition, the analysis highlighted the presence of some mitochondrial ribosomal proteins associated with the neurodegenerative disease: MRPS9, MRPS14, and MRPS24 [340].

In support of the co-localisation of stress granules foci with the protein aggregates, the immunocytochemistry analysis of phospho-elf2α demonstrated increased phosphorylation in the ECs lacking TCHP, confirming an activation of eIF2-GTP-tRNAiMet ternary complex, that stops translation through the block of polysome assembly, starting the process necessary for the formation of stress granules. Furthermore, TCHP knock-down ECs presented the RNA binding protein TTP in their cytoplasm, fundamental for the aggregation of stress granules.

The analysis suggests that the protein aggregates associated with the loss of TCHP could be stress granules. However, we did not detect a difference in the activation of HDAC6 between control and TCHP knock-down ECs. HDAC6 interacts with another stress granule protein, G3BP (Ras-GTPase-activating protein SH3 domain-binding protein 1). It is involved in the stress response by coordinating the formation of stress granules by mediating the motor-protein-driven movement of their components along microtubules [327].

The study reveals that the impairment of autophagy caused by the downregulation of TCHP causes the formation of stress granules in the cytoplasm of TCHP knock-down ECs, as confirmed by the enrichment analysis that revealed the presence of RNA binding proteins and stress granules related proteins and by the phosphorylation of elf2α and the presence of TTP in TCHP knock-down ECs. A co-localisation analysis between TTP and the protein aggregates will be performed in future experiments to confirm their association. The exact mechanism that links stress granules to disease is still poorly understood, and further research in this field is necessary to clarify the involvement of stress granules in the pathogenesis of neurovascular disease and help therapeutic interventions.

Guanabenz restores autophagy and reduces the accumulation of protein aggregates

To identify compounds that could reduce the accumulation of P62 and consequently reactivate autophagy, we performed a high-content phenotypic drug screen in collaboration with Edinburgh Phenotypic Assay Centre on 1280 FDA-approved compounds (Prestwick FDA Approved Drug Library) and 176 compounds including protease, epigenetics and kinase inhibitors. An experimental analysis previously performed in the lab demonstrated that BAY11-7082, an inhibitor of nuclear factor-κB (IκB) kinase (IKK), reduced the accumulation of P62 in TCHP knock-down cells. Furthermore, BAY11-7082 could reduce cytokine transcription and restore migratory capacity in TCHP knock-down ECs. In addition, this compound reduces NF-κB/p65 phosphorylation and, consequently, P62 accumulation [2].

To investigate if any compound could eliminate the protein aggregates in the cytoplasm of TCHP knock-down cells, I further tested *in vitro* two compounds, Milrinone and Guanabenz, and a small molecule, Calpain Inhibitor II.

Milrinone is a phosphodiesterase 3A inhibitor administered in patients with acute heart failure, pulmonary hypertension and chronic heart failure to improve cardiac contractility and vasodilatation and consequently increase cardiac output [341]. Milrinone blocks the degradation process of adenosine 3',5'-cyclic monophosphate (cAMP), increasing the intracellular concentration of cAMP. In addition, this compound showed anti-inflammatory properties in patients with severe heart failure, decreasing inflammatory biomarkers like IL-6 and TNFα [342]. Moreover, Milrinone treatment attenuated the activation of NF-κB and the inflammatory response in a mouse model of renal ischemia-reperfusion injury [328].

Guanabenz is an FDA-approved compound with anti-hypertensive properties and a centrally-acting alpha-2 adrenergic receptor agonist. It was previously described because it can enhance unfolded protein response (UPR) by prolonging eIF2α phosphorylation and consequently inhibiting protein synthesis in stressed cells [343]. Furthermore, it showed a protective action against ER stress in cardiac myocytes through the inhibition of the complex between protein phosphatase 1 regulatory subunit 15A and catalytic subunit of protein phosphatase 1 in the protein kinase RNA-like ER kinase (PERK) signalling pathway and the consequent impediment of stress-

induced dephosphorylation of eIF2α [344]. This mechanism was demonstrated in Hepatocellular Carcinoma Cells, where the phosphorylation of eIF2α led to apoptosis and autophagy through the inhibition of GADD34 (growth arrest and DNA damage-inducible transcript 34) and increased activation of the transcription factor ATF4 [345].

Guanabenz has been recently described in the context of neurodegenerative disorders. For example, in a rat model of spinal cord injury, Guanabenz increased lysosome biogenesis and unblocked autophagic flux through activation of TFEB and TFE3 and consequently restoring ER proteostasis [343, 346]. Furthermore, a Guanabenz analogue, PromISR-6, was able to reduce Huntingtin aggregates in a cellular model of Huntington's disease, selectively activating integrated stress response acting directly on PERK phosphorylation [347].

Calpain inhibitor II is a small molecule that restricts the activity of calpain, cathepsin L, and cathepsin B. Calpains are a family of calcium-activated cysteine proteases. They modulate the hypertrophic signalling pathway by activating NF-κB and protein degradation in cardiac hypertrophy [348]. The inhibition of calpain by endogenous calpain inhibitor calpastatin increased autophagosome levels reducing the number of aggregates present in the brain and improving motor signs and tremors in drosophila and in a mouse model of Huntington's disease [330]. Furthermore, calpains are aberrantly activated in Alzheimer's disease, where they are involved in the processing of amyloid precursor protein, and Tau [349] and a decrease in calpastatin level has been described in patients [350].

After treating HUVECs transduced with shRNA controls or shRNA TCHP lentiviral particles (20 MOI), the immunocytochemistry analysis performed using the PROTEOSTAT® dye demonstrated a significant reduction of the protein aggregates accumulation in TCHP knock-down ECs treated with Guanabenz. Conversely, no effects were shown by the treatment with Milrinone. On the other hand, an increase in the number of aggregates was shown after the treatment with Calpain Inhibitor II, possibly demonstrating a toxic effect on the cells. Whilst the drug screening analysed the reduction of the autophagic scaffold protein p62, the validation of the compounds here described was performed on Proteostat® aggresome detection kit. The Proteostat dye colocalizes with P62 [351] but the aggresome is constituted of

other misfolded proteins not processed by the cells. Consequently, we observed that some compounds that in the drug screening had a high score, like Milrinone, do not seem to have the same effect on the cells when immunocytochemistry analysis is performed. This can be due to the different markers analysed and that the analysis is not detecting only p62. One of the aims of the validation was also to investigate if the reduction of p62 corresponded to a reduction of the other misfolded proteins.

The described analyses to investigate the action of Guanabenz on autophagy confirmed that the alpha-2 adrenergic receptor agonist can restore the intracellular process. Indeed, immunocytochemistry demonstrated a reduction in p62 accumulation in TCHP knock-down ECs and a reduction of LC3 positive puncta. Furthermore, the accumulation of LC3 positive puncta is prominent in autophagy-deficient cells, where LC3-I is sequestered to P62 aggregates, and autophagosome formation is inhibited [352].

Guanabenz reduced the gene expression of the chemokine IL-8 and the transcription factor FOXM1. These two genes were previously found upregulated in ECs lacking TCHP [2]. More precisely, FOXM1 is involved in DNA break repair, cell differentiation, angiogenesis, apoptosis, and redox signalling and regulates cell cycle genes like cyclin B1 and cyclin D1. Moreover, it is often associated with tumour progression [353, 354]. IL-8 is a chemokine expressed by several types of cells, and its increase is associated with the senescence of endothelial cells. Senescent cells acquire a distinct phenotype known as SASP and secrete multiple inflammatory cytokines, growth factors, ROS, MMPs and proteases that contribute to ageing and the development of ageing-related disease. The increase of IL-8 has been documented in Alzheimer's disease and is associated with the induction of MMP2 and MMP9 activity [355]. Moreover, high cytokine levels contribute to chronic inflammation, facilitating vascular dysfunction and promoting endothelial apoptosis [234, 235, 356].

The decline in autophagic capacity provokes a low-grade inflammation. Indeed, typically autophagy is essential for the uptake of dysfunctional mitochondria that prevents excessive ROS production and, in that way, the activation of inflammasomes. When autophagic capacity declines, like during ageing, increased ROS production and aggregated proteins activate inflammasomes which provoke a low-grade inflammation in several tissues and, in that way, inhibit autophagy and

accelerate the ageing process. Furthermore, the decline in autophagy and the accumulation of protein aggregates affect cellular housekeeping functions, leading to the stimulation of NF-κB signalling that triggers a pro-inflammatory phenotype. This process might activate the NLRP3 and NLRP1 inflammatory risk sensors in specific tissues, such as the brain [127], which would then cause inflammatory responses in receptive tissues [357].

In this context, the decrease of inflammation and reactivation of autophagy through Guanabenz indicates that this compound may prove effective in clearing senescent cells in several aggregates-associated diseases.

Conclusions and future directions

In this chapter, I confirmed the impairment of autophagic flux in brain microvascular ECs lacking TCHP, demonstrated by the accumulation of autophagic receptor P62 and the delocalisation of PCM1, previously observed in HUVECS lacking TCHP. I then found stress granules-related proteins and increased phosphorylation of elf2α in the protein aggregates accumulated in the cytoplasm of these cells, supporting the hypothesis that there is a co-localisation between protein aggregates and biomolecular condensates. Finally, performing a high-throughput screening, I identified an FDA-approved compound, Guanabenz, that can restore the impaired autophagic process and decrease the inflammation associated with the decrease of TCHP. Further experiments will aim to investigate the effects of Guanabenz on ECs viability and *in vivo* in $Tchp^{EC}$ mice.

Chapter 6

Discussion

Chapter 6 Discussion

Cerebrovascular disease causes 15.4 thousand deaths per year in the UK, according to the last statistics data, and 160 thousand in the US, being the fifth cause of death worldwide [173]. Moreover, vascular dementia affects 150,000 people only in the UK, according to NHS [358]. Age-related cerebrovascular dysfunction plays a critical role in the pathogenesis of cerebrovascular disease, but therapeutic development has been largely unsuccessful until now. EC dysfunction is involved in the early stages of cerebrovascular disease, leading to altered cerebral blood flow and BBB impairment. In this context, identifying genes associated with endothelial dysfunction will help understand the role of ECs in BBB integrity and address new therapeutic targets.

TCHP has been identified as a ubiquitously expressed keratin-binding protein localised in mitochondria. It was then associated with cilia formation, cell cycle progression and finally, the regulation of ER-mitochondria tethering and mitophagy. Lately, the team has shown the role of TCHP in EC homeostasis and autophagy through stabilising PCM1 localisation and, consequently, its binding with the autophagic protein GABARAP. TCHP knock-down in ECs impaired migration and sprouting and led to inflammation. Protein aggregates were detected in ECs from $Tchp^{EC}$ mice and patients with CAD, presenting a decreased expression of TCHP [2]. Finally, endothelial-specific deletion of Tchp in mice reduced the blood flow recovery and vascularisation following hind-limb ischaemia.

The role of TCHP in brain vasculature has not been described yet. Therefore, the work described in this thesis was designed to investigate the role of TCHP *in vitro* and *in vivo* in the ECs of the BBB and what are the effects of its downregulation on EC homeostasis and BBB integrity, finally assessing the role of TCHP in autophagy regulation in brain ECs and identifying a compound that could restore endothelial dysfunction in this model.

TCHP knock-out impairs brain microvascular ECs homeostasis

TCHP knock-down has been associated with pro-inflammatory transcriptome and senescence in HUVECs [2]. The bulk RNA-seq and following validation by qPCR confirmed the activation of inflammatory pathways, such as chemokine and cytokine signalling, also in ECs isolated from the brain of $Tchp^{EC}$ mice and HBMVECs. Of note, Ccl5 was significantly upregulated when Tchp expression was downregulated. Ccl5 belongs to CCL5/CCR5 axis and is activated during chronic inflammation, maintaining inflammation and attracting immune cells via haptotaxis in the brain. Ccl5 is also responsible for inducing the expression of integrins and MMPs, which are fundamental for the passage of immune cells through the vascular wall [253]. CCL5 was expressed in patients with Alzheimer's disease and in a brain injury model, where it caused increased neuronal death [238, 254]. In support of the increased expression of Ccl5, gelatine zymography showed increased secretion of MMP9 in ECs with TCHP knock-out, suggesting the presence of inflammation and the possibility of TCHP knock-out affecting barrier integrity. In line with this, the permeability assay performed using ECIS® demonstrated an impairment of barrier function in the TCHP knock-down HBMVECs. Immunocytochemistry demonstrated a reduction of ZO-1 in the cells of $Tchp^{EC}$ mice. Inflammation has been reported to impair the BBB integrity by deregulating TJ assembly and Rho-kinase signalling necessary for the internalisation of TJs [92] and by activating MMPs [93]. Moreover, inflammation leads to the upregulation of the MAPK pathway and reduction of TJs [93] and causes an increased expression of cell adhesion molecules, involved in leukocyte infiltration from the blood [89]. In physiological conditions, MMPs are involved in the remodelling of the extracellular matrix to support angiogenesis and neurogenesis [63]. In disease, the continuous secretion of MMP causes a loss of BBB integrity by digesting TJs and basal membrane proteins. Increased MMP9 expression is involved in multiple sclerosis, stroke, Alzheimer's disease, cerebral aneurism and brain cancer [248].

In line with the impaired BBB integrity, TCHP knock-down caused an increased caveolae-mediated transport in HBMVECs. Brain ECs are characterised by a low vesicular rate, conversely to what happens in ECs of peripheral tissues like the heart

and lung. Increased caveolae-mediated trafficking has been associated with increased brain permeability in ischaemic stroke [232, 277]. Of note, it was reported that caveolae-mediated trafficking is prevented by the transporter Mfsd2a, which regulates lipid composition and BBB integrity [276]. TCHP was associated with the regulation of adipogenesis and its downregulation caused increased cholesterol levels. Further studies are necessary to understand if TCHP affects Mfsd2a expression and how it affects endocytosis.

Collectively, our data suggest that Tchp knock-out elicits inflammation and MMP9 secretion and affects caveolae-mediated trafficking, leading to an impairment of barrier integrity.

Tchp knock-out affects vascular permeability *in vivo*

The analysis *in vitro* suggested an impairment of barrier integrity associated with TCHP knock-down in HBMVECs and ECs isolated from $Tchp^{EC}$ mice. In Chapter 4, I described how the reduced expression of Tchp caused an increased vascular permeability *in vivo*. The intraperitoneal injection of dextran TRM 3 kDa and the following spectrofluorimetric analysis revealed an increased accumulation of fluorescent tracers in the brain of $Tchp^{EC}$ mice compared to the control. This is in line with the impaired barrier integrity observed *in vitro* and supports the hypothesis of an impaired BBB in $Tchp^{EC}$ mice. Of note, the increased vascular permeability was also confirmed in the heart of $Tchp^{EC}$ mice.

The analysis of the brain vascular network of $Tchp^{EC}$ mice showed significant alterations, decreased junctions, vessel length and reduced homogeneity of the vessels. Alterations of the vascular network have been observed in patients with cerebrovascular diseases, such as Alzheimer's disease [291] and traumatic brain injury [290], suggesting that Tchp knock-out affects endothelial functionality leading to a global modification of the brain's vasculature.

Collectively, the data suggest that the knock-out of Tchp negatively affects the brain vasculature. This aligns with the inflammatory transcriptome, MMP secretion and impairment of barrier function previously described.

TCHP and the regulation of autophagy in brain ECs

The team previously introduced the role of the keratin filament binding protein TCHP in regulating autophagy and, consequently, EC homeostasis, by controlling the localisation of PCM1 and its binding with the autophagic protein GABARAP [2]. In Chapter 5, I demonstrated how the knock-down of TCHP leads to the delocalisation of PCM1 and accumulation of P62 also in HBMVECs. Furthermore, the knock-out of Tchp caused an accumulation of protein aggregates in ECs isolated from the brain of $Tchp^{EC}$ mice. These features are typical of impaired autophagic flux and are associated with several neurodegenerative [160] and cardiovascular diseases [158]. Moreover, the mass spectrometry analysis of these aggregates revealed the presence of RNA-binding and stress granules-related proteins, suggesting that these aggregates could be stress granules, a category of biomolecular condensates. Immunocytochemistry analysis revealed increased phosphorylation of phospho-eIf2α in ECs lacking TCHP, suggesting activation of eIF2-GTP-tRNAiMet ternary complex that stops translation through the block of polysome assembly, starting the process necessary for the formation of stress granules. Furthermore, TCHP knock-down ECs are positive for the RNA-binding protein TTP, involved in the aggregation of stress granules. The assembling of stress granules is triggered by cellular stress and they are composed of translation factors, mRNAs, RNA-binding proteins and other proteins. Their main function is the translational arrest during a stress event, but they are also involved in disease [152]. Autophagy is involved in the clearance of stress granules and RNA-binding proteins [155, 157]; consequently, its impairment would lead to their accumulation. Accumulation of stress granules and protein aggregates leads to the production of ROS and inflammation, eliciting a pro-inflammatory phenotype in the ECs.

The high-throughput screening and the following immunocytochemistry analyses revealed that Guanabenz, an alpha-2 adrenergic receptor agonist FDA-approved compound, can reduce the protein aggregates accumulated in the cytoplasm of TCHP knock-down ECs and reduce inflammation by restoring autophagy, as demonstrated by the reduction in P62 accumulation in TCHP knock-down ECs and a reduction of LC3 positive puncta. Guanabenz acts on UPR by prolonging eIF2α phosphorylation

and consequently inhibiting protein synthesis in stressed cells [343]. Guanabenz was reported to inhibit the complex between protein phosphatase 1 regulatory subunit 15A and catalytic subunit of protein phosphatase 1 in the PERK signalling pathway and consequently prevent the stress-induced dephosphorylation of eIF2α in cardiac myocytes and Hepatocellular Carcinoma Cells [344, 345]. Furthermore, Guanabenz reactivated autophagic flux by activating TFEB and TFE3, restoring ER proteostasis in a rat model of spinal cord injury [346].

Overall, the data suggest that TCHP regulates autophagy also in brain ECs by stabilising the localisation of PCM1 and identifying Guanabenz as a compound to restore autophagy and reduce protein aggregates and inflammation in ECs.

Summary of key findings

Taken together, the data demonstrate that the knock-down of TCHP causes inflammation and secretion of MMPs, finally affecting barrier integrity. Furthermore, the impairment of barrier stability observed *in vitro* was finally confirmed *in vivo* in the $Tchp^{EC}$ mouse brain, where the fluorescent tracer dextran exited in the brain parenchyma and immunohistochemistry analysis revealed a reduction of vascular complexity.

The immunocytochemistry analysis revealed an accumulation of protein aggregates in the cytoplasm of ECs isolated from $Tchp^{EC}$ mice and TCHP knock-down HBMVECs. Furthermore, I confirmed the accumulation of P62 and the delocalisation of PCM1 in the HBMVECs lacking TCHP, suggesting an impairment of autophagy associated with the knock-down of TCHP as previously observed in peripheral ECs [2]. This mechanism will be analysed in ECs isolated from $Tchp^{EC}$ mice in the future. Impaired autophagy leads to inflammation and has been reported to affect TJs and BBB integrity, even if its role in the BBB is still controversial.

Of note, opposite to what was previously observed in HUVECs [2], I did not observe a modification of the cytoskeleton in TCHP knock-down ECs. This difference could be explained by brain microvascular EC resistance to actin remodelling. Indeed, conversely, to HUVECs and aortic ECs, HBMVECs were reported to resist cytoskeleton modification in response to shear stress or curvature [271, 359].

An increased caveolae-mediated transport was observed in TCHP knock-down ECs, supporting the impairment of barrier integrity associated with the lack of TCHP. CAV-1 expression is usually low in brain ECs and the increased endocytosis is a feature of impaired barrier integrity. Of note, CAV-1 is a negative regulator of autophagy by interacting with the ATG12-ATG5 regulatory system and maintaining the localisation of autophagosome components in lipid rafts, controlling autophagosome formation [360]. Also, CAV-1 is degraded by autophagy in a CAV-CAVIN-LC3B-mediated degradation. Consequently, impairment of autophagy would cause the accumulation of CAV-1 and more caveolae in the cytosol [361]. Conversely, Nah et al. reported that CAV1 acts as a positive regulator of autophagy under oxidative stress and cerebral ischemic injury by interacting with the BECN1/VPS34 complex and facilitating autophagosome formation [362]. Therefore, the increase in CAV-1 expression could be a compensatory mechanism to try to reactivate autophagy. Moreover, TCHP has been previously associated with CAV-1 in mesenchymal progenitors, where the elongated cilia, due to the depletion of TCHP prevented CAV-1 and GM3-positive lipid rafts from assembling at the cilium base [207]. Finally, CAV-1 expression in the ECs of the BBB is prevented by the transporter MFSD2A; consequently, further investigations of its expression in ECs lacking TCHP are necessary. Future studies are necessary to understand the link between TCHP and CAV-1 increase.

Finally, the high-throughput screening and immunocytochemistry analysis revealed that the anti-hypertensive agent Guanabenz can restore autophagy and reduce the accumulation of aggregates and inflammation. Further studies *in vitro* and *in vivo* are necessary to investigate if this compound could revert the inflammatory phenotype associated with Tchp knock-out.

Limitations of the study

The study presented in this thesis has some limitations. The culture of a large number of primary microvascular ECs isolated from the brain of a mouse model is difficult because of cell viability and handling. Consequently, immunocytochemistry analyses were performed on HBMVECs or HBEC-5i. The study described in the thesis was conducted in parallel in mouse and human cells and only concordant results were

considered; therefore, massive differences in the immunocytochemistry results are not expected. Nevertheless, some phenotype features discovered by immunocytochemistry and not confirmed yet in Tchp^{EC} mice must be investigated in the future. For the same reason, the drug screening and the following immunocytochemistry analysis were performed on HUVECs. The compound will be tested *in vitro* on HBMVEC functionality in the future.

In some analyses, sample size represented a limitation. During the PhD project, because of breeding issues, getting enough Tchp^{EC} mice for isolating ECs and enough power for some analyses was not possible.

The Tchp^{EC} mouse is a constitutive knock-out mouse model that exploits a cre under the promoter of the cadherin 5 (Cdh5) to get an endothelial-specific knock-out. However, the effects of the Tchp knock-out on embryos have yet to be studied and the constitutive knock-out could affect the development of the vasculature. To exclude that the observed phenotype is not due to an effect of the knock-out of Tchp in the developing brain, it will be necessary to confirm the phenotype using an inducible knockout and express it after birth. Furthermore, it would be interesting to perform an analysis on the embryos to understand what the effects of the knockout on the developing vasculature of the brain are. Further studies on how the knock-out could affect hemopoietic cells that transiently express VE-cadherin are necessary.

Finally, this study was deeply affected by the COVID-19 pandemic in 2020, which led to the impossibility of accessing the laboratories in the Centre for Cardiovascular Science, and to the interruption of the experimental analyses for 7 months (March 2020 to September 2020), slowing the research and the progress of the PhD studies.

Future perspectives

Characterisation of Tchp^{EC} mouse model: analysis of cerebral blood flow and behavioural tests

Future experiments will aim to clarify the effects of Tchp knock-out *in vivo*. Laser-speckle contrast imaging (Moor FLPI2 laser speckle contrast imager – Moor Instruments, UK) will be performed to understand how Tchp knock-out affects cortical cerebral perfusion. After anaesthesia, the skull will be exposed by a midline

incision and cortical perfusion measure will be recorded. Preliminary data show that Tchp knock-out affects cerebral perfusion with an increased flux compared to the WT (**Figure 6.1A**). This could be linked to microvasculature dysfunction that leads to reduced oxygen extraction and to a consequential compensating increase of the cerebral blood flow to balance the lack of oxygen and nutrients in the surrounding tissue. Studies described hyperaemia associated with abnormal capillaries features in young high-risk subjects for Alzheimer's disease. The same happens in acute ischaemic stroke when capillaries form functional shunts and oxygen becomes inaccessible to tissue [363].

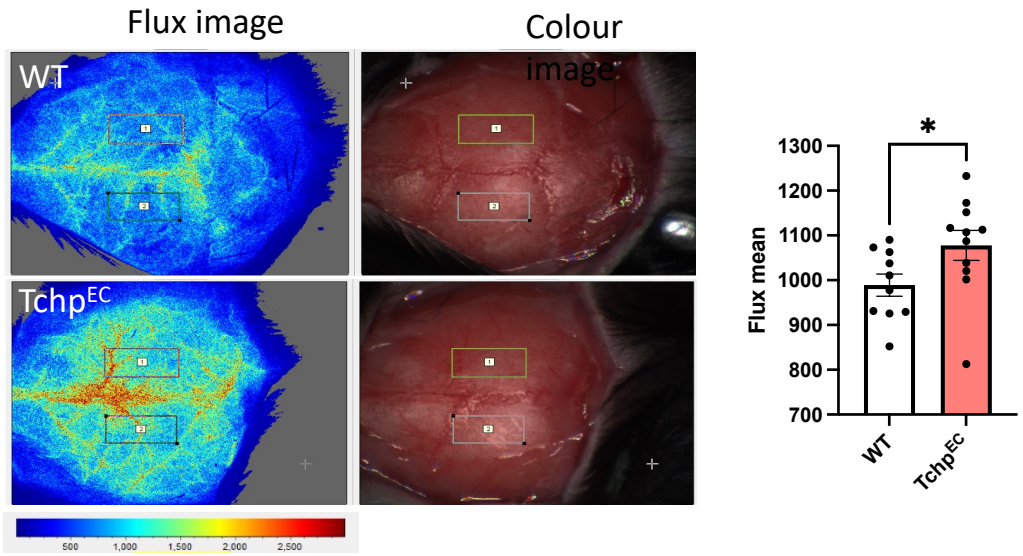
It is important to acknowledge the limitations of laser speckle contrast imaging, which can access only superficial areas of the brain, investigating mostly large vessels in the cortex, and does not allow a complete representation of the blood flux in the other areas of the brain. Other techniques that would allow a more complete view of cerebral blood flow in the brain are arterial spin labelling MRI and two photon imaging. The first one is a non-invasive technique that labels the protons in the arterial blood by radiofrequency pulses and the second one consists of the measurement of the speed of the red blood cells and vessel diameter by administrating dextran conjugated fluorescent dies. Future experiments will also aim to analyse blood pressure using The CODA™ Non-Invasive Blood Pressure System since the TCHP gene was associated with hypertension by gene-level phenotypic associations studies [212].

Magnetic Resonance Imaging (MRI) will be used to investigate BBB integrity (Figure 6.1B). Images will be acquired in a 400-mT/m gradient set 7 T Bruker scanner (Bruker Medical GmbH, Germany). The sequences will be collected in the following order: T2-weighted, T2*-weighted/SWI, T1-weighted RARE, and T1-map baseline RARE. After injection of 0.5 mmol kg^{-1} gadolinium-diethylenetriamine penta-acetic acid (Gd-DTPA), BioPAL, Inc., diluted in saline 1:7 via the tail vein at a rate of 600 µl min^{-1}, three further T1 maps each lasting 10 min will be recorded. Through MRI, it will be possible to have a precise characterisation of the brain regions interested in increased vascular permeability (**Figure 6.1B)**.

To further investigate the vessel leakage, other MW sizes of dextran (10 and 70 kDa) will be injected intraperitoneally in Tchp^{EC} mice and fluorescence will be analysed by spectrofluorimetric analysis.

Behavioural tests will be performed to investigate the effects of Tchp knock-out on behaviour. These tests include novel object recognition, open field, Y-maze, and elevated plus maze. In these tests, the willingness to explore, the anxiety, and the spatial working memory will be evaluated, to understand how Tchp affects the behaviour.

A



B

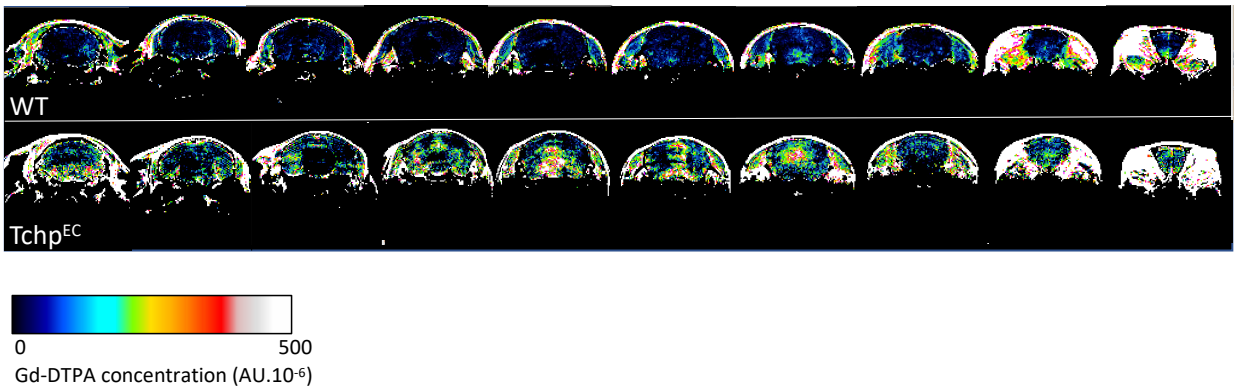


Figure 6.1| Characterization of cerebral blood flow and BBB integrity in Tchp^{EC} mouse.

A. Laser contrast speckle imaging and quantification of cortical perfusion on WT and Tchp^{EC} mice. P=*0.0473, unpaired t-test. **B.** Concentration of Gd-DTPA in WT and Tchp^{EC} mice measured by MRI scan.

To understand if endothelial-specific Tchp knock-out affects other cells of the BBB, pericytes coverage, astrocytes activation and microglia phenotype will be analysed by immunohistochemistry in the brain sections of Tchp^{EC} mice. A decrease in pericyte coverage has been associated with increased transcytosis, vessel leakage and impaired BBB integrity [54]. Moreover, the activation of astrocytes happens in

response to pathological conditions, leading to the secretion of inflammatory factors, such as IL-6 and MMPs [285]. Finally, the microglia phenotype will be investigated to confirm the data obtained by flow cytometry.

The increased caveolae-transport in TCHP knock-down ECs was demonstrated by a higher CAV-1 expression compared to control HBMVECs. The expression of CAV-1 has been linked with the transporter MFSD2A, which is fundamental for BBB development. Because of this, a deeper analysis of the expression of this transporter and the causes that lead to the increased expression of CAV-1 will be performed in brain ECs lacking TCHP. Preliminary qPCR data revealed the downregulation of MFSD2A in HBMVECs (**Figure 6.2**). In the future, the expression of this transporter will be investigated in Tchp^{EC} mice and a lipidomic analysis could help understand if Tchp knock-out affects brain EC lipidomic, affecting Mfsd2a.

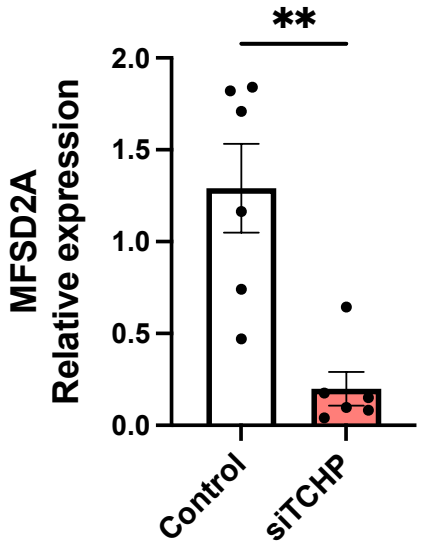


Figure 6.2| TCHP knockdown affects MFSD2A expression.

Expression of MFSD2A in control and TCHP knockdown HBMVECs (unpaired *t*-test;**P=0.0017).

In vitro and *in vivo* tests of Guanabenz

The high-throughput screening and the immunocytochemistry analysis suggested that the alpha-2 adrenergic receptor agonist Guanabenz can restore the impaired autophagy flux and reduce inflammation in TCHP knock-down HUVECs. Future experiments will aim to test this compound on HBMVECs, testing if the treatment with this compound can restore the impaired EC barrier using ECIS® and reduce

MMP9 production. If the test *in vitro* is successful, more tests will be performed *in vivo* on Tchp^{EC} mice to analyse if the treatment with this compound can reduce vascular permeability impairment and cortical perfusion.

Conclusive remarks

The thesis described the role of TCHP *in vitro* and *in vivo* in the ECs of the BBB and the effects of its downregulation on EC homeostasis and BBB integrity.

Tchp knock-down was associated with a decreased barrier function in HBMVECs and increased vascular permeability *in vivo*. Moreover, RNA-seq and gelatine zymography confirmed the inflammation and MMPs secretion associated with TCHP knock-down. Protein aggregates were found in the cytoplasm of brain microvascular ECs lacking TCHP, suggesting an impairment of autophagy, already studied in peripheral ECs. The proteomic characterisation of the insoluble-protein fraction revealed RNA-binding and proteasome-associated proteins, suggesting the toxicity of these aggregates for the cells. Finally, a pharmacological screening identified an FDA-approved compound activating autophagy and, thus, restoring EC function and reducing expression of inflammatory genes in EC lacking TCHP.

Overall, this study presents a novel role played by TCHP in the cerebrovascular endothelium and identifies a new mechanism by which the silencing of TCHP could link endothelial dysfunction to impaired BBB integrity.

References

1. Nishizawa, M., Izawa, I., Inoko, A., Hayashi, Y., Nagata, K. I., Yokoyama, T., Usukura, J. & Inagaki, M. (2005) Identification of trichoplein, a novel keratin filament-binding protein, *Journal of Cell Science*.
2. Martello, A., Lauriola, A., Mellis, D., Parish, E., Dawson, J. C., Imrie, L., Vidmar, M., Gammoh, N., Mitić, T., Brittan, M., Mills, N. L., Carragher, N. O., D'Arca, D. & Caporali, A. (2020) Trichoplein binds PCM 1 and controls endothelial cell function by regulating autophagy, *EMBO reports*.
3. Mameli, E., Martello, A. & Caporali, A. (2022) Autophagy at the interface of endothelial cell homeostasis and vascular disease, *Febs j.* **289**, 2976-2991.
4. Kisler, K., Nelson, A. R., Montagne, A. & Zlokovic, B. V. (2017) Cerebral blood flow regulation and neurovascular dysfunction in Alzheimer disease, *Nat Rev Neurosci.* **18**, 419-434.
5. Abbott, N. J., Rönnbäck, L. & Hansson, E. (2006) Astrocyte-endothelial interactions at the blood-brain barrier, *Nat Rev Neurosci.* **7**, 41-53.
6. Iadecola, C. (2017) The Neurovascular Unit Coming of Age: A Journey through Neurovascular Coupling in Health and Disease, *Neuron.* **96**, 17-42.
7. Zarekiani, P., Nogueira Pinto, H., Hol, E. M., Bugiani, M. & de Vries, H. E. (2022) The neurovascular unit in leukodystrophies: towards solving the puzzle, *Fluids Barriers CNS.* **19**, 18.
8. Sweeney, M. D., Zhao, Z., Montagne, A., Nelson, A. R. & Zlokovic, B. V. (2019) Blood-brain barrier: From physiology to disease and back, *Physiological Reviews.* **99**, 21-78.
9. Sweeney, M. D., Kisler, K., Montagne, A., Toga, A. W. & Zlokovic, B. V. (2018) The role of brain vasculature in neurodegenerative disorders, *Nature Neuroscience.* **21**, 1318-1331.
10. Kadry, H., Noorani, B. & Cucullo, L. (2020) A blood-brain barrier overview on structure, function, impairment, and biomarkers of integrity, *Fluids Barriers CNS.* **17**, 69.
11. Liebner, S., Dijkhuizen, R. M., Reiss, Y., Plate, K. H., Agalliu, D. & Constantin, G. (2018) Functional morphology of the blood-brain barrier in health and disease, *Acta Neuropathol.* **135**, 311-336.
12. Abbott, N. J., Patabendige, A. A., Dolman, D. E., Yusof, S. R. & Begley, D. J. (2010) Structure and function of the blood–brain barrier, *Neurobiology of disease.* **37**, 13-25.
13. Procter, T. V., Williams, A. & Montagne, A. (2021) Interplay between Brain Pericytes and Endothelial Cells in Dementia, *Am J Pathol.* **191**, 1917-1931.
14. Abbott, N. J. (2005) Dynamics of CNS barriers: evolution, differentiation, and modulation, *Cell Mol Neurobiol.* **25**, 5-23.
15. Hupe, M., Li, M. X., Kneitz, S., Davydova, D., Yokota, C., Kele, J., Hot, B., Stenman, J. M. & Gessler, M. (2017) Gene expression profiles of brain endothelial cells during embryonic development at bulk and single-cell levels, *Sci Signal.* **10**.
16. Wilhelm, I., Nyúl-Tóth, Á., Suciu, M., Hermenean, A. & Krizbai, I. A. (2016) Heterogeneity of the blood-brain barrier, *Tissue Barriers.* **4**, e1143544.

17. Noumbissi, M. E., Galasso, B. & Stins, M. F. (2018) Brain vascular heterogeneity: implications for disease pathogenesis and design of in vitro blood-brain barrier models, *Fluids Barriers CNS.* **15**, 12.
18. Matter, K. & Balda, M. S. (2003) Signalling to and from tight junctions, *Nat Rev Mol Cell Biol.* **4**, 225-36.
19. Taddei, A., Giampietro, C., Conti, A., Orsenigo, F., Breviario, F., Pirazzoli, V., Potente, M., Daly, C., Dimmeler, S. & Dejana, E. (2008) Endothelial adherens junctions control tight junctions by VE-cadherin-mediated upregulation of claudin-5, *Nat Cell Biol.* **10**, 923-34.
20. Tsukita, S., Furuse, M. & Itoh, M. (2001) Multifunctional strands in tight junctions, *Nat Rev Mol Cell Biol.* **2**, 285-93.
21. Cereijido, M., Valdés, J., Shoshani, L. & Contreras, R. G. (1998) Role of tight junctions in establishing and maintaining cell polarity, *Annu Rev Physiol.* **60**, 161-77.
22. Luissint, A. C., Artus, C., Glacial, F., Ganeshamoorthy, K. & Couraud, P. O. (2012) Tight junctions at the blood brain barrier: physiological architecture and disease-associated dysregulation, *Fluids Barriers CNS.* **9**, 23.
23. Sasson, E., Anzi, S., Bell, B., Yakovian, O., Zorsky, M., Deutsch, U., Engelhardt, B., Sherman, E., Vatine, G., Dzikowski, R. & Ben-Zvi, A. (2021) Nano-scale architecture of blood-brain barrier tight-junctions, *Elife.* **10**.
24. Engelhardt, B. & Liebner, S. (2014) Novel insights into the development and maintenance of the blood-brain barrier, *Cell Tissue Res.* **355**, 687-99.
25. Liebner, S., Fischmann, A., Rascher, G., Duffner, F., Grote, E. H., Kalbacher, H. & Wolburg, H. (2000) Claudin-1 and claudin-5 expression and tight junction morphology are altered in blood vessels of human glioblastoma multiforme, *Acta Neuropathol.* **100**, 323-31.
26. Liebner, S., Kniesel, U., Kalbacher, H. & Wolburg, H. (2000) Correlation of tight junction morphology with the expression of tight junction proteins in blood-brain barrier endothelial cells, *Eur J Cell Biol.* **79**, 707-17.
27. Lippoldt, A., Kniesel, U., Liebner, S., Kalbacher, H., Kirsch, T., Wolburg, H. & Haller, H. (2000) Structural alterations of tight junctions are associated with loss of polarity in stroke-prone spontaneously hypertensive rat blood-brain barrier endothelial cells, *Brain Res.* **885**, 251-61.
28. Berndt, P., Winkler, L., Cording, J., Breitkreuz-Korff, O., Rex, A., Dithmer, S., Rausch, V., Blasig, R., Richter, M., Sporbert, A., Wolburg, H., Blasig, I. E. & Haseloff, R. F. (2019) Tight junction proteins at the blood-brain barrier: far more than claudin-5, *Cell Mol Life Sci.* **76**, 1987-2002.
29. Uchida, Y., Sumiya, T., Tachikawa, M., Yamakawa, T., Murata, S., Yagi, Y., Sato, K., Stephan, A., Ito, K., Ohtsuki, S., Couraud, P. O., Suzuki, T. & Terasaki, T. (2019) Involvement of Claudin-11 in Disruption of Blood-Brain, -Spinal Cord, and -Arachnoid Barriers in Multiple Sclerosis, *Mol Neurobiol.* **56**, 2039-2056.
30. Ebnet, K., Brinkmann, B. F., Kummer, D., Misselwitz, S., Peddibhotla, S. S. & Tuncay, H. (2013) Tight junctions, junctional adhesion molecules (jams), and the blood brain barrier, *Tight junctions in cancer metastasis*, 119-129.
31. Ikenouchi, J., Furuse, M., Furuse, K., Sasaki, H., Tsukita, S. & Tsukita, S. (2005) Tricellulin constitutes a novel barrier at tricellular contacts of epithelial cells, *J Cell Biol.* **171**, 939-45.

32. Masuda, S., Oda, Y., Sasaki, H., Ikenouchi, J., Higashi, T., Akashi, M., Nishi, E. & Furuse, M. (2011) LSR defines cell corners for tricellular tight junction formation in epithelial cells, *J Cell Sci.* **124**, 548-55.
33. Sohet, F., Lin, C., Munji, R. N., Lee, S. Y., Ruderisch, N., Soung, A., Arnold, T. D., Derugin, N., Vexler, Z. S., Yen, F. T. & Daneman, R. (2015) LSR/angulin-1 is a tricellular tight junction protein involved in blood-brain barrier formation, *J Cell Biol.* **208**, 703-11.
34. Dejana, E. & Orsenigo, F. (2013) Endothelial adherens junctions at a glance, *J Cell Sci.* **126**, 2545-9.
35. Lai, C. H., Kuo, K. H. & Leo, J. M. (2005) Critical role of actin in modulating BBB permeability, *Brain Res Brain Res Rev.* **50**, 7-13.
36. Jones, J. C., Kam, C. Y., Harmon, R. M., Woychek, A. V., Hopkinson, S. B. & Green, K. J. (2017) Intermediate Filaments and the Plasma Membrane, *Cold Spring Harb Perspect Biol.* **9**.
37. Seetharaman, S. & Etienne-Manneville, S. (2019) Microtubules at focal adhesions - a double-edged sword, *J Cell Sci.* **132**.
38. Pardridge, W. M. (2015) Blood-brain barrier endogenous transporters as therapeutic targets: a new model for small molecule CNS drug discovery, *Expert Opin Ther Targets.* **19**, 1059-72.
39. Pardridge, W. M., Eisenberg, J. & Yang, J. (1985) Human blood-brain barrier insulin receptor, *J Neurochem.* **44**, 1771-8.
40. Zhang, Y. & Pardridge, W. M. (2001) Rapid transferrin efflux from brain to blood across the blood-brain barrier, *J Neurochem.* **76**, 1597-600.
41. Kido, Y., Tamai, I., Uchino, H., Suzuki, F., Sai, Y. & Tsuji, A. (2001) Molecular and functional identification of large neutral amino acid transporters LAT1 and LAT2 and their pharmacological relevance at the blood-brain barrier, *J Pharm Pharmacol.* **53**, 497-503.
42. Montagne, A., Zhao, Z. & Zlokovic, B. V. (2017) Alzheimer's disease: A matter of blood-brain barrier dysfunction?, *J Exp Med.* **214**, 3151-3169.
43. Bien-Ly, N., Yu, Y. J., Bumbaca, D., Elstrott, J., Boswell, C. A., Zhang, Y., Luk, W., Lu, Y., Dennis, M. S., Weimer, R. M., Chung, I. & Watts, R. J. (2014) Transferrin receptor (TfR) trafficking determines brain uptake of TfR antibody affinity variants, *J Exp Med.* **211**, 233-44.
44. Mayor, S., Parton, R. G. & Donaldson, J. G. (2014) Clathrin-independent pathways of endocytosis, *Cold Spring Harb Perspect Biol.* **6**.
45. Parton, R. G. & del Pozo, M. A. (2013) Caveolae as plasma membrane sensors, protectors and organizers, *Nat Rev Mol Cell Biol.* **14**, 98-112.
46. Andreone, B. J., Chow, B. W., Tata, A., Lacoste, B., Ben-Zvi, A., Bullock, K., Deik, A. A., Ginty, D. D., Clish, C. B. & Gu, C. (2017) Blood-Brain Barrier Permeability Is Regulated by Lipid Transport-Dependent Suppression of Caveolae-Mediated Transcytosis, *Neuron.* **94**, 581-594.e5.
47. Zhou, M., Shi, S. X., Liu, N., Jiang, Y., Karim, M. S., Vodovoz, S. J., Wang, X., Zhang, B. & Dumont, A. S. (2021) Caveolae-Mediated Endothelial Transcytosis across the Blood-Brain Barrier in Acute Ischemic Stroke, *J Clin Med.* **10**.
48. Kronstein, R., Seebach, J., Grossklaus, S., Minten, C., Engelhardt, B., Drab, M., Liebner, S., Arsenijevic, Y., Taha, A. A., Afanasieva, T. & Schnittler, H. J. (2012)

Caveolin-1 opens endothelial cell junctions by targeting catenins, *Cardiovasc Res.* **93**, 130-40.
49. O'Brown, N. M., Megason, S. G. & Gu, C. (2019) Suppression of transcytosis regulates zebrafish blood-brain barrier function, *Elife.* **8**.
50. Chow, B. W. & Gu, C. (2017) Gradual Suppression of Transcytosis Governs Functional Blood-Retinal Barrier Formation, *Neuron.* **93**, 1325-1333.e3.
51. Brown, L. S., Foster, C. G., Courtney, J. M., King, N. E., Howells, D. W. & Sutherland, B. A. (2019) Pericytes and Neurovascular Function in the Healthy and Diseased Brain, *Front Cell Neurosci.* **13**, 282.
52. Bell, R. D., Winkler, E. A., Sagare, A. P., Singh, I., LaRue, B., Deane, R. & Zlokovic, B. V. (2010) Pericytes control key neurovascular functions and neuronal phenotype in the adult brain and during brain aging, *Neuron.* **68**, 409-27.
53. Ribatti, D., Nico, B. & Crivellato, E. (2011) The role of pericytes in angiogenesis, *Int J Dev Biol.* **55**, 261-8.
54. Armulik, A., Genové, G., Mäe, M., Nisancioglu, M. H., Wallgard, E., Niaudet, C., He, L., Norlin, J., Lindblom, P., Strittmatter, K., Johansson, B. R. & Betsholtz, C. (2010) Pericytes regulate the blood–brain barrier, *Nature.* **468**, 557-561.
55. Mäe, M. A., He, L., Nordling, S., Vazquez-Liebanas, E., Nahar, K., Jung, B., Li, X., Tan, B. C., Chin Foo, J., Cazenave-Gassiot, A., Wenk, M. R., Zarb, Y., Lavina, B., Quaggin, S. E., Jeansson, M., Gu, C., Silver, D. L., Vanlandewijck, M., Butcher, E. C., Keller, A. & Betsholtz, C. (2021) Single-Cell Analysis of Blood-Brain Barrier Response to Pericyte Loss, *Circ Res.* **128**, e46-e62.
56. Grant, R. I., Hartmann, D. A., Underly, R. G., Berthiaume, A. A., Bhat, N. R. & Shih, A. Y. (2019) Organizational hierarchy and structural diversity of microvascular pericytes in adult mouse cortex, *J Cereb Blood Flow Metab.* **39**, 411-425.
57. Pfau, S. J., Langen, U. H., Fisher, T. M., Prakash, I., Nagpurwala, F., Lozoya, R. A., Lee, W.-C. A., Wu, Z. & Gu, C. (2021) Vascular and perivascular cell profiling reveals the molecular and cellular bases of blood-brain barrier heterogeneity, *bioRxiv*, 2021.04. 26.441465.
58. Chen, J., Luo, Y., Hui, H., Cai, T., Huang, H., Yang, F., Feng, J., Zhang, J. & Yan, X. (2017) CD146 coordinates brain endothelial cell-pericyte communication for blood-brain barrier development, *Proc Natl Acad Sci U S A.* **114**, E7622-e7631.
59. Paik, J. H., Skoura, A., Chae, S. S., Cowan, A. E., Han, D. K., Proia, R. L. & Hla, T. (2004) Sphingosine 1-phosphate receptor regulation of N-cadherin mediates vascular stabilization, *Genes Dev.* **18**, 2392-403.
60. Chua, X. Y., Chai, Y. L., Chew, W. S., Chong, J. R., Ang, H. L., Xiang, P., Camara, K., Howell, A. R., Torta, F., Wenk, M. R., Hilal, S., Venketasubramanian, N., Chen, C. P., Herr, D. R. & Lai, M. K. P. (2020) Immunomodulatory sphingosine-1-phosphates as plasma biomarkers of Alzheimer's disease and vascular cognitive impairment, *Alzheimers Res Ther.* **12**, 122.
61. Alarcon-Martinez, L., Yilmaz-Ozcan, S., Yemisci, M., Schallek, J., Kılıç, K., Can, A., Di Polo, A. & Dalkara, T. (2018) Capillary pericytes express α-smooth muscle actin, which requires prevention of filamentous-actin depolymerization for detection, *Elife.* **7**.
62. Herland, A., van der Meer, A. D., FitzGerald, E. A., Park, T. E., Sleeboom, J. J. & Ingber, D. E. (2016) Distinct Contributions of Astrocytes and Pericytes to

Neuroinflammation Identified in a 3D Human Blood-Brain Barrier on a Chip, *PLoS One.* **11**, e0150360.
63. Rosenberg, G. A. (2012) Neurological diseases in relation to the blood-brain barrier, *J Cereb Blood Flow Metab.* **32**, 1139-51.
64. Rustenhoven, J., Jansson, D., Smyth, L. C. & Dragunow, M. (2017) Brain Pericytes As Mediators of Neuroinflammation, *Trends Pharmacol Sci.* **38**, 291-304.
65. Sengillo, J. D., Winkler, E. A., Walker, C. T., Sullivan, J. S., Johnson, M. & Zlokovic, B. V. (2013) Deficiency in mural vascular cells coincides with blood-brain barrier disruption in Alzheimer's disease, *Brain Pathol.* **23**, 303-10.
66. Sagare, A. P., Bell, R. D., Zhao, Z., Ma, Q., Winkler, E. A., Ramanathan, A. & Zlokovic, B. V. (2013) Pericyte loss influences Alzheimer-like neurodegeneration in mice, *Nat Commun.* **4**, 2932.
67. Rhea, E. M. & Banks, W. A. (2019) Role of the Blood-Brain Barrier in Central Nervous System Insulin Resistance, *Front Neurosci.* **13**, 521.
68. Cheslow, L. & Alvarez, J. I. (2016) Glial-endothelial crosstalk regulates blood-brain barrier function, *Curr Opin Pharmacol.* **26**, 39-46.
69. Alvarez, J. I., Dodelet-Devillers, A., Kebir, H., Ifergan, I., Fabre, P. J., Terouz, S., Sabbagh, M., Wosik, K., Bourbonnière, L., Bernard, M., van Horssen, J., de Vries, H. E., Charron, F. & Prat, A. (2011) The Hedgehog pathway promotes blood-brain barrier integrity and CNS immune quiescence, *Science.* **334**, 1727-31.
70. Yao, Y., Chen, Z. L., Norris, E. H. & Strickland, S. (2014) Astrocytic laminin regulates pericyte differentiation and maintains blood brain barrier integrity, *Nat Commun.* **5**, 3413.
71. Langen, U. H., Ayloo, S. & Gu, C. (2019) Development and Cell Biology of the Blood-Brain Barrier, *Annu Rev Cell Dev Biol.* **35**, 591-613.
72. Dudiki, T., Meller, J., Mahajan, G., Liu, H., Zhevlakova, I., Stefl, S., Witherow, C., Podrez, E., Kothapalli, C. R. & Byzova, T. V. (2020) Microglia control vascular architecture via a TGFβ1 dependent paracrine mechanism linked to tissue mechanics, *Nat Commun.* **11**, 986.
73. Dixon, M. A., Greferath, U., Fletcher, E. L. & Jobling, A. I. (2021) The Contribution of Microglia to the Development and Maturation of the Visual System, *Front Cell Neurosci.* **15**, 659843.
74. Parkhurst, C. N., Yang, G., Ninan, I., Savas, J. N., Yates, J. R., 3rd, Lafaille, J. J., Hempstead, B. L., Littman, D. R. & Gan, W. B. (2013) Microglia promote learning-dependent synapse formation through brain-derived neurotrophic factor, *Cell.* **155**, 1596-609.
75. Subhramanyam, C. S., Wang, C., Hu, Q. & Dheen, S. T. (2019) Microglia-mediated neuroinflammation in neurodegenerative diseases, *Semin Cell Dev Biol.* **94**, 112-120.
76. Angelova, D. M. & Brown, D. R. (2019) Microglia and the aging brain: are senescent microglia the key to neurodegeneration?, *J Neurochem.* **151**, 676-688.
77. Qin, C., Zhou, L. Q., Ma, X. T., Hu, Z. W., Yang, S., Chen, M., Bosco, D. B., Wu, L. J. & Tian, D. S. (2019) Dual Functions of Microglia in Ischemic Stroke, *Neurosci Bull.* **35**, 921-933.
78. Merighi, S., Nigro, M., Travagli, A. & Gessi, S. (2022) Microglia and Alzheimer's Disease, *Int J Mol Sci.* **23**.

79. Haruwaka, K., Ikegami, A., Tachibana, Y., Ohno, N., Konishi, H., Hashimoto, A., Matsumoto, M., Kato, D., Ono, R., Kiyama, H., Moorhouse, A. J., Nabekura, J. & Wake, H. (2019) Dual microglia effects on blood brain barrier permeability induced by systemic inflammation, *Nat Commun.* **10**, 5816.
80. Jolivel, V., Bicker, F., Binamé, F., Ploen, R., Keller, S., Gollan, R., Jurek, B., Birkenstock, J., Poisa-Beiro, L., Bruttger, J., Opitz, V., Thal, S. C., Waisman, A., Bäuerle, T., Schäfer, M. K., Zipp, F. & Schmidt, M. H. H. (2015) Perivascular microglia promote blood vessel disintegration in the ischemic penumbra, *Acta Neuropathol.* **129**, 279-95.
81. Bialas, A. R., Presumey, J., Das, A., van der Poel, C. E., Lapchak, P. H., Mesin, L., Victora, G., Tsokos, G. C., Mawrin, C., Herbst, R. & Carroll, M. C. (2020) Retraction Note: Microglia-dependent synapse loss in type I interferon-mediated lupus, *Nature.* **578**, 177.
82. Whiteus, C., Freitas, C. & Grutzendler, J. (2014) Perturbed neural activity disrupts cerebral angiogenesis during a postnatal critical period, *Nature.* **505**, 407-11.
83. Hrvatin, S., Hochbaum, D. R., Nagy, M. A., Cicconet, M., Robertson, K., Cheadle, L., Zilionis, R., Ratner, A., Borges-Monroy, R., Klein, A. M., Sabatini, B. L. & Greenberg, M. E. (2018) Publisher Correction: Single-cell analysis of experience-dependent transcriptomic states in the mouse visual cortex, *Nat Neurosci.* **21**, 1017.
84. Augustin, H. G., Koh, G. Y., Thurston, G. & Alitalo, K. (2009) Control of vascular morphogenesis and homeostasis through the angiopoietin-Tie system, *Nat Rev Mol Cell Biol.* **10**, 165-77.
85. Vazana, U., Veksler, R., Pell, G. S., Prager, O., Fassler, M., Chassidim, Y., Roth, Y., Shahar, H., Zangen, A., Raccah, R., Onesti, E., Ceccanti, M., Colonnese, C., Santoro, A., Salvati, M., D'Elia, A., Nucciarelli, V., Inghilleri, M. & Friedman, A. (2016) Glutamate-Mediated Blood-Brain Barrier Opening: Implications for Neuroprotection and Drug Delivery, *J Neurosci.* **36**, 7727-39.
86. Kaplan, L., Chow, B. W. & Gu, C. (2020) Neuronal regulation of the blood-brain barrier and neurovascular coupling, *Nat Rev Neurosci.* **21**, 416-432.
87. Takata, F., Nakagawa, S., Matsumoto, J. & Dohgu, S. (2021) Blood-Brain Barrier Dysfunction Amplifies the Development of Neuroinflammation: Understanding of Cellular Events in Brain Microvascular Endothelial Cells for Prevention and Treatment of BBB Dysfunction, *Front Cell Neurosci.* **15**, 661838.
88. Zhao, Y., Gan, L., Ren, L., Lin, Y., Ma, C. & Lin, X. (2022) Factors influencing the blood-brain barrier permeability, *Brain Res.* **1788**, 147937.
89. Rajeev, V., Fann, D. Y., Dinh, Q. N., Kim, H. A., De Silva, T. M., Lai, M. K. P., Chen, C. L., Drummond, G. R., Sobey, C. G. & Arumugam, T. V. (2022) Pathophysiology of blood brain barrier dysfunction during chronic cerebral hypoperfusion in vascular cognitive impairment, *Theranostics.* **12**, 1639-1658.
90. Wang, F., Cao, Y., Ma, L., Pei, H., Rausch, W. D. & Li, H. (2018) Dysfunction of Cerebrovascular Endothelial Cells: Prelude to Vascular Dementia, *Front Aging Neurosci.* **10**, 376.
91. Utech, M., Mennigen, R. & Bruewer, M. (2010) Endocytosis and recycling of tight junction proteins in inflammation, *J Biomed Biotechnol.* **2010**, 484987.

92. Bauer, A. T., Bürgers, H. F., Rabie, T. & Marti, H. H. (2010) Matrix metalloproteinase-9 mediates hypoxia-induced vascular leakage in the brain via tight junction rearrangement, *J Cereb Blood Flow Metab.* **30**, 837-48.
93. Cardoso, F. L., Kittel, A., Veszelka, S., Palmela, I., Tóth, A., Brites, D., Deli, M. A. & Brito, M. A. (2012) Exposure to lipopolysaccharide and/or unconjugated bilirubin impair the integrity and function of brain microvascular endothelial cells, *PLoS One.* **7**, e35919.
94. Lochhead, J. J., Yang, J., Ronaldson, P. T. & Davis, T. P. (2020) Structure, Function, and Regulation of the Blood-Brain Barrier Tight Junction in Central Nervous System Disorders, *Front Physiol.* **11**, 914.
95. Kasza, K. E. & Zallen, J. A. (2011) Dynamics and regulation of contractile actin-myosin networks in morphogenesis, *Curr Opin Cell Biol.* **23**, 30-8.
96. Komarova, Y. A., Kruse, K., Mehta, D. & Malik, A. B. (2017) Protein Interactions at Endothelial Junctions and Signaling Mechanisms Regulating Endothelial Permeability, *Circ Res.* **120**, 179-206.
97. Wang, W. Y., Tan, M. S., Yu, J. T. & Tan, L. (2015) Role of pro-inflammatory cytokines released from microglia in Alzheimer's disease, *Ann Transl Med.* **3**, 136.
98. Réus, G. Z., Fries, G. R., Stertz, L., Badawy, M., Passos, I. C., Barichello, T., Kapczinski, F. & Quevedo, J. (2015) The role of inflammation and microglial activation in the pathophysiology of psychiatric disorders, *Neuroscience.* **300**, 141-54.
99. Muller, W. A. (2002) Leukocyte-endothelial cell interactions in the inflammatory response, *Lab Invest.* **82**, 521-33.
100. Vivier, E. & Malissen, B. (2005) Innate and adaptive immunity: specificities and signaling hierarchies revisited, *Nat Immunol.* **6**, 17-21.
101. Waldman, A. D., Fritz, J. M. & Lenardo, M. J. (2020) A guide to cancer immunotherapy: from T cell basic science to clinical practice, *Nat Rev Immunol.* **20**, 651-668.
102. Evans, L. E., Taylor, J. L., Smith, C. J., Pritchard, H. A. T., Greenstein, A. S. & Allan, S. M. (2021) Cardiovascular comorbidities, inflammation, and cerebral small vessel disease, *Cardiovasc Res.* **117**, 2575-2588.
103. Kamel, H. & Iadecola, C. (2012) Brain-immune interactions and ischemic stroke: clinical implications, *Arch Neurol.* **69**, 576-81.
104. Holland, P. R., Searcy, J. L., Salvadores, N., Scullion, G., Chen, G., Lawson, G., Scott, F., Bastin, M. E., Ihara, M., Kalaria, R., Wood, E. R., Smith, C., Wardlaw, J. M. & Horsburgh, K. (2015) Gliovascular disruption and cognitive deficits in a mouse model with features of small vessel disease, *J Cereb Blood Flow Metab.* **35**, 1005-14.
105. Mizushima, N. & Komatsu, M. (2011) Autophagy: Renovation of cells and tissues in
106. Schuck, S. (2020) Microautophagy - distinct molecular mechanisms handle cargoes of many sizes, *J Cell Sci.* **133**.
107. Kaushik, S. & Cuervo, A. M. (2018) The coming of age of chaperone-mediated autophagy in
108. Rabanal-Ruiz, Y., Otten, E. G. & Korolchuk, V. I. (2017) mTORC1 as the main gateway to autophagy, *Essays Biochem.* **61**, 565-584.

109. Lazarus, M. B., Novotny, C. J. & Shokat, K. M. (2015) Structure of the human autophagy initiating kinase ULK1 in complex with potent inhibitors, *ACS Chem Biol.* **10**, 257-61.
110. Gwinn, D. M., Shackelford, D. B., Egan, D. F., Mihaylova, M. M., Mery, A., Vasquez, D. S., Turk, B. E. & Shaw, R. J. (2008) AMPK phosphorylation of raptor mediates a metabolic checkpoint, *Mol Cell.* **30**, 214-26.
111. Ohashi, Y., Tremel, S. & Williams, R. L. (2019) VPS34 complexes from a structural perspective, *J Lipid Res.* **60**, 229-241.
112. Otomo, C., Metlagel, Z., Takaesu, G. & Otomo, T. (2013) Structure of the human ATG12~ATG5 conjugate required for LC3 lipidation in autophagy, *Nat Struct Mol Biol.* **20**, 59-66.
113. Birgisdottir Å, B., Mouilleron, S., Bhujabal, Z., Wirth, M., Sjøttem, E., Evjen, G., Zhang, W., Lee, R., O'Reilly, N., Tooze, S. A., Lamark, T. & Johansen, T. (2019) Members of the autophagy class III phosphatidylinositol 3-kinase complex I interact with GABARAP and GABARAPL1 via LIR motifs, *Autophagy.* **15**, 1333-1355.
114. Alemu, E. A., Lamark, T., Torgersen, K. M., Birgisdottir, A. B., Larsen, K. B., Jain, A., Olsvik, H., Øvervatn, A., Kirkin, V. & Johansen, T. (2012) ATG8 family proteins act as scaffolds for assembly of the ULK complex: sequence requirements for LC3-interacting region (LIR) motifs, *J Biol Chem.* **287**, 39275-90.
115. Kraft, C., Peter, M. & Hofmann, K. (2010) Selective autophagy: ubiquitin-mediated recognition and beyond, *Nat Cell Biol.* **12**, 836-41.
116. Joachim, J., Razi, M., Judith, D., Wirth, M., Calamita, E., Encheva, V., Dynlacht, B. D., Snijders, A. P., O'Reilly, N., Jefferies, H. B. J. & Tooze, S. A. (2017) Centriolar Satellites Control GABARAP Ubiquitination and GABARAP-Mediated Autophagy, *Current Biology*.
117. Spengler, K., Kryeziu, N., Große, S., Mosig, A. S. & Heller, R. (2020) VEGF Triggers Transient Induction of Autophagy in Endothelial Cells via AMPKα1, *Cells*.
118. Domigan, C. K., Warren, C. M., Antanesian, V., Happel, K., Ziyad, S., Lee, S., Krall, A., Duan, L., Torres-Collado, A. X., Castellani, L. W., Elashoff, D., Christofk, H. R., van der Bliek, A. M., Potente, M. & Iruela-Arispe, M. L. (2015) Autocrine VEGF maintains endothelial survival through regulation of metabolism and autophagy, *J Cell Sci.* **128**, 2236-48.
119. Zhao, X., Nedvetsky, P., Stanchi, F., Vion, A. C., Popp, O., Zühlke, K., Dittmar, G., Klussmann, E. & Gerhardt, H. (2019) Endothelial PKA activity regulates angiogenesis by limiting autophagy through phosphorylation of ATG16L1, *Elife.* **8**.
120. Liu, J., Bi, X., Chen, T., Zhang, Q., Wang, S. X., Chiu, J. J., Liu, G. S., Zhang, Y., Bu, P. & Jiang, F. (2015) Shear stress regulates endothelial cell autophagy via redox regulation and Sirt1 expression, *Cell Death Dis.* **6**, e1827.
121. Du, J., Teng, R. J., Guan, T., Eis, A., Kaul, S., Konduri, G. G. & Shi, Y. (2012) Role of autophagy in angiogenesis in aortic endothelial cells, *Am J Physiol Cell Physiol.* **302**, C383-91.
122. Schaaf, M. B., Houbaert, D., Meçe, O. & Agostinis, P. (2019) Autophagy in endothelial cells and tumor angiogenesis in
123. Bugatti, A., Marsico, S., Mazzuca, P., Schulze, K., Ebensen, T., Giagulli, C., Peña, E., Badimón, L., Slevin, M., Caruso, A., Guzman, C. A. & Caccuri, F. (2020) Role of autophagy in von willebrand factor secretion by endothelial cells and in the in vivo

thrombin-antithrombin complex formation promoted by the hiv-1 matrix protein p17, *International Journal of Molecular Sciences*.
124. Guo, F., Li, X., Peng, J., Tang, Y., Yang, Q., Liu, L., Wang, Z., Jiang, Z., Xiao, M., Ni, C., Chen, R., Wei, D. & Wang, G. X. (2014) Autophagy regulates vascular endothelial cell eNOS and ET-1 expression induced by laminar shear stress in an ex vivo perfused system, *Ann Biomed Eng.* **42**, 1978-88.
125. Fetterman, J. L., Holbrook, M., Flint, N., Feng, B., Bret'n-Romero, R., Linder, E. A., Berk, B. D., Duess, M. A., Farb, M. G., Gokce, N., Shirihai, O. S., Hamburg, N. M. & Vita, J. A. (2016) Restoration of autophagy in endothelial cells from patients with diabetes mellitus improves nitric oxide signaling, *Atherosclerosis*.
126. Larocca, T. J., Henson, G. D., Thorburn, A., Sindler, A. L., Pierce, G. L. & Seals, D. R. (2012) Translational evidence that impaired autophagy contributes to arterial ageing, *Journal of Physiology*.
127. De Rivero Vaccari, J. P., Lotocki, G., Alonso, O. F., Bramlett, H. M., Dietrich, W. D. & Keane, R. W. (2009) Therapeutic neutralization of the NLRP1 inflammasome reduces the innate immune response and improves histopathology after traumatic brain injury, *Journal of Cerebral Blood Flow and Metabolism*.
128. Salminen, A., Kaarniranta, K. & Kauppinen, A. (2012) Inflammaging: Disturbed interplay between autophagy and inflammasomes, *Aging.* **4**, 166-175.
129. Pacher, P., Beckman, J. S. & Liaudet, L. (2007) Nitric oxide and peroxynitrite in health and disease in
130. Ungvari, Z., Orosz, Z., Labinskyy, N., Rivera, A., Xiangmin, Z., Smith, K. & Csiszar, A. (2007) Increased mitochondrial H2O2 production promotes endothelial NF-κB activation in aged rat arteries, *American Journal of Physiology - Heart and Circulatory Physiology*.
131. Coppedè, F. & Migliore, L. (2015) DNA damage in neurodegenerative diseases in
132. Franceschi, C., BonafÈ, M., Valensin, S., Olivieri, F., De Luca, M., Ottaviani, E. & De Benedictis, G. (2006) Inflamm-aging: An Evolutionary Perspective on Immunosenescence, *Annals of the New York Academy of Sciences*.
133. Sánchez-Martín, P., Saito, T. & Komatsu, M. (2019) p62/SQSTM1: 'Jack of all trades' in health and cancer, *Febs j.* **286**, 8-23.
134. Duran, A., Linares, J. F., Galvez, A. S., Wikenheiser, K., Flores, J. M., Diaz-Meco, M. T. & Moscat, J. (2008) The signaling adaptor p62 is an important NF-kappaB mediator in tumorigenesis, *Cancer Cell.* **13**, 343-54.
135. Duran, A., Amanchy, R., Linares, J. F., Joshi, J., Abu-Baker, S., Porollo, A., Hansen, M., Moscat, J. & Diaz-Meco, M. T. (2011) p62 is a key regulator of nutrient sensing in the mTORC1 pathway, *Mol Cell.* **44**, 134-46.
136. Coleman, P., Hahn, C., Grimshaw, M., Lu, Y., Li, X., Brautigan, P., Beck, K., Stocker, R., Vadas, M. & Gamble, J. (2010) Stress-induced premature senescence mediated by a novel gene, SENEX, results in an anti-inflammatory phenotype in endothelial cells, *Blood.* **116**, 4016-40.
137. Powter, E., Coleman, P., Tran, M., Lay, A., Bertolino, P., Parton, R., Vadas, M. & Gamble, J. (2015) Caveolae control the anti-inflammatory phenotype of senescent endothelial cells, *Aging Cell.* **14**, 102-11.
138. Ting, K. K., Coleman, P., Zhao, Y., Vadas, M. A. & Gamble, J. R. (2021) The aging endothelium, *Vascular Biology.* **3**, R35-R47.

139. Guo, J., Huang, X., Dou, L., Yan, M., Shen, T., Tang, W. & Li, J. (2022) Aging and aging-related diseases: from molecular mechanisms to interventions and treatments, *Signal Transduction and Targeted Therapy.* **7**, 391.
140. Grunewald, M., Kumar, S., Sharife, H., Volinsky, E., Gileles-Hillel, A., Licht, T., Permyakova, A., Hinden, L., Azar, S., Friedmann, Y., Kupetz, P., Tzuberi, R., Anisimov, A., Alitalo, K., Horwitz, M., Leebhoff, S., Khoma, O. Z., Hlushchuk, R., Djonov, V., Abramovitch, R., Tam, J. & Keshet, E. (2021) Counteracting age-related VEGF signaling insufficiency promotes healthy aging and extends life span, *Science.* **373**, eabc8479.
141. Yousef, H., Czupalla, C. J., Lee, D., Chen, M. B., Burke, A. N., Zera, K. A., Zandstra, J., Berber, E., Lehallier, B., Mathur, V., Nair, R. V., Bonanno, L. N., Yang, A. C., Peterson, T., Hadeiba, H., Merkel, T., Körbelin, J., Schwaninger, M., Buckwalter, M. S., Quake, S. R., Butcher, E. C. & Wyss-Coray, T. (2019) Aged blood impairs hippocampal neural precursor activity and activates microglia via brain endothelial cell VCAM1, *Nature Medicine.* **25**, 988-1000.
142. Villeda, S. A., Plambeck, K. E., Middeldorp, J., Castellano, J. M., Mosher, K. I., Luo, J., Smith, L. K., Bieri, G., Lin, K., Berdnik, D., Wabl, R., Udeochu, J., Wheatley, E. G., Zou, B., Simmons, D. A., Xie, X. S., Longo, F. M. & Wyss-Coray, T. (2014) Young blood reverses age-related impairments in cognitive function and synaptic plasticity in mice, *Nature Medicine.* **20**, 659-663.
143. Jakab, M. & Augustin, H. G. (2020) Understanding angiodiversity: insights from single cell biology, *Development.* **147**.
144. Johnston, J. A., Ward, C. L. & Kopito, R. R. (1998) Aggresomes: a cellular response to misfolded proteins, *J Cell Biol.* **143**, 1883-98.
145. Lamark, T. & Johansen, T. (2012) Aggrephagy: selective disposal of protein aggregates by macroautophagy, *Int J Cell Biol.* **2012**, 736905.
146. Klaips, C. L., Jayaraj, G. G. & Hartl, F. U. (2018) Pathways of cellular proteostasis in aging and disease, *J Cell Biol.* **217**, 51-63.
147. Kopacz, A., Kloska, D., Targosz-Korecka, M., Zapotoczny, B., Cysewski, D., Personnic, N., Werner, E., Hajduk, K., Jozkowicz, A. & Grochot-Przeczek, A. (2020) Keap1 governs ageing-induced protein aggregation in endothelial cells, *Redox Biol.* **34**, 101572.
148. Hofmann, C., Katus, H. A. & Doroudgar, S. (2019) Protein Misfolding in Cardiac Disease, *Circulation.* **139**, 2085-2088.
149. Amodio, G., Moltedo, O., Faraonio, R. & Remondelli, P. (2018) Targeting the Endoplasmic Reticulum Unfolded Protein Response to Counteract the Oxidative Stress-Induced Endothelial Dysfunction, *Oxid Med Cell Longev.* **2018**, 4946289.
150. Deng, J., Lu, P. D., Zhang, Y., Scheuner, D., Kaufman, R. J., Sonenberg, N., Harding, H. P. & Ron, D. (2004) Translational repression mediates activation of nuclear factor kappa B by phosphorylated translation initiation factor 2, *Mol Cell Biol.* **24**, 10161-8.
151. Lee, J. & Ozcan, U. (2014) Unfolded protein response signaling and metabolic diseases, *J Biol Chem.* **289**, 1203-11.
152. Marcelo, A., Koppenol, R., de Almeida, L. P., Matos, C. A. & Nóbrega, C. (2021) Stress granules, RNA-binding proteins and polyglutamine diseases: too much aggregation?, *Cell Death Dis.* **12**, 592.
153. Anderson, P. & Kedersha, N. (2006) RNA granules, *J Cell Biol.* **172**, 803-8.

154. Hu, L. D., Chen, X. J., Liao, X. Y. & Yan, Y. B. (2017) Screening novel stress granule regulators from a natural compound library, *Protein Cell.* **8**, 618-622.
155. Buchan, J. R., Kolaitis, R. M., Taylor, J. P. & Parker, R. (2013) Eukaryotic stress granules are cleared by autophagy and Cdc48/VCP function, *Cell.* **153**, 1461-74.
156. Seguin, S. J., Morelli, F. F., Vinet, J., Amore, D., De Biasi, S., Poletti, A., Rubinsztein, D. C. & Carra, S. (2014) Inhibition of autophagy, lysosome and VCP function impairs stress granule assembly, *Cell Death & Differentiation.* **21**, 1838-1851.
157. Silva, J. M., Rodrigues, S., Sampaio-Marques, B., Gomes, P., Neves-Carvalho, A., Dioli, C., Soares-Cunha, C., Mazuik, B. F., Takashima, A., Ludovico, P., Wolozin, B., Sousa, N. & Sotiropoulos, I. (2019) Dysregulation of autophagy and stress granule-related proteins in stress-driven Tau pathology, *Cell Death Differ.* **26**, 1411-1427.
158. Herman, A. B., Silva Afonso, M., Kelemen, S. E., Ray, M., Vrakas, C. N., Burke, A. C., Scalia, R. G., Moore, K. & Autieri, M. V. (2019) Regulation of Stress Granule Formation by Inflammation, Vascular Injury, and Atherosclerosis, *Arterioscler Thromb Vasc Biol.* **39**, 2014-2027.
159. Patel, A., Lee, H. O., Jawerth, L., Maharana, S., Jahnel, M., Hein, M. Y., Stoynov, S., Mahamid, J., Saha, S., Franzmann, T. M., Pozniakovski, A., Poser, I., Maghelli, N., Royer, L. A., Weigert, M., Myers, E. W., Grill, S., Drechsel, D., Hyman, A. A. & Alberti, S. (2015) A Liquid-to-Solid Phase Transition of the ALS Protein FUS Accelerated by Disease Mutation, *Cell.* **162**, 1066-77.
160. Ambadipudi, S., Biernat, J., Riedel, D., Mandelkow, E. & Zweckstetter, M. (2017) Liquid-liquid phase separation of the microtubule-binding repeats of the Alzheimer-related protein Tau, *Nat Commun.* **8**, 275.
161. Shi, W., Wei, X., Wang, Z., Han, H., Fu, Y., Liu, J., Zhang, Y., Guo, J., Dong, C., Zhou, D., Zhou, Q., Chen, Y. & Yi, F. (2016) HDAC9 exacerbates endothelial injury in cerebral ischaemia/reperfusion injury, *J Cell Mol Med.* **20**, 1139-49.
162. Li, H., Gao, A., Feng, D., Wang, Y., Zhang, L., Cui, Y., Li, B., Wang, Z. & Chen, G. (2014) Evaluation of the Protective Potential of Brain Microvascular Endothelial Cell Autophagy on Blood-Brain Barrier Integrity During Experimental Cerebral Ischemia-Reperfusion Injury, *Translational Stroke Research*.
163. Saha, K., Ganapathy, A. S., Wang, A., Morris, N. M., Suchanec, E., Ding, W., Yochum, G., Koltun, W., Nighot, M., Ma, T. & Nighot, P. (2022) Autophagy Reduces the Degradation and Promotes Membrane Localization of Occludin to Enhance the Intestinal Epithelial Tight Junction Barrier against Paracellular Macromolecule Flux, *J Crohns Colitis*.
164. Liu, J., Weaver, J., Jin, X., Zhang, Y., Xu, J., Liu, K. J., Li, W. & Liu, W. (2016) Nitric Oxide Interacts with Caveolin-1 to Facilitate Autophagy-Lysosome-Mediated Claudin-5 Degradation in Oxygen-Glucose Deprivation-Treated Endothelial Cells, *Molecular Neurobiology*.
165. Kim, K. A., Kim, D., Kim, J. H., Shin, Y. J., Kim, E. S., Akram, M., Kim, E. H., Majid, A., Baek, S. H. & Bae, O. N. (2020) Autophagy-mediated occludin degradation contributes to blood-brain barrier disruption during ischemia in bEnd.3 brain endothelial cells and rat ischemic stroke models, *Fluids Barriers CNS.* **17**, 21.
166. Wei, N., Yu, S. P., Gu, X. H., Chen, D. D., Whalin, M. K., Xu, G. L., Liu, X. F. & Wei, L. (2013) The involvement of autophagy pathway in exaggerated ischemic brain damage in diabetic mice, *CNS Neuroscience and Therapeutics*.

167. Yang, Z., Lin, P., Chen, B., Zhang, X., Xiao, W., Wu, S., Huang, C., Feng, D., Zhang, W. & Zhang, J. (2021) Autophagy alleviates hypoxia-induced blood-brain barrier injury via regulation of CLDN5 (claudin 5), *Autophagy.* **17**, 3048-3067.
168. Wang, J., Whiteman, M. W., Lian, H., Wang, G., Singh, A., Huang, D. & Denmark, T. (2009) A non-canonical MEK/ERK signaling pathway regulates autophagy via regulating Beclin 1, *J Biol Chem.* **284**, 21412-24.
169. Basuroy, S., Seth, A., Elias, B., Naren, A. P. & Rao, R. (2006) MAPK interacts with occludin and mediates EGF-induced prevention of tight junction disruption by hydrogen peroxide, *Biochem J.* **393**, 69-77.
170. Saha, K., Subramenium Ganapathy, A., Wang, A., Michael Morris, N., Suchanec, E., Ding, W., Yochum, G., Koltun, W., Nighot, M., Ma, T. & Nighot, P. (2023) Autophagy Reduces the Degradation and Promotes Membrane Localization of Occludin to Enhance the Intestinal Epithelial Tight Junction Barrier against Paracellular Macromolecule Flux, *J Crohns Colitis.* **17**, 433-449.
171. Li, W. D., Li, N. P., Song, D. D., Rong, J. J., Qian, A. M. & Li, X. Q. (2017) Metformin inhibits endothelial progenitor cell migration by decreasing matrix metalloproteinases, MMP-2 and MMP-9, via the AMPK/mTOR/autophagy pathway, *Int J Mol Med.* **39**, 1262-1268.
172. Meng, Q., Pu, L., Qi, M., Li, S., Sun, B., Wang, Y., Liu, B. & Li, F. (2022) Laminar shear stress inhibits inflammation by activating autophagy in human aortic endothelial cells through HMGB1 nuclear translocation, *Commun Biol.* **5**, 425.
173. Surgeons, A. A. o. N.
174. https://www.stroke.org.uk/what-is-stroke/stroke-statistics#:~:text=Key%20statistics%3A, s. s. i. t. U. in
175. Love, S. (2005) Neuropathological investigation of dementia: a guide for neurologists, *J Neurol Neurosurg Psychiatry.* **76 Suppl 5**, v8-14.
176. https://www.alzheimers.org.uk/about-dementia/types-dementia/types-of-vascular-dementia#1.
177. Martins-Filho, R. K., Zotin, M. C., Rodrigues, G. & Pontes-Neto, O. (2020) Biomarkers Related to Endothelial Dysfunction and Vascular Cognitive Impairment: A Systematic Review, *Dementia and Geriatric Cognitive Disorders.* **49**, 365-374.
178. Wang, W., Qiao, O., Ji, H., Zhang, X., Han, X., Zhang, Y., Wang, J., Li, X. & Gao, W. (2021) Autophagy in vascular dementia and natural products with autophagy regulating activity, *Pharmacological Research.* **170**, 105756.
179. Xu, L., Qu, C., Qu, C., Shen, J., Song, H., Li, Y., Li, T., Zheng, J. & Zhang, J. (2020) Improvement of autophagy dysfunction as a potential mechanism for environmental enrichment to protect blood-brain barrier in rats with vascular cognitive impairment, *Neuroscience Letters.* **739**, 135437.
180. Tian, J., Shi, J. & Mann, D. M. (2004) Cerebral amyloid angiopathy and dementia, *Panminerva Med.* **46**, 253-64.
181. Liu, B., Tang, J., Zhang, J., Li, S., Yuan, M. & Wang, R. (2014) Autophagy activation aggravates neuronal injury in the hippocampus of vascular dementia rats, *Neural Regen Res.* **9**, 1288-96.
182. Liu, B., Liu, J., Zhang, J., Mao, W. & Li, S. (2019) Effects of autophagy on synaptic-plasticity-related protein expression in the hippocampus CA1 of a rat model of vascular dementia, *Neurosci Lett.* **707**, 134312.

183. Wang, X., Fu, Y. F., Liu, X., Feng, G., Xiong, D., Mu, G. F. & Chen, F. P. (2018) ROS Promote Ox-LDL-Induced Platelet Activation by Up-Regulating Autophagy Through the Inhibition of the PI3K/AKT/mTOR Pathway, *Cell Physiol Biochem.* **50**, 1779-1793.
184. Li, F., Yang, B., Li, T., Gong, X., Zhou, F. & Hu, Z. (2019) HSPB8 over-expression prevents disruption of blood-brain barrier by promoting autophagic flux after cerebral ischemia/reperfusion injury, *J Neurochem.* **148**, 97-113.
185. Kido, Y., Yin, J., Zuo, G., Zhang, J. & Chen, G. (2012) Role of autophagy in early brain injury after experimental subarachnoid hemorrhage, *J Mol Neurosci.* **46**, 192-202.
186. DeSai C, H. S. A. C. I. U. A. I. S. I. T. I. F. S. P. J.-A. f.
187. Liu, J., Weaver, J., Jin, X., Zhang, Y., Xu, J., Liu, K. J., Li, W. & Liu, W. (2016) Nitric Oxide Interacts with Caveolin-1 to Facilitate Autophagy-Lysosome-Mediated Claudin-5 Degradation in Oxygen-Glucose Deprivation-Treated Endothelial Cells, *Mol Neurobiol.* **53**, 5935-5947.
188. Kim, K. A., Kim, D., Kim, J. H., Shin, Y. J., Kim, E. S., Akram, M., Kim, E. H., Majid, A., Baek, S. H. & Bae, O. N. (2020) Autophagy-mediated occludin degradation contributes to blood-brain barrier disruption during ischemia in bEnd.3 brain endothelial cells and rat ischemic stroke models, *Fluids and Barriers of the CNS*.
189. Wang, S., Han, X., Mao, Z., Xin, Y., Maharjan, S. & Zhang, B. (2019) MALAT1 lncRNA Induces Autophagy and Protects Brain Microvascular Endothelial Cells Against Oxygen-Glucose Deprivation by Binding to miR-200c-3p and Upregulating SIRT1 Expression, *Neuroscience.* **397**, 116-126.
190. Yang, G., Wang, N., Seto, S. W., Chang, D. & Liang, H. (2018) Hydroxysafflor yellow a protects brain microvascular endothelial cells against oxygen glucose deprivation/reoxygenation injury: Involvement of inhibiting autophagy via class I PI3K/Akt/mTOR signaling pathway, *Brain Res Bull.* **140**, 243-257.
191. Zhang, S., An, Q., Wang, T., Gao, S. & Zhou, G. (2018) Autophagy- and MMP-2/9-mediated Reduction and Redistribution of ZO-1 Contribute to Hyperglycemia-increased Blood-Brain Barrier Permeability During Early Reperfusion in Stroke, *Neuroscience.* **377**, 126-137.
192. Li, H., Gao, A., Feng, D., Wang, Y., Zhang, L., Cui, Y., Li, B., Wang, Z. & Chen, G. (2014) Evaluation of the protective potential of brain microvascular endothelial cell autophagy on blood-brain barrier integrity during experimental cerebral ischemia-reperfusion injury, *Transl Stroke Res.* **5**, 618-26.
193. Steinert, P. M., Parry, D. A. & Marekov, L. N. (2003) Trichohyalin mechanically strengthens the hair follicle: multiple cross-bridging roles in the inner root sheath, *J Biol Chem.* **278**, 41409-19.
194. Leung, C. L., Green, K. J. & Liem, R. K. (2002) Plakins: a family of versatile cytolinker proteins, *Trends Cell Biol.* **12**, 37-45.
195. Vecchione, A., Fassan, M., Anesti, V., Morrione, A., Goldoni, S., Baldassarre, G., Byrne, D., D'Arca, D., Palazzo, J. P., Lloyd, J., Scorrano, L., Gomella, L. G., Iozzo, R. V. & Baffa, R. (2009) MITOSTATIN, a putative tumor suppressor on chromosome 12q24.1, is downregulated in human bladder and breast cancer, *Oncogene*.
196. Cerqua, C., Anesti, V., Pyakurel, A., Liu, D., Naon, D., Wiche, G., Baffa, R., Dimmer, K. S. & Scorrano, L. (2010) Trichoplein/mitostatin regulates endoplasmic reticulum-mitochondria juxtaposition, *EMBO Rep.* **11**, 854-60.

197. Neill, T., Torres, A., Buraschi, S., Owens, R. T., Hoek, J. B., Baffa, R. & Iozzo, R. V. (2014) Decorin induces mitophagy in breast carcinoma cells via peroxisome proliferator-activated receptor γ coactivator-1α (PGC-1α) and mitostatin, *Journal of Biological Chemistry*.
198. Neill, T., Andreuzzi, E., Wang, Z. X., Peiper, S. C., Mongiat, M. & Iozzo, R. V. (2018) Endorepellin remodels the endothelial transcriptome toward a pro-autophagic and pro-mitophagic gene signature, *J Biol Chem.* **293**, 12137-12148.
199. Silvander, J. S. G., Kvarnström, S. M., Kumari-Ilieva, A., Shrestha, A., Alam, C. M. & Toivola, D. M. (2017) Keratins regulate β-cell mitochondrial morphology, motility, and homeostasis, *Faseb j.* **31**, 4578-4587.
200. Ibi, M., Zou, P., Inoko, A., Shiromizu, T., Matsuyama, M., Hayashi, Y., Enomoto, M., Mori, D., Hirotsune, S., Kiyono, T., Tsukita, S., Goto, H. & Inagaki, M. (2011) Trichoplein controls microtubule anchoring at the centrosome by binding to Odf2 and ninein, *J Cell Sci.* **124**, 857-64.
201. Inoko, A., Matsuyama, M., Goto, H., Ohmuro-Matsuyama, Y., Hayashi, Y., Enomoto, M., Ibi, M., Urano, T., Yonemura, S., Kiyono, T., Izawa, I. & Inagaki, M. (2012) Trichoplein and Aurora A block aberrant primary cilia assembly in proliferating cells, *Journal of Cell Biology*.
202. Kasahara, K., Kawakami, Y., Kiyono, T., Yonemura, S., Kawamura, Y., Era, S., Matsuzaki, F., Goshima, N. & Inagaki, M. (2014) Ubiquitin-proteasome system controls ciliogenesis at the initial step of axoneme extension, *Nat Commun.* **5**, 5081.
203. Kasahara, K., Aoki, H., Kiyono, T., Wang, S., Kagiwada, H., Yuge, M., Tanaka, T., Nishimura, Y., Mizoguchi, A., Goshima, N. & Inagaki, M. (2018) EGF receptor kinase suppresses ciliogenesis through activation of USP8 deubiquitinase, *Nat Commun.* **9**, 758.
204. Huang, M., Kong, X., Tang, Z., Lin, Z., He, R., Cao, M. & Zhang, X. (2022) Cell cycle arrest induced by trichoplein depletion is independent of cilia assembly, *J Cell Physiol.* **237**, 2703-2712.
205. Lauriola, A., Martello, A., Fantini, S., Marverti, G., Zanocco-Marani, T., Davalli, P., Guardavaccaro, D., Mai, S., Caporali, A. & D'Arca, D. (2020) Depletion of Trichoplein (TpMs) Causes Chromosome Mis-Segregation, DNA Damage and Chromosome Instability in Cancer Cells, *Cancers (Basel).* **12**.
206. Lauriola, A., Davalli, P., Marverti, G., Caporali, A., Mai, S. & D'Arca, D. (2022) Telomere Dysfunction Is Associated with Altered DNA Organization in Trichoplein/Tchp/Mitostatin (TpMs) Depleted Cells, *Biomedicines.* **10**.
207. Yamakawa, D., Katoh, D., Kasahara, K., Shiromizu, T., Matsuyama, M., Matsuda, C., Maeno, Y., Watanabe, M., Nishimura, Y. & Inagaki, M. (2021) Primary cilia-dependent lipid raft/caveolin dynamics regulate adipogenesis, *Cell Rep.* **34**, 108817.
208. Yamakawa, D., Tsuboi, J., Kasahara, K., Matsuda, C., Nishimura, Y., Kodama, T., Katayama, N., Watanabe, M. & Inagaki, M. (2022) Cilia-Mediated Insulin/Akt and ST2/JNK Signaling Pathways Regulate the Recovery of Muscle Injury, *Adv Sci (Weinh).* **10**, e2202632.
209. Caporali, A., Meloni, M., Völlenkle, C., Bonci, D., Sala-Newby, G. B., Addis, R., Spinetti, G., Losa, S., Masson, R., Baker, A. H., Agami, R., Le Sage, C., Condorelli, G., Madeddu, P., Martelli, F. & Emanueli, C. (2011) Deregulation of microRNA-503

contributes to diabetes mellitus-induced impairment of endothelial function and reparative angiogenesis after Limb Ischemia, *Circulation*.
210. Caporali, A., Meloni, M., Nailor, A., Mitić, T., Shantikumar, S., Riu, F., Sala-Newby, G. B., Rose, L., Besnier, M., Katare, R., Voellenkle, C., Verkade, P., Martelli, F., Madeddu, P. & Emanueli, C. (2015) P75NTR-dependent activation of NF-κB regulates microRNA-503 transcription and pericyte-endothelial crosstalk in diabetes after limb ischaemia, *Nature Communications*.
211. Weidberg, H., Shvets, E., Shpilka, T., Shimron, F., Shinder, V. & Elazar, Z. (2010) LC3 and GATE-16/GABARAP subfamilies are both essential yet act differently in autophagosome biogenesis, *EMBO Journal*.
212. Partnership, A. M. Common Metabolic Diseases Knowledge Portal. in
213. Malik, R.Chauhan, G.Traylor, M.Sargurupremraj, M.Okada, Y.Mishra, A.Rutten-Jacobs, L.Giese, A. K.van der Laan, S. W.Gretarsdottir, S.Anderson, C. D.Chong, M.Adams, H. H. H.Ago, T.Almgren, P.Amouyel, P.Ay, H.Bartz, T. M.Benavente, O. R.Bevan, S.Boncoraglio, G. B.Brown, R. D., Jr.Butterworth, A. S.Carrera, C.Carty, C. L.Chasman, D. I.Chen, W. M.Cole, J. W.Correa, A.Cotlarciuc, I.Cruchaga, C.Danesh, J.de Bakker, P. I. W.DeStefano, A. L.den Hoed, M.Duan, Q.Engelter, S. T.Falcone, G. J.Gottesman, R. F.Grewal, R. P.Gudnason, V.Gustafsson, S.Haessler, J.Harris, T. B.Hassan, A.Havulinna, A. S.Heckbert, S. R.Holliday, E. G.Howard, G.Hsu, F. C.Hyacinth, H. I.Ikram, M. A.Ingelsson, E.Irvin, M. R.Jian, X.Jiménez-Conde, J.Johnson, J. A.Jukema, J. W.Kanai, M.Keene, K. L.Kissela, B. M.Kleindorfer, D. O.Kooperberg, C.Kubo, M.Lange, L. A.Langefeld, C. D.Langenberg, C.Launer, L. J.Lee, J. M.Lemmens, R.Leys, D.Lewis, C. M.Lin, W. Y.Lindgren, A. G.Lorentzen, E.Magnusson, P. K.Maguire, J.Manichaikul, A.McArdle, P. F.Meschia, J. F.Mitchell, B. D.Mosley, T. H.Nalls, M. A.Ninomiya, T.O'Donnell, M. J.Psaty, B. M.Pulit, S. L.Rannikmäe, K.Reiner, A. P.Rexrode, K. M.Rice, K.Rich, S. S.Ridker, P. M.Rost, N. S.Rothwell, P. M.Rotter, J. I.Rundek, T.Sacco, R. L.Sakaue, S.Sale, M. M., et al. (2018) Multiancestry genome-wide association study of 520,000 subjects identifies 32 loci associated with stroke and stroke subtypes, *Nat Genet.* **50**, 524-537.
214. Staley, J. R., Blackshaw, J., Kamat, M. A., Ellis, S., Surendran, P., Sun, B. B., Paul, D. S., Freitag, D., Burgess, S., Danesh, J., Young, R. & Butterworth, A. S. (2016) PhenoScanner: a database of human genotype-phenotype associations, *Bioinformatics.* **32**, 3207-3209.
215. Kamat, M. A., Blackshaw, J. A., Young, R., Surendran, P., Burgess, S., Danesh, J., Butterworth, A. S. & Staley, J. R. (2019) PhenoScanner V2: an expanded tool for searching human genotype-phenotype associations, *Bioinformatics.* **35**, 4851-4853.
216. Schunkert, H.König, I. R.Kathiresan, S.Reilly, M. P.Assimes, T. L.Holm, H.Preuss, M.Stewart, A. F. R.Barbalic, M.Gieger, C.Absher, D.Aherrahrou, Z.Allayee, H.Altshuler, D.Anand, S. S.Andersen, K.Anderson, J. L.Ardissino, D.Ball, S. G.Balmforth, A. J.Barnes, T. A.Becker, D. M.Becker, L. C.Berger, K.Bis, J. C.Boekholdt, S. M.Boerwinkle, E.Braund, P. S.Brown, M. J.Burnett, M. S.Buysschaert, I.Carlquist, J. F.Chen, L.Cichon, S.Codd, V.Davies, R. W.Dedoussis, G.Dehghan, A.Demissie, S.Devaney, J. M.Diemert, P.Do, R.Doering, A.Eifert, S.Mokhtari, N. E. E.Ellis, S. G.Elosua, R.Engert, J. C.Epstein, S. E.De Faire, U.Fischer, M.Folsom, A. R.Freyer, J.Gigante, B.Girelli, D.Gretarsdottir, S.Gudnason, V.Gulcher, J. R.Halperin, E.Hammond, N.Hazen, S. L.Hofman, A.Horne, B. D.Illig, T.Iribarren, C.Jones, G. T.Jukema, J. W.Kaiser, M. A.Kaplan, L. M.Kastelein, J. J. P.Khaw, K. T.Knowles, J.

W.Kolovou, G.Kong, A.Laaksonen, R.Lambrechts, D.Leander, K.Lettre, G.Li, M.Lieb, W.Loley, C.Lotery, A. J.Mannucci, P. M.Maouche, S.Martinelli, N.McKeown, P. P.Meisinger, C.Meitinger, T.Melander, O.Merlini, P. A.Mooser, V.Morgan, T.Mühleisen, T. W.Muhlestein, J. B.Münzel, T.Musunuru, K.Nahrstaedt, J.Nelson, C. P.Nöthen, M. M.Olivieri, O., et al. (2011) Large-scale association analysis identifies 13 new susceptibility loci for coronary artery disease, *Nature Genetics*.
217. MGI MGI.
218. consortium, I. M. P. IMPC.
219. Assmann, J., Müller, K., Wenzel, J., Walther, T., Brands, J., Thornton, P., Allan, S. & Schwaninger, M. (2017) Isolation and Cultivation of Primary Brain Endothelial Cells from Adult Mice, *Bio-Protocol.* **7**, 1-16.
220. Wiśniewski, J. R., Hein, M. Y., Cox, J. & Mann, M. (2014) A "proteomic ruler" for protein copy number and concentration estimation without spike-in standards, *Mol Cell Proteomics.* **13**, 3497-506.
221. Schmittgen, T. D. & Livak, K. J. (2008) Analyzing real-time PCR data by the comparative C(T) method, *Nat Protoc.* **3**, 1101-8.
222. Love, M. I., Huber, W. & Anders, S. (2014) Moderated estimation of fold change and dispersion for RNA-seq data with DESeq2, *Genome Biol.* **15**, 550.
223. Klickstein, J. A., Mukkavalli, S. & Raman, M. (2020) AggreCount: an unbiased image analysis tool for identifying and quantifying cellular aggregates in a spatially defined manner, *Journal of Biological Chemistry.* **295**, 17672-17683.
224. Zudaire, E., Gambardella, L., Kurcz, C. & Vermeren, S. (2011) A computational tool for quantitative analysis of vascular networks, *PLoS One.* **6**, e27385.
225. Frangi, R., Niessen, W. J., Vincken, K. & Viergever, M. (2000) Multiscale Vessel Enhancement Filtering, *Med Image Comput Comput Assist Interv.* **1496**.
226. Manniesing, R., Viergever, M. A. & Niessen, W. J. (2006) Vessel enhancing diffusion: A scale space representation of vessel structures, *Medical Image Analysis.* **10**, 815-825.
227. Lee, T. C., Kashyap, R. L. & Chu, C. N. (1994) Building Skeleton Models via 3-D Medial Surface Axis Thinning Algorithms, *CVGIP: Graphical Models and Image Processing.* **56**, 462-478.
228. Berg, S., Kutra, D., Kroeger, T., Straehle, C. N., Kausler, B. X., Haubold, C., Schiegg, M., Ales, J., Beier, T., Rudy, M., Eren, K., Cervantes, J. I., Xu, B., Beuttenmueller, F., Wolny, A., Zhang, C., Koethe, U., Hamprecht, F. A. & Kreshuk, A. (2019) ilastik: interactive machine learning for (bio)image analysis, *Nature Methods.* **16**, 1226-1232.
229. Davies, C. L., Patir, A. & McColl, B. W. (2019) Myeloid Cell and Transcriptome Signatures Associated With Inflammation Resolution in a Model of Self-Limiting Acute Brain Inflammation, *Front Immunol.* **10**, 1048.
230. Ruxton, G. D. (2006) The unequal variance t-test is an underused alternative to Student's t-test and the Mann–Whitney U test, *Behavioral Ecology.* **17**, 688-690.
231. Kadl, A. & Leitinger, N. (2005) The role of endothelial cells in the resolution of acute inflammation, *Antioxid Redox Signal.* **7**, 1744-54.
232. Knowland, D., Arac, A., Sekiguchi, K. J., Hsu, M., Lutz, S. E., Perrino, J., Steinberg, G. K., Barres, B. A., Nimmerjahn, A. & Agalliu, D. (2014) Stepwise recruitment of transcellular and paracellular pathways underlies blood-brain barrier breakdown in stroke, *Neuron.* **82**, 603-17.

233. Kalaria, R. N. (2010) Vascular basis for brain degeneration: Faltering controls and risk factors for dementia, *Nutrition Reviews*.
234. Arenas, I. A., Xu, Y. & Davidge, S. T. (2006) Age-associated impairment in vasorelaxation to fluid shear stress in the female vasculature is improved by TNF-α antagonism, *American Journal of Physiology - Heart and Circulatory Physiology*.
235. Donato, A. J., Black, A. D., Jablonski, K. L., Gano, L. B. & Seals, D. R. (2008) Aging is associated with greater nuclear NFκB, reduced IκBα, and increased expression of proinflammatory cytokines in vascular endothelial cells of healthy humans, *Aging Cell*.
236. Zuliani, G., Ranzini, M., Guerra, G., Rossi, L., Munari, M. R., Zurlo, A., Volpato, S., Atti, A. R., Blè, A. & Fellin, R. (2007) Plasma cytokines profile in older subjects with late onset Alzheimer's disease or vascular dementia, *Journal of Psychiatric Research*.
237. Li, P., Wang, L., Zhou, Y., Gan, Y., Zhu, W., Xia, Y., Jiang, X., Watkins, S., Vazquez, A., Thomson, A. W., Chen, J., Yu, W. & Hu, X. (2017) C-C Chemokine Receptor Type 5 (CCR5)-Mediated Docking of Transferred Tregs Protects Against Early Blood-Brain Barrier Disruption After Stroke, *J Am Heart Assoc.* **6**.
238. Azizi, G., Khannazer, N. & Mirshafiey, A. (2014) The Potential Role of Chemokines in Alzheimer's Disease Pathogenesis, *Am J Alzheimers Dis Other Demen.* **29**, 415-25.
239. Cartier, L., Hartley, O., Dubois-Dauphin, M. & Krause, K. H. (2005) Chemokine receptors in the central nervous system: role in brain inflammation and neurodegenerative diseases, *Brain Res Brain Res Rev.* **48**, 16-42.
240. Warde-Farley, D., Donaldson, S. L., Comes, O., Zuberi, K., Badrawi, R., Chao, P., Franz, M., Grouios, C., Kazi, F., Lopes, C. T., Maitland, A., Mostafavi, S., Montojo, J., Shao, Q., Wright, G., Bader, G. D. & Morris, Q. (2010) The GeneMANIA prediction server: biological network integration for gene prioritization and predicting gene function, *Nucleic Acids Res.* **38**, W214-20.
241. Park, L., Wang, G., Zhou, P., Zhou, J., Pitstick, R., Previti, M. L., Younkin, L., Younkin, S. G., Van Nostrand, W. E., Cho, S., Anrather, J., Carlson, G. A. & Iadecola, C. (2011) Scavenger receptor CD36 is essential for the cerebrovascular oxidative stress and neurovascular dysfunction induced by amyloid-beta, *Proc Natl Acad Sci U S A.* **108**, 5063-8.
242. Sheedy, F. J., Grebe, A., Rayner, K. J., Kalantari, P., Ramkhelawon, B., Carpenter, S. B., Becker, C. E., Ediriweera, H. N., Mullick, A. E., Golenbock, D. T., Stuart, L. M., Latz, E., Fitzgerald, K. A. & Moore, K. J. (2013) CD36 coordinates NLRP3 inflammasome activation by facilitating intracellular nucleation of soluble ligands into particulate ligands in sterile inflammation, *Nat Immunol.* **14**, 812-20.
243. Le, K., Mo, S., Lu, X., Idriss Ali, A., Yu, D. & Guo, Y. (2018) Association of circulating blood HMGB1 levels with ischemic stroke: a systematic review and meta-analysis, *Neurol Res.* **40**, 907-916.
244. Paudel, Y. N., Shaikh, M. F., Chakraborti, A., Kumari, Y., Aledo-Serrano, Á., Aleksovska, K., Alvim, M. K. M. & Othman, I. (2018) HMGB1: A Common Biomarker and Potential Target for TBI, Neuroinflammation, Epilepsy, and Cognitive Dysfunction, *Frontiers in Neuroscience.* **12**, 628.

245. Schneider, M., Hansen, J. L. & Sheikh, S. P. (2008) S100A4: a common mediator of epithelial-mesenchymal transition, fibrosis and regeneration in diseases?, *J Mol Med (Berl).* **86**, 507-22.
246. Nishioku, T., Furusho, K., Tomita, A., Ohishi, H., Dohgu, S., Shuto, H., Yamauchi, A. & Kataoka, Y. (2011) Potential role for S100A4 in the disruption of the blood-brain barrier in collagen-induced arthritic mice, an animal model of rheumatoid arthritis, *Neuroscience.* **189**, 286-92.
247. Månberg, A., Skene, N., Sanders, F., Trusohamn, M., Remnestål, J., Szczepińska, A., Aksoylu, I. S., Lönnerberg, P., Ebarasi, L., Wouters, S., Lehmann, M., Olofsson, J., von Gohren Antequera, I., Domaniku, A., De Schaepdryver, M., De Vocht, J., Poesen, K., Uhlén, M., Anink, J., Mijnsbergen, C., Vergunst-Bosch, H., Hübers, A., Kläppe, U., Rodriguez-Vieitez, E., Gilthorpe, J. D., Hedlund, E., Harris, R. A., Aronica, E., Van Damme, P., Ludolph, A., Veldink, J., Ingre, C., Nilsson, P. & Lewandowski, S. A. (2021) Altered perivascular fibroblast activity precedes ALS disease onset, *Nat Med.* **27**, 640-646.
248. Rempe, R. G., Hartz, A. M. S. & Bauer, B. (2016) Matrix metalloproteinases in the brain and blood-brain barrier: Versatile breakers and makers, *J Cereb Blood Flow Metab.* **36**, 1481-507.
249. Turner, R. J. & Sharp, F. R. (2016) Implications of MMP9 for Blood Brain Barrier Disruption and Hemorrhagic Transformation Following Ischemic Stroke, *Front Cell Neurosci.* **10**, 56.
250. Seghezzi, G., Patel, S., Ren, C. J., Gualandris, A., Pintucci, G., Robbins, E. S., Shapiro, R. L., Galloway, A. C., Rifkin, D. B. & Mignatti, P. (1998) Fibroblast growth factor-2 (FGF-2) induces vascular endothelial growth factor (VEGF) expression in the endothelial cells of forming capillaries: an autocrine mechanism contributing to angiogenesis, *J Cell Biol.* **141**, 1659-73.
251. Beardsley, A., Fang, K., Mertz, H., Castranova, V., Friend, S. & Liu, J. (2005) Loss of caveolin-1 polarity impedes endothelial cell polarization and directional movement, *J Biol Chem.* **280**, 3541-7.
252. Bayir, E. & Sendemir, A. (2021) Role of Intermediate Filaments in Blood-Brain Barrier in Health and Disease, *Cells.* **10**.
253. Krensky, A. M. & Ahn, Y. T. (2007) Mechanisms of disease: regulation of RANTES (CCL5) in renal disease, *Nat Clin Pract Nephrol.* **3**, 164-70.
254. Lumpkins, K., Bochicchio, G. V., Zagol, B., Ulloa, K., Simard, J. M., Schaub, S., Meyer, W. & Scalea, T. (2008) Plasma levels of the beta chemokine regulated upon activation, normal T cell expressed, and secreted (RANTES) correlate with severe brain injury, *J Trauma.* **64**, 358-61.
255. Vion, A. C., Kheloufi, M., Hammoutene, A., Poisson, J., Lasselin, J., Devue, C., Pic, I., Dupont, N., Busse, J., Stark, K., Lafaurie-Janvore, J., Barakat, A. I., Loyer, X., Souyri, M., Viollet, B., Julia, P., Tedgui, A., Codogno, P., Boulanger, C. M. & Rautou, P. E. (2017) Autophagy is required for endothelial cell alignment and atheroprotection under physiological blood flow, *Proceedings of the National Academy of Sciences of the United States of America*.
256. LaRocca, T. J., Gioscia-Ryan, R. A., Hearon, C. M. & Seals, D. R. (2013) The autophagy enhancer spermidine reverses arterial aging, *Mechanisms of Ageing and Development*.

257. Laberge, R. M., Sun, Y., Orjalo, A. V., Patil, C. K., Freund, A., Zhou, L., Curran, S. C., Davalos, A. R., Wilson-Edell, K. A., Liu, S., Limbad, C., Demaria, M., Li, P., Hubbard, G. B., Ikeno, Y., Javors, M., Desprez, P. Y., Benz, C. C., Kapahi, P., Nelson, P. S. & Campisi, J. (2015) MTOR regulates the pro-tumorigenic senescence-associated secretory phenotype by promoting IL1A translation, *Nat Cell Biol.* **17**, 1049-61.
258. Nussenzweig, S. C., Verma, S. & Finkel, T. (2015) The role of autophagy in vascular biology in
259. Kim, Y., Kim, Y. K., Kim, N. K., Kim, S. H., Kim, O. J. & Oh, S. H. (2014) Circulating matrix metalloproteinase-9 level is associated with cerebral white matter hyperintensities in non-stroke individuals, *Eur Neurol.* **72**, 234-40.
260. Daneman, R., Zhou, L., Kebede, A. A. & Barres, B. A. (2010) Pericytes are required for blood-brain barrier integrity during embryogenesis, *Nature.* **468**, 562-6.
261. Bell, R. D., Winkler, E. A., Singh, I., Sagare, A. P., Deane, R., Wu, Z., Holtzman, D. M., Betsholtz, C., Armulik, A., Sallstrom, J., Berk, B. C. & Zlokovic, B. V. (2012) Apolipoprotein E controls cerebrovascular integrity via cyclophilin A, *Nature.* **485**, 512-6.
262. Ethell, D. W., Kinloch, R. & Green, D. R. (2002) Metalloproteinase shedding of Fas ligand regulates beta-amyloid neurotoxicity, *Curr Biol.* **12**, 1595-600.
263. Stamenkovic, I. (2003) Extracellular matrix remodelling: the role of matrix metalloproteinases, *J Pathol.* **200**, 448-64.
264. Black, R. A., Rauch, C. T., Kozlosky, C. J., Peschon, J. J., Slack, J. L., Wolfson, M. F., Castner, B. J., Stocking, K. L., Reddy, P., Srinivasan, S., Nelson, N., Boiani, N., Schooley, K. A., Gerhart, M., Davis, R., Fitzner, J. N., Johnson, R. S., Paxton, R. J., March, C. J. & Cerretti, D. P. (1997) A metalloproteinase disintegrin that releases tumour-necrosis factor-alpha from cells, *Nature.* **385**, 729-33.
265. English, W. R., Puente, X. S., Freije, J. M., Knauper, V., Amour, A., Merryweather, A., Lopez-Otin, C. & Murphy, G. (2000) Membrane type 4 matrix metalloproteinase (MMP17) has tumor necrosis factor-alpha convertase activity but does not activate pro-MMP2, *J Biol Chem.* **275**, 14046-55.
266. Powell, W. C., Fingleton, B., Wilson, C. L., Boothby, M. & Matrisian, L. M. (1999) The metalloproteinase matrilysin proteolytically generates active soluble Fas ligand and potentiates epithelial cell apoptosis, *Curr Biol.* **9**, 1441-7.
267. Chen, Q., Moulder, K., Tenkova, T., Hardy, K., Olney, J. W. & Romano, C. (1999) Excitotoxic cell death dependent on inhibitory receptor activation, *Exp Neurol.* **160**, 215-25.
268. King, D., Skehel, P. A., Dando, O., Emelianova, K., Barron, R. & Wishart, T. M. (2021) Microarray profiling emphasizes transcriptomic differences between hippocampal in vivo tissue and in vitro cultures, *Brain Commun.* **3**, fcab152.
269. Goldeman, C., Ozgür, B. & Brodin, B. (2020) Culture-induced changes in mRNA expression levels of efflux and SLC-transporters in brain endothelial cells, *Fluids Barriers CNS.* **17**, 32.
270. Llufrio, E. M., Wang, L., Naser, F. J. & Patti, G. J. (2018) Sorting cells alters their redox state and cellular metabolome, *Redox Biol.* **16**, 381-387.
271. Reinitz, A., DeStefano, J., Ye, M., Wong, A. D. & Searson, P. C. (2015) Human brain microvascular endothelial cells resist elongation due to shear stress, *Microvasc Res.* **99**, 8-18.

272. Osmanagic-Myers, S., Rus, S., Wolfram, M., Brunner, D., Goldmann, W. H., Bonakdar, N., Fischer, I., Reipert, S., Zuzuarregui, A., Walko, G. & Wiche, G. (2015) Plectin reinforces vascular integrity by mediating crosstalk between the vimentin and the actin networks, *J Cell Sci.* **128**, 4138-50.
273. Bhattacharya, R., Gonzalez, A. M., Debiase, P. J., Trejo, H. E., Goldman, R. D., Flitney, F. W. & Jones, J. C. (2009) Recruitment of vimentin to the cell surface by beta3 integrin and plectin mediates adhesion strength, *J Cell Sci.* **122**, 1390-400.
274. Tsuruta, D. & Jones, J. C. (2003) The vimentin cytoskeleton regulates focal contact size and adhesion of endothelial cells subjected to shear stress, *J Cell Sci.* **116**, 4977-84.
275. Shi, Y., Zhang, L., Pu, H., Mao, L., Hu, X., Jiang, X., Xu, N., Stetler, R. A., Zhang, F., Liu, X., Leak, R. K., Keep, R. F., Ji, X. & Chen, J. (2016) Rapid endothelial cytoskeletal reorganization enables early blood-brain barrier disruption and long-term ischaemic reperfusion brain injury, *Nat Commun.* **7**, 10523.
276. Ben-Zvi, A., Lacoste, B., Kur, E., Andreone, B. J., Mayshar, Y., Yan, H. & Gu, C. (2014) Mfsd2a is critical for the formation and function of the blood-brain barrier, *Nature.* **509**, 507-11.
277. Haley, M. J. & Lawrence, C. B. (2017) The blood-brain barrier after stroke: Structural studies and the role of transcytotic vesicles, *J Cereb Blood Flow Metab.* **37**, 456-470.
278. Lourenço, C. F., Ledo, A., Barbosa, R. M. & Laranjinha, J. (2017) Neurovascular-neuroenergetic coupling axis in the brain: master regulation by nitric oxide and consequences in aging and neurodegeneration, *Free Radic Biol Med.* **108**, 668-682.
279. Förstermann, U. (2010) Nitric oxide and oxidative stress in vascular disease, *Pflugers Arch.* **459**, 923-39.
280. Kettenmann, H., Hanisch, U. K., Noda, M. & Verkhratsky, A. (2011) Physiology of microglia, *Physiol Rev.* **91**, 461-553.
281. Zlokovic, B. V. (2008) The blood-brain barrier in health and chronic neurodegenerative disorders, *Neuron.* **57**, 178-201.
282. Chen, A. Q., Fang, Z., Chen, X. L., Yang, S., Zhou, Y. F., Mao, L., Xia, Y. P., Jin, H. J., Li, Y. N., You, M. F., Wang, X. X., Lei, H., He, Q. W. & Hu, B. (2019) Microglia-derived TNF-α mediates endothelial necroptosis aggravating blood brain-barrier disruption after ischemic stroke, *Cell Death Dis.* **10**, 487.
283. Davalos, D., Ryu, J. K., Merlini, M., Baeten, K. M., Le Moan, N., Petersen, M. A., Deerinck, T. J., Smirnoff, D. S., Bedard, C., Hakozaki, H., Gonias Murray, S., Ling, J. B., Lassmann, H., Degen, J. L., Ellisman, M. H. & Akassoglou, K. (2012) Fibrinogen-induced perivascular microglial clustering is required for the development of axonal damage in neuroinflammation, *Nat Commun.* **3**, 1227.
284. Takata, F., Dohgu, S., Matsumoto, J., Takahashi, H., Machida, T., Wakigawa, T., Harada, E., Miyaji, H., Koga, M., Nishioku, T., Yamauchi, A. & Kataoka, Y. (2011) Brain pericytes among cells constituting the blood-brain barrier are highly sensitive to tumor necrosis factor-α, releasing matrix metalloproteinase-9 and migrating in vitro, *J Neuroinflammation.* **8**, 106.
285. Shan, Y., Tan, S., Lin, Y., Liao, S., Zhang, B., Chen, X., Wang, J., Deng, Z., Zeng, Q., Zhang, L., Wang, Y., Hu, X., Qiu, W., Peng, L. & Lu, Z. (2019) The glucagon-like peptide-1 receptor agonist reduces inflammation and blood-brain barrier

breakdown in an astrocyte-dependent manner in experimental stroke, *J Neuroinflammation.* **16**, 242.
286. Takeshita, Y., Obermeier, B., Cotleur, A. C., Spampinato, S. F., Shimizu, F., Yamamoto, E., Sano, Y., Kryzer, T. J., Lennon, V. A., Kanda, T. & Ransohoff, R. M. (2017) Effects of neuromyelitis optica-IgG at the blood-brain barrier in vitro, *Neurol Neuroimmunol Neuroinflamm.* **4**, e311.
287. Ensoli, F., Fiorelli, V., Lugaresi, A., Farina, D., De Cristofaro, M., Collacchi, B., Muratori, D. S., Scala, E., Di Gioacchino, M., Paganelli, R. & Aiuti, F. (2002) Lymphomononuclear cells from multiple sclerosis patients spontaneously produce high levels of oncostatin M, tumor necrosis factors alpha and beta, and interferon gamma, *Mult Scler.* **8**, 284-8.
288. Hamel, E., Royea, J., Ongali, B. & Tong, X. K. (2016) Neurovascular and Cognitive failure in Alzheimer's Disease: Benefits of Cardiovascular Therapy, *Cell Mol Neurobiol.* **36**, 219-32.
289. Donnelly, J., Budohoski, K. P., Smielewski, P. & Czosnyka, M. (2016) Regulation of the cerebral circulation: bedside assessment and clinical implications, *Crit Care.* **20**, 129.
290. Obenaus, A., Ng, M., Orantes, A. M., Kinney-Lang, E., Rashid, F., Hamer, M., DeFazio, R. A., Tang, J., Zhang, J. H. & Pearce, W. J. (2017) Traumatic brain injury results in acute rarefication of the vascular network, *Sci Rep.* **7**, 239.
291. Hassler, O. (1967) Arterial deformities in senile brains. The occurrence of the deformities in a large autopsy series and some aspects of their functional significance, *Acta Neuropathol.* **8**, 219-29.
292. Beckmann, N., Schuler, A., Mueggler, T., Meyer, E. P., Wiederhold, K. H., Staufenbiel, M. & Krucker, T. (2003) Age-dependent cerebrovascular abnormalities and blood flow disturbances in APP23 mice modeling Alzheimer's disease, *J Neurosci.* **23**, 8453-9.
293. Kimura, T., Hashimura, T. & Miyakawa, T. (1991) Observations of microvessels in the brain with Alzheimer's disease by the scanning electron microscopy, *Jpn J Psychiatry Neurol.* **45**, 671-6.
294. Hamel, E., Nicolakakis, N., Aboulkassim, T., Ongali, B. & Tong, X. K. (2008) Oxidative stress and cerebrovascular dysfunction in mouse models of Alzheimer's disease, *Exp Physiol.* **93**, 116-20.
295. Tong, X. K., Nicolakakis, N., Kocharyan, A. & Hamel, E. (2005) Vascular remodeling versus amyloid beta-induced oxidative stress in the cerebrovascular dysfunctions associated with Alzheimer's disease, *J Neurosci.* **25**, 11165-74.
296. Iadecola, C., Zhang, F., Niwa, K., Eckman, C., Turner, S. K., Fischer, E., Younkin, S., Borchelt, D. R., Hsiao, K. K. & Carlson, G. A. (1999) SOD1 rescues cerebral endothelial dysfunction in mice overexpressing amyloid precursor protein, *Nat Neurosci.* **2**, 157-61.
297. Erdös, B., Snipes, J. A., Miller, A. W. & Busija, D. W. (2004) Cerebrovascular dysfunction in Zucker obese rats is mediated by oxidative stress and protein kinase C, *Diabetes.* **53**, 1352-9.
298. Dias, R. A., Dias, L., Azevedo, E. & Castro, P. (2021) Acute Inflammation in Cerebrovascular Disease: A Critical Reappraisal with Focus on Human Studies, *Life (Basel).* **11**.

299. Leng, F. & Edison, P. (2021) Neuroinflammation and microglial activation in Alzheimer disease: where do we go from here?, *Nat Rev Neurol.* **17**, 157-172.
300. Gómez Morillas, A., Besson, V. C. & Lerouet, D. (2021) Microglia and Neuroinflammation: What Place for P2RY12?, *Int J Mol Sci.* **22**.
301. Haynes, S. E., Hollopeter, G., Yang, G., Kurpius, D., Dailey, M. E., Gan, W. B. & Julius, D. (2006) The P2Y12 receptor regulates microglial activation by extracellular nucleotides, *Nat Neurosci.* **9**, 1512-9.
302. Moore, C. S., Ase, A. R., Kinsara, A., Rao, V. T., Michell-Robinson, M., Leong, S. Y., Butovsky, O., Ludwin, S. K., Séguéla, P., Bar-Or, A. & Antel, J. P. (2015) P2Y12 expression and function in alternatively activated human microglia, *Neurol Neuroimmunol Neuroinflamm.* **2**, e80.
303. Amadio, S., Parisi, C., Montilli, C., Carrubba, A. S., Apolloni, S. & Volonté, C. (2014) P2Y(12) receptor on the verge of a neuroinflammatory breakdown, *Mediators Inflamm.* **2014**, 975849.
304. Sipe, G. O., Lowery, R. L., Tremblay, M., Kelly, E. A., Lamantia, C. E. & Majewska, A. K. (2016) Microglial P2Y12 is necessary for synaptic plasticity in mouse visual cortex, *Nat Commun.* **7**, 10905.
305. Cosenza-Nashat, M. A., Kim, M. O., Zhao, M. L., Suh, H. S. & Lee, S. C. (2006) CD45 isoform expression in microglia and inflammatory cells in HIV-1 encephalitis, *Brain Pathol.* **16**, 256-65.
306. Ning, M., Furie, K. L., Koroshetz, W. J., Lee, H., Barron, M., Lederer, M., Wang, X., Zhu, M., Sorensen, A. G., Lo, E. H. & Kelly, P. J. (2006) Association between tPA therapy and raised early matrix metalloproteinase-9 in acute stroke, *Neurology.* **66**, 1550-5.
307. Rosell, A., Ortega-Aznar, A., Alvarez-Sabín, J., Fernández-Cadenas, I., Ribó, M., Molina, C. A., Lo, E. H. & Montaner, J. (2006) Increased brain expression of matrix metalloproteinase-9 after ischemic and hemorrhagic human stroke, *Stroke.* **37**, 1399-406.
308. Lorenzl, S., Albers, D. S., Relkin, N., Ngyuen, T., Hilgenberg, S. L., Chirichigno, J., Cudkowicz, M. E. & Beal, M. F. (2003) Increased plasma levels of matrix metalloproteinase-9 in patients with Alzheimer's disease, *Neurochem Int.* **43**, 191-6.
309. Agrawal, S., Anderson, P., Durbeej, M., van Rooijen, N., Ivars, F., Opdenakker, G. & Sorokin, L. M. (2006) Dystroglycan is selectively cleaved at the parenchymal basement membrane at sites of leukocyte extravasation in experimental autoimmune encephalomyelitis, *J Exp Med.* **203**, 1007-19.
310. Li, W. D., Hu, N., Lei, F. R., Wei, S., Rong, J. J., Zhuang, H. & Li, X. Q. (2015) Autophagy inhibits endothelial progenitor cells migration via the regulation of MMP2, MMP9 and uPA under normoxia condition, *Biochem Biophys Res Commun.* **466**, 376-80.
311. Feng, Y., He, D., Yao, Z. & Klionsky, D. J. (2014) The machinery of macroautophagy, *Cell Res.* **24**, 24-41.
312. Du, J., Teng, R. J., Guan, T., Eis, A., Kaul, S., Konduri, G. G. & Shi, Y. (2012) Role of autophagy in angiogenesis in aortic endothelial cells, *American Journal of Physiology - Cell Physiology*.
313. Bharath, L. P., Mueller, R., Li, Y., Ruan, T., Kunz, D., Goodrich, R., Mills, T., Deeter, L., Sargsyan, A., Babu, P. V. A., Graham, T. E. & Symons, J. D. (2014) Impairment of autophagy in endothelial cells prevents shear-stress-induced

increases in nitric oxide bioavailability1, *Canadian Journal of Physiology and Pharmacology*.
314. Pallet, N., Sirois, I., Bell, C., Hanafi, L. A., Hamelin, K., Dieudé, M., Rondeau, C., Thibault, P., Desjardins, M. & Hebert, M. J. (2013) A comprehensive characterization of membrane vesicles released by autophagic human endothelial cells, *Proteomics.* **13**, 1108-20.
315. Patella, F., Neilson, L. J., Athineos, D., Erami, Z., Anderson, K. I., Blyth, K., Ryan, K. M. & Zanivan, S. (2016) In-Depth Proteomics Identifies a Role for Autophagy in Controlling Reactive Oxygen Species Mediated Endothelial Permeability, *J Proteome Res.* **15**, 2187-97.
316. Ross, C. A. & Poirier, M. A. (2004) Protein aggregation and neurodegenerative disease, *Nat Med.* **10 Suppl**, S10-7.
317. Wu, S. & Du, L. (2021) Protein Aggregation in the Pathogenesis of Ischemic Stroke, *Cell Mol Neurobiol.* **41**, 1183-1194.
318. Conti, B. A. & Oppikofer, M. (2022) Biomolecular condensates: new opportunities for drug discovery and RNA therapeutics, *Trends Pharmacol Sci.* **43**, 820-837.
319. Asadi, M. R., Sadat Moslehian, M., Sabaie, H., Jalaiei, A., Ghafouri-Fard, S., Taheri, M. & Rezazadeh, M. (2021) Stress Granules and Neurodegenerative Disorders: A Scoping Review, *Front Aging Neurosci.* **13**, 650740.
320. Suzuki, H. I. & Onimaru, K. (2022) Biomolecular condensates in cancer biology, *Cancer Sci.* **113**, 382-391.
321. Risso-Ballester, J., Galloux, M., Cao, J., Le Goffic, R., Hontonnou, F., Jobart-Malfait, A., Desquesnes, A., Sake, S. M., Haid, S., Du, M., Zhang, X., Zhang, H., Wang, Z., Rincheval, V., Zhang, Y., Pietschmann, T., Eléouët, J. F., Rameix-Welti, M. A. & Altmeyer, R. (2021) A condensate-hardening drug blocks RSV replication in vivo, *Nature.* **595**, 596-599.
322. Alberti, S. & Hyman, A. A. (2021) Biomolecular condensates at the nexus of cellular stress, protein aggregation disease and ageing, *Nat Rev Mol Cell Biol.* **22**, 196-213.
323. Martello, A., Lauriola, A., Mellis, D., Parish, E., Dawson, J. C., Imrie, L., Vidmar, M., Gammoh, N., Mitic, T., Brittan, M., Carragher, N. O., Arca, D. D. & Caporali, A. Trichoplein binds PCM1 and controls endothelial cell function by regulating autophagy.
324. Lopez Sanchez, M. I. G., Krüger, A., Shiriaev, D. I., Liu, Y. & Rorbach, J. (2021) Human Mitoribosome Biogenesis and Its Emerging Links to Disease, *Int J Mol Sci.* **22**.
325. Kedersha, N., Chen, S., Gilks, N., Li, W., Miller, I. J., Stahl, J. & Anderson, P. (2002) Evidence that ternary complex (eIF2-GTP-tRNA(i)(Met))-deficient preinitiation complexes are core constituents of mammalian stress granules, *Mol Biol Cell.* **13**, 195-210.
326. Mahboubi, H. & Stochaj, U. (2017) Cytoplasmic stress granules: Dynamic modulators of cell signaling and disease, *Biochim Biophys Acta Mol Basis Dis.* **1863**, 884-895.
327. Kwon, S., Zhang, Y. & Matthias, P. (2007) The deacetylase HDAC6 is a novel critical component of stress granules involved in the stress response, *Genes Dev.* **21**, 3381-94.

328. Jung, H. S., Joo, J. D., Kim, D. W., In, J. H., Roh, M., Jeong, J. T., Noh, S. J. & Choi, J. W. (2014) Effect of milrinone on the inflammatory response and NF-kB activation in renal ischemia-reperfusion injury in mice, *Korean J Anesthesiol.* **66**, 136-42.
329. Ong, S. B., Lee, W. H., Shao, N. Y., Ismail, N. I., Katwadi, K., Lim, M. M., Kwek, X. Y., Michel, N. A., Li, J., Newson, J., Tahmasebi, S., Rehman, J., Kodo, K., Jang, H. R. & Ong, S. G. (2019) Calpain Inhibition Restores Autophagy and Prevents Mitochondrial Fragmentation in a Human iPSC Model of Diabetic Endotheliopathy, *Stem Cell Reports.* **12**, 597-610.
330. Menzies, F. M., Garcia-Arencibia, M., Imarisio, S., O'Sullivan, N. C., Ricketts, T., Kent, B. A., Rao, M. V., Lam, W., Green-Thompson, Z. W., Nixon, R. A., Saksida, L. M., Bussey, T. J., O'Kane, C. J. & Rubinsztein, D. C. (2015) Calpain inhibition mediates autophagy-dependent protection against polyglutamine toxicity, *Cell Death Differ.* **22**, 433-44.
331. Tsaytler, P., Harding, H. P., Ron, D. & Bertolotti, A. (2011) Selective inhibition of a regulatory subunit of protein phosphatase 1 restores proteostasis, *Science.* **332**, 91-4.
332. Humeau, J., Leduc, M., Cerrato, G., Loos, F., Kepp, O. & Kroemer, G. (2020) Phosphorylation of eukaryotic initiation factor-2α (eIF2α) in autophagy, *Cell Death Dis.* **11**, 433.
333. Jucker, M. & Walker, L. C. (2013) Self-propagation of pathogenic protein aggregates in neurodegenerative diseases, *Nature.* **501**, 45-51.
334. Li, J. Y., Englund, E., Holton, J. L., Soulet, D., Hagell, P., Lees, A. J., Lashley, T., Quinn, N. P., Rehncrona, S., Björklund, A., Widner, H., Revesz, T., Lindvall, O. & Brundin, P. (2008) Lewy bodies in grafted neurons in subjects with Parkinson's disease suggest host-to-graft disease propagation, *Nat Med.* **14**, 501-3.
335. Ugalde, C. L., Finkelstein, D. I., Lawson, V. A. & Hill, A. F. (2016) Pathogenic mechanisms of prion protein, amyloid-β and α-synuclein misfolding: the prion concept and neurotoxicity of protein oligomers, *J Neurochem.* **139**, 162-180.
336. Jeon, I., Cicchetti, F., Cisbani, G., Lee, S., Li, E., Bae, J., Lee, N., Li, L., Im, W., Kim, M., Kim, H. S., Oh, S. H., Kim, T. A., Ko, J. J., Aubé, B., Oueslati, A., Kim, Y. J. & Song, J. (2016) Human-to-mouse prion-like propagation of mutant huntingtin protein, *Acta Neuropathol.* **132**, 577-92.
337. He, Z., Guo, J. L., McBride, J. D., Narasimhan, S., Kim, H., Changolkar, L., Zhang, B., Gathagan, R. J., Yue, C., Dengler, C., Stieber, A., Nitla, M., Coulter, D. A., Abel, T., Brunden, K. R., Trojanowski, J. Q. & Lee, V. M. (2018) Amyloid-β plaques enhance Alzheimer's brain tau-seeded pathologies by facilitating neuritic plaque tau aggregation, *Nat Med.* **24**, 29-38.
338. Kahl, A., Blanco, I., Jackman, K., Baskar, J., Milaganur Mohan, H., Rodney-Sandy, R., Zhang, S., Iadecola, C. & Hochrainer, K. (2018) Cerebral ischemia induces the aggregation of proteins linked to neurodegenerative diseases, *Sci Rep.* **8**, 2701.
339. Bentmann, E., Haass, C. & Dormann, D. (2013) Stress granules in neurodegeneration--lessons learnt from TAR DNA binding protein of 43 kDa and fused in sarcoma, *Febs j.* **280**, 4348-70.
340. Gopisetty, G. & Thangarajan, R. (2016) Mammalian mitochondrial ribosomal small subunit (MRPS) genes: A putative role in human disease, *Gene.* **589**, 27-35.
341. Ayres, J. K. & Maani, C. V. (2022) Milrinone in *StatPearls*, StatPearls Publishing

Copyright © 2022, StatPearls Publishing LLC., Treasure Island (FL).
342. Lanfear, D. E., Hasan, R., Gupta, R. C., Williams, C., Czerska, B., Tita, C., Bazari, R. & Sabbah, H. N. (2009) Short term effects of milrinone on biomarkers of necrosis, apoptosis, and inflammation in patients with severe heart failure, *J Transl Med.* **7**, 67.
343. Bisicchia, E., Mastrantonio, R., Nobili, A., Palazzo, C., La Barbera, L., Latini, L., Millozzi, F., Sasso, V., Palacios, D., D'Amelio, M. & Viscomi, M. T. (2022) Restoration of ER proteostasis attenuates remote apoptotic cell death after spinal cord injury by reducing autophagosome overload, *Cell Death Dis.* **13**, 381.
344. Neuber, C., Uebeler, J., Schulze, T., Sotoud, H., El-Armouche, A. & Eschenhagen, T. (2014) Guanabenz interferes with ER stress and exerts protective effects in cardiac myocytes, *PLoS One.* **9**, e98893.
345. Kang, H. J., Seol, H. S., Lee, S. E., Suh, Y. A., Kim, J., Jang, S. J. & Yu, E. (2019) Guanabenz Acetate Induces Endoplasmic Reticulum Stress-Related Cell Death in Hepatocellular Carcinoma Cells, *J Pathol Transl Med.* **53**, 94-103.
346. Zhou, K., Zheng, Z., Li, Y., Han, W., Zhang, J., Mao, Y., Chen, H., Zhang, W., Liu, M., Xie, L., Zhang, H., Xu, H. & Xiao, J. (2020) TFE3, a potential therapeutic target for Spinal Cord Injury via augmenting autophagy flux and alleviating ER stress, *Theranostics.* **10**, 9280-9302.
347. Sundaram, J. R., Wu, Y., Lee, I. C., George, S. E., Hota, M., Ghosh, S., Kesavapany, S., Ahmed, M., Tan, E. K. & Shenolikar, S. (2019) PromISR-6, a Guanabenz Analogue, Improves Cellular Survival in an Experimental Model of Huntington's Disease, *ACS Chem Neurosci.* **10**, 3575-3589.
348. Stansfield, W. E., Ranek, M., Pendse, A., Schisler, J. C., Wang, S., Pulinilkunnil, T. & Willis, M. S. (2014) Chapter 4 - The Pathophysiology of Cardiac Hypertrophy and Heart Failure in *Cellular and Molecular Pathobiology of Cardiovascular Disease* (Willis, M. S., Homeister, J. W. & Stone, J. R., eds) pp. 51-78, Academic Press, San Diego.
349. Saito, K., Elce, J. S., Hamos, J. E. & Nixon, R. A. (1993) Widespread activation of calcium-activated neutral proteinase (calpain) in the brain in Alzheimer disease: a potential molecular basis for neuronal degeneration, *Proc Natl Acad Sci U S A.* **90**, 2628-32.
350. Rao, M. V., Mohan, P. S., Peterhoff, C. M., Yang, D. S., Schmidt, S. D., Stavrides, P. H., Campbell, J., Chen, Y., Jiang, Y., Paskevich, P. A., Cataldo, A. M., Haroutunian, V. & Nixon, R. A. (2008) Marked calpastatin (CAST) depletion in Alzheimer's disease accelerates cytoskeleton disruption and neurodegeneration: neuroprotection by CAST overexpression, *J Neurosci.* **28**, 12241-54.
351. https://www.enzolifesciences.com/ENZ-51035/proteostat-aggresome-detection-kit/#:~:text=Aggresomes%20within%20HeLa%20cells%2C%20previously, a. o. b. f. m.
352. Runwal, G., Stamatakou, E., Siddiqi, F. H., Puri, C., Zhu, Y. & Rubinsztein, D. C. (2019) LC3-positive structures are prominent in autophagy-deficient cells, *Sci Rep.* **9**, 10147.
353. Kalathil, D., John, S. & Nair, A. S. (2020) FOXM1 and Cancer: Faulty Cellular Signaling Derails Homeostasis, *Front Oncol.* **10**, 626836.

354. Tan, Y., Raychaudhuri, P. & Costa, R. H. (2007) Chk2 mediates stabilization of the FoxM1 transcription factor to stimulate expression of DNA repair genes, *Mol Cell Biol.* **27**, 1007-16.
355. Thirumangalakudi, L., Yin, L., Rao, H. V. & Grammas, P. (2007) IL-8 induces expression of matrix metalloproteinases, cell cycle and pro-apoptotic proteins, and cell death in cultured neurons, *J Alzheimers Dis.* **11**, 305-11.
356. Zou, Y., Yoon, S., Kyung, J. J., Chul, H. K., Tae, G. S., Kim, M. S., You, J. K., Lee, J., Byung, P. Y. & Hae, Y. C. (2006) Upregulation of aortic adhesion molecules during aging, *Journals of Gerontology - Series A Biological Sciences and Medical Sciences*.
357. Salminen, A., Kaarniranta, K. & Kauppinen, A. (2012) Inflammaging: Disturbed interplay between autophagy and inflammasomes, *Aging*.
358. NHS.
359. Ye, M., Sanchez, H. M., Hultz, M., Yang, Z., Bogorad, M., Wong, A. D. & Searson, P. C. (2014) Brain microvascular endothelial cells resist elongation due to curvature and shear stress, *Sci Rep.* **4**, 4681.
360. Zhang, X., Ramírez, C. M., Aryal, B., Madrigal-Matute, J., Liu, X., Diaz, A., Torrecilla-Parra, M., Suárez, Y., Cuervo, A. M., Sessa, W. C. & Fernández-Hernando, C. (2020) Cav-1 (Caveolin-1) Deficiency Increases Autophagy in the Endothelium and Attenuates Vascular Inflammation and Atherosclerosis, *Arterioscler Thromb Vasc Biol.* **40**, 1510-1522.
361. Bai, X., Yang, X., Jia, X., Rong, Y., Chen, L., Zeng, T., Deng, X., Li, W., Wu, G., Wang, L., Li, Y., Zhang, J., Xiong, Z., Xiong, L., Wang, Y., Zhu, L., Zhao, Y. & Jin, S. (2020) CAV1-CAVIN1-LC3B-mediated autophagy regulates high glucose-stimulated LDL transcytosis, *Autophagy.* **16**, 1111-1129.
362. Nah, J., Yoo, S.-M., Jung, S., Jeong, E. I., Park, M., Kaang, B.-K. & Jung, Y.-K. (2017) Phosphorylated CAV1 activates autophagy through an interaction with BECN1 under oxidative stress, *Cell Death & Disease.* **8**, e2822-e2822.
363. Østergaard, L., Jespersen, S. N., Engedahl, T., Gutiérrez Jiménez, E., Ashkanian, M., Hansen, M. B., Eskildsen, S. & Mouridsen, K. (2015) Capillary dysfunction: its detection and causative role in dementias and stroke, *Curr Neurol Neurosci Rep.* **15**, 37.